The pulsations and energy transfers in a double-orifice combustor

C. K. Beale

The Pulsations and Energy Transfers in a Double-Orifice Combustor

by

C. K. Beale, B.Sc.

Thesis submitted for the degree of
Doctor of Philosophy in the
University of Durham.

Department of Engineering Science

March 1975

I should like to thank my supervisor, Dr. P.H. Clarke, for his assistance and encouragement; the technical staff of the Department of Engineering Science for their invaluable help with the experimental apparatus; and the Science Research Council for the grant for the work.

ABSTRACT

This work examines the effect of longitudinal oscillations on the heat transfer in a naturally-aspirating, propane-fuelled combustor. Previous investigations in the field have been predominantly experimental in nature, although theoretical studies of the effect of oscillations on local heat transfer coefficients have been made. In this work, a linearised wave equation, which governs the propagation of sound waves in a gas confined by a straight tube and exhibiting an axial temperature variation, is used to correlate local heat transfer coefficients by a quasi-steady-state method. An apparatus was constructed, and measurements of the gas, wall and water temperatures and of the gas pressure amplitudes were taken in a concentric tube heat exchanger, which formed part of the resonating section.

CONTENTS

SYMBOLS AND CONSTANTS

Section 1

A_1, A_2, A_3, B	constants	
$\bar{c}$	time-averaged velocity of sound	m/s
c_p	specific heat at constant pressure	kJ/kg K
c_v	specific heat at constant volume	kJ/kg K
$\hat{E}$	amplitude of kinetic energy in oscillation	kJ
$\bar{E}$	time-averaged kinetic energy of flow	kJ
f	frequency	Hz
Gz	Graetz number	
L	length	m
n	integer	
N	rotational speed	rev/minute
$\overline{Nu_p}$	time-averaged Nusselt number in pulsating flow	
Nu	Nusselt number in steady flow	
$\hat{p}$	pressure amplitude	N/m^2
$\bar{p}$	time-averaged pressure	N/m^2
ΔP	pressure amplitude of Koshkin (37)	N/m^2
$\bar{P}$	working pressure of Koshkin (37)	N/m^2
Pr	Prandtl number	
Re	Reynolds number	
SPL	sound pressure level	dB
$\hat{u}$	velocity amplitude	m/s
$\bar{u}$	time-averaged velocity	m/s
x	axial distance	m
λ	wavelength	m
γ	ratio of cp/cv	
ρ	density	kg/m^3
ϕ_{AT}	pulsation energy attenuation factor of Galitseysky et al. (38)	

ω	angular frequency	radian/s

Section 2

A	constant	
B_A	bulk modulus of air	N/m^2
c_o	velocity of sound at x = 0	m/s
e	specific internal energy	kJ/kg
E_c	Eckert number	
h	local heat transfer coefficient	$W/m^2 K$
J_n	Bessel function of first kind - order n	
k	thermal conductivity	W/m K
L	length	m
M_1	constant defined by equation 2.2.28	
$\dot{m}$	mass flowrate	kg/h
N_1	constant defined by equation 2.2.29	
p	pressure	N/m^2
$\hat{p}_o$	pressure amplitude at x = 0	N/m^2
q	heat transfer	kJ
R	specific gas constant for air 0.2871	kJ/kg
S	Strouhal number $= \frac{\omega d}{u}$	
t	time	s
T	temperature	°C
T_o	temperature at x = 0	°C
u	velocity	m/s
x	axial distance	m
X	function of x	
Y_n	Bessel function of second kind - order n	
y	coordinate	m
z	change of variable	
Z	coordinate	m

ξ	axial displacement of pressure wave	m
α	constant	
θ	function of time	
λ	wavelength	m
ϕ	function	
μ	dynamic viscosity	kg/m s
ρ	density	kg/m^3

Section 3

D_I	diameter of aerodynamic valve	m
h	damping ratio	
L_n	connecting length for pressure transducer	m
$\dot{m}_{GC}$	mass flowrate of chamber coolant	kg/h
$\dot{m}_P$	mass flowrate of propane	kg/h
$\dot{m}_W$	mass flowrate of water	kg/h
P_{An}	pressure amplitude at site n	N/m^2
P_P	regulated pressure of propane	Bar
r	radius of connecting tube	m
T_{An}	temperature of air at site n	°C
T_P	temperature of propane in flowmeter	°C
T_{gn}	surface temperature at site n	°C
T_{WIN}	outlet temperature of water from injector	°C
T_{Wn}	temperature of water at site n	°C
x_{AUG}	axial position of augmenter	m
ω_n	natural frequency	radian/s

Section 4

c	velocity of sound	m/s
D_{EQ}	equivalent diameter of annulus	m
D_I	diameter of aerodynamic valve	m

D_o	diameter of inner tube of heat exchanger A	m
f	frequency	Hz
h_{AS}	heat transfer coefficient between air and tube surface	W/m^2 K
h_{SW}	heat transfer coefficient between tube surface and water	W/m^2 K
k_A	thermal conductivity of air	W/m K
k_W	thermal conductivity of water	W/m K
L	length	m
L_A	length of heat exchanger A	m
$\dot{m}_{AA}$	mass flowrate of air through resonating section	kg/h
$\dot{m}_P$	mass flowrate of propane	kg/h
n	wave number	
n	integer	
$p_{A(x)}$	pressure amplitude at point x	N/m^2
$\hat{p}_{A(x)}$	maximum pressure amplitude	N/m^2
p_{Ac}	combustion chamber pressure amplitude	N/m^2
$\overline{Re}_A$	time-averaged Reynolds number of air flow	
Re_W	Reynolds number of water flow	
S	Strouhal number	
S_S	surface area of section of heat exchanger A	m^2
$T_{A(x)}$	temperature of air at point x	°C
T_{An}	temperature of air at site n	°C
$\overline{T}_A$	mean air temperature in section	°C
$\overline{T}_S$	mean surface temperature in section	°C
$\overline{T}_W$	mean water temperature in section	°C
$\overline{u}_A$	time-averaged velocity of air flow	m/s
$\hat{u}$	velocity amplitude of air	m/s
x	axial distance	m
ρ_A	density of air	kg/m^3
μ_A	dynamic viscosity of air	kg/m s
η_{th}	thermal efficiency	

Section 6

a_g	gravitational acceleration	m/s^2
c	velocity of sound	m/s
C_c	capitance of connecting leads	pF
C_i	capitance of amplifier input	pF
C_m	capitance of microphone	nF
c_{pA}	specific heat at constant pressure of air	kJ/kg K
c_{pw}	specific heat at constant pressure of water	kJ/kg K
D_{L1}	internal diameter of chamber lagging	m
D_{L2}	external diameter of chamber lagging	m
d_o	diameter of inner tube of heat exchanger	m
d_{SH}	diameter of sheath	m
$f(x)$	function of x	
f	frequency	Hz
g_o	constant in Newton's Second Law	kg m/N s^2
h	mean heat transfer coefficient	W/m^2 K
h	specific enthalpy of pure substance	kJ/kg
h_c	convection heat transfer coefficient	W/m^2 K
h_r	radiation heat transfer coefficient	W/m^2 K
k_{LAG}	thermal conductivity of chamber lagging	W/m K
k_{SH}	thermal conductivity of sheath	W/m K
L	immersion of thermocouple	m
L	length of tube	m
L_A	length of Heat exchanger A	m
L_{CL}	length of chamber lagging	m
$\dot{m}_A$	mass flowrate of fluid	kg/h
$\dot{m}_{AA}$	mass flowrate of air through resonating section	kg/h
$\dot{m}_{ABC}$	mass flowrate of air through Heat exchangers B & C	kg/h
$\dot{m}_{CC}$	mass flowrate of chamber coolant	kg/h
$\dot{m}_p$	mass flowrate of propane	kg/h

$\dot{m}_w$	mass flowrate of water	kg/h
$\dot{m}_1$	defined by equation 6 - C.7	
Nu_d	Nusselt number based on tube diameter	
p	pressure	N/m^2
P_{AO}	ambient pressure	N/m^2
P_o	reference pressure 1.01325×10^5	n/m^2
$\dot{Q}$	rate of heat transfer	W
$\dot{Q}_{LCL}$	rate of heat transfer through chamber lagging	W
r	radial ordinate	m
R	radius of tube	m
R_d	Reynolds number of flow in tube	
S_B	surface area of thermocouple bead	m
S_{CHARGE}	charge sensitivity of microphone	$pC/N/m^2$
S_V	voltage sensitivity of microphone	$mV/\mu Bar$
$S_{V(C)}$	connected sensitivity of microphone	$mV/\mu Bar$
T_{Am}	mean air temperature over length Δx	°C
T_{Am}	connected air temperature	°C
T'_{Am}	temperature recorded by thermocouple	°C
T_{AO}	ambient temperature	°C
T_{EXIT}	exhaust gas temperature	°C
T_{LAG}	outer surface temperature of chamber lagging	°C
T_o	reference temperature 273.16	K
T_{SC}	chamber surface temperature	°C
t_{SH}	thickness of sheath wall	m
T_{wm}	mean water temperature over length Δx	°C
u	specific internal energy of substance	kJ/kg
$\dot{W}_x$	rate of external work	W
x	axial distance along tube	m
x_c	cold end of Heat exchanger A	m
x_H	hot end of Heat exchanger A	m

y	change of variable	
z	elevation of system above arbitrary datum	m
$\Delta \dot{H}$	rate of change of enthalpy	W
$[\Delta \dot{H}']_{t_0}$	rate of increase of enthalpy of propane fuel in isothermal reaction	W
ΔT_w	change in water temperature over Δx	K
ε_B	normal total emissivity of bead	
ε_{SH}	normal total emissivity of sheath	
σ	Stefan-Boltzmann constant 5.67×10^{-8}	$W/m^2\ K^4$
ρ	density	kg/m^3
$\bar{\rho}$	time-averaged density	kg/m^3
ω	angular frequency	radian/s
η_{th}	thermal efficiency	
E_c	ECKERT Nº $= \dfrac{\bar{u}^2}{c_p \Delta T}$	

1. Introduction

This work studies the effect of combustion-driven oscillations on the process of heat transfer in a double-orifice pulsating combustor. Such a combustor consists of a combustion chamber, into which fuel and air are admitted, and a resonating exhaust tube in which convective heat transfer occurs. When in operation, the predominant oscillations occur in a standing, longitudinal mode and are sustained by a correctly-phased variation in the rate of energy release in the combustion chamber. The oscillations are regarded as stable when the pressure amplitude neither increases nor decreases, which indicates that the energy added to the wave motion is exactly damped out by viscous dissipation. The advantages of constant volume over constant pressure combustion are generally held to be increased volumetric combustion rate, increased combustion efficiency and increased rate of convective heat transfer, the chief disadvantage being noise. Although considerable interest has been shown in the pulsating combustor, there have been few commercial applications.

One of the earliest observations of combustion-driven oscillations was recorded by Higgins (1) in 1777 when he found that a hydrogen diffusion flame, enclosed by a large tube (open at both ends), oscillated audibly for certain lengths of the fuel supply line. In 1859 Reijke (2) reported an acoustically-driven oscillation in an air column when a hot metal gauze was positioned one quarter of the way up a vertical open-ended tube. In 1883 Mallard and Le Chatelier (3) noticed that a flame, propagating from the open to the closed end of a tube, began to oscillate with increasing violence until detonation occurred.

In 1904 Lemale and Armengaud (4) built one of the first constant pressure gas turbines but obtained no external shaft power as the

output of the turbine was absorbed by the compressor. Holzwarth (5) recognised that the negative compression work had to be reduced and suggested that a constant volume combustion process should be employed. A number of patents were taken out - by Esnault-Pelterie in 1905 (6), Karawodine, 1906 (7) Armengaud, 1907 (8) and Marconnet, 1910 (9). Each of these designs consisted principally of a rigid volume with two openings, one for the injection of the combustible mixture and the other for the expulsion of the combustion products. In these valve-actuated chambers, the constant-volume combustion produced a considerable pressure gain although this pressure could only be expanded in the turbine with a poor efficiency, due to the variation in the exhaust gas velocity. In the course of these early experiments, it was observed that the transmission of energy from the intermittent flow of exhaust gases to the cooled walls of the outlet tubes was very apparent, and this led to the development of a steam boiler, the Velox, by the Brown Boveri Company.

In 1930 Schmidt (10) patented a pulsating combustion tube which was designed to thrust a column of air out of the open end by means of the "rapidly repeated combustion of fuel and air in small quantities" at the accoustically closed end. It was this tube, 'Das Schmidt-Rohr', that was later developed by the Argus Engine Company to propel the 'Vergeltungswaffe - 1' flying bomb, shown in Figure 1.1. Manganiello (10) has reported that a replica of the propulsion unit developed up to 520 kW at the operating frequency of 40 Hz.

In 1933 Reynst (11) patented a combustion chamber which consisted of a rigid volume with only one opening for the alternate passage of fresh mixture and exhaust products. Reynst took out a further patent (12) in 1938, concerning an invention, based on his earlier patent, to

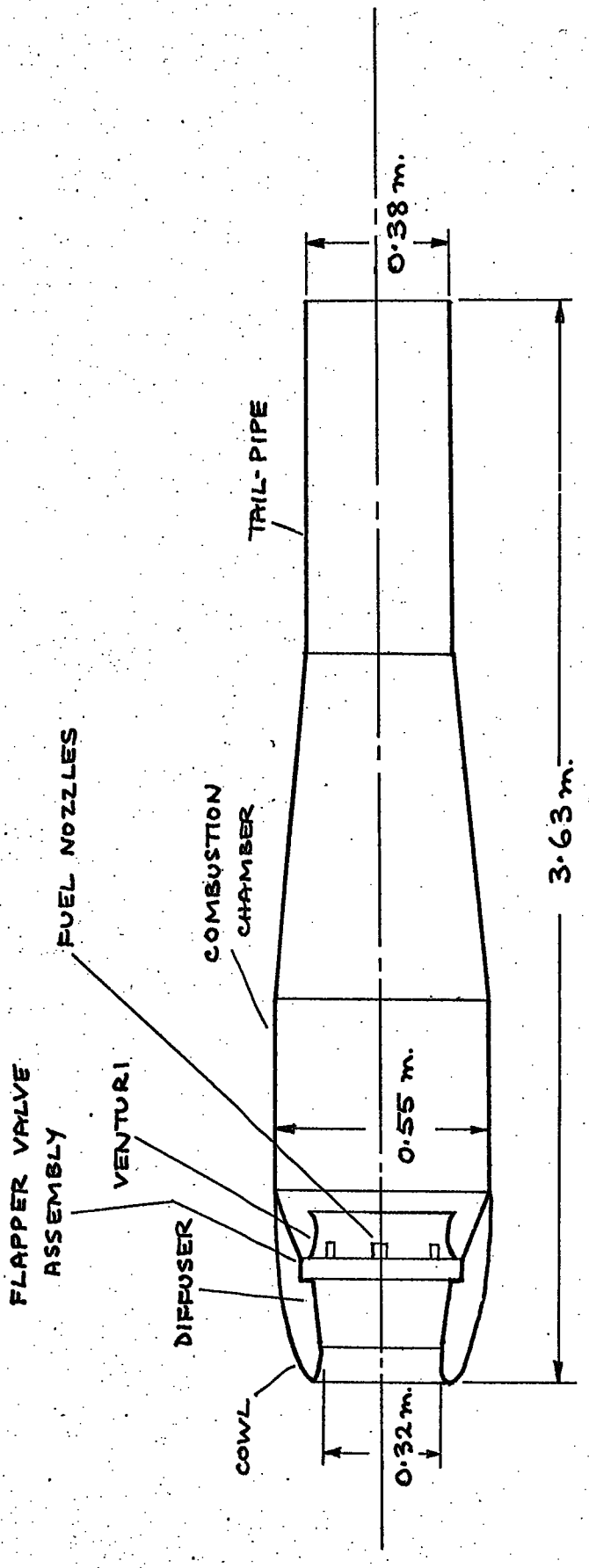

FIGURE 1.1 : THE SCHMIDT TUBE

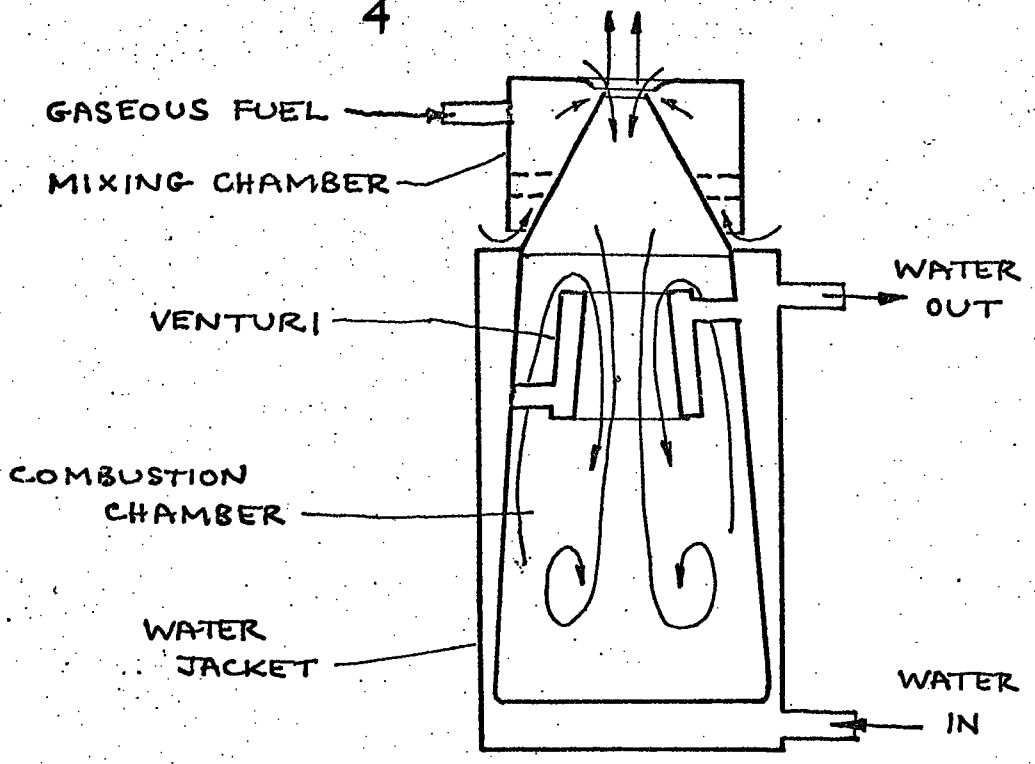

FIGURE 1.2 : THE REYNST POT

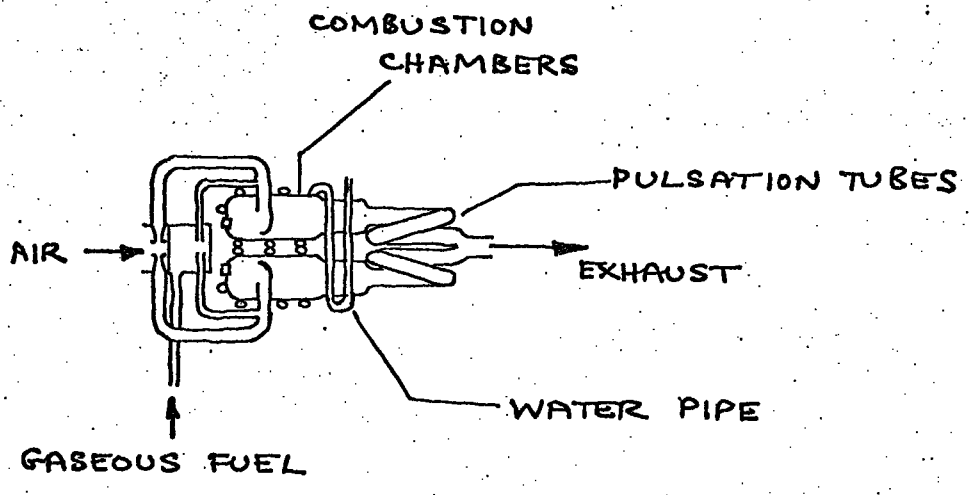

FIGURE 1.3 : HUBER WATER HEATER

produce and transfer heat efficiently by means of a detonative combustion process (see Figure 1.2).

1.1 Water/air heating pulsating combustors

In 1943 Reynst (13) reported work on a single-orifice combustor; volumetric combustion rate was 17.5 MW/m^3 at an operating frequency of 128 Hz, and the maximum rate of heat transfer was 0.28 W/m^2K for an outlet water temperature of 50°C. An analysis of the exhaust gases gave 13% CO_2, 1.5% O_2 and 0% CO, and the unit was said to be unpleasantly noisy. In 1948 Huber (14) began to market the 'Schwingfeuergerat'; this unit incorporated a two-orifice combustor, fuelled by petrol at first, but by natural gas after 1950. The device was intended to preheat the cooling water of internal combustion engines prior to starting in cold weather, and was rated at 5.8 kW. Huber later developed the 'Schwing Calor' air-heater for the heating of temporary shelters and, more recently, a continuous-flow water heater (Figure 1.3) in conjunction with the Junkers Company. This unit comprised a pair of twc-orifice pulsating combustors coupled at their inlet ends. Each chamber (Figure 1.4) worked alternately; the fuel was drawn from a common chamber into a mixing tube, and the resultant mixture passed into the combustion chamber via a funnel and burned explosively. The combustion-driven oscillations occurred first in one chamber and then the other, and most of the hot gases were expelled through the heat exchangers at the end of the combustion chambers into the pulsation tubes. A small proportion of the hot gases were forced back through the mixing tube, due to the relatively low resistance to flow in the inlet tubes; these were connected to restrict this back-flow. The operating frequency of the heater was 130 Hz on town gas, and 122 Hz

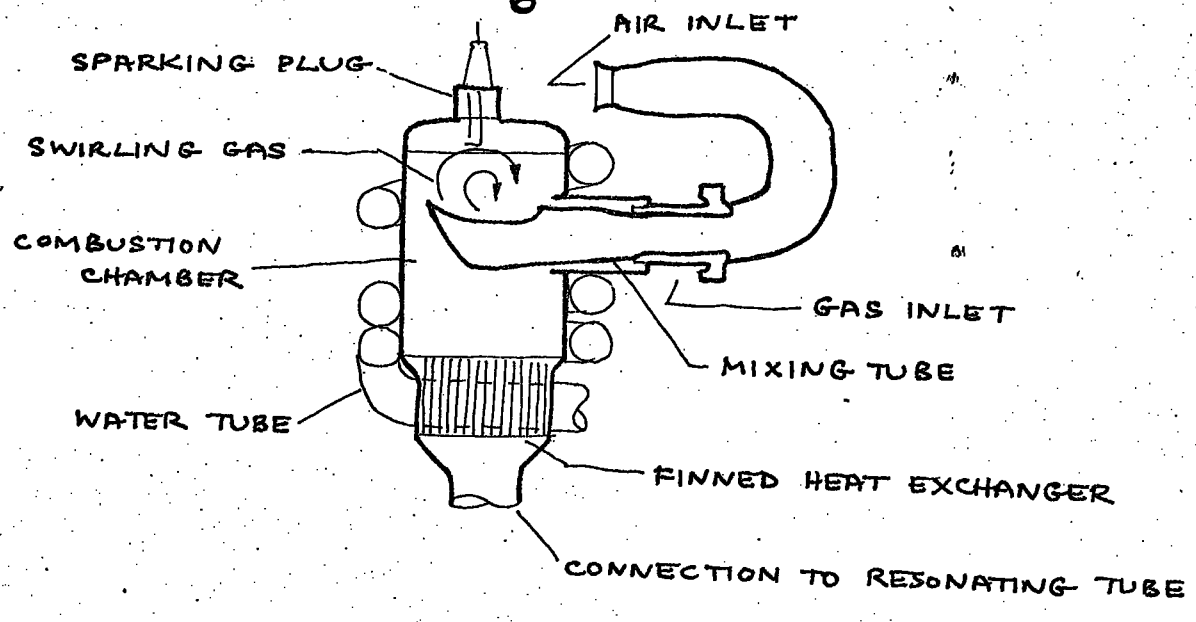

FIGURE 1.4 : HUBER COMBUSTION CHAMBER

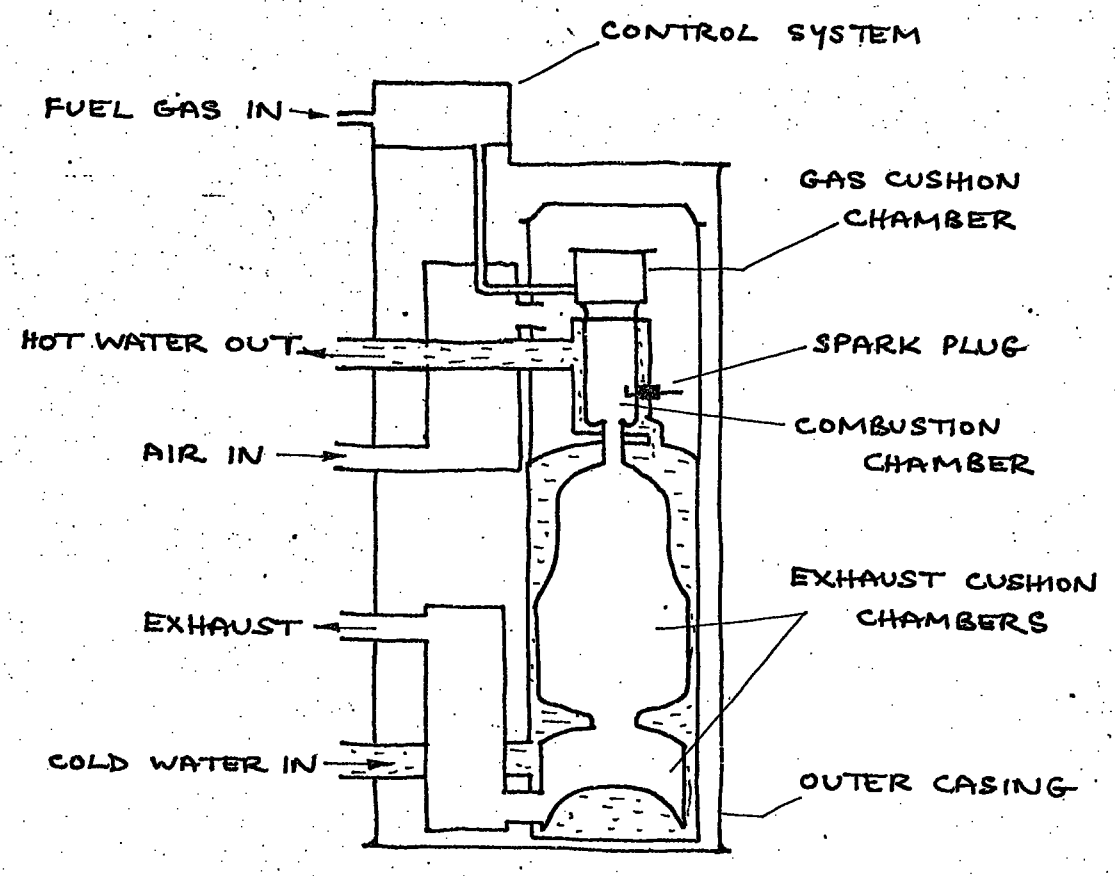

FIGURE 1.5 : PULSAMATIC WATER HEATER

with propane, due to the different temperature profile, and it was rated at 23.2 kW.

Another commercial application of pulsating combustion has been to central heating. The 'Pulsamatic' (see Figure 1.5) was developed in Canada and was rated at 30 kW. This boiler was investigated by Alebon et al (15) with a view to improving the method of silencing. They found that the volumetric combustion rate was 44.5 MW/m^3 at an operating frequency of 70 Hz, the overall rate of heat transfer was 58.6 kW/m^2, and an exhaust gas analysis gave 8.56% CO_2, 3.06% O_2 and 0.0% CO. The overall thermal efficiency of the unit varied between 87% and 93% and the water outlet temperature varied between 32°C and 95°C. The authors managed to reduce the noise output from the device from 107 dB to 68 dB. A notable feature was that physically it was smaller than designs for steady combustion of a similar rating. However, it was noted by Bottoms (16) that the CO content in the exhaust gases increased when the unit was operated at less than its maximum rating.

In 1963 Francis et al (17) reported a preliminary study by the Gas Council on pulsating combustors to assess their use in industry, particularly for heating water and air. Two types of combustor were examined - 'Schmidt' and 'Helmholtz' (see Figure 1.6) - were examined for quality of combustion, thermal efficiency and stability of operation. The dimensions of these units were typically of 50-75 mm. internal diameter and between 2.1 m and 3.3 m long, and were fired by natural gas; both aerodynamic and mechanical values were studied for their effect on performance. The authors concluded that the combustion in their devices was efficient, provided that ;

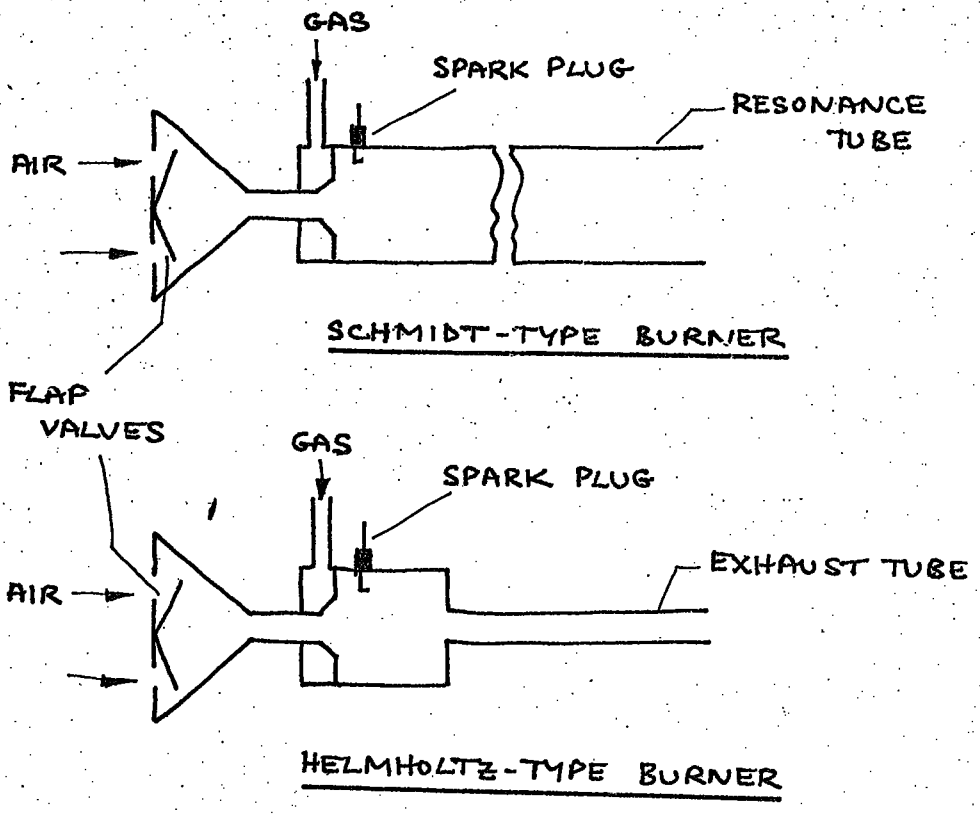

FIGURE 1.6 : FRANCIS BURNER CLASSIFICATION

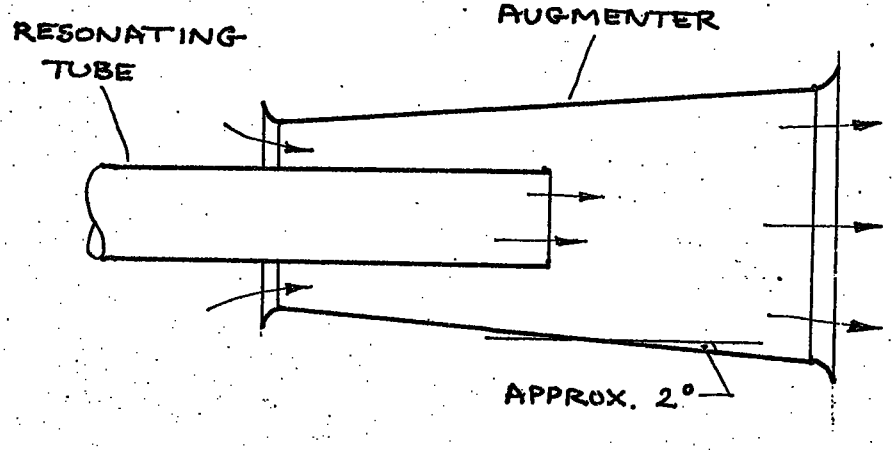

FIGURE 1.7 : MULLER AUGMENTER

a) multiple gas jets were used to achieve a uniform air/fuel mixture;

b) the fuel flowrate was not excessive;

c) the combustors were 'well-tuned'.

The authors found that extending the exhaust tube of the combustor moved the pressure anti-node of the acoustic oscillation away from the flame, thus adversely affecting the stability of the oscillation. This observation was explained by the criterion of Rayleigh (18). Their correlation between this expression and experiment was not conclusive, and it was recommended that more attention should be paid to the effect of the inlet valve section on combustor frequency and to the effect of axial temperature gradients on exhaust pipe frequency.

Further work by the Gas Council has been reported by Reay (20). It was found that the thermal efficiencies of the combustors ranged between 70% and 80%, and the noise levels of 125 dB from the unsilenced state could be reduced to approximately 80 dB using Burgess 'straight-through' absorption silencers. It was also found that the thermal efficiencies under pulsating flow conditions were from 30% to 50% higher than those predicted theoretically for steady flow. The equation used by Reay for this comparison assumed that the heat transfer in the combustors was predominantly convective, and it is possible that neglecting radiation led to slightly low values of the steady combustion efficiency. It was observed that no fully satisfactory design procedure for these units had yet been evolved and that the effect of the many parameters on combustion stability was not clear.

In 1967 Muller (19) reported the development of a resonant combustion heater for drying applications. Simple acoustic theory was used to design two combustors, one of the Helmholtz type and the other

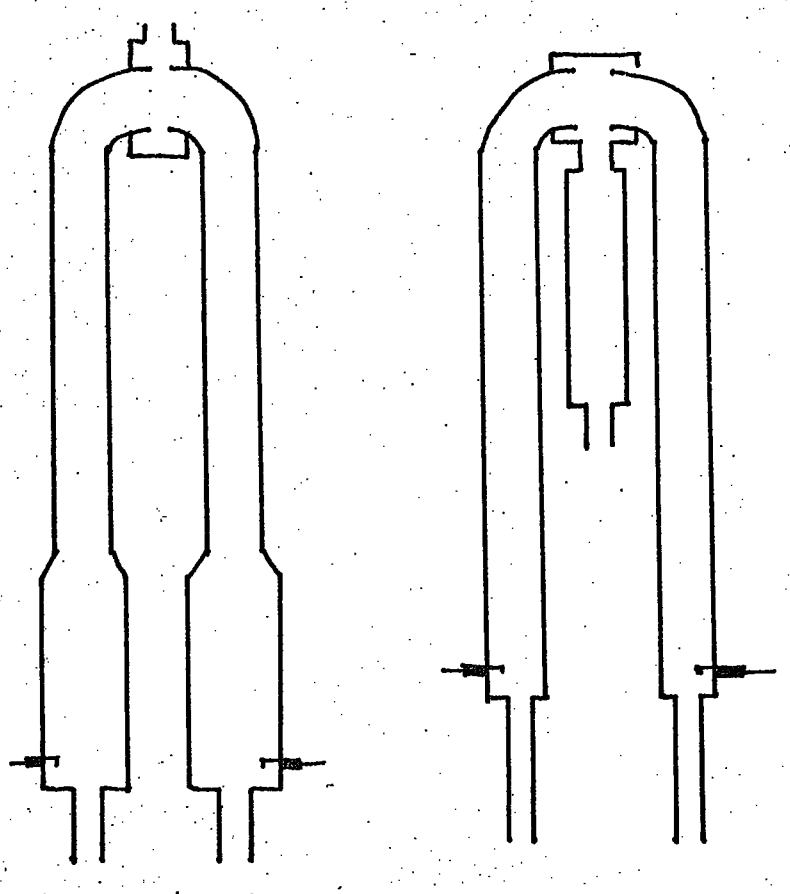

HELMHOLTZ UNITS

SCHMIDT TUBES

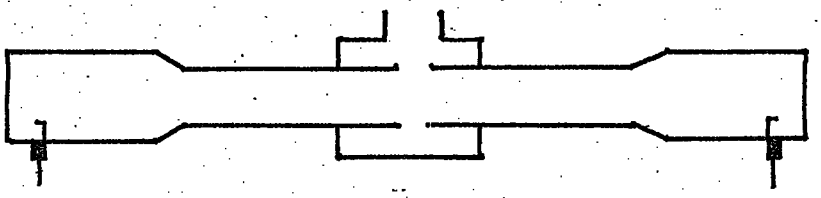

HELMHOLTZ UNITS WITH TANGENTIAL INJECTION

FIGURE 1.8 : BRIFFA BURNER CONFIGURATIONS

of a mixture of Helmholtz and Schmidt types. Both units developed approximately 90 kW of LPG; the volumetric combustion rate of the first was 71 MW/m^3 at a frequency of 153 Hz (estimated), and that of the second was 150 MW/m^3 at a frequency of 210 Hz. Muller made use of augmenters (see Figure 1.7) to increase the quantity of air pumped by his combustors, and noted that the length of the augmenter had an important influence on performance and had to be such that its natural frequency was some multiple of the combustor frequency.

In 1971 Briffa et al. (21) reported work on both Schmidt and Helmholtz type combustors (Figure 1.8) which were fuelled by a mixture of methane and air injected into short inlet tubes. The aims of the study were to examine methods of noise suppression. It was concluded that some reduction in noise was obtained by coupling the exhausts of two identical pulsating combustors and that reductions of up to 30 dB were attained when the coupled units operated in opposed phase and produced identical pressure waveforms. It was also noted that the Schmidt combustors gave a smoother and more sinusoidal pressure wave than the Helmholtx combustors and were thus more suitable for the method of anti-phase silencing.

1.2 Pulsating combustors in steam generating plant

In 1948 Reynst (22) advocated the use of pulsating combustion in boiler furnaces fired by pulverized solid fuels to increase the volumetric combustion rate. This idea was pursued by Sommers 1954 (23) who reported the conversion of a tube boiler to pulsating combustion. Preliminary experiments were undertaken on a double-orifice combustor fitted with a mechanical valve. It was found that, when the combustor was water-cooled, it would operate only with an

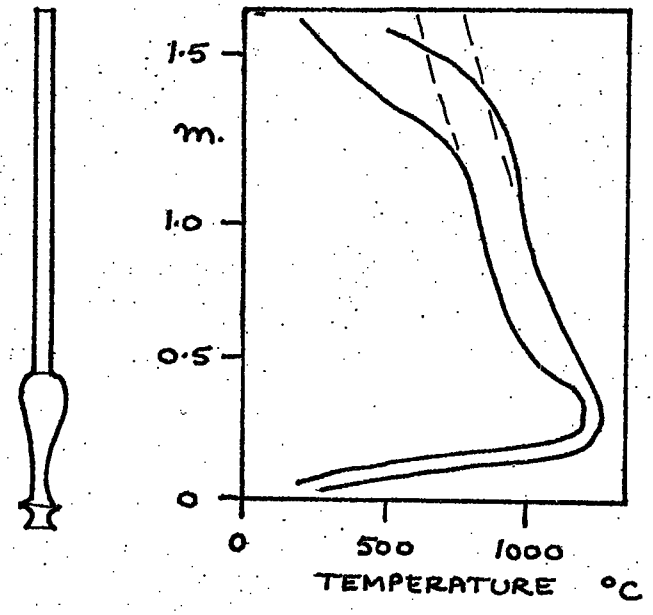

FIGURE 1.9 : GAS TEMPERATURE DISTRIBUTION IN PULSATING COMBUSTOR

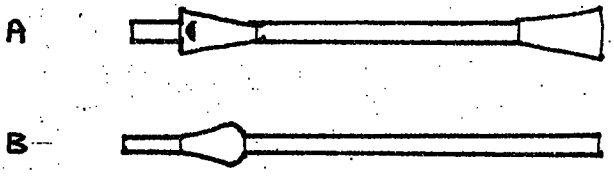

FIGURE 1.10 : TYPICAL PULSATING COMBUSTOR FORMS :

A : GOOD ASPIRATION

B : GOOD COMBUSTION

approximately stoichiometric mixture, whereas, when the combustor was either uncooled or lagged and supplied with pre-heated air, the mixture ratio could be varied widely. It was noted that the combustion-driven oscillations ceased when the maximum temperature in the combustion chamber fell below 1200°C. Sommers estimated that the amplitude of the oscillations was approximately 0.65m by extrapolating the slope of the temperature distributions (Figure 1.9) in the combustor towards the open end.

Sommers carried out a study of the effect of tube shape and type of inlet valve on the intensity of pulsation, and a wide range of configurations were tested. The results for the work on aerodynamic valves, are summarized in Figure 1.10. Configuration A was found to present the most resistance to back-flow through the inlet valve and to inflow at the exhaust end; whereas configuration B proved to be the best shape for complete combustion, particularly if the combustion chamber was maintained at a high temperature.

Sommers finally installed a double-orifice combustor, developed from the earlier work, in a tube boiler (see Figure 1.11). The maximum volumetric combustion rate attained was 21MW/m^3 at a coal consumption rate of 1900kg/h and an operating frequency of 35Hz. The volumetric combustion rate was estimated to be several times that of a contemporary cyclone burner. Sommers concluded that attention to the design of both the aerodynamic valve and the pulsating tube would improve performance.

In 1965 Babkin (24) reported a project similar to that of Sommers. The investigation into pulsating combustion had been undertaken in 1958 with the purpose of intensifying combustion and heat transfer in the furnaces of steam boilers. A preliminary study was made of the

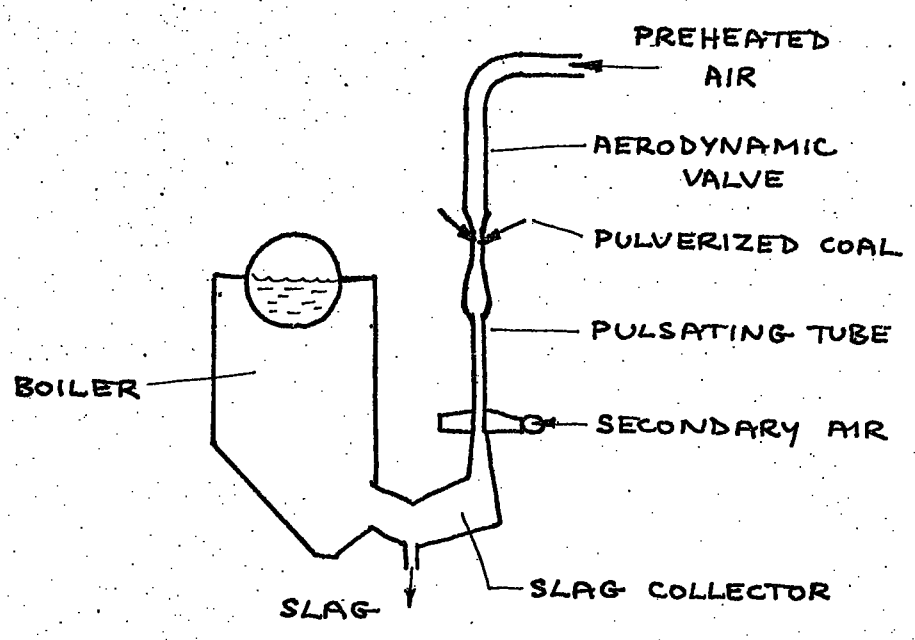

FIGURE 1.11 : SHAMROCK TEST PLANT

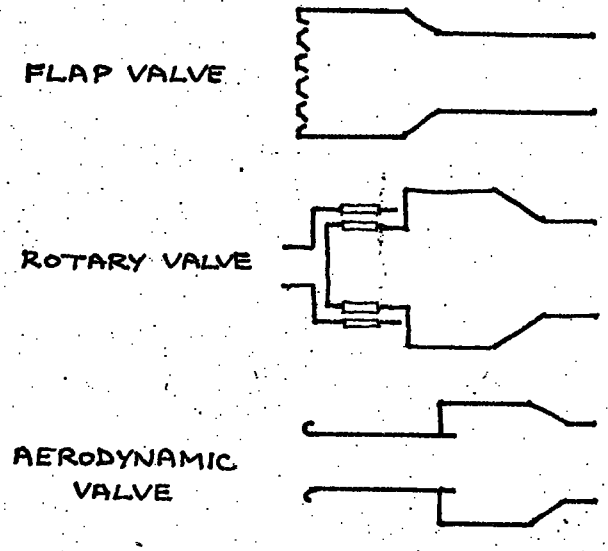

FIGURE 1.12 : MECHANICAL AND AERODYNAMIC VALVES

two types of valve - mechanical (flap and rotary) and aerodynamic (see Figure 1.12). Tests showed that intense pulsating combustion and self-aspiration were easily obtained in chambers fitted with flap valves but these suffered from fatigue failure. Rotary valves were tested but they were found to be impractical for chambers of more than 15 MW. rating. Aerodynamic valves were then studied, and it was found that:

a) the ability of the pulsating combustion chamber to self-aspirate was sharply diminished when air preheat was introduced;

b) the pressure amplitude of the oscillations increased when the inlet pipe length was increased, but, beyond a critical length, the oscillations would break down;

c) the oscillations ceased if the aerodynamic valve was connected to any inlet duct, even of much greater cross-section.

The design of the aerodynamic valve used in the investigation is shown in Figure 1.13; it consisted of a hemi-spherical stabilizer, telescopic connecting piece through which the fuel oil was fed, and turoidal shield. It was found that combustion of heavy fuel oils was particularly efficient in chambers fitted with such a valve which did not completely prevent back-flow and thus permitted a certain amplitude of flame movement in the region of the fuel injector. In 1960 a double-tube counter-phase pulsating combustion unit was installed in a steam boiler (see Figure 1.14 and A in Table 1.A). On the basis of measurements taken from this apparatus, a further unit was designed and installed in another boiler (see Figure 1.15 and B in Table 1.A) in 1963. Both furnaces were fired by fuel oil. It is apparent from Table 1.A that the volumetric combustion rate of B was less than half that of A.

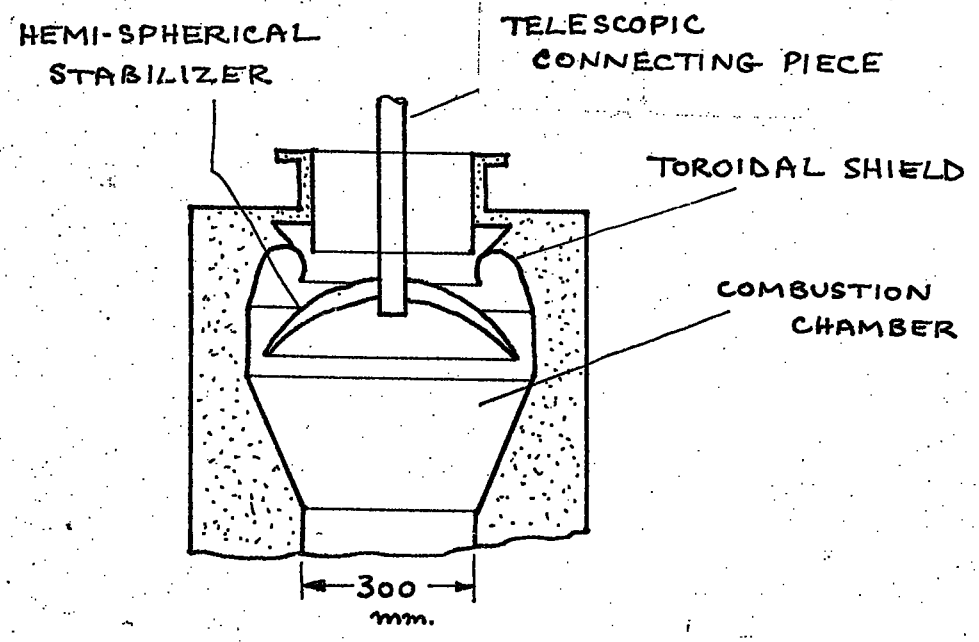

FIGURE 1.13 : AERODYNAMIC VALVE OF BABKIN

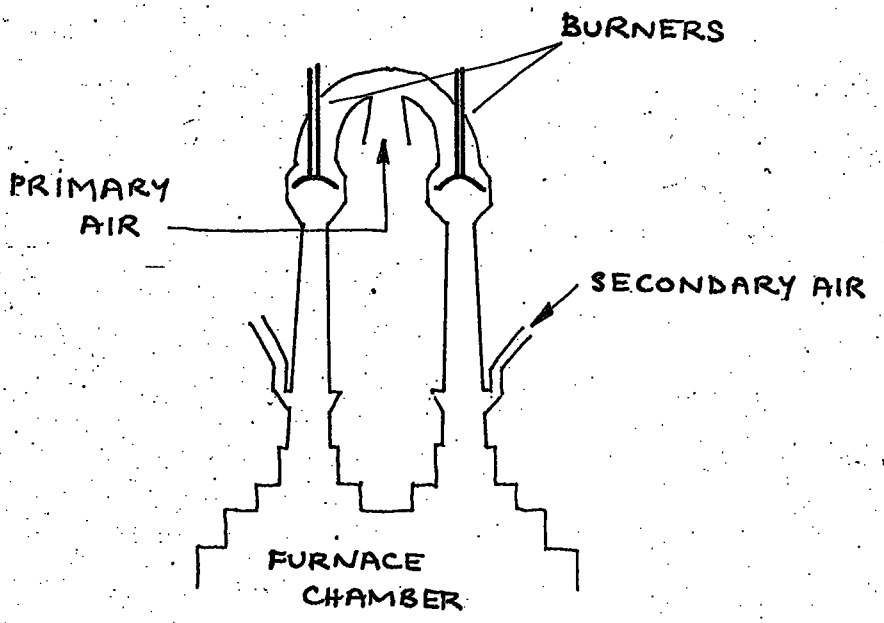

FIGURE 1.14 : COUNTER-PHASE PULSATING COMBUSTER

FIGURE 1.15 : FURNACE INSTALLATION

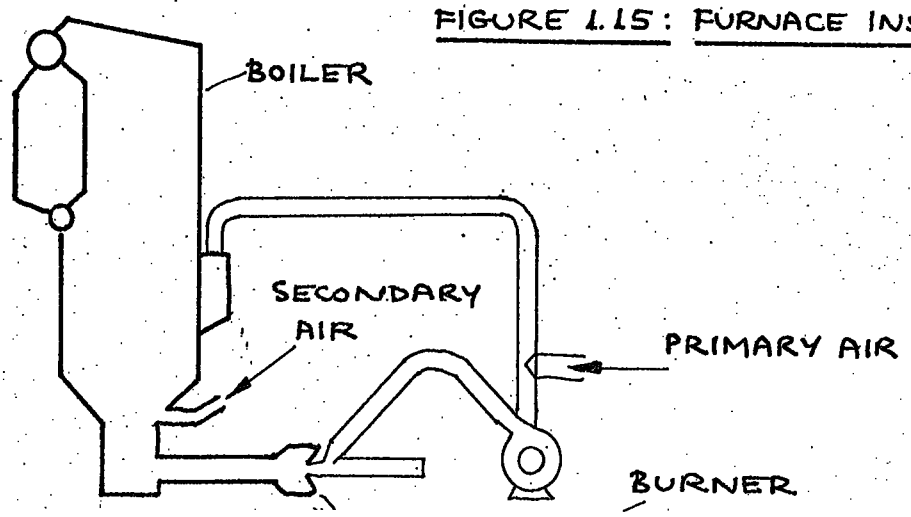

Table 1.A Furnaces of Babkin

PULSATING COMBUSTION FURNACE	A	B	
Total rate of oil consumption	1500	4200	kg/h
Frequency of oscillations	68	31	Hz
Pressure amplitude of oscillations	30	15	kN/m^2
Volumetric combustion rate	18.6	7.2	MW/m^3

In 1968 Hanby and Brown (25) reported an investigation into a pulsating combustor fired by pulverized coal. A full-scale perspex model of the combustor design was used to study the effect of various designs of fuel injectors on the mixing process. The flows of air through the inlet pipe and of fuel through the injectors were modelled by water and by chemical tracer respectively. The quality of the injection process was then assessed by sampling the mixture at a number of points in the combustor model. The final design (Figure 1.16), which was similar to that of Sommers, was constructed in steel, the combustion chamber and first part of the exhaust tube being lined with refractory material. It was found that the volumetric combustion rate was 8.3 MW/m^3 on a coal consumption of 23 kg/h. at an operation frequency of 75 Hz., and the gas temperature distribution in the combustor is shown in Figure 1.17. It is interesting to note that the sharp change in gas temperature gradient observed by Sommers near the open end of his early combustor (see Figure 1.9) is not evident here. The combustor of Sommers operated at pressure amplitudes up to 100 kN/m^2 while that of Hanby and Brown attained a maximum of 12.5 kN/m^2.

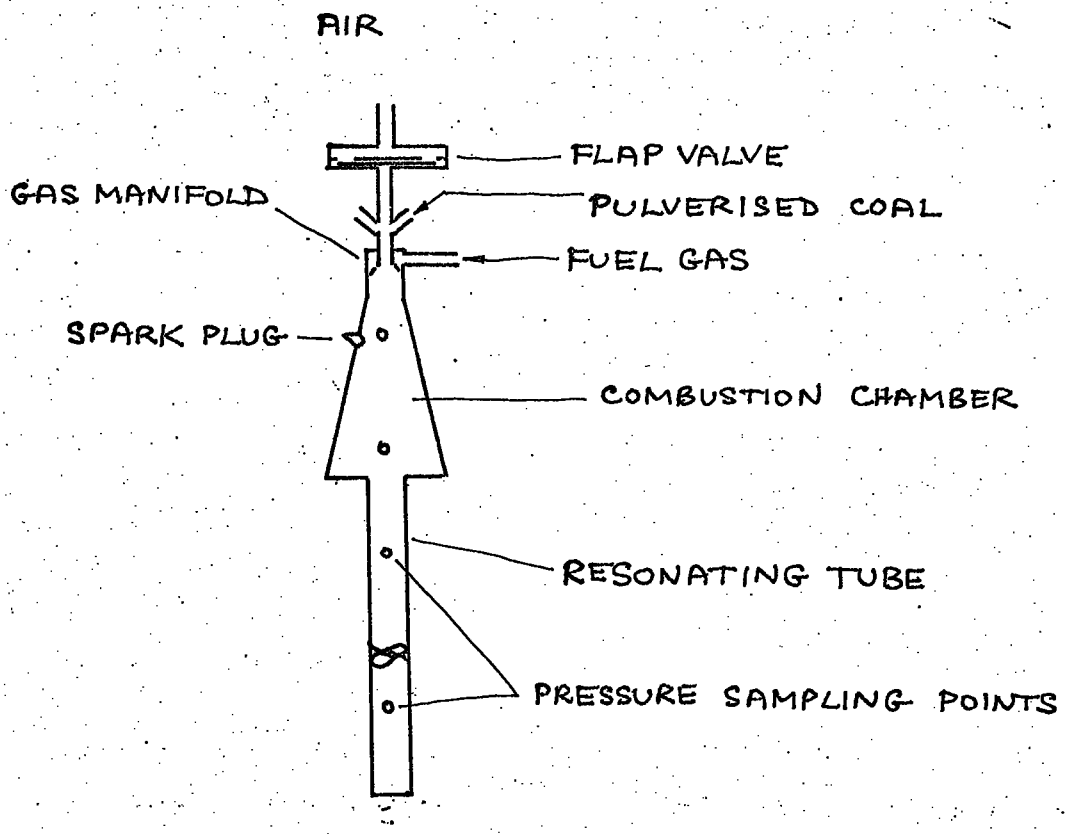

FIGURE 1.16: PULSATING COMBUSTOR OF HANBY & BROWN

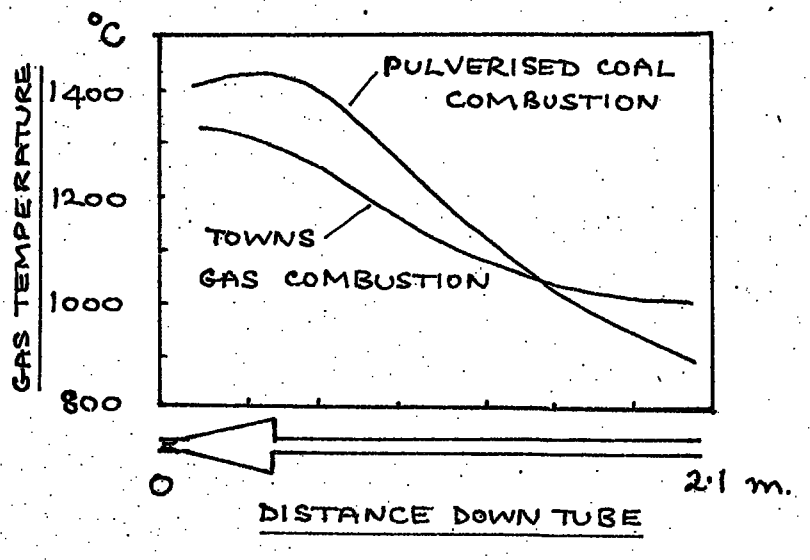

FIGURE 1.17: GAS TEMPERATURE DISTRIBUTION

Therefore the reverse flow of cool air up the exhaust tube occurred to a far greater extent in the combustor of Sommers than in that of Hanby and Brown, and this perhaps explains the difference in shape of the gas temperature distributions in the two combustors. Hanby and Brown finally measured a noise level of 80 dB. near their furnace and concluded that considerable work on this aspect of pulsating combustion was necessary before an industrial use of the process could be envisaged.

1.3 Heat transfer in unsteady flow

The subject of heat transfer in unsteady flow has received considerable attention since the work of Martinelli and Boelter (26) in 1938. They found that the rate of heat transfer increased with increasing amplitude of vibration beyond a critical value of Reynolds number of approximately 1000.

In 1943 Martinelli et al. (27) measured heat transfer between condensing steam and water flowing in a vertical concentric-tube heat exchanger. The data for the heat transfer coefficients in steady flow were obtained using a centrifugal pump, and those for periodic flow, using a reciprocating pump.

The oscillating flow was not strictly sinusoinal. Keeping the stroke of the reciprocating pump constant and varying the rotational speed, N, in the range 13 N 265 r.p.m., enabled the periodic heat transfer to be examined over the range of frequency, f, $0.22 < f < 44.2$ Hz. and over 'the periodic Reynolds number', Re, range of $2660 < Re < 77300$. The experiments showed that frequency per se had little effect on Nuselt number and that the velocity emplitude was the main parameter. The results were correlated by the quasi-steady-state method (see

Section 2.4.2), previously used by Schultz-Grunow (28) and Estel (29).

In 1959 Jackson et al. (30) reported an experimental study of the effect of acoustic vibrations on the heat transfer of air flowing through a vertical brass tube, 95 mm. internal diameter by 1.5 m. long. The wall temperature of the tube was maintained at a constant temperature by the condensation of saturated steam at atmospheric pressure onto its outer surface. Heat transfer coefficients were deduced from the quantity of condensate collected by ten collecting cups, equally spaced down the tube. The working fluid, air, was passed through the test section from a plenum chamber by a centrifugal fan and was excited by a horn at the lower end of the tube, the sound pressure level being measured at the mouth of the tube in the plenum chamber. Results were presented for Reynolds number of 2300 over a range of sound pressure level, $108 < SPL < 138$ dB., at a frequency of 520 Hz., the third harmonic of the tube under the experimental conditions. It was found that the sound pressure level had little effect upon the heat transfer up to 118 dB., above which the effect was quite marked. This is evident from Figure 1.18, where the distribution of the ratio:

$$\frac{\overline{Nu}_p}{Nu} = \frac{\text{time-averaged Nusselt number in pulsating flow}}{\text{steady state Nusselt number}}$$

against axial displacement has been replotted for two sound pressure levels, 118 dB. and 129 dB., from the data of Jackson. The ratio $\frac{\overline{Nu}_p}{Nu}$ rises to a maximum of 1.8 at $x/L = 0.3$, corresponding to the position of a velocity antinode, and thereafter diminishes approximately linearly, the overall effect being one of an improvement in the heat

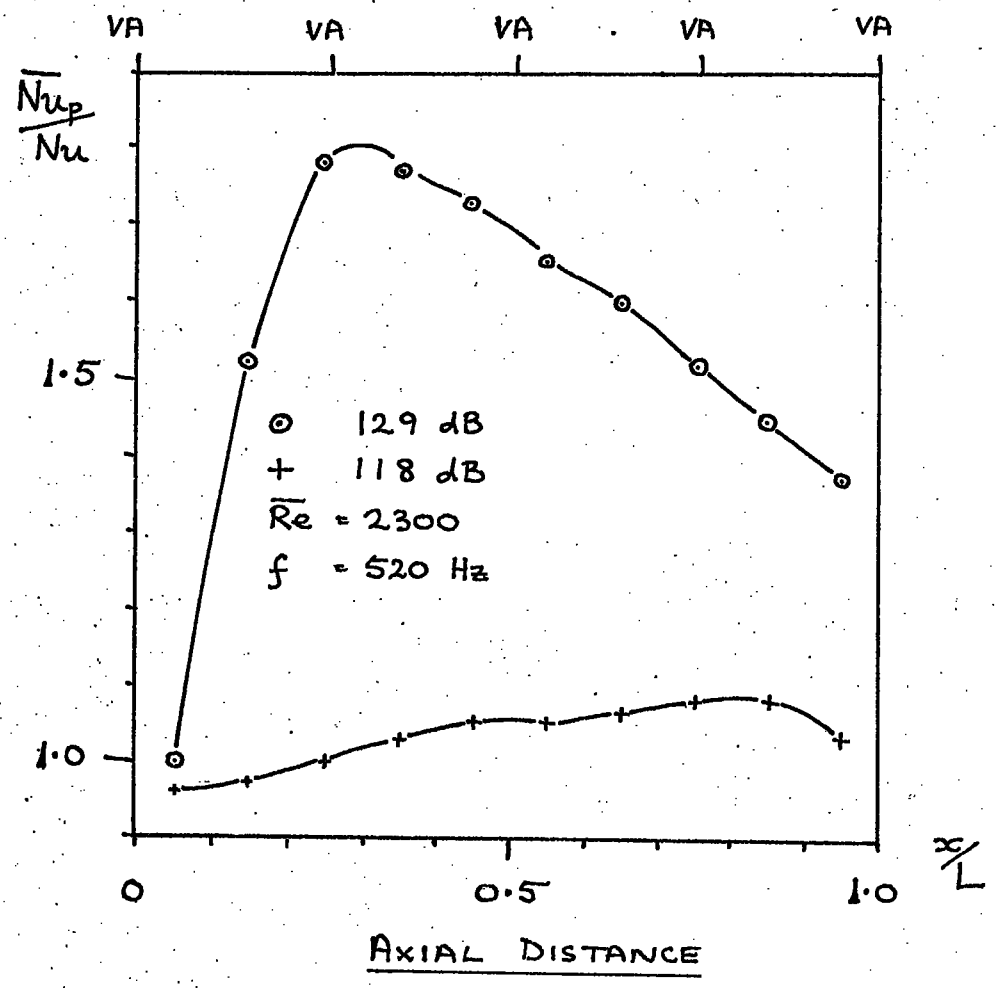

FIGURE 1.18 : GRAPH OF NUSSELT NUMBER RATIO AGAINST DISTANCE FROM DATA OF JACKSON ET AL

transfer. The authors sought a relationship between the Nusselt number at any cross-section of the tube and the sound pressure level, as measured by the microphone, and gave:

$$\overline{Nu}_{px} = 2{\cdot}52 \left\{ \frac{\exp(SPL/69{\cdot}5)}{(\overline{Re})^{0{\cdot}25}} \right\} \sqrt{Gz_x} \qquad 1.3.1$$

which was claimed to be valid within ± 25% for SPL > 118 dB. Using further data for resonant frequencies of 125, 250 and 2000 Hz. obtained under otherwise similar conditions, a further empirical relationship, incorporating a frequency term, was given:

$$\overline{Nu}_{px} = 5{\cdot}7 \left\{ \frac{\exp(SPL/69{\cdot}5)}{(\overline{Re})^{0{\cdot}25} f} \right\} \sqrt{Gz_x} \qquad 1.3.2$$

which was valid within ± 16% if the data for 125 Hz. were ignored. The authors concluded that it was difficult to separate the effect of frequency upon heat transfer from that of sound pressure level, an observation also made by Martinelli.

In 1961 Zartmann and Churchill (31) reported an investigation into the effect of combustion-driven oscillations on the local heat transfer coefficients in a water-cooled cylindrical burner, 125 mm. internal diameter and 0.68 m. long. Preliminary studies (32) had shown that intense longitudinal and transverse oscillations could be attained in such a tube over the range of flow, Re = 5000 to 20000. The frequency of the longitudinal oscillations in the water-cooled burner was found to be 350 Hz, and that of the transverse oscillations to be 4000 Hz. The combustion was stabilized by a bluff-body flame-holder, upstream of which was sited a microphone to measure the sound pressure level.

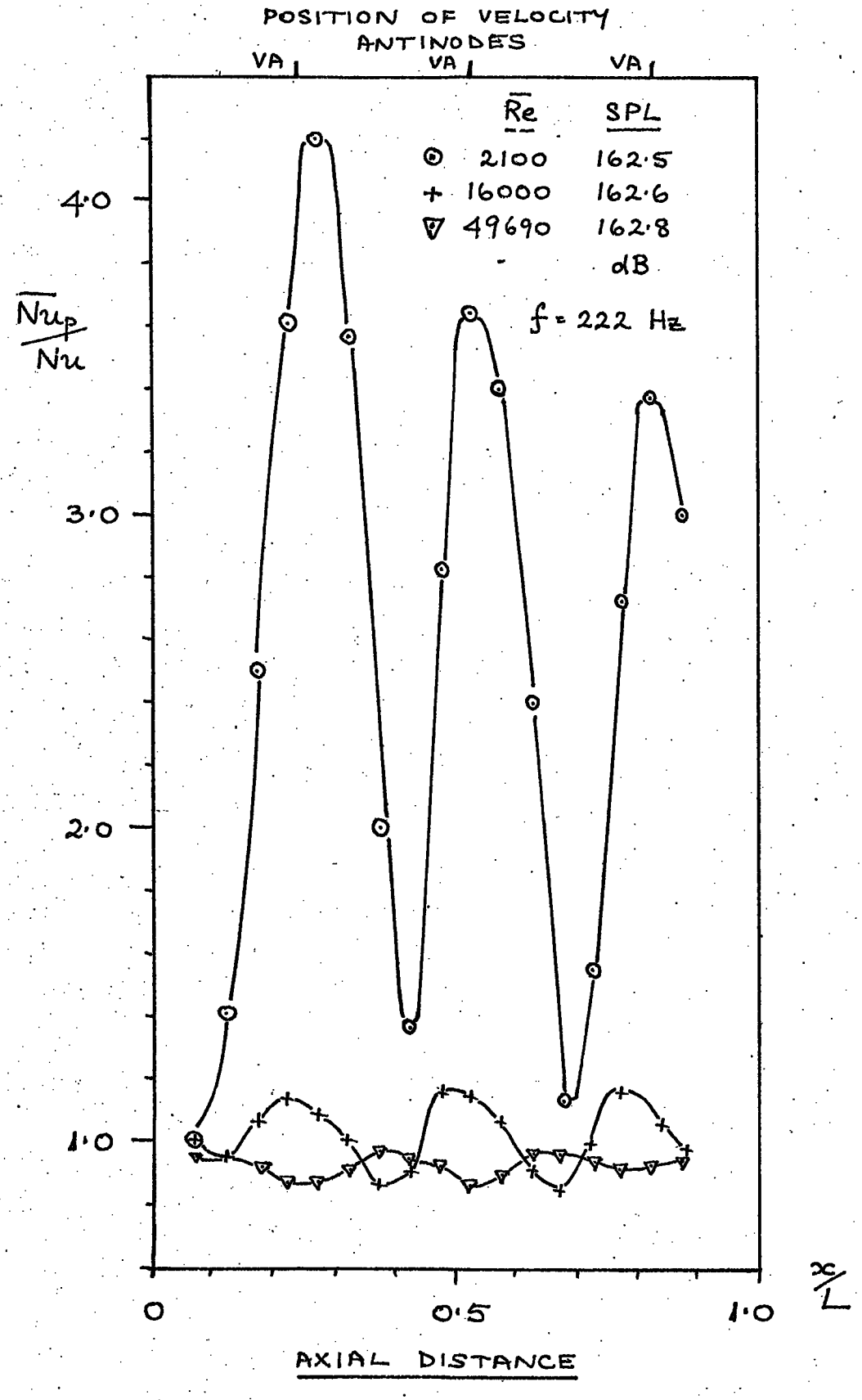

FIGURE 1.19 : GRAPH OF NUSSELT NUMBER RATIO AGAINST DISTANCE FROM JACKSON & PURDY

This was found to be 130 dB. in the absence of oscillations, and to vary from 148 to 155 dB with oscillations. From measurements of the local heat transfer coefficient with and without oscillations, the authors obtained a linear correlation between $\overline{Nu}_p$ and $\hat{p}$ of the form:

$$\frac{\overline{Nu}_p}{Nu} = A \frac{\hat{p}}{\bar{p}} + B$$

where A and B are constants. This result was consistent with that of Harrje (33) who also observed a linear increase in forced convection heat transfer with pressure amplitude.

In 1965 Jackson and Purdy (34) reported a study of the performance of a simple convective heat exchanger under the influence of acoustic oscillations. The apparatus was similarly constructed to that of (30), except that it was sited horizontally. Air was passed through a copper tube, 98 mm. internal diameter by 3.0 m. long, the walls of which were maintained at a constant temperature. The sound field was introduced by a horn placed at the exit of the tube, and the sound pressure level could be measured at any cross-section by a microphone mounted on a rod inserted into the tube from the upstream end. Heat transfer coefficients were deduced from the quantity of condensate cooled over lengths of 153 mm., and the range of experimental conditions was $2000 < Re < 200{,}000$ and $0 < SPL < 163$ dB. Results were presented for Re = 2100, 16,000 and 49,690 for the sound pressure level range of 152 to 163 dB., and three of the tests have been replotted in Figure 1.19, which again shows the variation of the ratio $\frac{\overline{Nu}_p}{Nu}$ with axial displacement, x/L. It is evident from the graph that, except for Re = 49,690, the maximum values of $\frac{\overline{Nu}_p}{Nu}$ occur at the velocity antinodes,

that the maxima of $\frac{\overline{Nu_p}}{Nu}$ for Re = 2100 decrease along the tube, and that the effect of the oscillations at Re = 16000 and 49,690 is considerably less than at Re = 2100. The authors correlated the ratio $\frac{\overline{Nu_p}}{Nu}$ with axial position in the tube using the relationships given in Table 1.B.

Table 1.B Correlations of Jackson and Purdy

$\overline{Re}$	$\frac{\overline{Nu_p}}{Nu}$
2100	$\left[1 + \frac{A_3}{Pr^{0.167}}\left(\frac{\lambda}{\nu}\right)\frac{\hat{u}^2}{\bar{u}}\cos^2\left(\frac{2\pi x}{\lambda}\right)\cos^2(\omega t)\right]^{0.4}$
16000	$A_2\left(\frac{\hat{u}}{\bar{u}}\right)^{0.8}\left[1 + \cos\left(\frac{4\pi x}{\lambda}\right)\right]^{0.4}$
49690	$1 - A_1\left(\frac{\hat{u}}{\bar{u}}\right)^2\left\{1 + \cos\left(\frac{4\pi x}{\lambda}\right)\right\}$
	where A_1 A_2 A_3 are constants.

It is interesting to note that, apart from the transcendental terms, the ratio $\frac{\hat{u}}{\bar{u}}$ occurs in each equation. This ratio signifies

$$\frac{\text{velocity amplitude of the oscillation}}{\text{mean flow velocity}}$$

at any cross-section of the tube, and, for an acoustic oscillation in an isothermal gas, varies sinusiodally in amplitude along the tube. From the information provided in the paper, the values of $\frac{\hat{u}}{\bar{u}}$ at the velocity antinodes have been calculated and are given in Table 1.C., together with the corresponding mean values of $\frac{\overline{Nu_p}}{Nu}$.

Table 1.C Calculated $\hat{u}/\bar{u}$ from Jackson and Purdy

$\bar{Re}$	$\overline{Nu}_p / Nu$	$\hat{u}/\bar{u}$
2100	3.74	26.3
16000	1.16	3.5
49690	0.87	1.1

Table 1.C has been plotted in Figure 1.20 and may be seen to be approximately linear, although it is unfortunate that there is a lack of data in the range $6 < \hat{u}/\bar{u} < 22$. The equation of the line is:

$$\frac{\overline{Nu}_p}{Nu} = 0.72 + 0.114 \frac{\hat{u}}{\bar{u}} \qquad 1.3.3$$

It may be concluded tentatively from these estimates that, at any cross-section of the tube, the heat transfer coefficient is linearly dependent on the dimensionless velocity amplitude. In this paper, Jackson and Purdy regarded the flow of air through the tube at Re = 2100 as laminar, which is a questionable assumption. The transition from the laminar to the turbulent regime has been studied by Miller and Fejer (35) who examined the flow of air over a flat plate under the influence of oscillations produced by a set of rotating butterfly valves. The frequency of the oscillations could be varied from 4 to 125 Hz., and the range of dimensionless velocity amplitude was $0.585 < \hat{u}/\bar{u} < 0.667$. The value of the transitional Reynolds number was found to be 954,000 under steady flow conditions but, under the influence of the oscillations, it varied from only 350,000 to 200,000 and was independent of frequency.

FIGURE 1.20: GRAPH OF NUSSELT NUMBER RATIO AGAINST VELOCITY AMPLITUDE RATIO FROM DATA OF JACKSON & PURDY

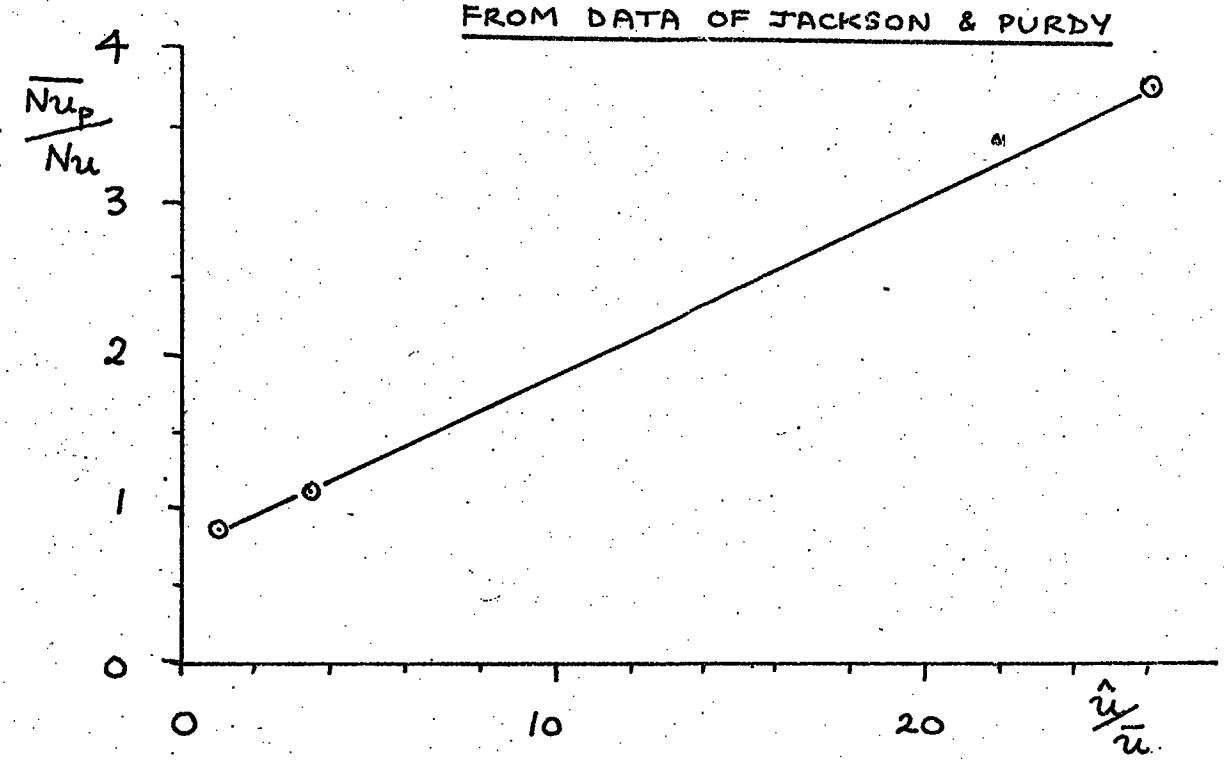

FIGURE 1.21: GRAPH OF NUSSELT NUMBER RATIO AGAINST DISTANCE FROM KOSHKIN

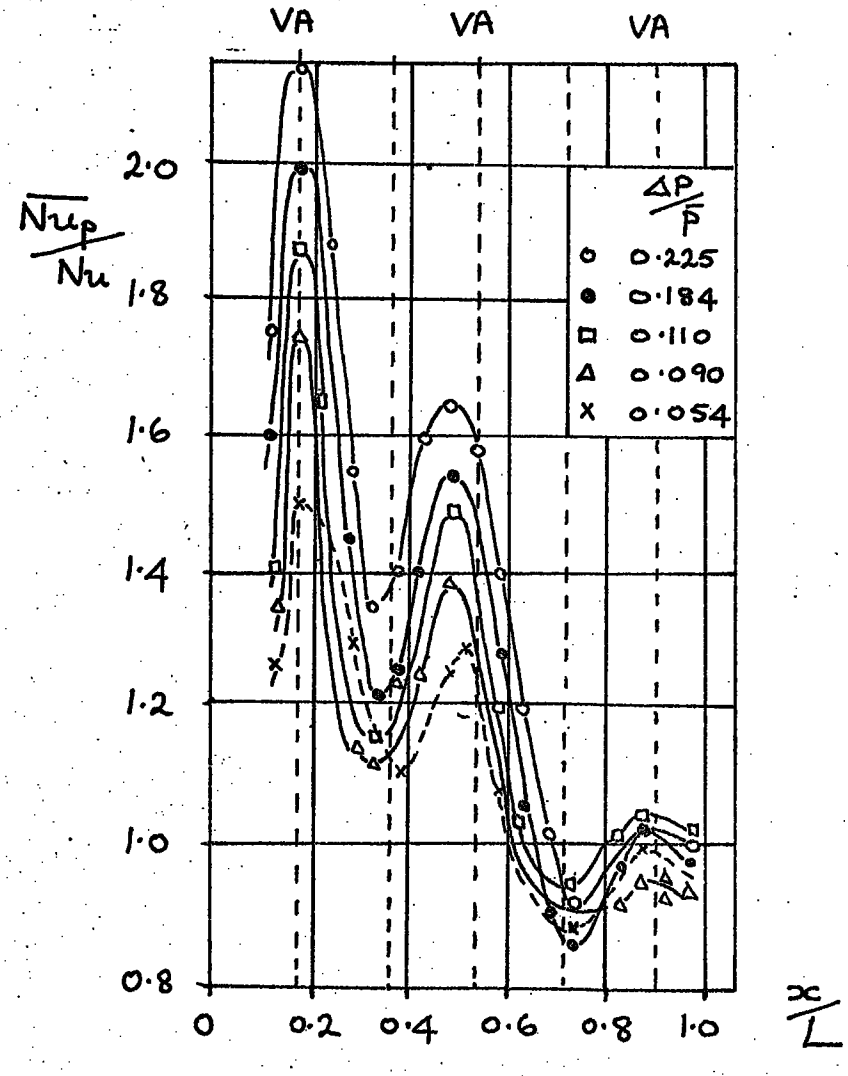

These results are not directly applicable to flow through tubes, as the Reynolds numbers are based on length, but the work indicates that the onset of transition is advanced by macroscopic oscillations in a flow and that the transitional Reynolds number decreased with increasing dimensionless velocity amplitude. In 1964 Purdy et al. (36) reported a theoretical examination of the effect of oscillations on laminar flow and supported their hypothesis of 'standing vortices' with a visualization study, using a smoke-filled transparent tube. It is notable that, in these experiments, the flow did not exceed a Reynolds number of 478. Furthermore, Martinelli and Boelter (26) observed that the rate of heat transfer increased with increasing velocity amplitude only when a Reynolds number of 1000 was exceeded. This worker feels that, for moderate values of Reynolds number and of dimensionless velocity amplitude, an approximate estimate of the transition from the laminar to the turbulent regime in oscillating flow through a tube may be gained by consideration of the instantaneous Reynolds number; if, at any instant during the cycle of oscillation, the instantaneous Reynolds number approaches 2000, then the flow may be regarded as on the point of transition.

In 1966 Koshkin et al. (37) reported a study of time-averaged heat transfer rates in an acoustically-closed tube for a wide range of experimental conditions. The apparatus consisted of a stainless steel tube, 5.4 mm. internal diameter by 1.2 mm. long, which was heated by passing low voltage alternating current through its length. Ambient air was passed through the tube at pressures between 5 to 20 bar for Reynolds numbers of 10,000 and 100,000 and was excited by a rotating valve at the resonant frequencies of the tube, 90, 180, 270

360 and 450 Hz. The pressure amplitude was expressed as a fraction of the working pressure, and the range studied was $0.01 < \frac{\Delta P}{\bar{P}} < 0.25$. The flow was claimed to be hydrodynamically developed at the entrance to the test section. The results of the work showed that the maxima of $\frac{\overline{Nu}_p}{Nu}$ occurred at the velocity antinodes, as is evident in Figure 1.21. For this range of Reynolds numbers, the evidence conflicts with that of Jackson and Purdy (Figure 1.19), although the frequencies of the two sets of data, 270 and 222 Hz. respectively, are not dissimilar. It is possible that the ratio $\hat{u}/\bar{u}$ in the work of Koshkin et al was far greater than in the case of Jackson (see Table 1.C) but, due to the method of presentation of the experimental conditions, the values of $\hat{u}/\bar{u}$ in the Russian work remain obscure and further comparison is of dubious value. Koshkin et al. made an analysis of the effects of the oscillations on heat transfer in their apparatus and proposed that the ratio $\frac{\overline{Nu}_p}{Nu}$ was proportional to $\hat{E}/\bar{E}$, given by:

$$\frac{\hat{E}}{\bar{E}} = \frac{\text{amplitude of kinetic energy in oscillation}}{\text{mean kinetic energy of flow}}$$

The analysis took into account energy dissipation down the tube and also considered the non-isothermal effects in the flow. Due to the temperature gradient in the tube, the velocity of sound was regarded as a function of axial distance, and thus mean velocity of sound was given by:

$$\bar{c}_x = \frac{1}{x} \int_0^x c(x)\, dx \qquad 1.3.4$$

It was concluded that for any value of $\frac{\Delta P}{\bar{P}}$ the distribution of $\frac{\overline{Nu_p}}{Nu}$ along the tube followed that of $\frac{\hat{E}}{\bar{E}}$ closely, but, due to the method used to normalize coefficients, again it is difficult to pursue the analyses further.

In 1967 Galitseysky et al. (38) reported a study of the effect of longitudinal oscillations on heat transfer in a tube when the driving frequency was displaced from resonance. The apparatus and experimental conditions were very similar to those of Koshkin (37) except that the tube diameter was 9.7 mm. and the frequency range 45 to 135 Hz. The experiments showed that the maximum value of $\frac{\overline{Nu_p}}{Nu}$ occurred at 90 Hz., the fundamental of the tube, and that at the extreme anti-resonant frequencies of 45 and 135 Hz., the heat transfer data compared closely with the steady state values. The authors made an analyses in this paper of the non-isothermal and dissipation effects in the tube. The velocity of sound, c, was, as before, regarded as a function of the axial co-ordinate, x, and, by introducing a change of variable, q_x, the acoustic wave equation was re-expressed:

$$\frac{\partial^2 \Delta(\rho u)}{\partial t^2} = \frac{\partial^2 \Delta(\rho u)}{\partial q_x^2} \qquad 1.3.5$$

where $$q_x = \int_0^x \frac{dx}{c(x)}$$

Then, by assuming a perfect gas, the distribution of $\frac{\hat{E}}{\bar{E}}$ in the tube was obtained:

$$\frac{\hat{E}}{\bar{E}} = \frac{1}{2\mu}\left(\frac{\Delta P}{\bar{P}}\right)^2_{max} \left\{\sin\left(n\pi \frac{q_x^*}{q_L^*}\right)\right\}^2 \qquad 1.3.6$$

where $\frac{q_x^*}{q_L^*}$ represented a further change of variable to permit the

analysis of resonant frequencies. This expression, 1.3.6, was expanded to the case of non-isothermal flow of a viscous gas by assuming that the kinetic energy of the oscillations attenuated exponentially along the tube:

$$\frac{\hat{E}}{\bar{E}} = \frac{1}{2\mu}\left(\frac{\Delta P}{\bar{P}}\right)^2_{max} \exp\left(-\phi_{AT}\frac{q^*_x}{q^*_L}\right)\left\{\sin\left(n\pi\frac{q^*_x}{q^*_L}\right)\right\}^2 \qquad 1.3.7$$

where ϕ_{AT} was the pulsation energy attenuation factor.

In 1968 Hanby (39) reported an experimental investigation of the effect of combustion-driven oscillations on convective heat transfer. The apparatus consisted of a stainless steel tube, 51 mm. internal diameter by 1.9 m. long, which was water cooled for most of its length. Propane and air were injected under pressure at one end of the tube, which, being thus constricted, behaved as an acoustically-closed end. Two water-cooled cylinders with adjustable pistons were attached to the main tube at the closed end, so that the amplitude of the oscillations could be controlled. The local heat transfer coefficients were measured directly at five points along the tube by means of a heat flux transducer. Results were obtained for Reynolds numbers of 6000 to 16,000, and, from the data provided, $\frac{\overline{Nu}_p}{Nu}$ has been plotted against x/L in Figure 1.22. It is evident that these results are in accord with those of Jackson and Purdy in Figure 1.19 over this range of Reynolds numbers. The maximum of $\frac{\overline{Nu}_p}{Nu}$ occurs in the region of the velocity antinode at the open end of the tube, and the minimum near the combustion zone, a velocity node. In these experiments, the pressure amplitude was found to vary approximately sinusoidally along the tube, from a maximum of 38 kN/m^2 (186 dB.) to

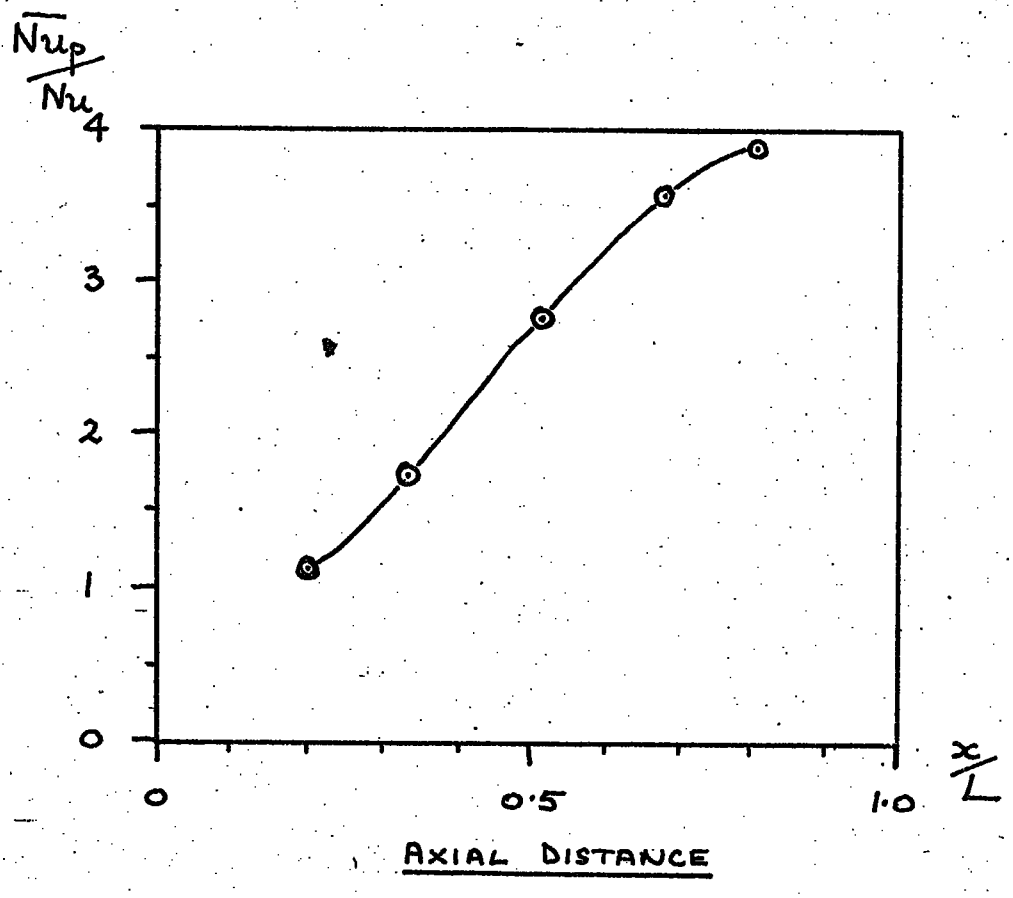

FIGURE 1.22 : GRAPH OF NUSSELT NUMBER RATIO AGAINST DISTANCE FROM HANBY

zero at the open end. This level is greatly in excess of those found in the apparatus of Jackson et al. (30) or Jackson and Purdy (34). Hanby used acoustic relationships, based on the one-dimensional wave equation, to derive an expression for the dimensionless velocity amplitude:

$$\frac{\hat{u}}{\bar{u}} = \frac{\hat{p}}{\bar{p}} \frac{c}{\nu} \tan\left(\frac{2\pi x}{\lambda}\right) \qquad 1.3.8$$

An analysis of the effect of the oscillations on heat transfer was made, using the quasi-steady state approach (see Section 2.4.2); then, by assuming that the gas particle velocity in an acoustic wave superimposed on a mean flow could be represented by:

$$u = \bar{u}\left(1 + \frac{\hat{u}}{\bar{u}} \cos \omega t\right) \qquad 1.3.9$$

it was shown that:

$$\frac{\overline{Nu_p}}{Nu} = \frac{1}{2\pi} \int_0^{2\pi} \left(\left| 1 + \frac{\hat{u}}{\bar{u}} \cos \omega t \right|\right)^{0.8} d\omega t \qquad 1.3.10$$

The result of a numerical integration of 1.3.10 is shown in Figure 2.6, and Hanby found that his experimental data fitted this curve to a standard deviation of ±5% over the range of possible values, $0.5 < \frac{\hat{u}}{\bar{u}} < 4.8$. This graph, 2.6, is very similar to that of Figure 1.20, as both show an approximately linear increase in $\frac{\overline{Nu_p}}{Nu}$ with $\hat{u}/\bar{u}$ greater that 1.0, but the slopes are not the same, being 0.377 and 0.114 respectively.

1.4 Aims of the Investigation

The review of previous work revealed that studies of the effect of longitudinal oscillations on local heat transfer coefficients using sirens and microphones were reasonably numerous. Also there existed a number of investigations into pulsating combustors of various designs. The only studies of local heat transfer coefficients in pulsating combustors were those of Hanby and Reay, who used a closed-open organ pipe and flap-valves respectively. It was decided to study a pulsating combustor with an aerodynamic valve, and to measure local heat transfer coefficients between the hot combusted gases and the heat exchanger wall. The results of this could be correlated in a similar manner to that used by Hanby, whose work indicated a dependence of $\frac{\overline{Nu}_p}{Nu}$ on the local dimensionless velocity amplitude, $\frac{\hat{u}}{\bar{u}}$. As Hanby had ignored non-isothermal effects, it was decided to make an analysis the propagation of sound waves through a gas exhibiting a severe temperature gradient in one direction. Due to the complexity of operation of combustors with aerodynamic valves, it was hoped to make a contribution to the understanding of the subject. Finally, it was decided to attempt a simplified analysis of the flow capacity of the aerodynamic valve.

2.1 Acoustic Wave Equation - Isothermal Fluid

The acoustic wave equation for plane waves of small waves of small amplitude propagating through an isothermal compressible fluid is:

$$\frac{\partial^2 \}}{\partial t^2} = c^2 \frac{\partial^2 \}}{\partial x^2} \qquad 2.1.1$$

The solutions to this equation for the case of standing waves in a straight, rigid duct of large L/d, closed at x = 0 and open at x = L, are:

$$\}(x,t) = \frac{\hat{p}_o c}{\omega B_A} \sin(\omega t) \sin\left(\frac{\omega x}{c}\right) \qquad 2.1.2$$

$$u(x,t) = \frac{\hat{p}_o c}{B_A} \sin\left(\omega t + \frac{\pi}{2}\right) \sin\left(\frac{\omega x}{c}\right) \qquad 2.1.3$$

$$p(x,t) = \hat{p}_o \sin(\omega t) \cos\left(\frac{\omega x}{c}\right) \qquad 2.1.4$$

$$\omega = \frac{\pi c (2n-1)}{2L} \qquad n = 1, 2, 3 \ldots \qquad 2.1.5$$

The boundary conditions and co-ordinates for this system are shown in Figure 2.1.

2.2 Acoustic Wave Equation - Exponential variation of Fluid Temperature

Now consider the propagation of plane waves of small amplitude through a compressible fluid which, as before, is confined in a straight, rigid duct of large L/d but whose temperature varies exponentially along it, as shown in Figure 2.2. For a perfect gas, the velocity of sound is a function of the absolute temperature only. Therefore, if the variation in the fluid temperature is written:

$$T = T_o e^{-2\alpha x} \qquad 2.2.1$$

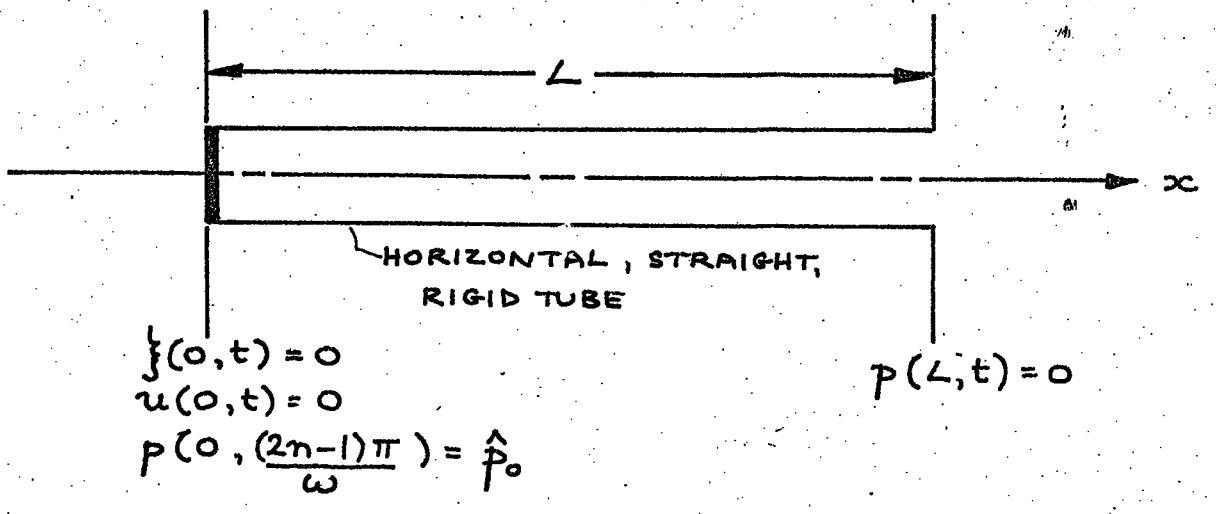

FIGURE 2.1 : BOUNDARY CONDITIONS & CO-ORDINATE SYSTEM FOR ISOTHERMAL FLUID

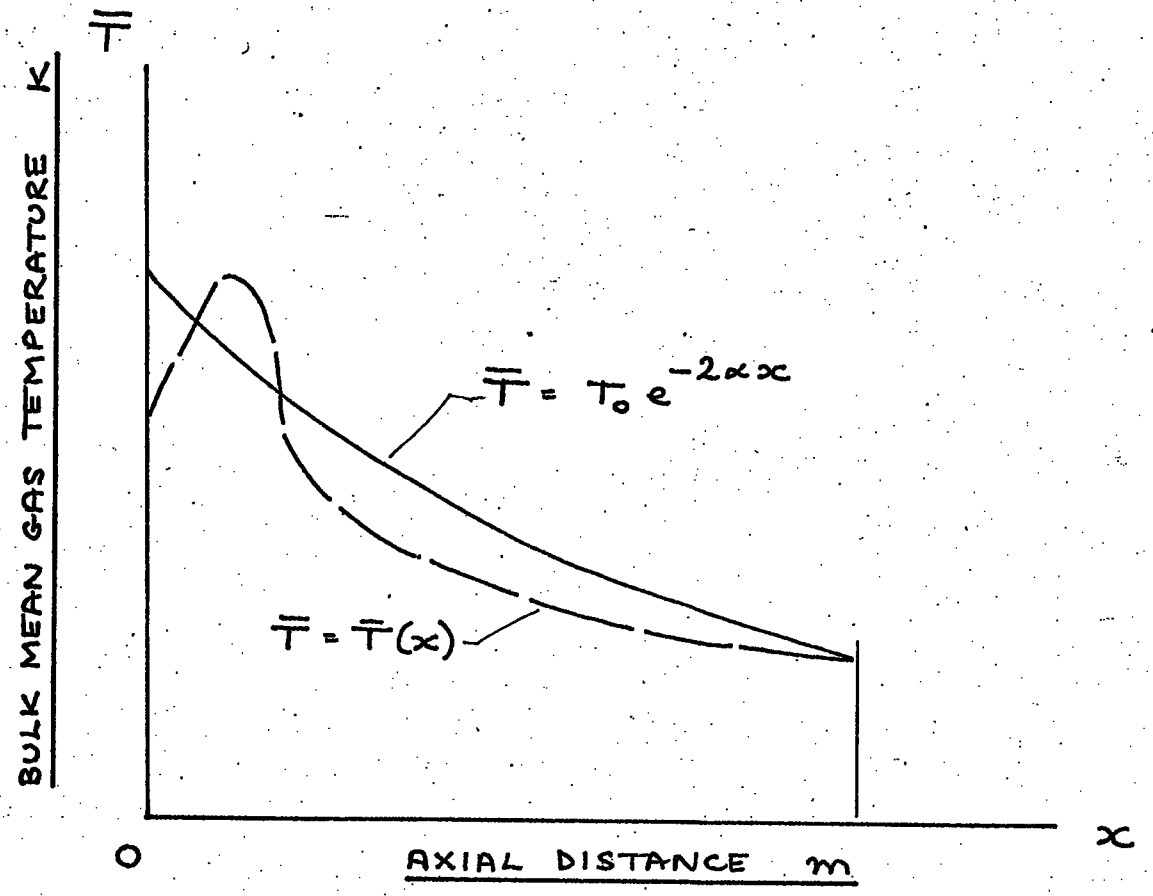

FIGURE 2.2 : EXPONENTIAL AND GENERAL VARIATIONS OF GAS TEMPERATURE ALONG TUBE

the variation in the velocity of sound becomes:

$$c = c_0 e^{-\alpha x} \qquad 2.2.2$$

The wave equation 2.1.1 may be solved with c now being a function of x. Putting:

$$\psi(x,t) = X(x)\,\theta(t) \qquad 2.2.3$$

and separating variables, 2.1.1 becomes:

$$c^2 \frac{X''}{X} = \frac{\ddot{\theta}}{\theta} = -\omega^2 \qquad 2.2.4$$

where ω is the separation constant. Thus

$$\ddot{\theta} + \omega^2 \theta = 0 \qquad 2.2.5$$

and $$X'' + \frac{\omega^2}{c^2} X = 0 \qquad 2.2.6$$

The solution to equation 2.2.5 is:

$$\theta(t) = A \sin(\omega t + \varepsilon) \qquad 2.2.7$$

where A and ε are constants. Substitution of 2.2.2 into equation 2.2.6 yields:

$$X'' + \lambda^2 e^{2\alpha x} X = 0 \qquad 2.2.8$$

where $$\lambda = \omega / c_0 \qquad 2.2.9$$

Now putting $$z = \frac{\lambda}{\alpha} e^{\alpha x} \qquad 2.2.10$$

and substituting into equation 2.2.8 gives:

$$\frac{d^2X}{dz^2} + \frac{1}{z}\frac{dX}{dz} + X = 0 \qquad 2.2.11$$

provided that $\alpha \neq 0$. Equation 2.2.11 is Bessel's Function of the Second Kind, and the general solution is:

$$X(z) = M_1 J_0(z) + N_1 Y_0(z) \qquad 2.2.12$$

where M and N are constants. Thus the general solution to 2.1.1 for an exponential variation in the velocity of sound is, from 2.2.3:

$$\xi(x,t) = \left\{M_1 J_0(z) + N_1 Y_0(z)\right\} A \sin(\omega t + \varepsilon) \qquad 2.2.13$$

Noting that the displacement and pressure in an acoustic wave are related by:

$$p = - B_A \frac{\partial \xi}{\partial x} \qquad 2.2.14$$

where B_A is the adiabatic bulk modulus of elasticity of the fluid and is independent of temperature, the variation in pressure may be obtained:

$$p(x,t) = - \left\{M_1 J_1(z) + N_1 Y_1(z)\right\} A\lambda e^{\alpha x} B_A \sin(\omega t + \varepsilon) \qquad 2.2.15$$

Application of the boundary conditions:

$$u(0,t) = 0$$

and

$$p(L,t) = 0$$

from Figure 2.1 yields respectively:

$$M_1 J_1(z_0) + N_1 Y_1(z_0) = 0 \qquad 2.2.16$$

and

$$M_1 J_1(z_L) + N_1 Y_1(z_L) = 0 \qquad 2.2.17$$

where $$z_0 = \lambda/\alpha \qquad 2.2.18$$

$$z_L = \lambda/\alpha\, e^{\alpha L} \qquad 2.2.19$$

The equations 2.2.16 and 2.2.17 must be solved simultaneously for λ :

$$f(\lambda) \equiv J_0(b\lambda)\,Y_1(a\lambda) - J_1(a\lambda)\,Y_0(b\lambda) = 0 \qquad 2.2.20$$

where $$a = \frac{1}{\alpha}\, e^{\alpha L} \qquad 2.2.21$$

$$b = 1/\alpha \qquad 2.2.22$$

The Newton-Raphson method may be used to find the zeroes of $f(\lambda)$ and is of the form:

$$\lambda_{m+1} = \lambda_m - \frac{f(\lambda_m)}{f'(\lambda_m)} \qquad 2.2.23$$

where $f'(\lambda)$ is given by:

$$\begin{aligned} f'(\lambda) = -\tfrac{1}{2}\{ & a\,Y_0(b\lambda)\left[J_0(a\lambda) - J_2(a\lambda)\right] \\ & + b\,J_1(a\lambda)\left[-2\,Y_1(b\lambda)\right] - b\,Y_1(a\lambda)\left[-2\,J_1(b\lambda)\right] \\ & - a\,J_0(b\lambda)\left[Y_0(a\lambda) - Y_2(a\lambda)\right]\} \end{aligned} \qquad 2.2.24$$

The particular solutions to the wave equation 2.1.1 for an exponential variation in the velocity of sound are, therefore:

$$\xi(x,t) = \frac{\hat{p}_0\, c_0}{\omega\, B_A} \sin(\omega t)\left\{M_1 J_0(z) + N_1 Y_0(z)\right\} \qquad 2.2.25$$

$$u(x,t) = \frac{\hat{p}_0\, c_0}{B_A} \sin(\omega t + \pi/2)\left\{M_1 J_0(z) + N_1 Y_0(z)\right\} \qquad 2.2.26$$

$$p(x,t) = \hat{p}_0 \sin(\omega t)\, e^{\alpha x}\left\{M_1 J_1(z) + N_1 Y_1(z)\right\} \qquad 2.2.27$$

where $$M_1 = \frac{-Y_0(z_0)}{\left[J_0(z_0)\,Y_1(z_0) - J_1(z_0)\,Y_0(z_0)\right]} \qquad 2.2.28$$

$$N_1 = \frac{J_0(z_0)}{\left[J_0(z_0)\,Y_1(z_0) - J_1(z_0)\,Y_0(z_0)\right]} \qquad 2.2.29$$

2.3 General Wave Equation - Arbitrary Variation in Fluid Temperature

Consider now a flow of hot gas through a smooth, horizontal tube, the hot end of which behaves as though acoustically closed, and the cold end of which as though acoustically open (see Figure 2.3). As convective heat transfer occurs between the hot gas and the externally-cooled wall of the tube, the temperature of the gas falls in the direction of flow as shown in Figure 2.2. Therefore, the time-averaged temperature, $\bar{T}$, may be regarded as a function of x:

$$\bar{T} = \bar{T}(x) \qquad 2.3.1$$

and, as the problem is effectively one-dimensional, changes in the y and z directions may be ignored. Consider the elemental control volume in Figure 2.4; equating the rate of increase of mass within the control volume with the rate of efflux minus the rate of influx yields:

$$\frac{\partial \rho}{\partial t}\,\delta x\,\delta y\,\delta z = \left(\rho + \frac{\partial \rho}{\partial x}\delta x\right)\left(u + \frac{\partial u}{\partial x}\delta x\right)\delta y\,\delta z - \rho u\,\delta y\,\delta z$$

Ignoring quadratic terms, the conservation of mass equation becomes:

$$\frac{\partial \rho}{\partial t} + u\frac{\partial \rho}{\partial x} + \rho\frac{\partial u}{\partial x} = 0 \qquad 2.3.2$$

Equating the forces acting on the element with the rate of change of momentum yields:

$$p\,\delta y\,\delta z - \left(p + \frac{\partial p}{\partial x}\delta x\right)\delta y\,\delta z = -\rho\,\delta x\,\delta y\,\delta z\,\frac{Du}{Dt}$$

and the equation of motion becomes, for an inviscid fluid:

$$\frac{\partial p}{\partial x} + \rho\frac{\partial u}{\partial t} + \rho u\frac{\partial u}{\partial x} = 0 \qquad 2.3.3$$

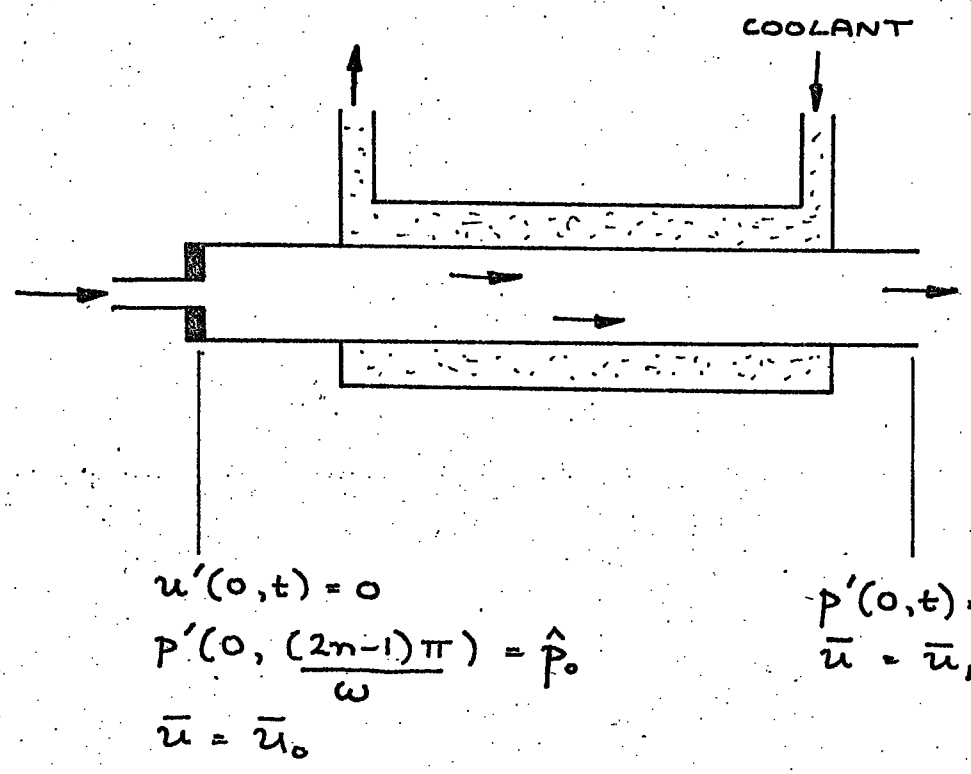

FIGURE 2.3: OSCILLATING FLOW OF COMPRESSIBLE FLUID THROUGH SIMPLE HEAT EXCHANGER

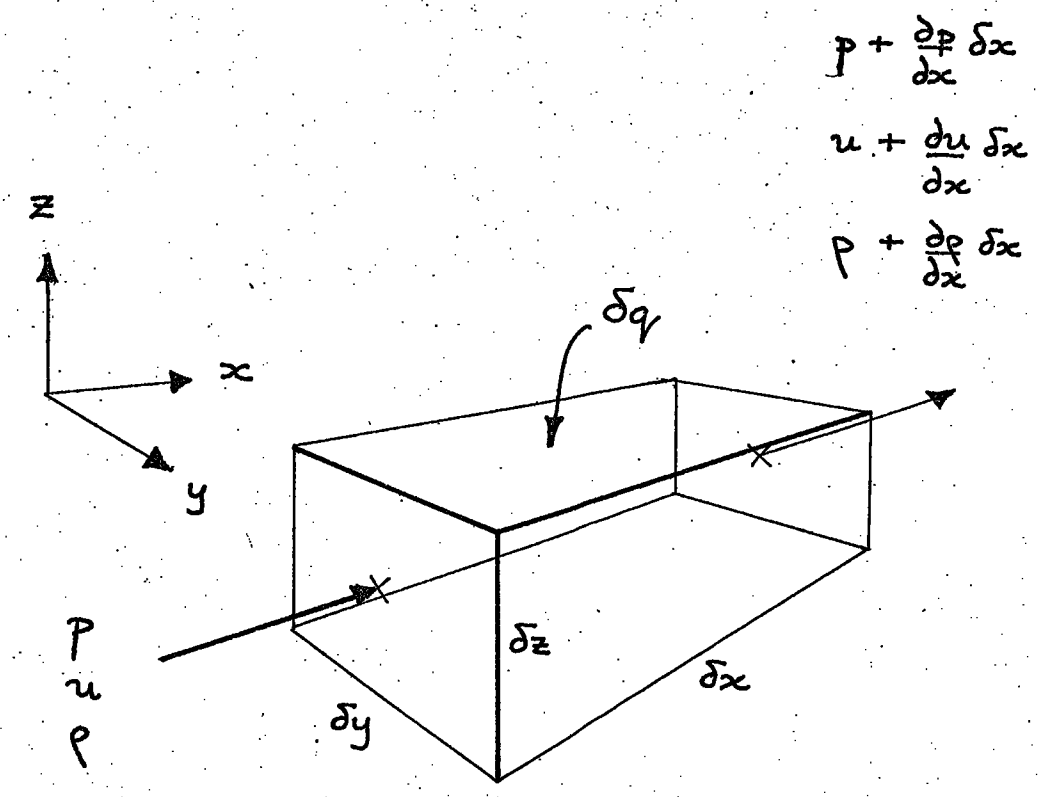

FIGURE 2.4 : ELEMENTAL CONTROL VOLUME OF THE SYSTEM SHOWN IN FIGURE 2.3

Equating the rate of change of internal energy of the element with the heat and work transfers from the surroundings yields:

$$\rho \delta x \delta y \delta z \frac{De}{Dt} = p u \delta y \delta z - \left\{\left(p + \frac{\partial p}{\partial x}\delta x\right) \times \left(u + \frac{\partial u}{\partial x}\delta x\right)\delta y \delta z\right\} + \delta q \, 2(\delta x \delta y + \delta x \delta z)$$

and the conservation of energy equation, in the absence of capillary, magnetic and electric effects, becomes:

$$\rho \frac{De}{Dt} + u \frac{\partial p}{\partial x} + p \frac{\partial u}{\partial x} = \frac{\partial q}{\partial x} \qquad 2.3.4$$

Consider now the effect of small perturbations on the flow, such that:

$$p = \bar{p} + p' \qquad 2.3.5.$$

$$u = \bar{u} + u' \qquad 2.3.6$$

$$\rho = \bar{\rho} + \rho' \qquad 2.3.7$$

the equations 2.2.3, 2.3.3 and 2.3.4 may now be examined again. From the equation of state of a perfect gas, it is evident that:

$$\frac{p'}{\bar{p}} = \frac{\rho'}{\bar{\rho}} \qquad 2.3.8$$

The analysis will now be limited to pressure amplitudes, $\hat{p}'$, such that:

$$\frac{\hat{p}'}{\bar{p}} < 0.15 \qquad 2.3.9$$

as recommended by Bogdanoff (40). The approximations may then be made:

$$\frac{\partial p}{\partial x} \simeq \frac{\partial \bar{p}}{\partial x} \qquad \frac{\partial \rho}{\partial x} \simeq \frac{\partial \bar{\rho}}{\partial x} \qquad 2.3.10$$

Consider:

$$\left| u \frac{\partial u}{\partial x} \Big/ \frac{\partial u}{\partial t} \right| = O\left(\frac{u^2}{L} \Big/ \omega c\right) \qquad 2.3.11$$

$$= O\left(\frac{u}{c}\right)^2$$

from equation 2.1.5. Thus, for flows of low Mach number, the term $u\frac{\partial u}{\partial x}$ is negligible compared with $\frac{\partial u}{\partial t}$. Assuming that the time-averaged pressure drop along the tube is negligible:

$$\frac{\partial \bar{p}}{\partial x} \simeq 0 \qquad 2.3.12$$

and using the definitions:

$$\frac{\partial p}{\partial t} \simeq \frac{\partial p'}{\partial t} \qquad \frac{\partial \rho}{\partial t} \simeq \frac{\partial \rho'}{\partial t} \qquad 2.3.13$$

the equations 2.3.2 and 2.3.3 become, respectively:

$$\frac{\partial \rho'}{\partial t} + u\frac{\partial \bar{\rho}}{\partial x} + \bar{\rho}\frac{\partial u}{\partial x} = 0 \qquad 2.3.14$$

$$\frac{\partial u}{\partial t} + \frac{1}{\bar{\rho}}\frac{\partial p'}{\partial x} = 0 \qquad 2.3.15$$

and using equation 2.3.14, the energy equation 2.3.4 becomes:

$$\rho\frac{De}{Dt} = \frac{p}{\bar{\rho}}\left\{\frac{\partial \rho'}{\partial t} + u\frac{\partial \bar{\rho}}{\partial x}\right\} + \frac{\partial q}{\partial x} \qquad 2.3.16$$

For the flow of a perfect gas with negligible kinetic energy, the specific internal energy, e, may be expressed:

$$e = c_v T = \frac{1}{\nu - 1}\frac{p}{\rho}$$

Therefore:

$$\frac{De}{Dt} = \frac{1}{\nu-1}\left\{\frac{1}{\rho}\left(\frac{\partial p}{\partial t} + u\frac{\partial p}{\partial x}\right) - \frac{p}{\rho^2}\left(\frac{\partial \rho}{\partial t} + u\frac{\partial \rho}{\partial x}\right)\right\}$$

Using 2.3.10, 2.3.12 and 2.3.13 and noting that:

$$c^2 = \nu R T$$

equation 2.3.16 becomes:

$$\frac{\partial p'}{\partial t} = c^2\left(\frac{\partial \rho'}{\partial t} + u\frac{\partial \bar{\rho}}{\partial x}\right) + (\nu - 1)\frac{\partial q}{\partial x}$$

Thus equations 2.3.2, 2.3.3 and 2.3.4 have been reduced to 2.3.14, 2.3.15 and 2.3.18 respectively. Differentiation of equation 2.3.14 with respect to t yields:

$$\frac{\partial^2 u}{\partial x \partial t} = \left\{ \frac{1}{\bar{\rho}^2} \frac{\partial p'}{\partial x} \frac{\partial \bar{\rho}}{\partial x} - \frac{1}{\bar{\rho}} \frac{\partial^2 p'}{\partial x^2} \right\} \qquad 2.3.19$$

and differentiation of equation 2.3.15 with respect to x yields:

$$\frac{\partial^2 u}{\partial t \partial x} = \frac{\partial}{\partial t} \left\{ -\frac{1}{\bar{\rho}} \left[\frac{1}{c^2} \frac{\partial p'}{\partial t} + (1-\nu) \frac{\partial q}{\partial x} \right] \right\} \qquad 2.3.20$$

using equation 2.3.18. Equating 2.3.19 and 2.3.20 yields:

$$\frac{\partial^2 p'}{\partial x^2} - \frac{1}{\bar{\rho}} \frac{\partial \bar{\rho}}{\partial x} \frac{\partial p'}{\partial x} - \frac{1}{c^2} \frac{\partial^2 p'}{\partial t^2} = \frac{1-\nu}{\bar{\rho}} \frac{\partial^2 q}{\partial t \partial x} \qquad 2.3.21$$

Now q, the heat flux, is dependent on the difference between the bulk mean gas temperature and the tube wall temperature, and thus is dependent on x. For high frequencies, this temperature difference may be regarded as independent of time, due to the thermal inertia of the wall and the small oscillations in the gas temperature. Therefore:

$$\frac{\partial}{\partial t} \left(\frac{\partial q}{\partial x} \right) \simeq 0 \qquad 2.3.22$$

If sinusoidal oscillations of p', u' and ρ' are now assumed, a solution of the type:

$$p' = p_x \sin(\omega t) \qquad 2.3.23$$

may be used. Equation 2.3.21 then becomes:

$$\frac{\partial^2 p_x}{\partial x^2} - \left(\frac{1}{\bar{\rho}} \frac{\partial \bar{\rho}}{\partial x} \right) \frac{\partial p_x}{\partial x} + \frac{\omega^2}{c^2} p_x = 0 \qquad 2.3.24$$

or

$$\frac{d^2 p_x}{dx^2} + \left(\frac{1}{\bar{T}} \frac{\partial \bar{T}}{\partial x} \right) \frac{d p_x}{dx} + \frac{\omega^2}{\nu R T} p_x = 0 \qquad 2.3.25$$

Equation 2.3.25 requires numerical solution, and the Runge-Kutta method was used, (see Appendix A). As in the case of the exponential

temperature variation, it is necessary to obtain ω by an iterative procedure from the boundary condition:

$$p_x(L) = 0$$

In this section, a general wave equation, similar to that of Kapur et al. (41), has been derived for the propagation of small amplitude waves at high frequency through a non-isothermal, perfect gas, flowing at small Mach number through a horizontal, straight tube. It may be noted that equation 2.3.21 reduces to the one-dimensional acoustic wave for a static, isothermal gas.

2.4 Forced convection heat transfer and longitudinal oscillations

2.4.1 Dimensional Analysis

Some insight into the important parameters of heat transfer in oscillating flow may be gained by the application of dimensional analysis. Consider first the steady flow of a gas in a straight, horizontal tube of circular cross-section, as shown in Figure 2.5; assuming that the flow of hot gas upstream of the heat exchanging section is hydro-dynamically developed and that the effects of natural convection are negligible, the local heat transfer coefficient becomes a function of nine parameters:

$$h = \phi(\rho, T, \mu, k, c_p, T_s, u, x, D) \qquad 2.4.1$$

By selecting ρ, c_p, u and T as the repeating variables and using Buckingham's Pi Theorem, the following relationship is established:

$$Nu = \phi\left(Re, Pr, \frac{x}{D}, \frac{T}{T_s}, E_c\right) \qquad 2.4.2$$

Now, by superimposing small oscillations on the flow, and assuming that they may be characterized by the angular frequency, ω, and the local velocity amplitude, $\hat{u}$, equation 2.4.1 becomes:

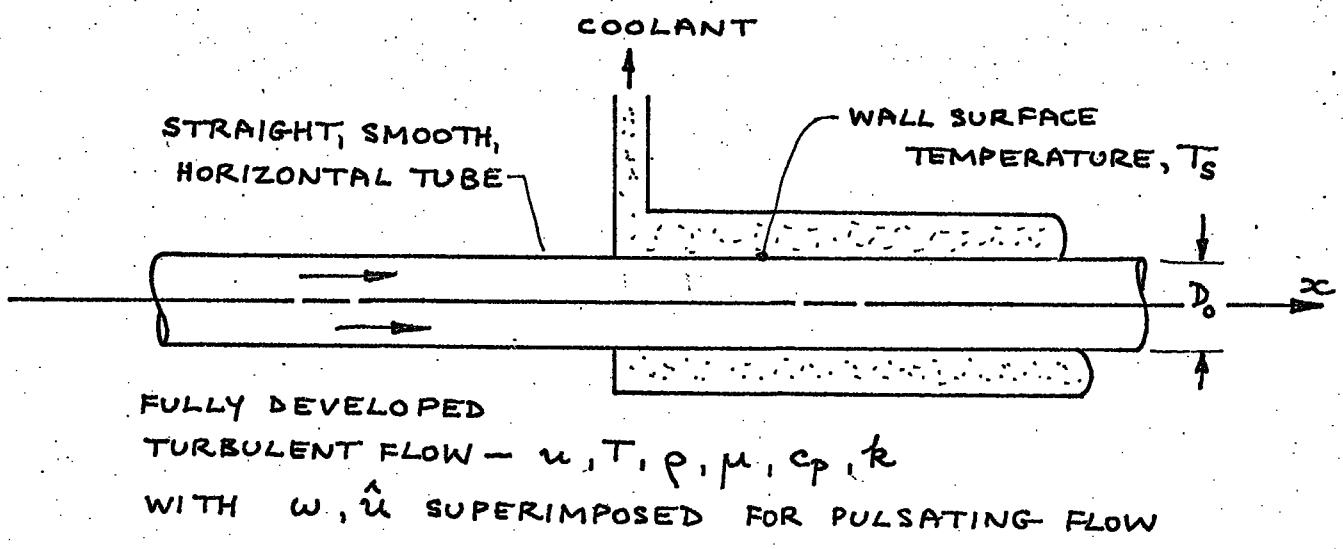

FIGURE 2.5: PARAMETERS OF THE FLOW

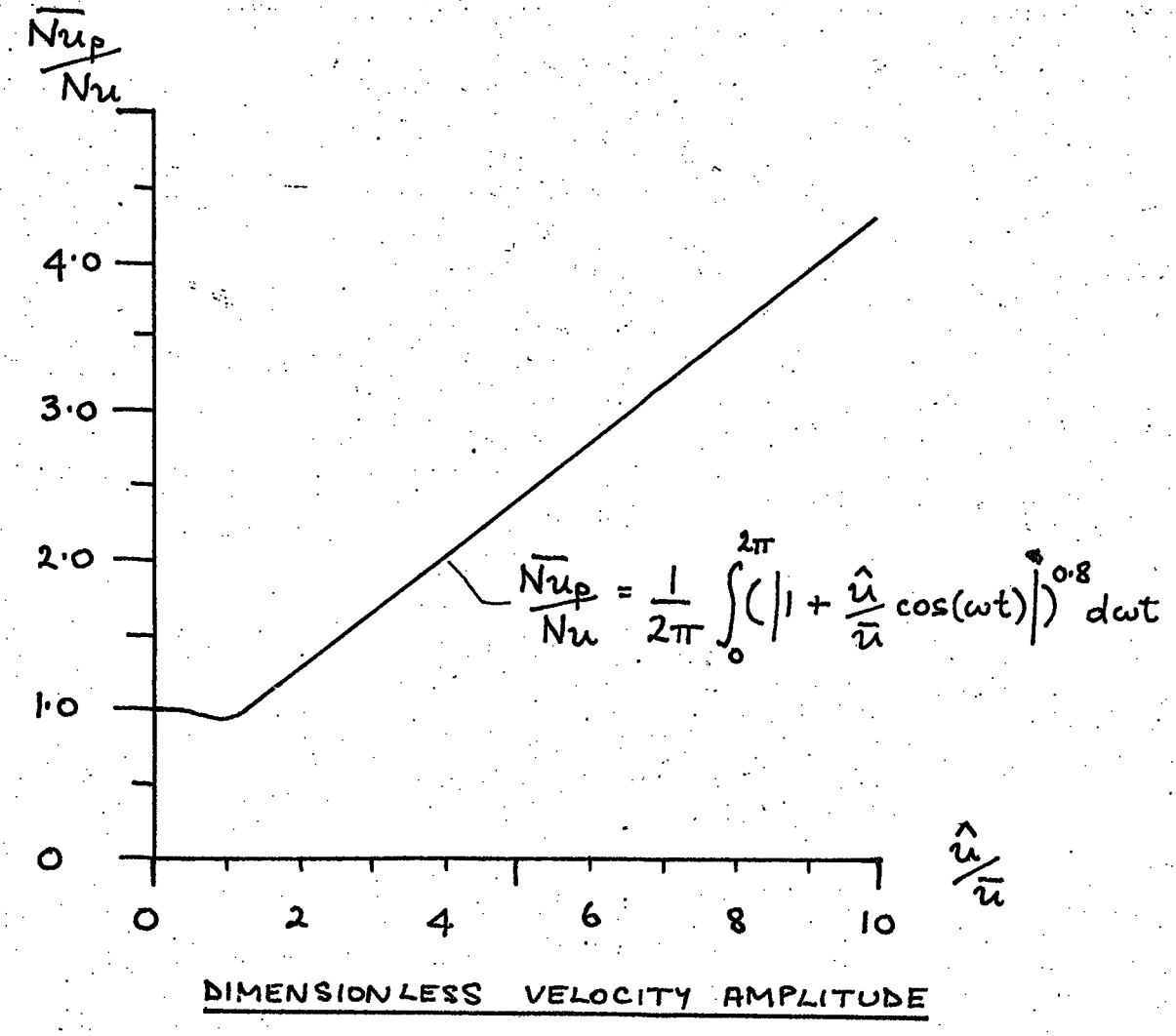

FIGURE 2.6: QUASI-STEADY STATE THEORY

$$\bar{h}_p = \phi(\bar{\rho}, \bar{T}, \mu, k, c_p, T_s, \bar{u}, x, D, \omega, \hat{u})$$

which leads to:

$$\overline{Nu}_p = \phi(\overline{Re}, Pr, \frac{x}{D}, \frac{\bar{T}}{T_s}, \bar{E}_c, \frac{\hat{u}}{\bar{u}}, S) \qquad 2.4.4$$

Thus the superimposition of small oscillations on the flow gives rise to two additional π factors, the dimensionless velocity amplitude $\frac{\hat{u}}{\bar{u}}$ and the Strouhal number, S. As the analysis of the slow is confined to flows of small Mach number (see Section 2.3), the effect of the Eckert number, $\bar{E}_c$, upon the heat transfer may be ignored. Therefore, if the other parameters are kept constant, a relationship may be sought between $\overline{Nu}_p$, $\frac{\hat{u}}{\bar{u}}$ and S.

2.4.2. Quasi-steady-state Analysis

The principle of this method, which has been used by Schultz-Grunow (28), Martinelli (27), Morell (42) and Hanby (39), is that an empirical relationship for forced convection in steady flow may be applied during any instant of the cycle of oscillation superimposed on the flow. The chief objection to this approach is that the velocity and temperature profiles will change throughout the cycle, and this in turn affects the accuracy of the relationship. For turbulent flow, the equation of Sieder and Tate (43) was chosen:

$$Nu = 0.027 (Re)^{0.8} (Pr)^{0.33} \left(\frac{\mu}{\mu_s}\right)^{0.14} \qquad 2.4.5.$$

This expression is valid for $\frac{L}{d} > 60$, for $(\bar{T} - T_s) > 56°C$ and for $0.7 < Pr < 16700$. All properties are evaluated at the bulk mean gas temperature, except for μ_s, which is evaluated at the tube surface temperature. Now from equations 2.3.6 and 2.3.23, the velocity at any instant may be expressed:

$$u = \bar{u} + \hat{u} \cos(\omega t) \qquad 2.4.6$$

Equation 2.4.5 becomes, on substitution of equation 2.4.6:

$$Nu_p = 0.027(\bar{Re})^{0.8}(Pr)^{0.33}\left(\frac{\mu}{\mu_s}\right)^{0.14}\left[1 + \frac{\hat{u}}{\bar{u}}\cos(\omega t)\right]^{0.8} \qquad 2.4.7$$

Dividing 2.4.7 by 2.4.5 and integrating over the period of one oscillation yields:

$$\frac{\overline{Nu_p}}{Nu} = \frac{1}{2\pi}\int_0^{2\pi}\left(\left|1 + \frac{\hat{u}}{\bar{u}}\cos(\omega t)\right|\right)^{0.8} d\omega t \qquad 2.4.8$$

This curve is shown in Figure 2.6.

The effects predicted by these analyses were calculated for the arrangement as shown in Figure 2.4. A comparison between equations 2.1.4 and 2.2.27 is shown in Figure 2.7, where it is apparent that a temperature gradient causes a nodal shift towards the cooler end of the tube. The maximum pressure amplitude increases by approximately 30%. Figure 2.8 illustrates the increase in local heat transfer coefficient predicted by the quasi-steady approach. At velocity antinodes the increases range from 20 to 200%. Figure 2.9 demonstrates the increases to be expected in overall heat transfer rates. These are less dramatic, ranging from 0 to 17.5%. At higher frequencies, increases are approximately 2% more than at low.

2.4.3 Dimensionless velocity amplitude

From the acoustic wave equation, the dimensionless velocity amplitude for the isothermal state is given by:

$$\frac{\hat{u}}{\bar{u}} = \frac{\hat{p}_o c}{\bar{u} B_A}\sin\left(\frac{\omega x}{c}\right) \qquad 2.4.9$$

and for the exponential temperature variation:

$$\frac{\hat{u}}{\bar{u}} = \frac{\hat{p}_o c_o}{\bar{u} B_A}\left\{M_1 J_0(z) + N_1 Y_0(z)\right\} \qquad 2.4.10$$

FIGURE 2.7: VARIATION OF PRESSURE AMPLITUDE ALONG COMBUSTOR FOR LINEAR TEMPERATURE GRADIENT. COMPARISON OF GENERAL SOLUTION WITH SIMPLE ACOUSTIC THEORY.

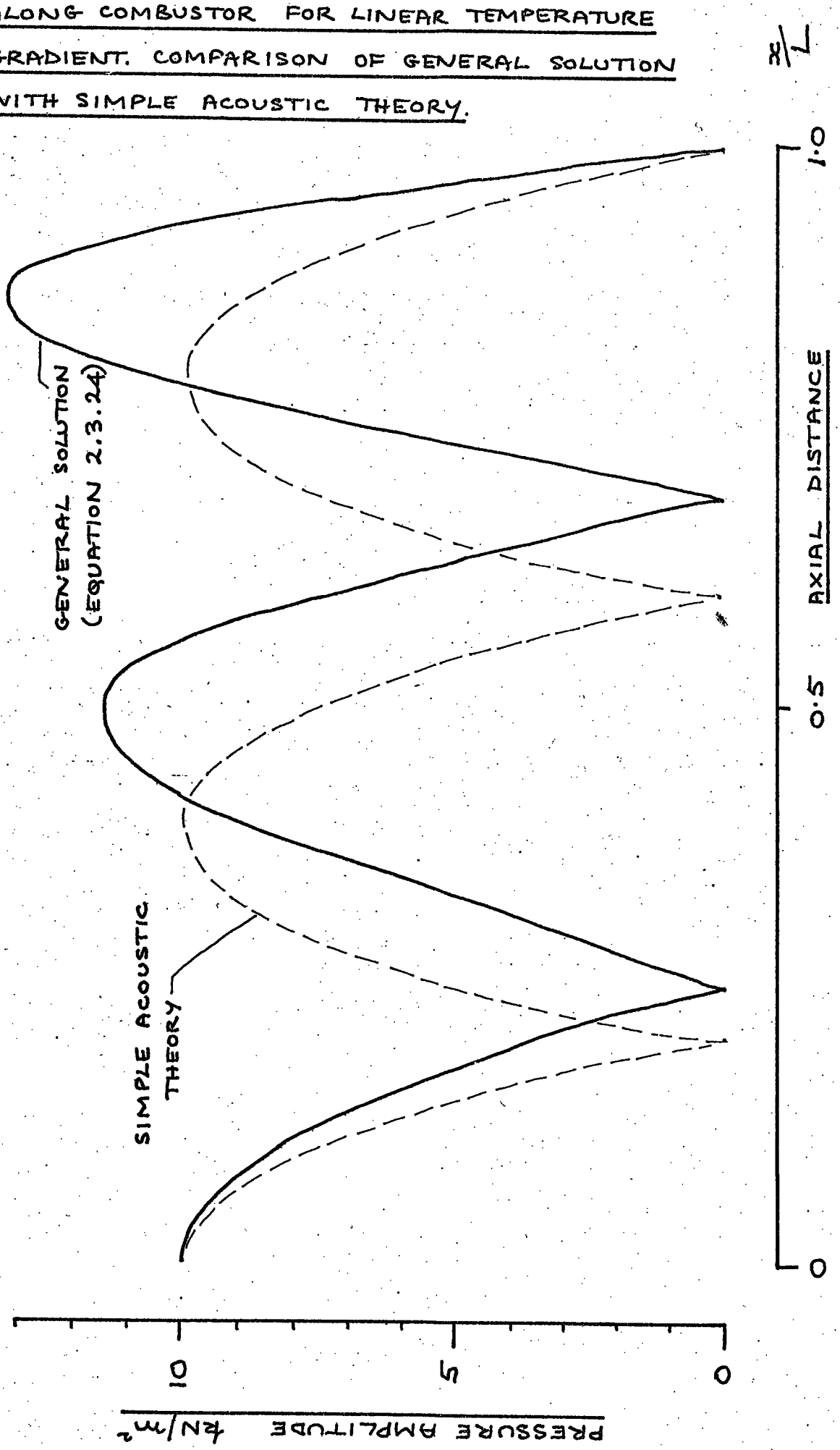

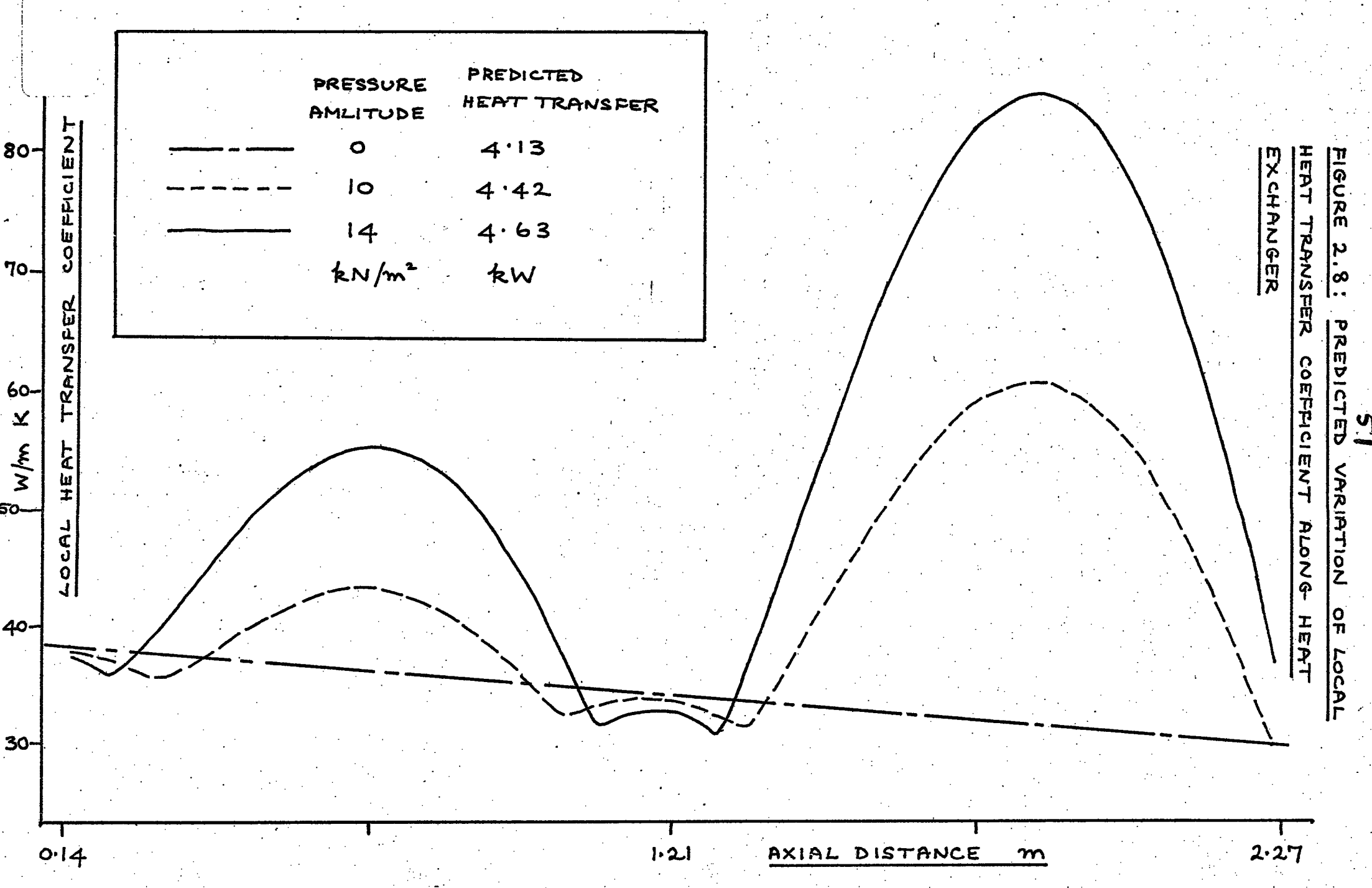

FIGURE 2.8: PREDICTED VARIATION OF LOCAL HEAT TRANSFER COEFFICIENT ALONG HEAT EXCHANGER

FIGURE 2.9 : PREDICTED VARIATION OF OVERALL HEAT TRANSFER IMPROVEMENT RATIO FOR FOUR HARMONICS

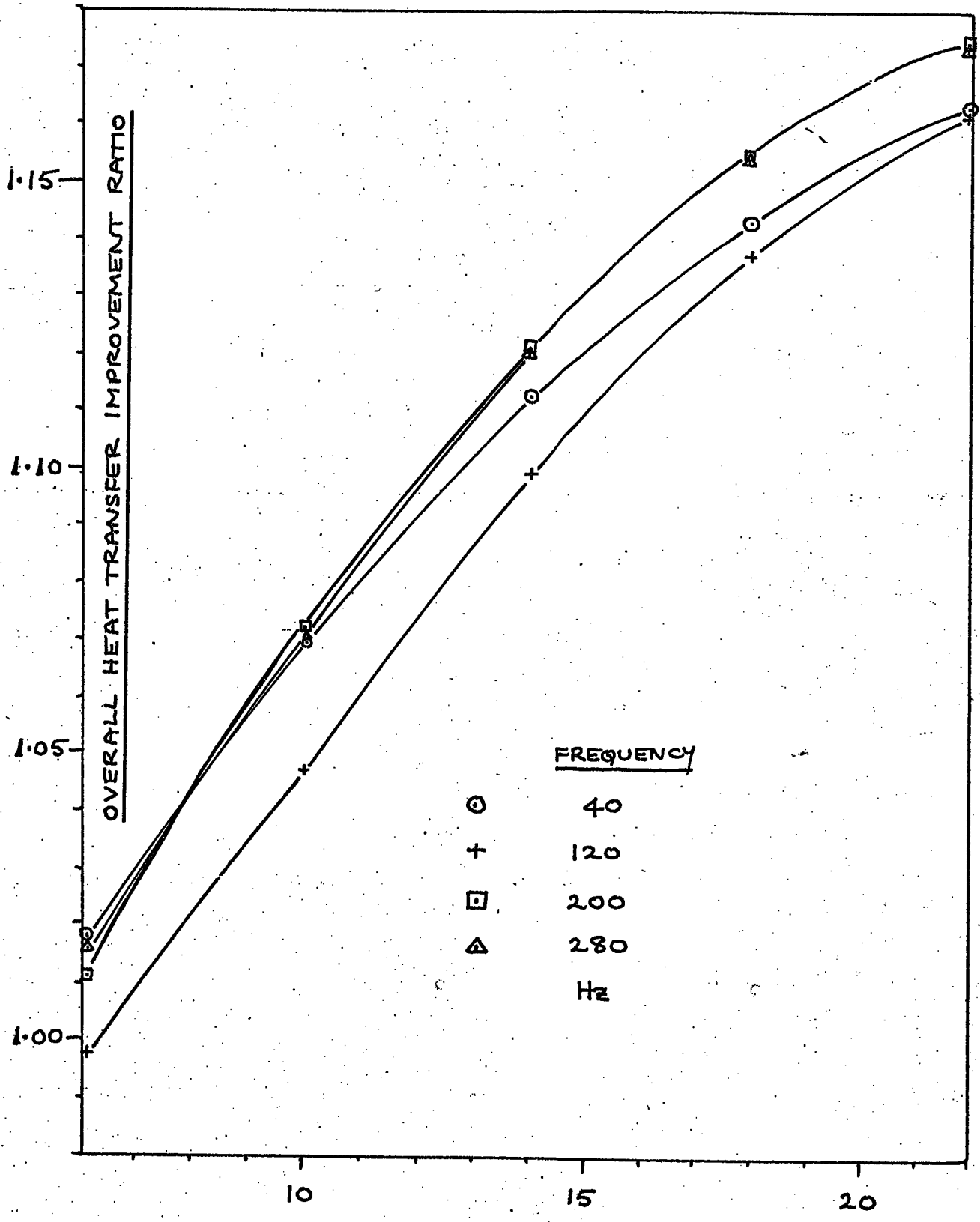

For the general case, $\bar{T} = \bar{T}(x)$, it is necessary to solve equation 2.3.25 and derive u from equations 2.3.25 and 2.3.23:

$$\frac{\partial u}{\partial t} = -\frac{1}{\bar{\rho}} \frac{\partial p_x}{\partial x} \sin(\omega t) \qquad 2.4.11$$

Integration gives:

$$u = \bar{u} + \frac{1}{\omega \bar{\rho}} \frac{\partial p_x}{\partial x} \cos(\omega t) \qquad 2.4.12$$

from which

$$\frac{\hat{u}}{\bar{u}} = \frac{1}{\bar{u} \omega \bar{\rho}} \frac{\partial p_x}{\partial x} \qquad 2.4.13$$

2.5 Analysis of aerodynamic valve

It was decided to analyse the flow through the aerodynamic valve in order to predict the net mass flowrate of air through it for a given pressure variation in the combustion chamber. During the induction part of the cycle, air, and possibly rejected gases of the previous cycle, are drawn into the combustion chamber. After the expansion of the combustion process, hot products are rejected back through the valve. It was decided to simplify the problem by assuming that the induced fluid was air at atmospheric temperature and that the exhausted fluid was air at a high temperature. The analysis uses a quasi-steady state approach. From Lewitt (44), the isentropic steady state relation for the frictionless flow of a gas through a nozzle is:

$$\dot{m} = A_e \left\{ 2 p_1 \rho_1 \left(\frac{\nu}{\nu - 1} \right) \left(\frac{p_2}{p_1} \right)^{2/\nu} \left[1 - \left(\frac{p_2}{p_1} \right)^{\frac{\nu-1}{\nu}} \right] \right\}^{1/2} \qquad 2.5.1$$

where ν is evaluated at T_2. The velocity at 2 is given by:

$$u_2 = \left\{ 2 \frac{p_1}{\rho_1} \left(\frac{\nu}{\nu - 1} \right) \left[1 - \left(\frac{p_2}{p_1} \right)^{\frac{\nu-1}{\nu}} \right] \right\}^{1/2} \qquad 2.5.2$$

The situation is illustrated in Figure 2.10. The effective area of the valve is less than its actual cross-sectional area, and is given by Shapiro (45) to be:

$$A_e = A \times C_d \qquad 2.5.3$$

C_d, the coefficient of discharge is given by:

$$C_d = \frac{1}{\mu M^2}\left\{\left[1+\left(\frac{\mu-1}{2}\right)M^2\right]^{\frac{\mu}{\mu-1}} - 1\right\} \qquad 2.5.4$$

M, being the Mach number of the flow through the nozzle at 2. Using the binomial series to expand equation 2.5.4 and simplifying, the coefficient of discharge becomes, approximately:

$$C_d = \tfrac{1}{2} + \frac{M^2}{8} + \frac{M^4}{24} \qquad 2.5.5$$

provided $M < 1$.

The oscillation of pressure within the combustion chamber is assumed to be sinusoidal, and the steady state flow relation through the valve is assumed to hold over the whole cycle. The induction and exhaust sequence is shown in Figure 2.11.

Induction

At any instant then:

$$\dot{m}_{IN} = A_e\left\{2 p_1 \rho_1 \left(\frac{\mu_2}{\mu_2-1}\right)\left(\frac{p_2}{p_1}\right)^{2/\mu_2}\left[1-\left(\frac{p_2}{p_1}\right)^{\frac{\mu_2-1}{\mu_2}}\right]\right\}^{1/2} \qquad 2.5.6$$

Equation 2.5.6 must be integrated over the time:

$$\frac{\pi}{\omega} \leq t \leq \frac{2\pi}{\omega} \qquad 2.5.7$$

when the pressure in the combustion chamber is less than atmospheric. Thus ;

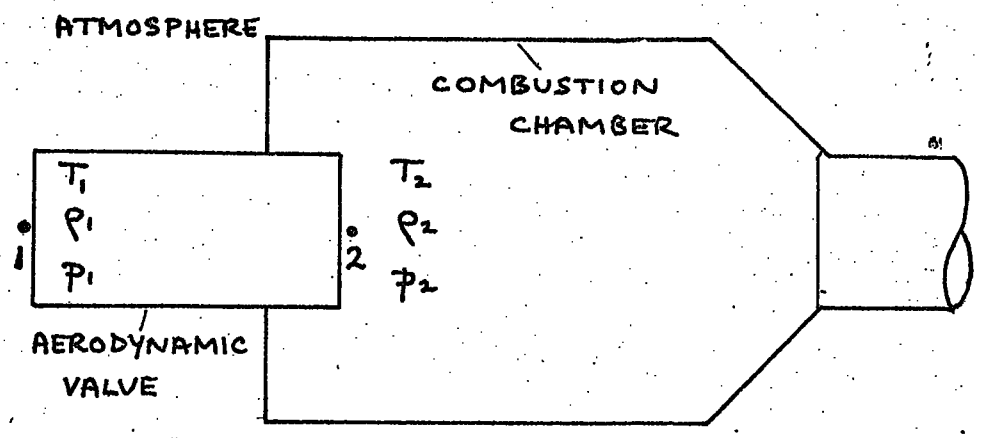

FIGURE 2.10: FRICTIONLESS FLOW OF GAS THROUGH AERODYNAMIC VALVE

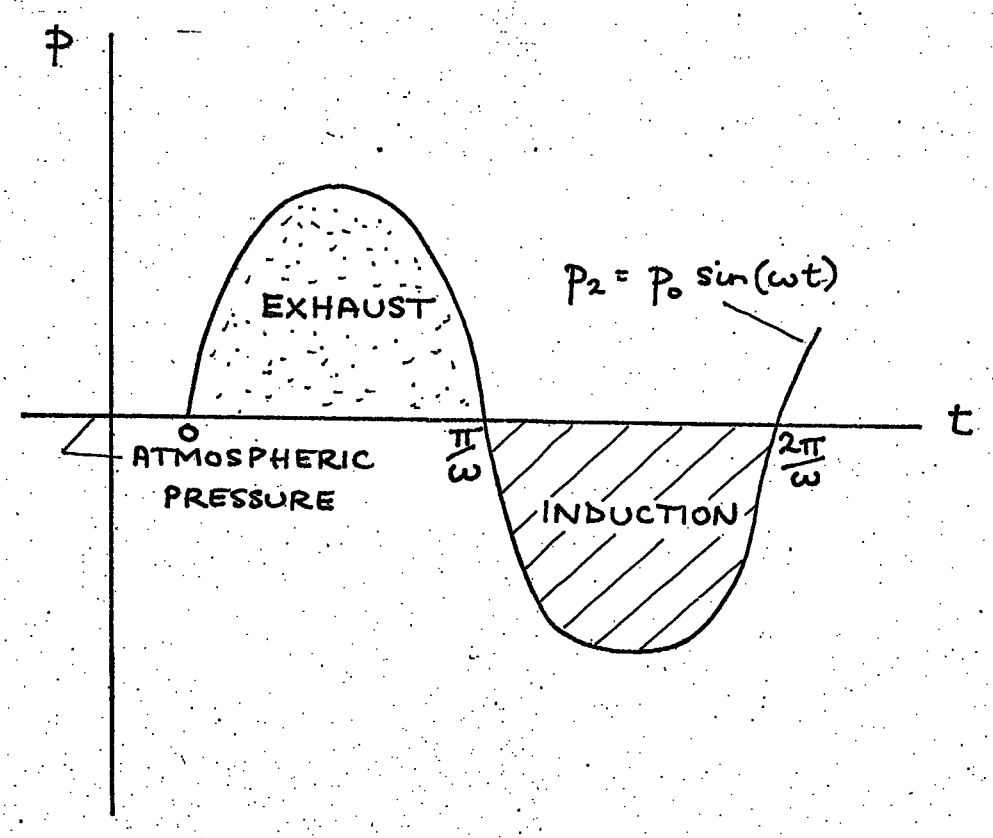

FIGURE 2.11: INDUCTION AND EXHAUST SEQUENCE THROUGH VALVE

$$\Sigma \dot{m}_{IN} = \left\{2 p_1 \rho_1 \left(\frac{\mu_2}{\mu_2 - 1}\right)\right\}^{1/2} \int_{\pi/\omega}^{2\pi/\omega} A_e \left(\frac{p_2}{p_1}\right)^{1/\mu} \left\{1 - \left(\frac{p_2}{p_1}\right)^{\frac{\mu_2 - 1}{\mu_2}}\right\}^{1/2} dt \quad 2.5.8$$

and

$$u_2 = \left\{2 \frac{p_1}{\rho_1} \left(\frac{\mu_2}{\mu_2 - 1}\right)\left[1 - \left(\frac{p_2}{p_1}\right)^{\frac{\mu_2 - 1}{\mu_2}}\right]\right\}^{1/2} \quad 2.5.9$$

Exhaust

By similar considerations, for when the pressure in the combustion chamber exceeds atmospheric, the total mass of air exhausted is given by:

$$\Sigma \dot{m}_{OUT} = \left\{2 p_2 \rho_2 \left(\frac{\mu_1}{\mu_1 - 1}\right)\right\}^{1/2} \int_{0}^{\pi/\omega} A_e \left(\frac{p_1}{p_2}\right)^{1/\mu} \left\{1 - \left(\frac{p_1}{p_2}\right)^{\frac{\mu_1 - 1}{\mu_1}}\right\}^{1/2} dt \quad 2.5.10$$

and

$$u_1 = \left\{2 \frac{p_2}{\rho_2} \left(\frac{\mu_1}{\mu_1 - 1}\right)\left[1 - \left(\frac{p_1}{p_2}\right)^{\frac{\mu_1 - 1}{\mu_1}}\right]\right\}^{1/2} \quad 2.5.11$$

ρ_2 may be expressed in terms of ρ_1, by the isentropic relation:

$$\rho_2 = \rho_1 \left(\frac{p_2}{p_1}\right)^{1/\mu} \quad 2.5.12$$

The necessary integrations may be carried out using Simpsons Rule. The net flow of air into the combustion is then given by:

$$\dot{m}_{AA} = \Sigma \dot{m}_{IN} + \Sigma \dot{m}_{OUT} \quad 2.5.13$$

3. Experimental Work

As stated in Section 1.4, it was decided that a pulsating combustor, comprising an aerodynamic valve, combustion chamber and heat exchanger, should be constructed with an exhaust tube dimension of 26 mm. internal diameter. Due to the lack of experience in the field, a preliminary investigation into the general behaviour of a pulsating combustor was carried out. This work is reported in Appendix B, and the conclusions were:

a) a Helmholtz-type combustor was suitable for the purpose of the work;

b) the aerodynamic valve should be 50 mm. long and 12 - 26 mm. internal diameter;

c) the apparatus should include two heat exchangers, one through which the reverse flow back past the valve could be arranged to pass.

The general arrangement of the apparatus is shown in Figure 3.1. It was mounted on a rigid steel framework, which was tilted a few degrees from the horizontal to allow condensate to drain. The apparatus was separated from the frame by wooden vee-blocks to reduce conduction losses and permit expansion. The exhaust gases vented at atmospheric pressure into the laboratory beside an extractor fan that pumped them away. The inlets to the combustor were placed near an open window to ensure a continuous supply of fresh air. The apparatus was constructed in several sections which were flanged and bolted together, sealed by copper gaskets.

3.1 The Resonating Section

The resonating section of the apparatus is shown in Figure 3.2 and comprised a combustion chamber with aerodynamic valve, settling

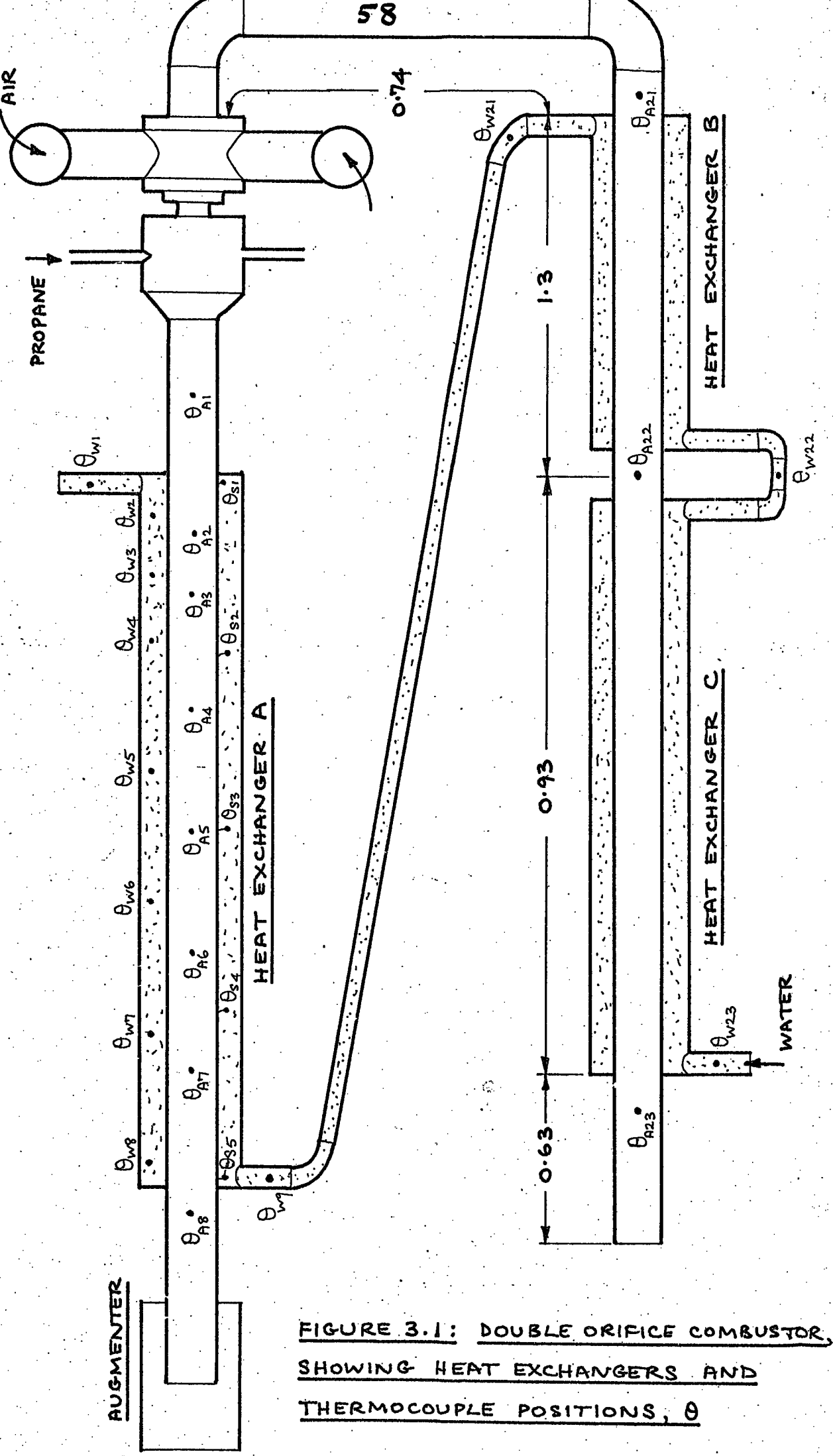

FIGURE 3.1: DOUBLE ORIFICE COMBUSTOR, SHOWING HEAT EXCHANGERS AND THERMOCOUPLE POSITIONS, θ

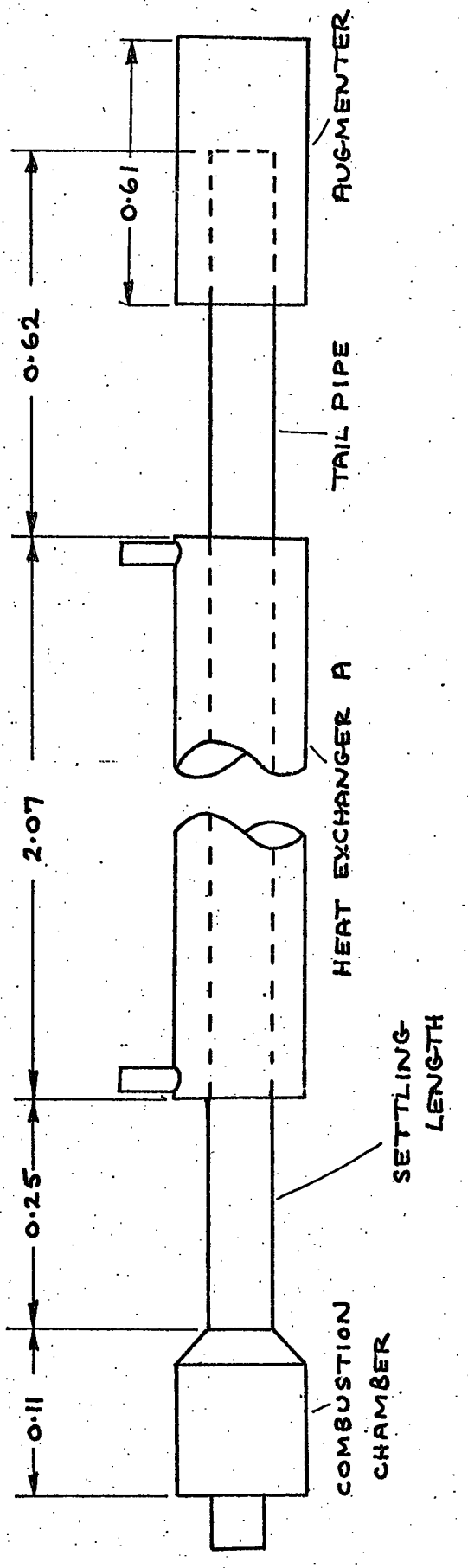

FIGURE 3.2: MAIN RESONATING SECTION

length, heat exchanger A , tail-pipe and augmenter. The total length of the section was 3.05 m. and therefore was 0.65 m. longer than the development combustor. The purpose of this increase was to permit the use of a longer heat exchanger (2.07 m. compared to 1.65 m.) and a settling length of approximately 10 tube diameters between the combustion chamber and the heat exchanger. It was found necessary also to increase the length of the augmenter from 0.276 to 0.61 m.

3.1.1 The Combustion Chamber

The combustion chamber is shown in Figure 3.3. Internally it was an exact reproduction of the chambers used in earlier experiments. The chamber itself was constructed from a bar of stainless steel. It had six radial holes into which components could be screwed, of which the fuel injector and sparking plug are shown. Due to trouble experienced with proprietory sparking plugs, a special one was built. This consisted of a stainless steel body into which a long-reach KLG electrode and insulator fitted, being retained by a threaded ring. This design proved to be very convenient for cleaning the electrode of deposits and for realignment, often necessary after a prolonged period of combustor operation. The cooling annulus around the chamber was intended to provide some control over the chamber wall temperature, so that the gas temperature gradient, and hence the operating mode, could be changed if required. The metal temperature was measured by Chromel-Alumel thermocouple only one measurement being taken as it was felt that this temperature was not critical. Also shown in Figure 3.3 is an aerodynamic valve screwed into the combustion chamber. The valves, which were 51 mm. long and from 9.5 to 25 mm. internal diameter, were constructed from stainless steel hexagon bar. Apart from removing sharp corners, no attempt was made to streamline the bores. An air

THREADED TAPPING FOR KISTLER PRESSURE TRANSDUCER AT POINT 'X'

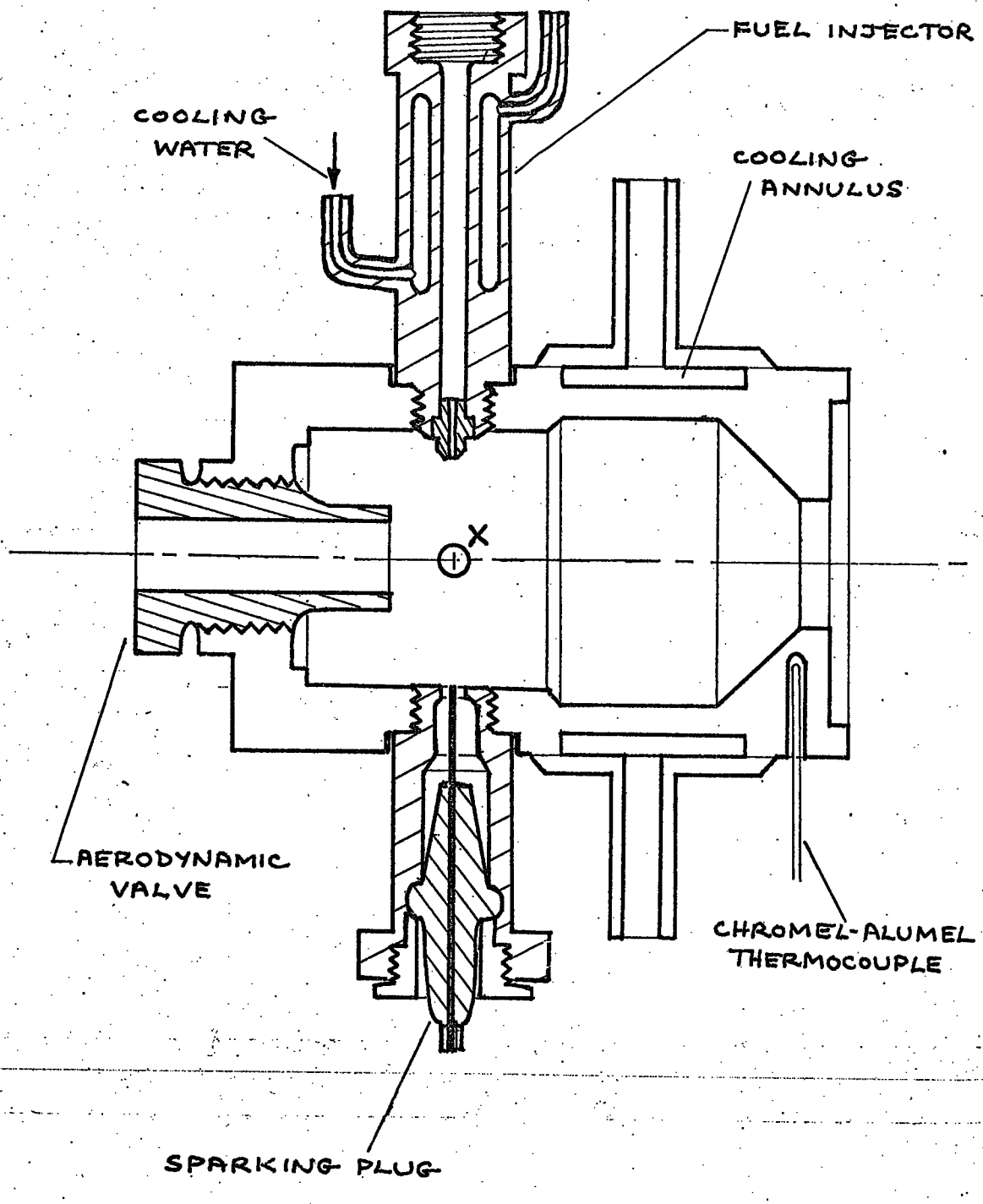

FIGURE 3.3 : COMBUSTION CHAMBER

SCALE : 3/4 FULL SIZE

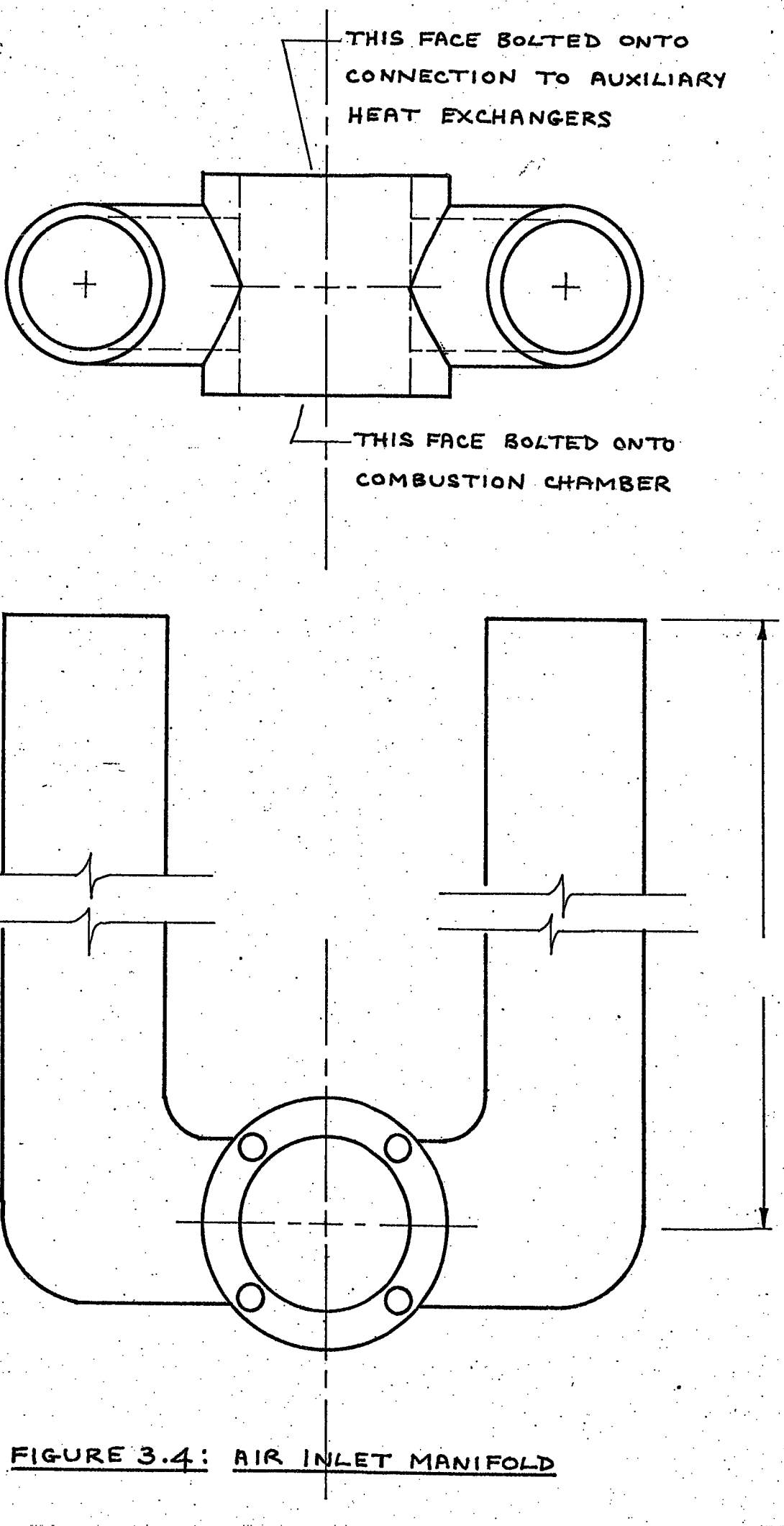

FIGURE 3.4: AIR INLET MANIFOLD

inlet manifold, which enclosed the valve, was bolted to the end of the combustion chamber and is shown in Figure 3.4. The purpose of the manifold was to guide the air inducted by the combustor into the valve and thus, by using a suitable flowmeter, to make a direct measurement of the flow.

The combustion chamber and ancillaries were lagged by winding asbestos rope around them, and enclosing that with preformed sections of calcium silicate, 0.23 m. outside diameter, obtained from Newalls Insulation Company.

3.1.2 Heat Exchanger A

As heat exchanger A formed part of the resonating section of the apparatus, it was constructed so that measurements of local heat transfer coefficients and of local pressure amplitudes could be made. It consisted principally of two concentric copper tubes, of 26 and 38 mm. nominal diameter, which were located at the ends by two brass adaptors. The arrangement is shown in Figure 3.5. The exchanger, which was 2.14 m. long overall, had a heat exchange surface of 2.07 m. length, giving a surface area (based on the outside diameter, 28.3 mm., of the inner tube) of 0.184 m^2. Along this length, were sited six instrument mountings, into which a temperature probe (see Section 3.4.1) or a pressure transducer (see Section 3.5.2) could be screwed. Seven thermocouples were mounted in the annular space to measure the water temperature (see Section 3.4.2), and five other thermocouples were soldered to the heat exchange surface to measure the wall temperature. The seven water thermocouples were threaded through mounting pads and bent to face upstream to oppose the water flow. This meant that the wires led axially away from the junction and thus not along an isotherm, but it was felt that, as the axial temperature gradient in the water flow did not exceed 0.05 $^{o}C/mm.$, the error due to conduction along the

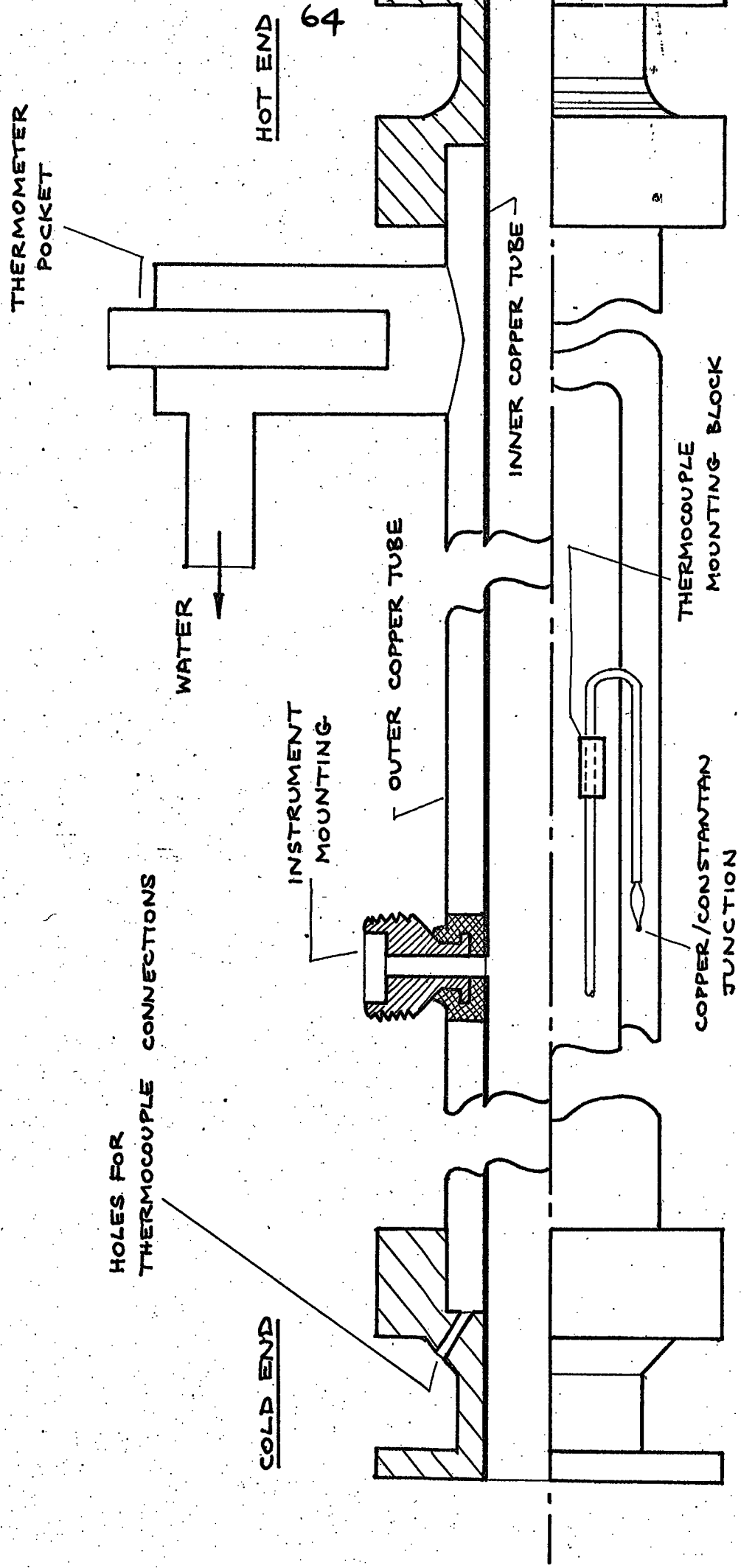

FIGURE 3.5: HEAT EXCHANGER A

wires was small. The thermocouples were laid adjacently where possible and clamped with wire to the inner tube. The free ends were passed through holes in the brass adaptor at the cold end and connected to copper wires in an isothermal wooden box, clamped to the tail-pipe.

The water connections to heat exchanger A consisted of vertical thermometer pockets at each end, to which 13 mm. diameter tubes were soldered for connection to the water system. The exchanger was lagged by preformed glass-fibre sections of 82 mm. outside diameter. During the construction of this piece of apparatus, a solid 25 mm. diameter mild steel bar was passed through the inner tube in order to minimise distortion during the welding operations. When complete, the annulus was tested up to 270 kN/m^2 water pressure; minor leaks were found and these were repaired with araldite.

3.1.3 The Tail-pipe and Augmenter

The tail-pipe was constructed from a piece of copper tube, 26 mm. nominal diameter and 0.62 m. long. Onto the outer end were glued three steel rods of small diameter and 38 mm. long, over which the augmenter could slide axially. The augmenter consisted of a piece of tube, 38 mm. nominal diameter and 0.61 m. long. The arrangement is shown in Figure 3.6.

3.2 The Fuel System

The fuel used in the investigation was commercial grade propane (B.S.4250:1968) obtained from the British Oxygen Company in quantities of 47 kg. in the liquid state. The arrangement of the fuel system is shown in Figure 3.7. The flowrate was measured by a viscous flowmeter,

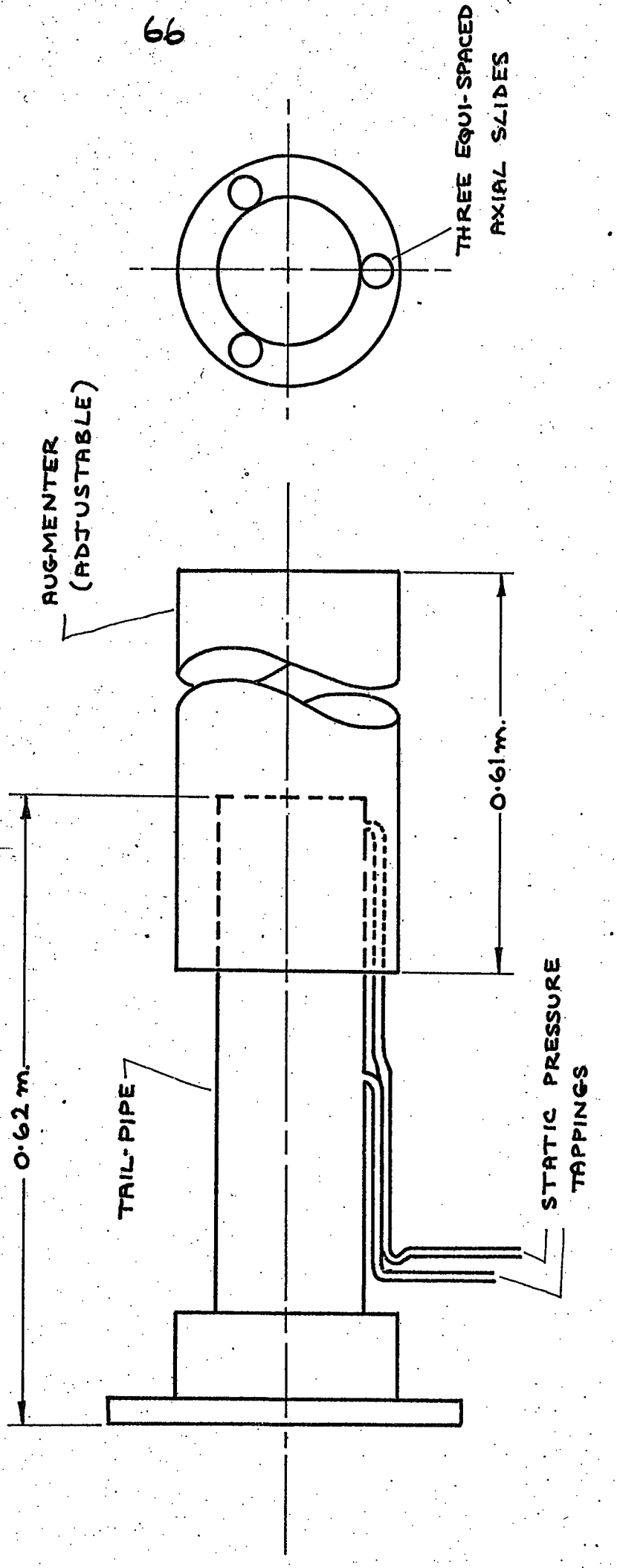

FIGURE 3.6 : TAIL-PIPE AND AUGMENTER

Type R837951/G, supplied by the Rotameter Manufacturing Company and calibrated over the range 0.13 to 1.3 kg/h. at standard atmospheric conditions to ± 2 per cent of indicated flow. The pressure in the flowmeter was displayed by a Bourdon gauge, supplied by the Budenburg Gauge Company and calibrated to ± 0.25 per cent of indicated pressure. The pressure drop at maximum flow through the meter was quoted (46) to be 0.1 kN/m^2. It was thus negligible compared with the working pressure. The temperature of the propane was measured to ± 2 per cent by a Type T thermocouple inserted into the top of the meter and was controlled at 20 ± 3 °C by manual adjustment of the isothermal bath temperature. A straight, settling length of 0.6 m. was placed between the heat exchanger coil and the meter to damp out disturbances in the flow, and this was lagged to reduce heat losses. The rate of flow of the fuel was controlled by a precision pressure regulator and a needle valve, with a shut-off valve in case of emergency.

The fuel was forced radially into the combustion chamber through a water-cooled injector, (see Figure 3.3). Brass jets, which were obtained from Amal in sizes ranging from 0.2 to 2.5 mm. internal diameter, screwed into the injector. This was water-cooled to prevent premature decomposition of the fuel due to the high chamber temperature.

It was found that a jet of 0.86 mm. internal diameter performed best in the fuel injector. If a larger jet was fitted, the pressure drop across it was less, and the oscillations in the chamber affected the propane flowmeter. If a smaller one was fitted, the combustor did not always oscillate smoothly, and the flame occasionally failed. This was possibly due to the high injection velocity which could have prevented good mixing in the chamber and retarded the rate of reaction.

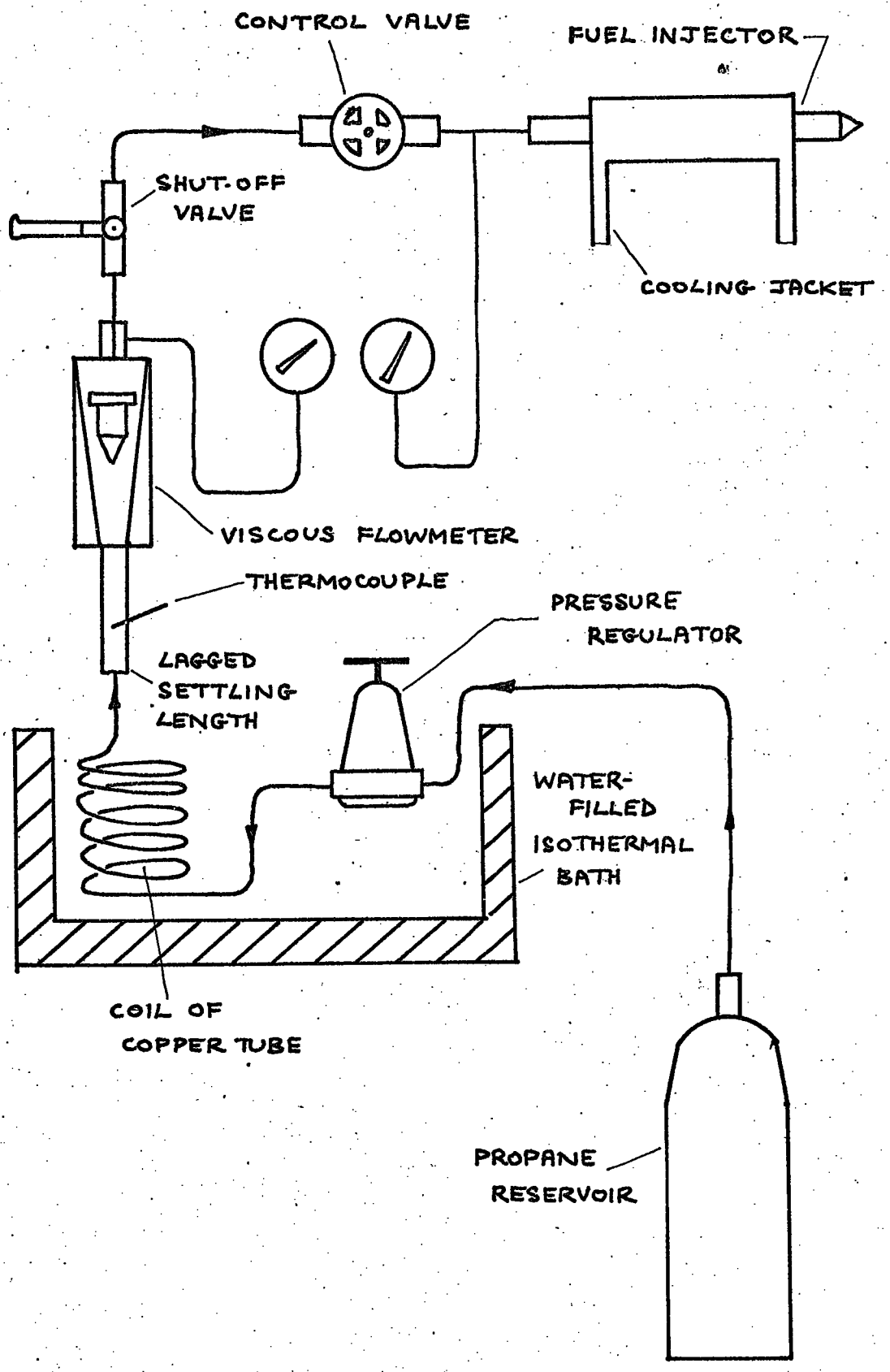

FIGURE 3.7: LAY-OUT OF FUEL SYSTEM

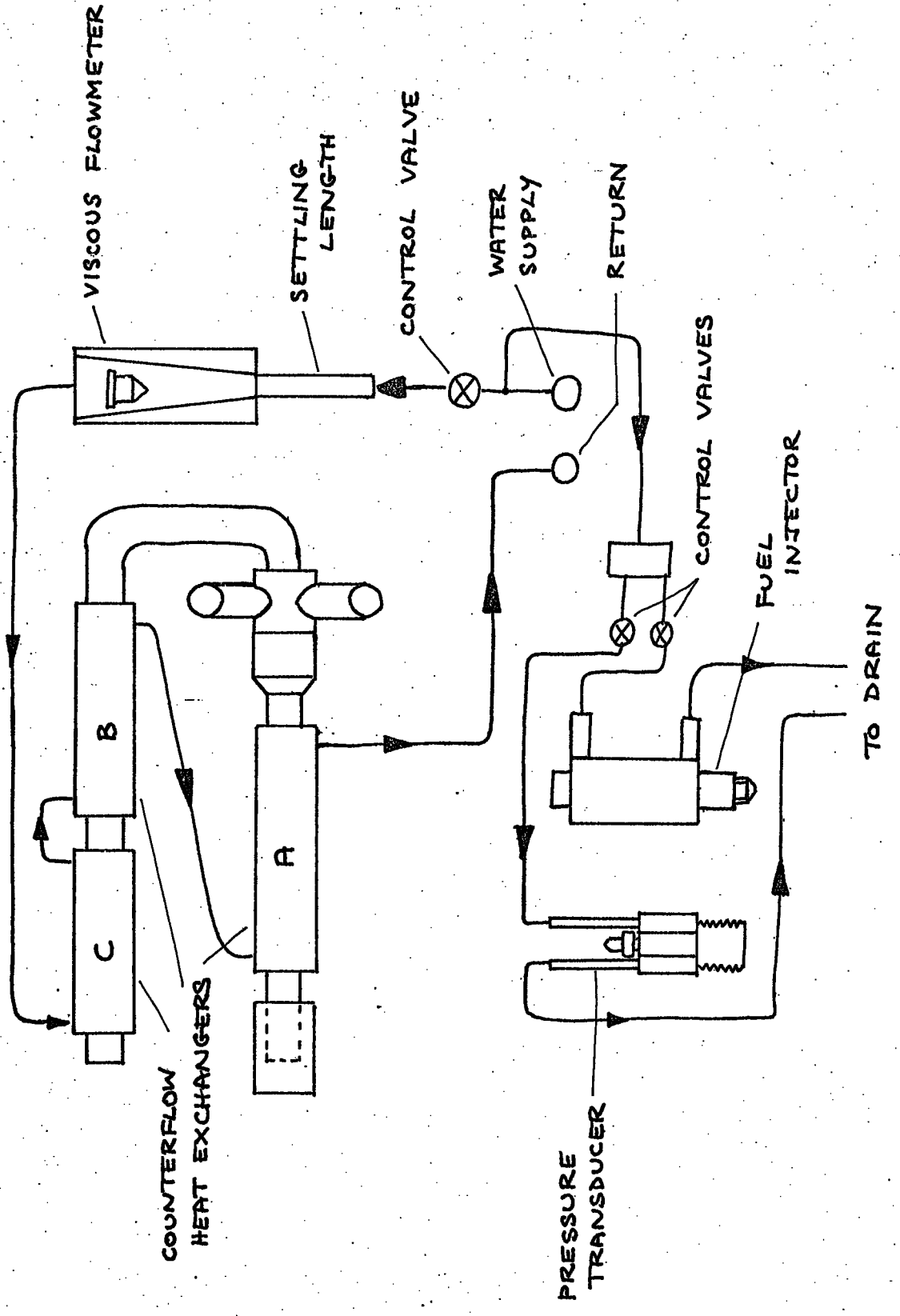

FIGURE 3.8: COOLING WATER SYSTEM

In addition a small jet set a limit on the maximum fuel flowrate, as the maximum propane regulator pressure was approximately 270 kN/m^2.

3.3 The Water System

The water, which was passed in a counterflow direction through heat exchangers A, B and C, was drawn from the Laboratory cooling system for heat engines. A diagram of the circuit is shown in Figure 3.8. The rate of flow was measured by a viscous flowmeter, Rotameter Type Metric 24E. A scale, graduated in litres/minute, was supplied with this instrument but, as only the lower part of it was used during the experiments, it was necessary to improve the accuracy of $\pm$ 5 per cent full scale reading. A calibration of the flowmeter was therefore made, using a vessel, a weighing machine and a stopwatch to measure the mass of water flowing per second for a given scale reading. The result is shown in Figure 3.9, the accuracy being improved to $\pm$ 0.5 per cent of indicated flow. As the laboratory cooling water contained small quantities of grit and rust, it was necessary to clean the tube and float occasionally.

The flowrates of cooling water through the fuel injector and through the transducer adaptor were each measured with a graduated flask and a stopwatch, the method being accurate to $\pm$ 0.3 per cent of the reading.

3.4 Measurement of Temperature

The measurement of gas and water temperatures within the apparatus was made with thermocouples and thermometers of the types shown in Table 3.1, and the circuit used for all the thermocouples is shown in Figure 3.10.

FIGURE 3.9 : CALIBRATION OF ROTAMETER TYPE METRIC 24E FOR WATER

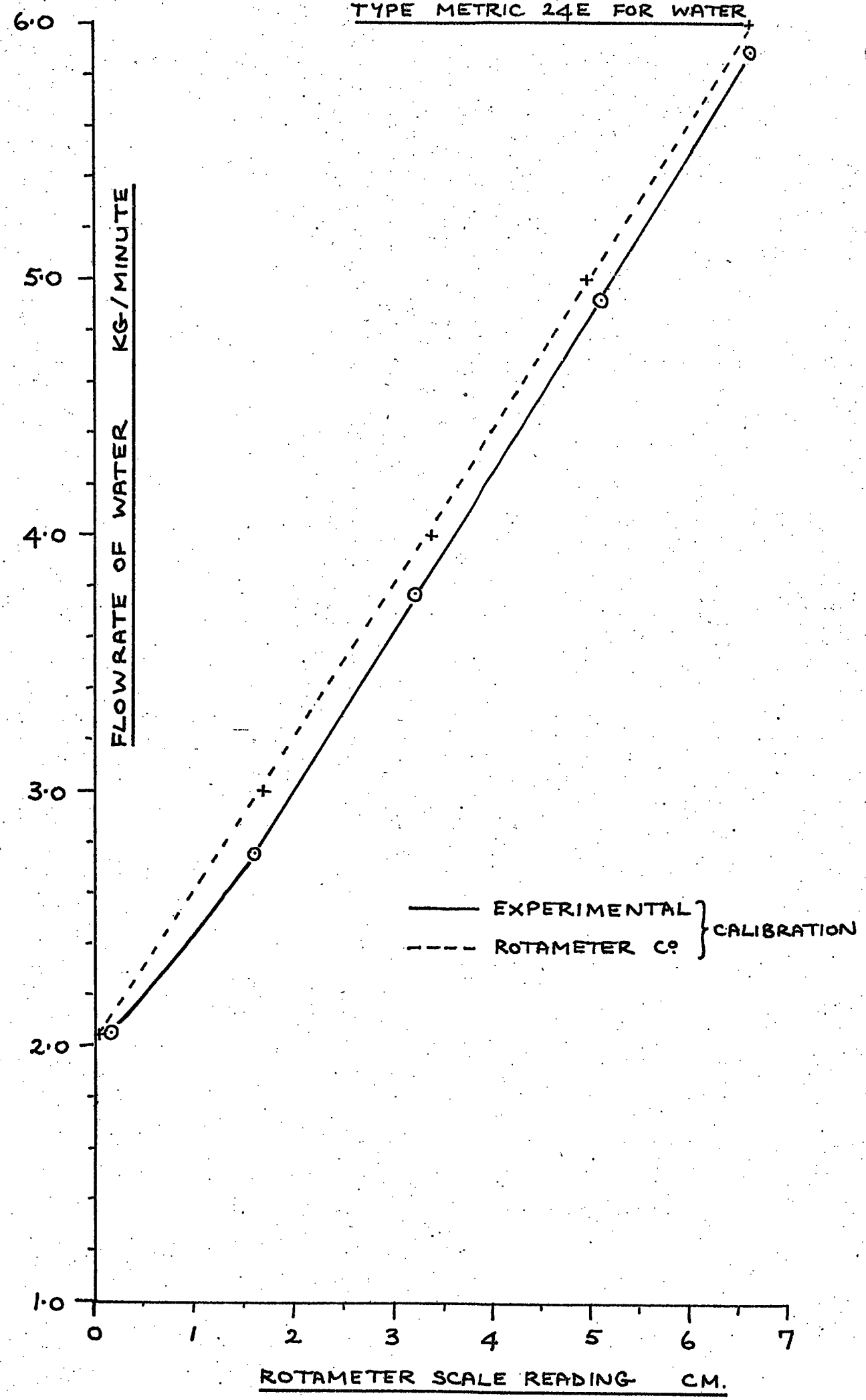

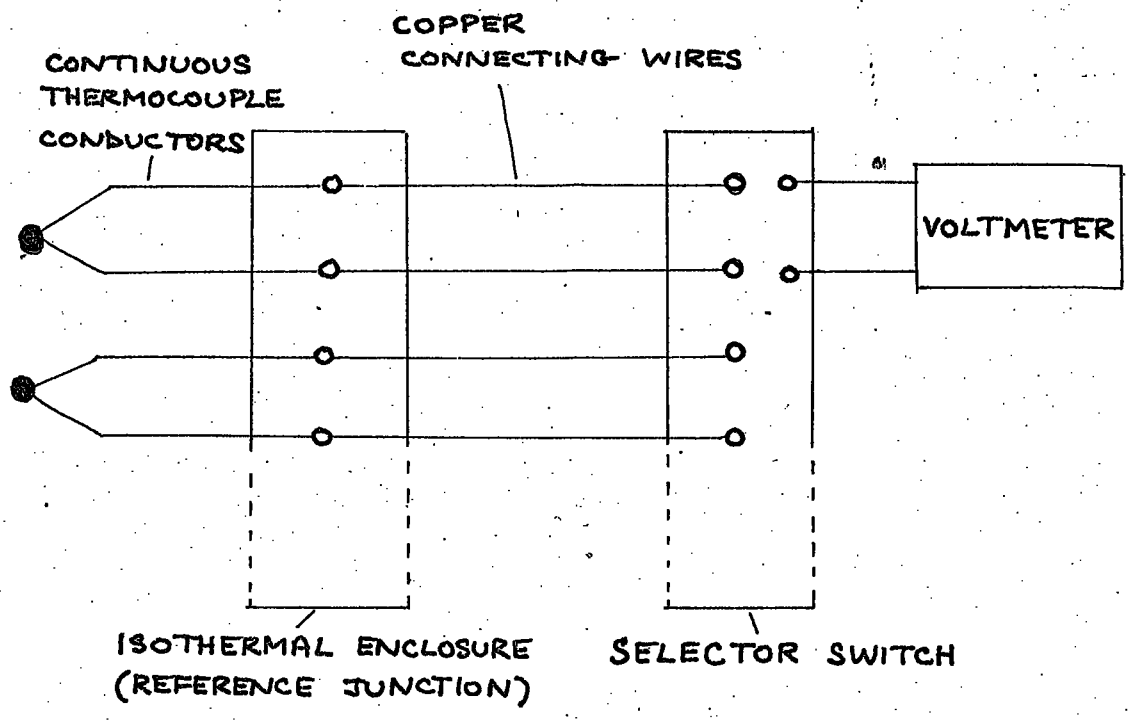

FIGURE 3.10 : THERMOCOUPLE CIRCUIT

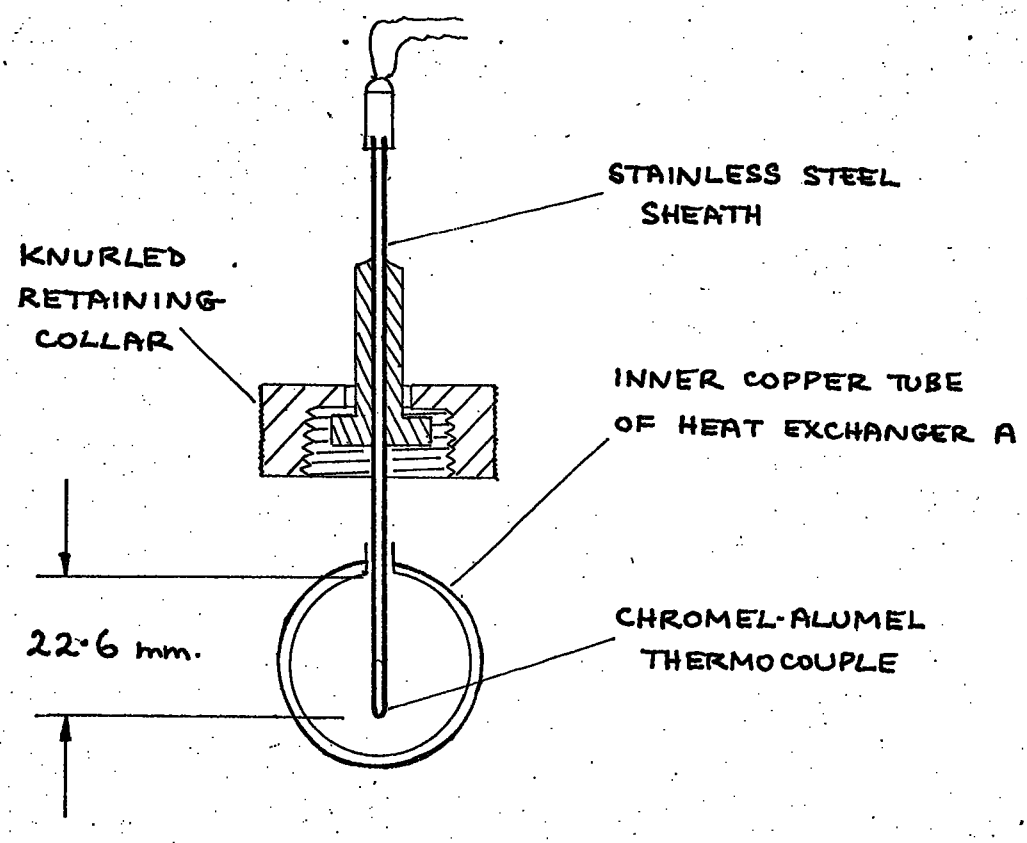

FIGURE 3.11 : GAS TEMPERATURE THERMOCOUPLE — TYPE K

Table 3.1 Types of thermocouple and thermometer

Thermocouple	Type K	Ni-Ch/Ni-Al	± 3°C < 400 °C ± 0.75% > 400°C
Thermocouple	Type S	Pt-10%Rh/Pt	± 1.5%
Thermocouple	Type T	Cu/Con	± 1°C
Thermometer		Hg-in-glass	± 0.2°C

The unbroken thermocouple wires were led to an isothermal enclosure, comprising a wooden box, where connections were made, using electrical 'tagstrip', to the copper connection wires. These wires were connected to a selecting switch, mounted on an isothermal enclosure, again using the 'tagstrip'. The selecting switches were supplied by the Croydon Precision Instrument Company and had silver-plated terminals. The output terminals were connected to a digital voltmeter, Solartron Type LM.1420.2.

3.4.1 Gas Temperature

The gas temperatures, $T_{A2} - T_{A8}$, were each measured by screwing into the instrument sites the probe shown in Figure 3.11. When in position, the thermocouple junction projected approximately 22 mm. into the tube. The temperature of the junction was not that of the flowing gas as it was influenced by the effects of radiation, conduction and convection. Corrections were complicated by the presence of the oscillations. An analysis of the errors of this measurement has been made in Appendix C. The highest gas temperature, T_{A1}, was measured by a thermocouple mounted in a silica tube, shown in Figure 3.12. The tube, which had a nominal outside diameter of 4.8 mm., possessed twin

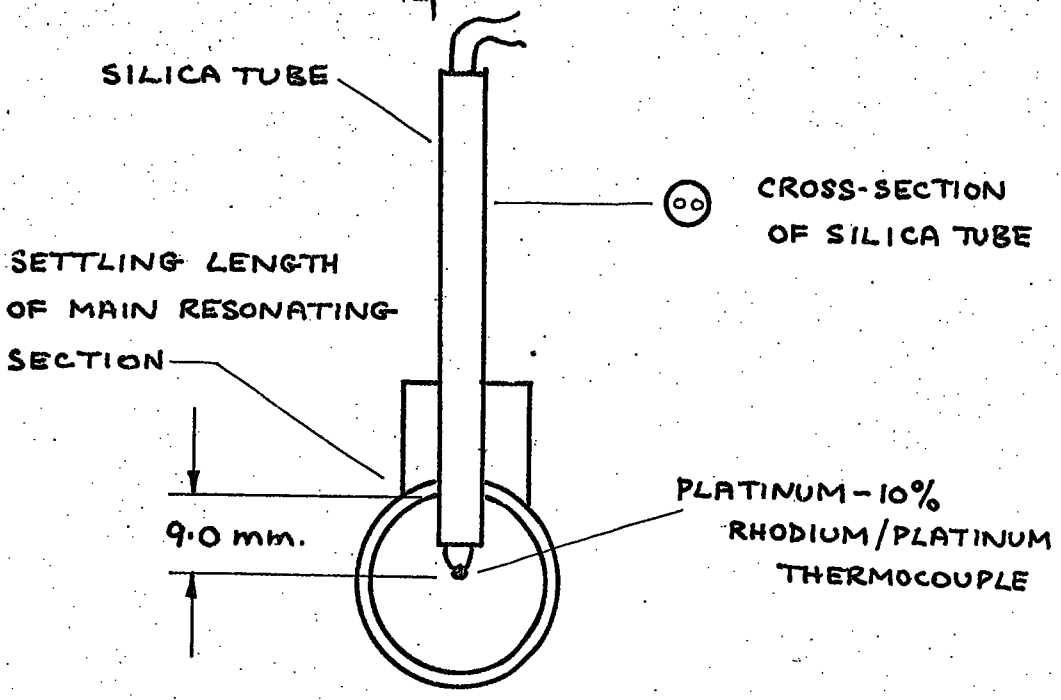

FIGURE 3.12: GAS TEMPERATURE THERMOCOUPLE – TYPE S

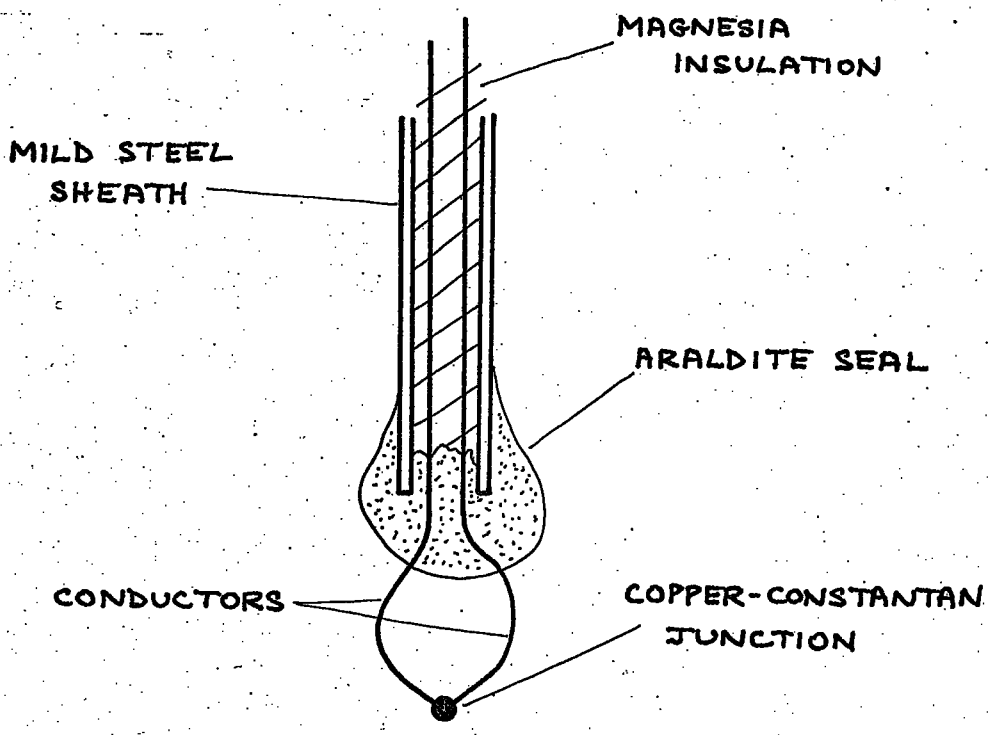

FIGURE 3.13: DETAIL OF CONSTRUCTED THERMOCOUPLES

bores, through which the thermocouple wires were passed, and was obtained from Thermal Syndicate.

The gas temperatures, T_{A21}, T_{A22} and T_{A23} were measured in a manner exactly similar to that described earlier in this section except that three thermocouples were used and fixed in place permanently.

3.4.2 Water Temperature

The seven Type T thermocouples in Heat Exchanger A, used to measure the water temperature, were constructed from a continuous coil of thermocouple cable. This consisted of a mild steel sheath, 1.6 mm. outside diameter, containing the copper and constantan conductors packed in magnesia insulation. It was obtained from Pyrotenax. The construction of the junctions was a delicate operation, and the advice contained in their manual (47), was followed. Due to the hygroscopic nature of the refractory insulant, the two ends of the thermocouple were dried and sealed with Araldite. The finished thermocouples (see Figure 3.13) were checked to ensure that the insulation resistance between conductors and sheath exceeded 100 $k\Omega$ and that the electrical circuit was continuous.

The remaining water temperatures, T_{W1}, T_{W9}, T_{W21}, T_{W22}, T_{W23}, T_{WTR}, and T_{WIN} were all measured with mercury-in-glass thermometers, Type TJ-070, obtained from Gallenkamp. These were total immersion thermometers, graduated in 0.2 ^{o}C with a range -5 to 105 ^{o}C. They were immersed in oil in thermometer pockets of the type illustrated in Figure 3.14 in the case of T_{W1}, T_{W9}, T_{W21}, T_{W22} and T_{W23}, and of the type shown in Figure 3.14 in the case of T_{WTR} and T_{WIN}. The corrections to the readings due to the incorrect immersion is considered in Appendix C.

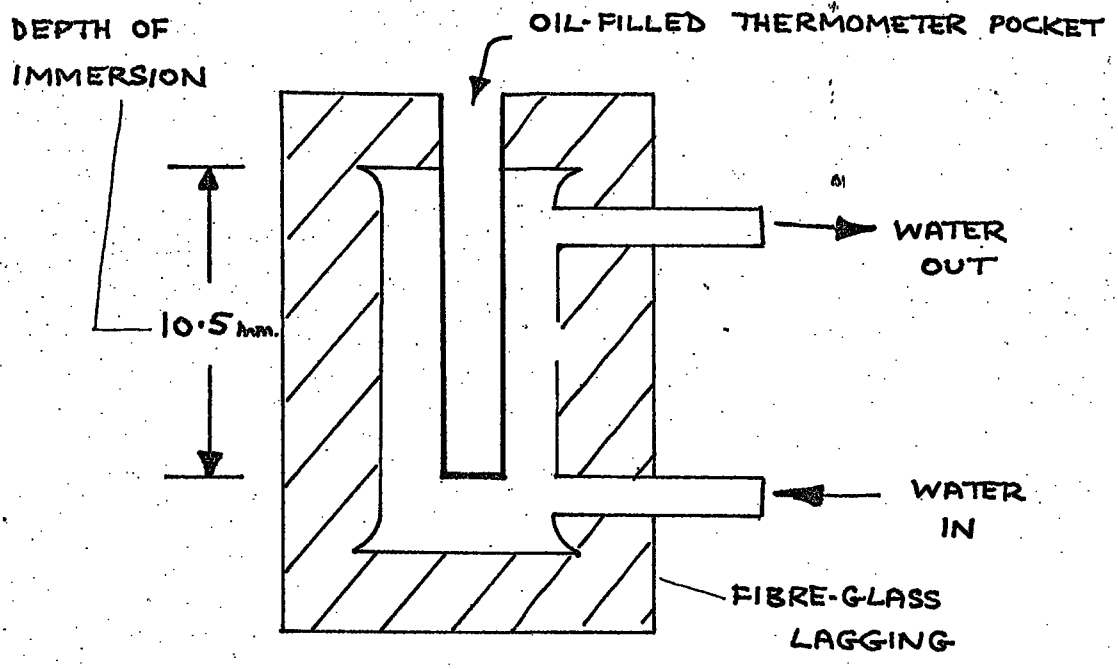

FIGURE 3.14: THERMOMETER POCKET

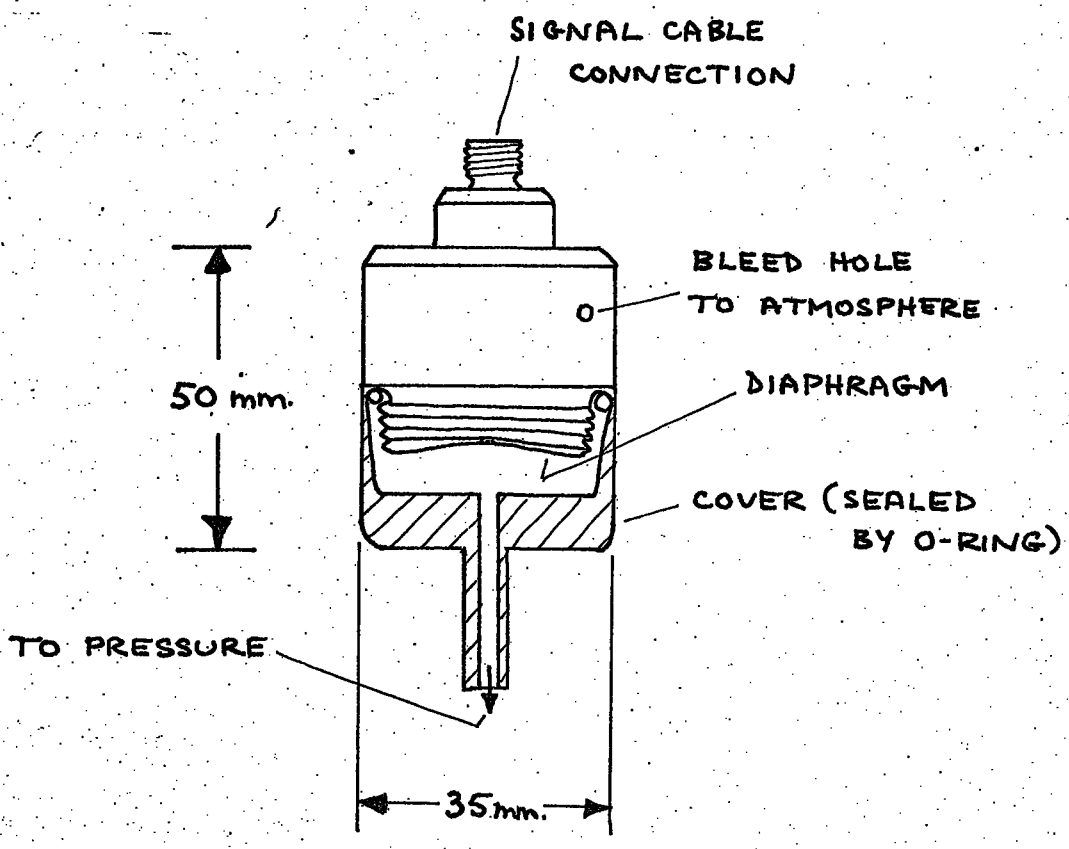

FIGURE 3.15: KISTLER TYPE 412 PRESSURE TRANSDUCER

3.5 Measurement of Pressure

A very important measurement in the experiments was that of pressure. It was found in the preliminary experiments that:

a) the pressure waveform of the oscillations was approximately sinusoidal;

b) the mean static pressure throughout the combustor was approximately atmospheric.

Therefore it was decided not to take any further measurements of the static mean pressure, and to assume that the pressure oscillated about the mean atmospheric value.

There were ten sites on the resonating section where measurements of pressure amplitude could be taken. They are listed in Table 3.2. It was decided to use one transducer, and this was inserted into each of the sites in turn.

Table 3.2 Axial Position of Measuring Sites

	x
P_{AC}	0.032
P_{A1}	0.190
P_{A2}	0.476
P_{A3}	0.654
P_{A4}	1.010
P_{A5}	1.365
P_{A6}	1.721
P_{A7}	2.076
P_{A8}	2.451
P_{A9}	2.821
P_{A10}	3.047
	m.

3.5.1 Time-dependent static gas pressure

The preliminary investigation showed that the instrument used for measuring the pressure variations in the hot gases had to be sensitive to oscillations between 30 and 300 Hz, to pressure amplitudes in the range 1 to 20 Hz and to be independent of temperature. It was decided to use a transducer available in the laboratory and manufactured by the Kistler Instrument Ag. Details are given in Table 3.3 and Figure 3.15.

Table 3.3 Transducer data

Kistler Type 412 static pressure transducer Serial No. SN33502		
Max. measuring range	0 - 10	Atm.
Calibrated partial ranges	0 - +1 -1 - 0	" "
Resolution	1.5×10^{-5}	"
Sensitivity	2230	pc/Atm
Resonant frequency	7500	Hz
" with cover	350	Hz
Max. error for each range	1	%
Working temperature range	-150 - +240	^{o}C

The mounting for the pressure transducer is shown in Figure 3.16, where it is illustrated connected to a site on the heat exchanger. The two longer lengths of tube were found to be necessary due, firstly, to the high wall temperature of the combustion chamber and, secondly, to the augmenter sliding over the exhaust pipe, thus limiting access to it, as shown by Figure 3.6.

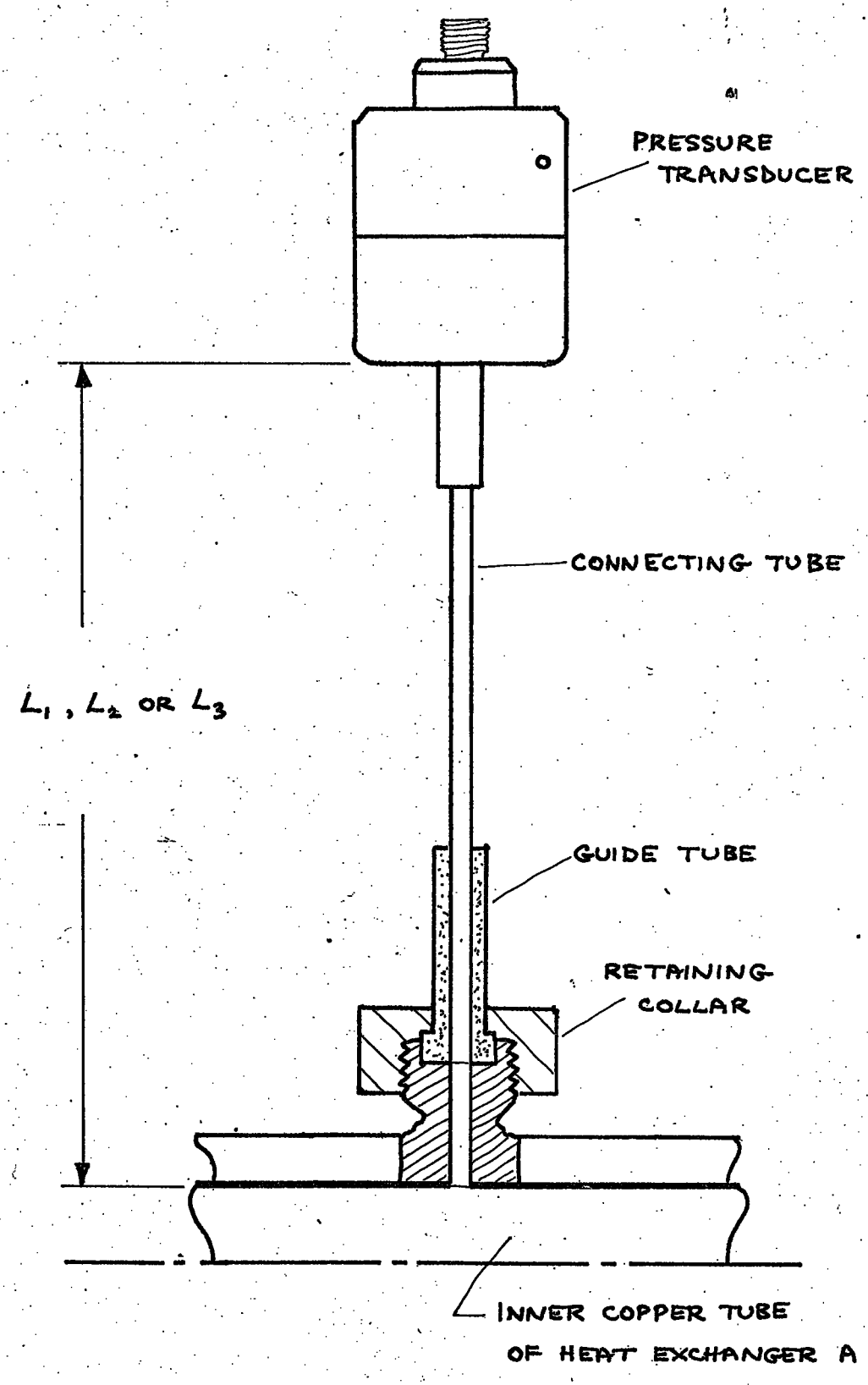

FIGURE 3.16 : PRESSURE TRANSDUCER MOUNTING

Considering the system shown in Figure 3.17, the attenuation of p_o, the pressure signal, is given by Holman (48) to be:

$$\left|\frac{p}{p_o}\right| = 1/\left\{\left[1-\left(\frac{\omega}{\omega_n}\right)^2\right]^2 + 4h^2\left(\frac{\omega}{\omega_n}\right)^2\right\}^{1/2} \qquad 3.5.1$$

where the natural frequency, ω_n, of the transmitting volume is:

$$\omega_n = \left\{\frac{3\pi r^2 c^2}{4LV}\right\}^{1/2} \qquad 3.5.2$$

The damping ratio, h, which is expressed as a laminar frictional resistance, is given by:

$$h = \frac{2\mu}{\rho c r^3}\left\{\frac{3LV}{\pi}\right\}^{1/2} \qquad 3.5.3$$

and the phase angle for the pressure signal is:

$$\phi_{ph} = \tan^{-1}\left\{\frac{-2h\left(\frac{\omega}{\omega_n}\right)}{1-\left(\frac{\omega}{\omega_n}\right)^2}\right\} \qquad 3.5.4$$

It was assumed that the fluid in the connecting tube and dead volume was air at 20 ^{o}C and the following data was put into equations 3.5.2 and 3.3.3;

$V = 1.5 \times 10^{-6}\ m^3$

$r = 0.8\ mm.$

$\mu = 1.85 \times 10^{-5}\ kg/m\ s$

$\rho = 1.18\ kg/m^3$

$c = 345\ m/s$

Evaluation of the equations gives:

$$\omega_n = \frac{345}{\sqrt{L}} \qquad 3.5.5$$

$$h = 0.0213\sqrt{L} \qquad 3.5.6$$

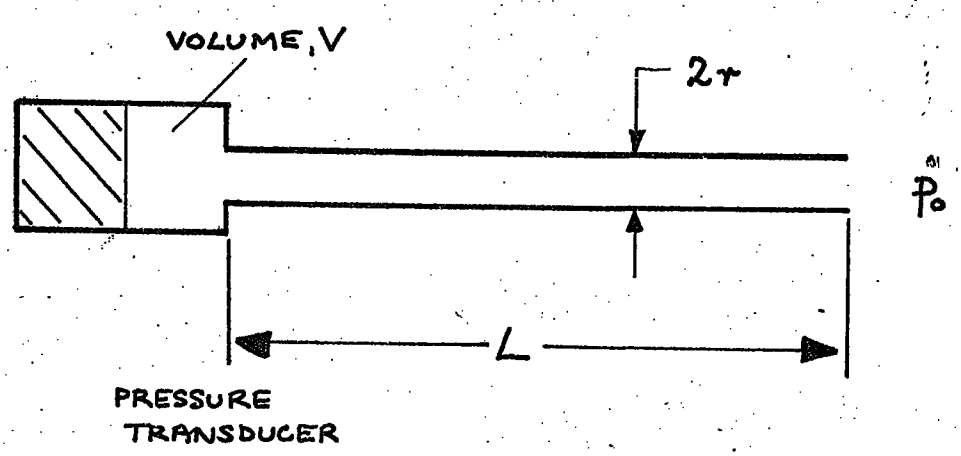

FIGURE 3.17 : IDEALISED PRESSURE MEASURING SYSTEM

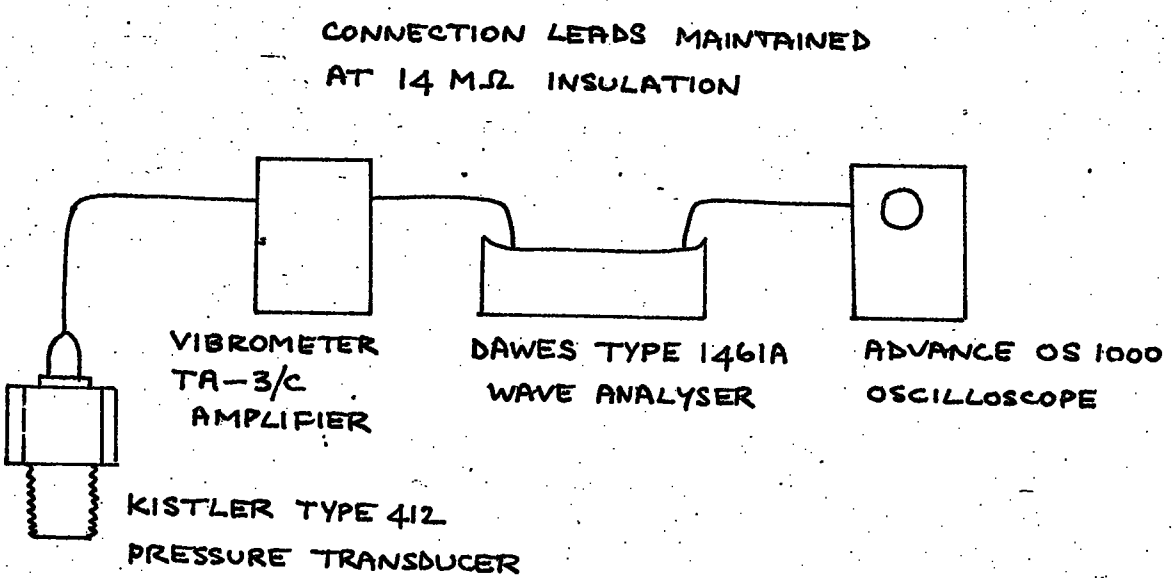

FIGURE 3.19 : APPARATUS FOR AMPLIFICATION AND ANALYSIS OF PRESSURE SIGNALS

FIGURE 3.18 : VARIATION OF PRESSURE SIGNAL ATTENUATION WITH FREQUENCY FOR THREE LENGTHS OF CONNECTING TUBE

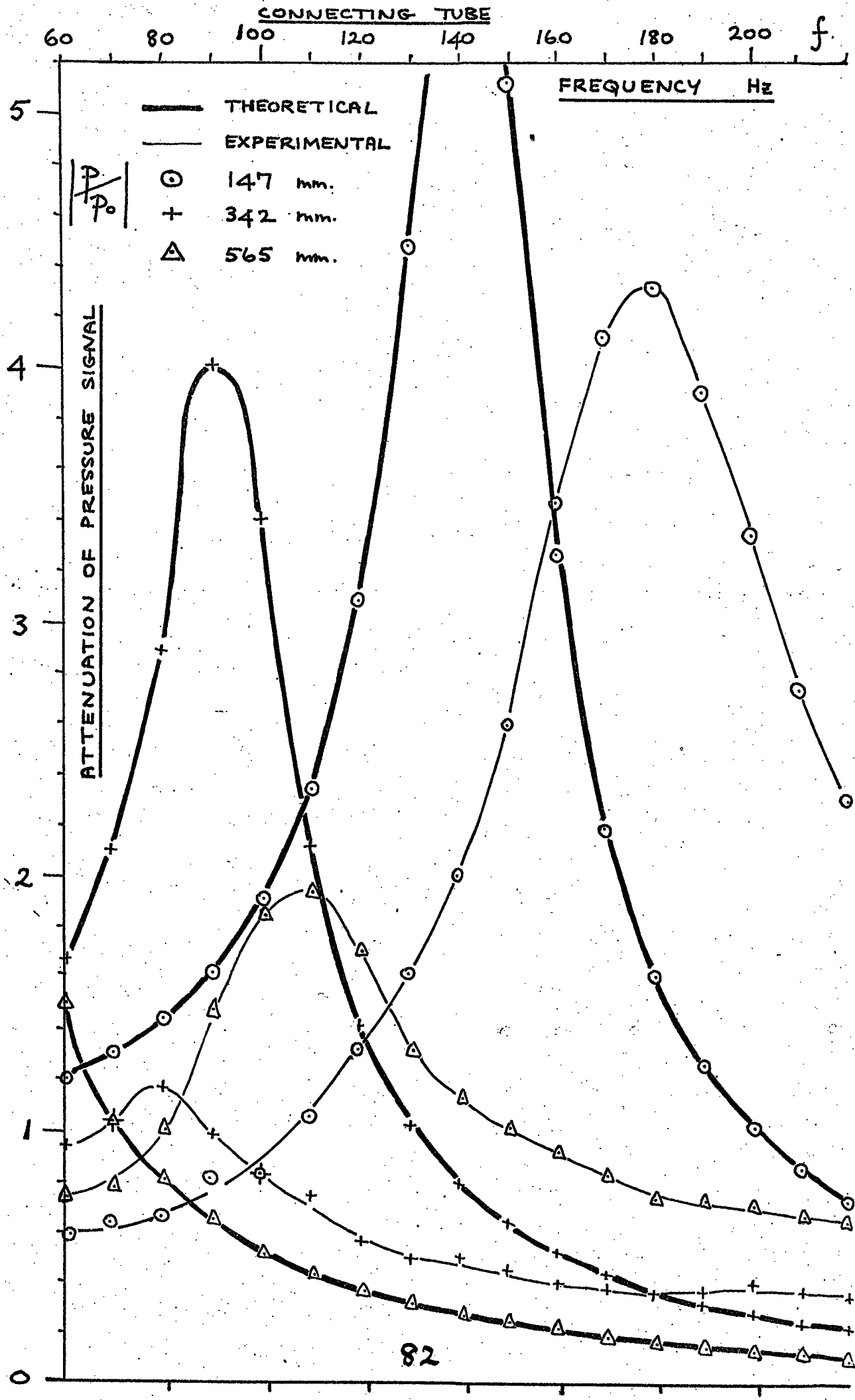

The resonant frequencies and damping factors are therefore:

$\omega_{n_1} = 143$ Hz $\quad h_1 = 0.0815$

$\omega_{n_2} = 94$ Hz $\quad h_2 = 0.1246$

$\omega_{n_3} = 73$ Hz $\quad h_3 = 0.1600$

for $L_1 = 147$ mm.

$L_2 = 342$ mm.

$L_3 = 565$ mm.

respectively.

It was decided to calibrate the transducer mountings experimentally, using a loudspeaker, driven by an audio wave generator, and a microphone of known response. The details of the experiment are given in Appendix D. The results of the experiment and of equation 3.5.1 are shown in Figure 3.18, where attenuation $\left|P/P_0\right|$ is plotted against frequency for the range 60 to 220 Hz. The main observations from the graph are summarised in Table 3.4, where the three different transducer mountings are identified by connecting tube length.

Table 3.4 Maxima from Figure 3.18

	Theoretical		Experimental	
Length	Attenuation	Frequency	Attenuation	Frequency
147	6.16	143	4.30	180
342	4.0	90	1.16	80
565	-	-	1.94	108
mm.		Hz		Hz

Numerically there is little agreement between the two sets of values. With respect to shape, the curves are substantially similar, the

resonances being displaced by from 10 Hz in the case of L_2 = 342 mm. up to approximately 90 Hz in the case of L_3 = 565 mm. The reason for this is not clear. The lower peak value of the experimental resonances is in all probability due to underestimation of the frictional losses in the connecting tube fluid.

The response of the Kistler transducer without cover and connecting tubes was compared, using the same method and apparatus, with that of the microphone. The two agreed to within $\pm$ 0.5% over the whole range. The disparity between the experimental calibration and the theoretical one was probably caused by distortion in the sound field so close to the loud speaker cone. This would have been accentuated by the difference in cross-sectional area between the microphone diaphragm and the connecting tube end, which were 1960 and 2.01 mm^2 respectively. As it was impossible to estimate accurately the errors in the experiment it was decided that the analysis of Holman should be used to determine the attenuation of the pressure waves within the transducer connections.

Figure 3.19 shows a diagram of the apparatus used to amplify the signal from the Kistler transducer. The charge amplifier was Type TA-3/C, manufactured by Vibro-Meter Ag. The amplified signal from it was filtered by a Dawe Type 1461 A Wave Analyser, and the filtered signal was displayed on an Advance OS 1000 oscilloscope. The magnitude of the pressure amplitude was measured by means of the graticule on the screen, graduated in millimetres. The signal connections were made with coaxial leads, and it was vital, when settling up the equipment, to maintain the insulation resistance to 14 MΩ. This was achieved with a Freon aerosol sprayed onto the

plugs and sockets before connection. The oscilloscope had a facility for rapid calibration of the y amplification and this was also done before experiments. This was always adjusted, when taking readings, so that the waveform filled the graticule. This procedure minimised reading errors. The oscilloscope was equipped with a single-shot facility and a mounting for a Polaroid camera. This permitted recordings of any pressure waveform to be obtained with difficulty. It was necessary only to set the brightness of the trace low, open the camera shutter, press the single-shot button and release the shutter. The film used was Kodak 107 and was developed in the recommended way.

The transducer sensitivity was 2230 ± 5 pc/Atm (Kistler calibration) and the charge amplifier potentiometer was set such that the system sensitivity was 0.199 ± 0.006 kN/m^2 per mm. on the oscilloscope graticule.

3.6.1 The Independent Variables

The independent variables for the experiments are listed in Table 3.5. Of the five, the preliminary investigation (Appendix B) showed that the effects of changes in B, C and E were small compared to changes in A and D.

Table 3.5 Independent Variables

A	Fuel flowrate	$0.13 < \dot{m}_p < 0.8$ kg/h
B	Water flowrate	$120 < \dot{m}_w < 588$ kg/h
C	Coolant flowrate	$1 < \dot{m}_{gc} < 10$ kg/h
D	Aero' valve diameter	$D_t = 13, 16, 19$ mm.
E	Augmenter position	$2.08 < x_{AUG} < 3.05$ m.

The following experiments were therefore carried out:

1) the combustor was operated to establish an energy balance for values of D = 13,16,19 mm. and $\dot{m}_p$ in the range 0.13 to 0.6 kg/h. Application of the First Law to a control volume around the apparatus permitted a table of energy exchanges to be drawn up;

2) the combustor was operated at gradually increasing fuel flowrates, and measurements of frequency and gas and chamber temperatures were taken. By this means, the resonant frequencies of the combustor were found for varying gas temperature distributions;

3) the combustor was finally operated to obtain data from which the local and overall heat transfer coefficients could be calculated. Pressure amplitudes were measured also, and the velocity amplitude of the gas was deduced by assuming a sinusoidal variation with time. From these results correlations of $\frac{Nu_p}{Nu}$ against x were plotted.

3.6.2 Experimental Technique

The combustor was started by supplying a combustible mixture of fuel and air to the chamber and igniting it with a high tension spark. A flow of propane in the range $0.19 < \dot{m}_p < 0.49$ kg/h was required for this purpose, and a suitable flow of air, directed into the aerodynamic valve, was found by experiment. Once the combustor had started, the forced air supply could be shut off, although the combustion would sometimes quench if this was done when the chamber walls were below approximately 260 °C. Great care was taken when using the trembler coil to ensure that all the electronic apparatus was grounded. Failure to follow this precaution could have led to an instrument malfunction due to the inductance of the connecting signal leads.

It was found that the combustor required nearly an hour to reach thermal equilibrium. This condition was taken to be when the chamber temperature varied by less than 2 °C per minute. Clearly the process was accelerated by setting a high fuel flowrate. Before readings could be recorded, it was necessary to check that the fuel gauge pressure, P_p, and temperature, T_p, were set correctly, and that the water flowrate was steady. For all experiments the local atmospheric pressure and temperature were recorded before and after the readings were taken.

The operation of the apparatus for experiment 1 presented no particular difficulties. Readings were taken every 5 minutes for a period of 30 minutes. For experiment 2, the combustor had to be operated at first at a very low fuel flowrate to obtain its lowest resonant frequency, and the pressure amplitude was found to be very

unsteady. The combustor also did not remain in thermal equilibrium as its lowest frequency. For these reasons, it was necessary to collect the data briskly and thus the accuracy of the experiment suffered. For higher fuel flowrates and thus higher frequencies, the combustor did reach equilibrium, and the accuracy improved.

During experiment 3, it was found that the combustion became slightly unstable when the caps on the instrument sites were removed. Thus several minutes were allowed to elapse while the apparatus, and the inserted instrument, reached equilibrium once more.

4.1. The Energy Balance

The results of Experiment 1 are presented in Appendix E. The double-orifice pulsating combustor is a flow process and, therefore, by drawing a Control Volume around the apparatus, as in Figure 4.1., the First Law of Thermodynamics may be applied in the form of the Steady Flow Energy Equation. The discrepancy between the two sides of the equation lay within the range -5.7 to +10.0%. This was regarded to be acceptable. The calculations also yielded the variation of the thermal efficiency with the fuel flowrate, and this has been plotted in Figure 4.2. The graph shows that the thermal efficiency decreases with increasing fuel flowrate. This trend was found with earlier combustors, as shown in Figure 3.5. and was observed by Hanby (39) and Reay (20). The thermal efficiency varies from 0.74 to a maximum of 0.94. It is difficult to choose an aerodynamic valve which performs best. D_I = 13mm. gave the best efficiency over the range of fuel flowrate but D_I = 16mm. attained the maximum efficiency.

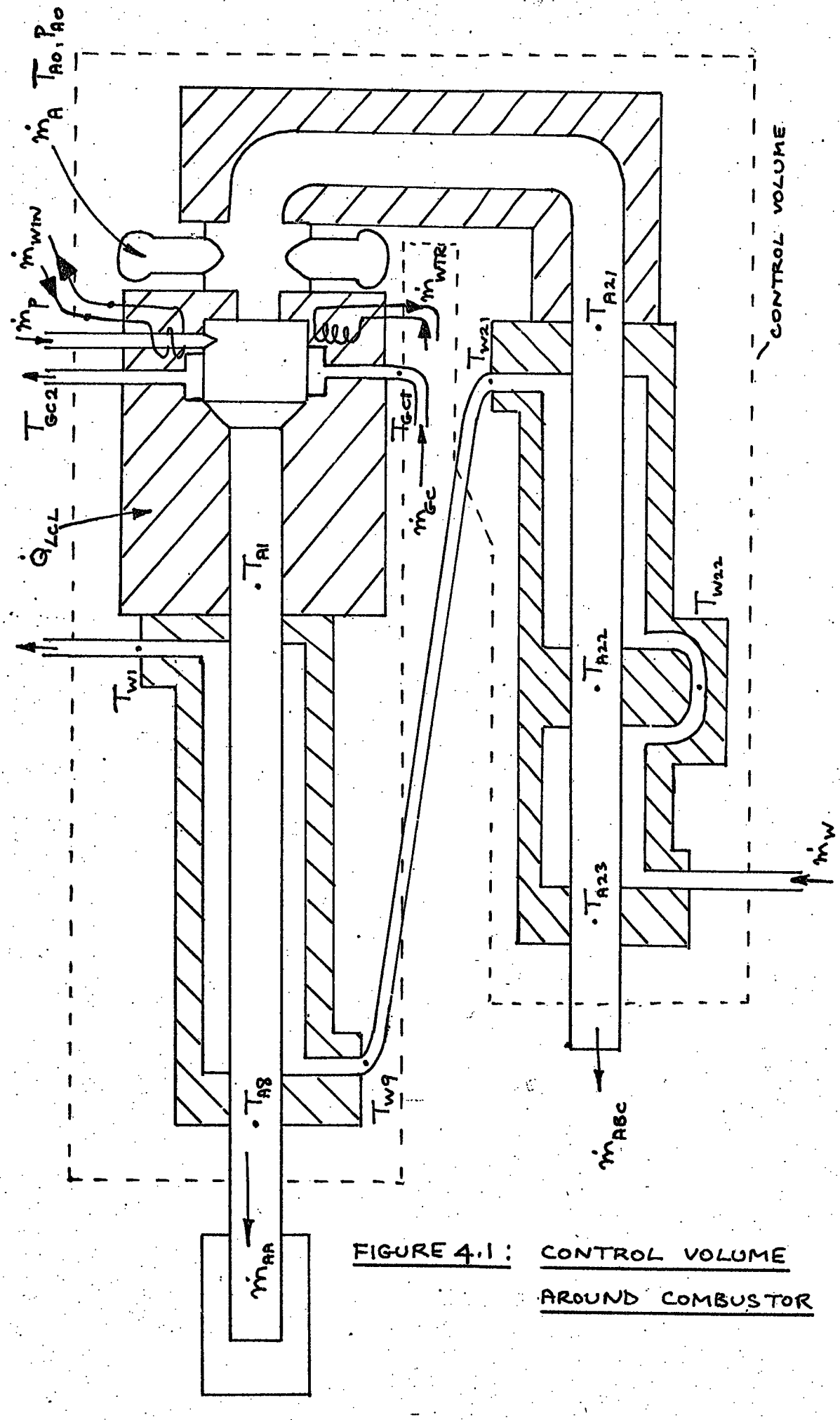

FIGURE 4.1 : CONTROL VOLUME AROUND COMBUSTOR

	D_I	
⊙	19	mm.
×	16	mm.
△	13	mm.

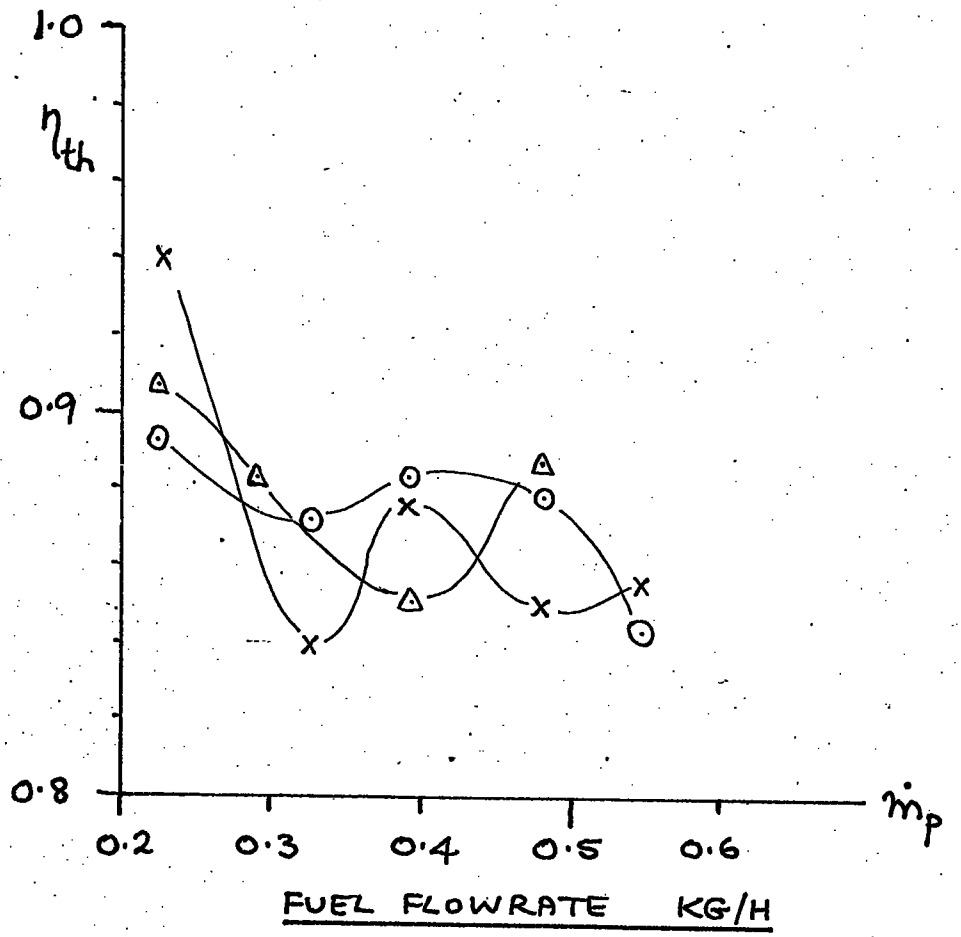

FIGURE 4.2: VARIATION OF THERMAL EFFICIENCY OF COMBUSTOR WITH FUEL FLOWRATE

4.2. The Aerodynamic Valve

The net flow of air, $\dot{m}_{AR}$, through the aerodynamic valve was deduced from the results using equation E.1.17. Knowing the corresponding pressure amplitude in the combustion chamber, it was possible to compare the experimental results with the values obtained by the quasi-steady state approach of Section 2.5. The comparison may be made in Figure 4.3.

It is evident that the experimental curves follow the theoretical ones approximately in shape, but, except the theoretical ones for D_I = 13mm., do not agree in magnitude. It is interesting to note that the pressure amplitude reaches its maximum value for D_I = 19mm. The curves verify the experimentally observed fact that the combustor pumps its own combustion air through itself. The difference between the curves is due to the assumptions made in the quasi-steady state approach. These were that the flow was a) isentropic and b) frictionless, and that c) the kinetic energy of the fluid entering the valve during the cycle was negligible compared to that leaving it, and that d) the equation held at all instants of time. Of these assumptions, b) and d) are the most suspect. In addition, the fluid during the exhaust part of the cycle was hot combustion gas. It was assumed that the inlet air was at 520 °C by taking a mean of the profile shown in Figure 4.4. A Type K thermocouple was mounted on a probe, and the probe onto a rack mechanism, and fed into the valve and chamber. It shows that the mean temperature of the gases in the aerodynamic valve to rose from 215 °C at entry to 850 °C for = 0.409 kg/h. Figure 4.5. shows a temperature traverse of the combustion chamber itself for the same fuel flowrate. The maximum temperature of the gases occurs at the axis of the chamber, and the minimum at the walls. There appears to be an annulus of relatively cooler gas extending from the valve lip into the chamber along the axis. Also from Figure 4.5. this low temperature gas extends across the cross-section in Plane 7. This gas is cooler due to the heat exchange between it and the valve walls. The core is clearly highly turbulent from its rapid rise in temperature - 830 °C just past Plane Y

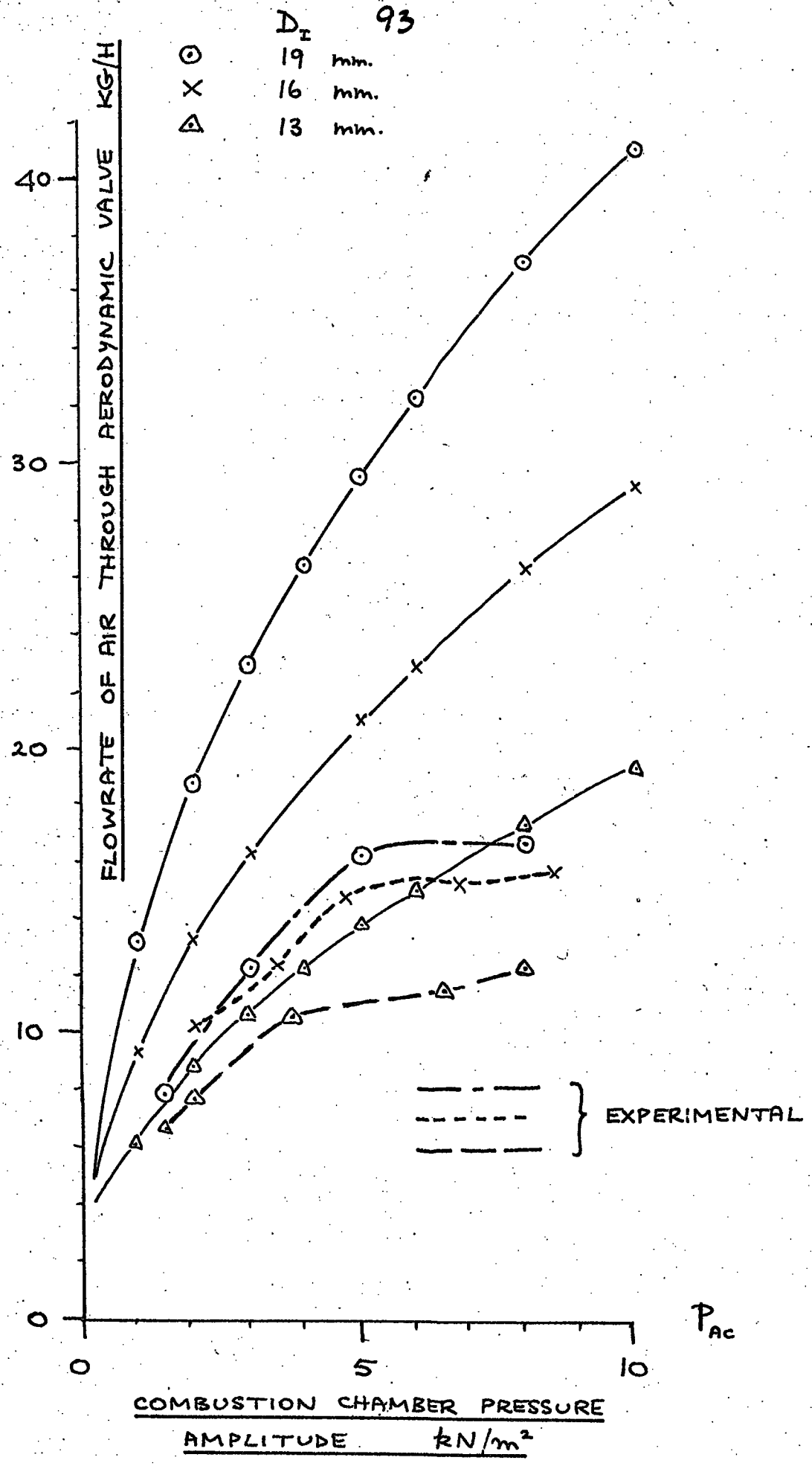

FIGURE 4.3 : NET FLOW THROUGH AERODYNAMIC VALVE — COMPARISON OF EXPERIMENTAL VALUES WITH THEORETICAL

FIGURE 4.4: AXIAL (TIME-AVERAGED) TEMPERATURE PROFILE OF GASES WITHIN COMBUSTION CHAMBER — $\dot{m}_p = 0.41$ kg/h

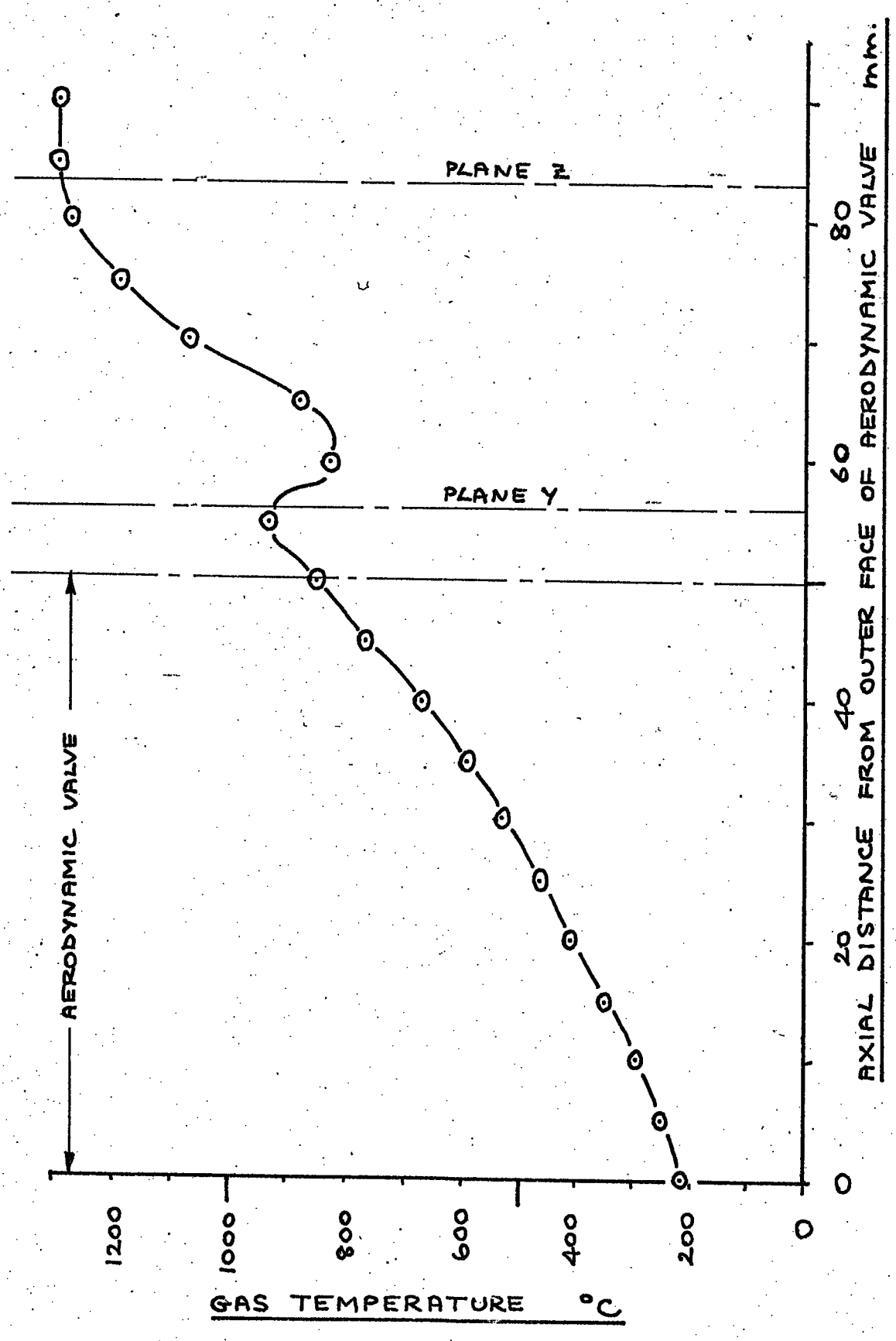

FIGURE 4.5 : TEMPERATURE TRAVERSES ACROSS COMBUSTION CHAMBER FOR TWO FUEL FLOWRATES

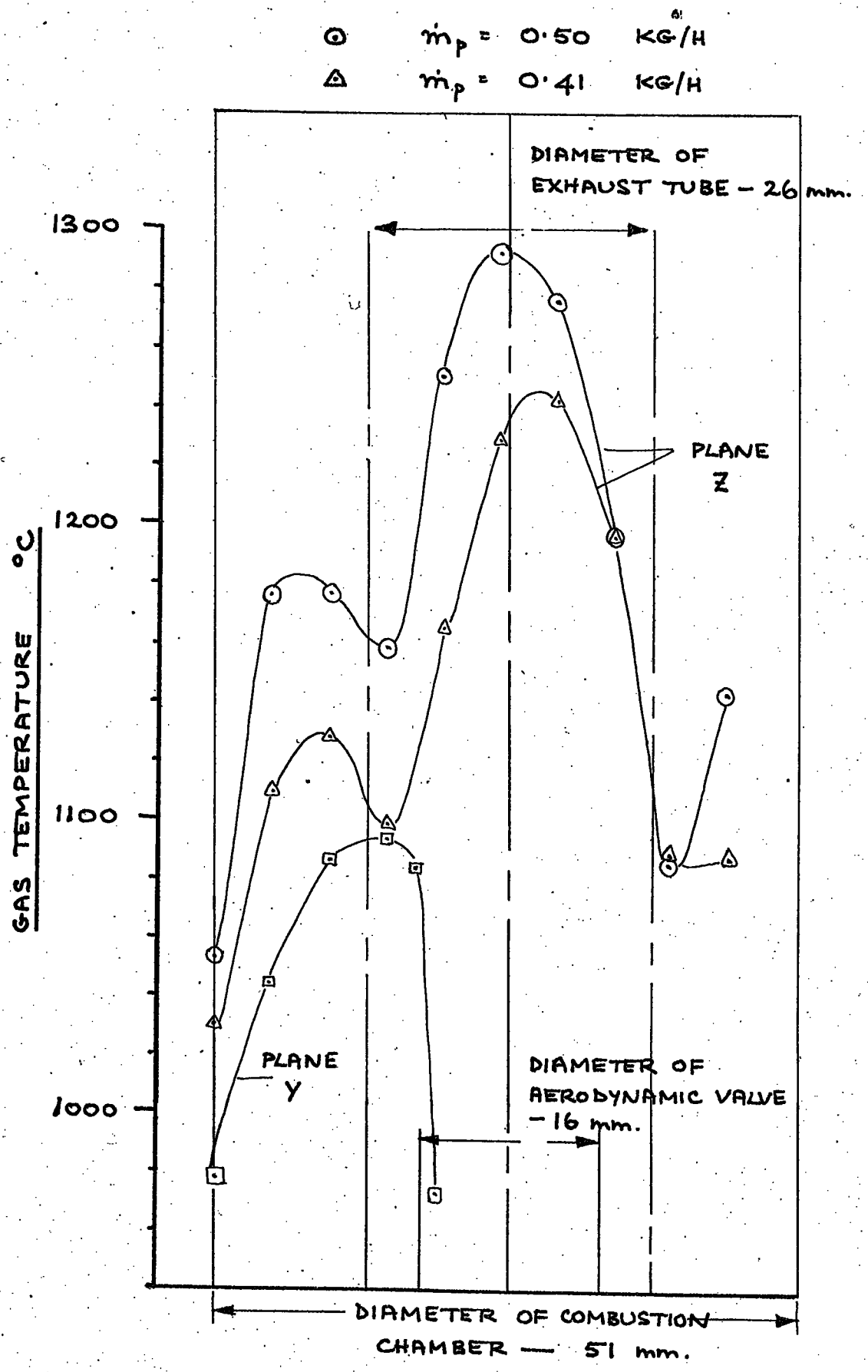

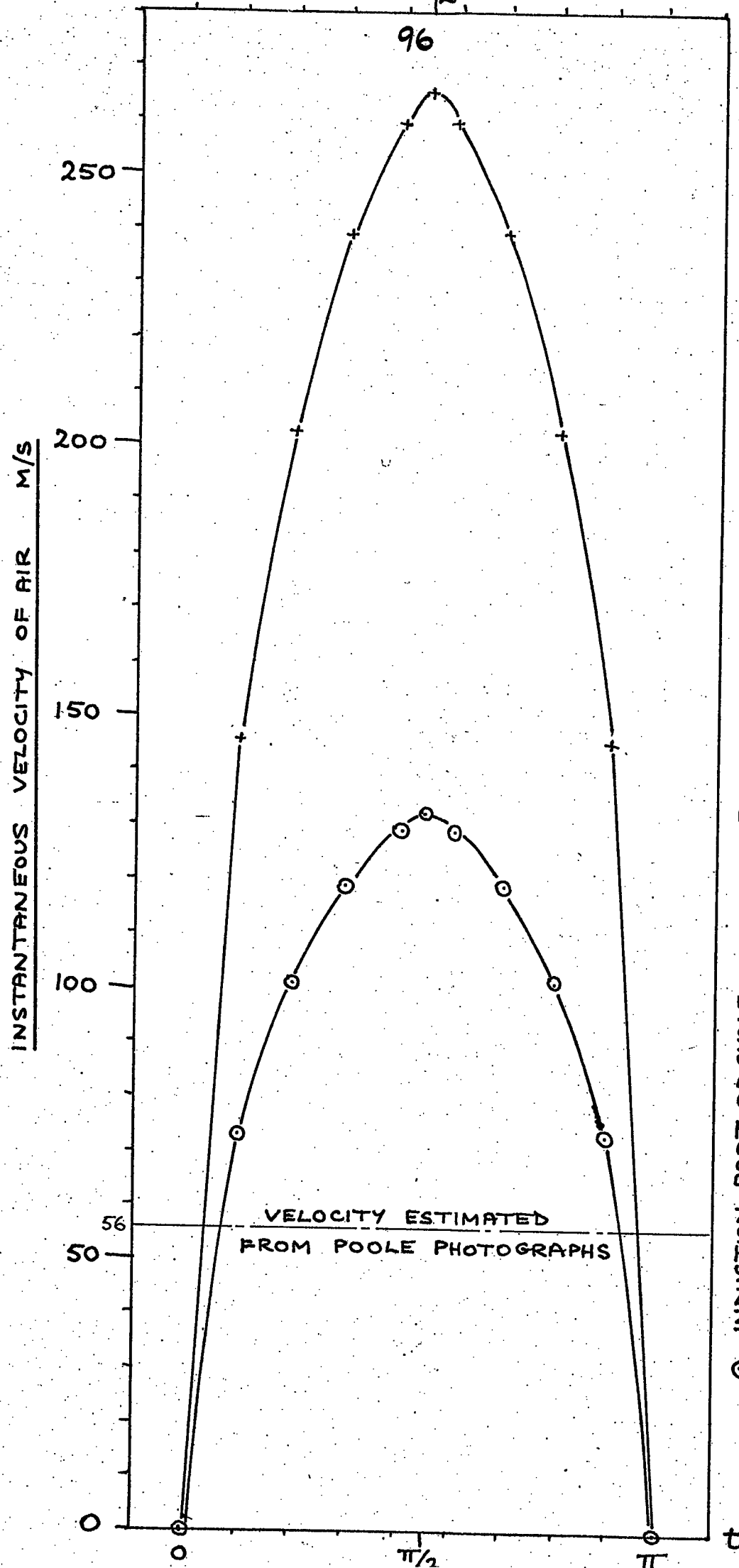

FIGURE 4.6: INSTANTANEOUS VELOCITY OF GASES WITHIN AERODYNAMIC VALVE

to 1300 °C at Plane Z, 27 mm. into the chamber. It is important to remember these are time-mean temperatures, and that events are occurring in reality at the rate of one cycle in 4 mS. The abrupt cooling of the gases in Plane Y may be due to a nozzle expansion effect. At high fuel flowrates, the combustion process emerged from the aerodynamic valve. It was the energy dissipation represented by this flame that led to the addition of heat exchangers B and C.

Using equations 2.5.9. and 2.5.11., the velocity of the gases passing through the aerodynamic valve were calculated for regular intervals during the cycle. These have been plotted in Figure 4.6., and show that the exit velocity of the gases is higher than the induction velocity. Given the discrepancy in Figure 4.3., it is probable that these velocities are generally too high. Tentative confirmation of this view was provided in a photographic study by Poole (49). Poole studied a pulsating combustor whose combustion chamber was fitted with quartz windows. Using a schieren technique, the combustion was filmed with a rotating prism high-speed camera at a rate of 8000 pictures per second. A typical sequence of 5 frames is shown in Figure 4.7. The pictures show a column of gas progressing along the axis of the combustion chamber, whose dimensions were similar to those employed in this study, the main difference being that the cross-section of the Poole chamber was square. The scale of the pictures is 1:1.695 and the time interval between them is 50 μS. The mean velocity of the line, marked A, over the five pictures is 56 m/s. This compares favourably with the values of Figure 4.6. The difficulty in making a strict comparison is to place the sequence of pictures correctly during the cycle. Examination of several whole cycles of pictures, and further work of Poole synchronising the pressure amplitude onto the film, suggests that the sequence of events in Figure 4.7. occurs approximately $\frac{\omega}{12\pi}$ before the maximum pressure in the chamber.

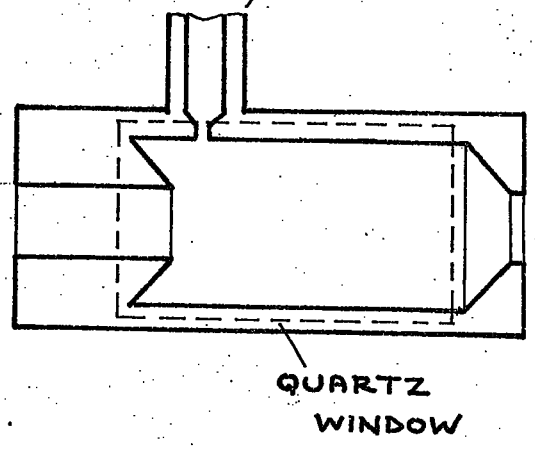

APPARATUS OF POOLE

The original of this photograph is held in the Science Library in the top copy.

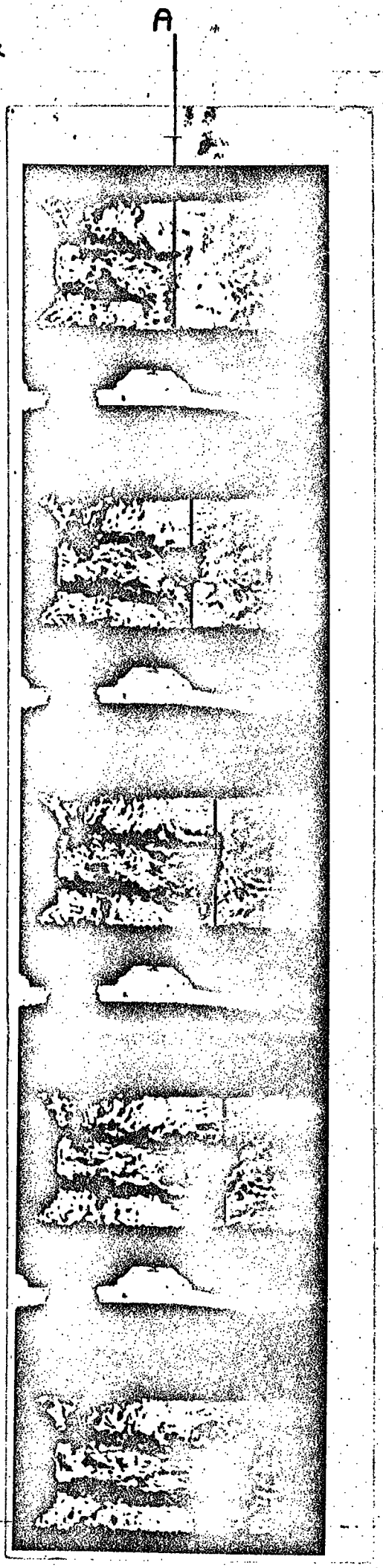

FIGURE 4.7: SCHLIEREN PHOTOGRAPHS FROM WORK BY K. POOLE

4.3. Characteristics of Resonating Section

The first result of experiment 2 is shown in Figure 4.8., where the operating frequency of the combustor is plotted against fuel flowrate. The graph has been divided into four parts by lines A, B, C and D. Up to A, the pressure oscillations in the combustion chamber were too small and irregular to be measured with any certainty. In the region AB the frequency varied from 59 to 70 Hz for D_I = 13 and 16 mm., and from 74 - 93 Hz for D_I = 19 mm. Then by increasing the fuel flowrate to and beyond B, the frequency would begin to jump and settle on a higher note. For D_I = 13 and 16 mm. this was approximately 117 Hz, and, for D_I = 19 mm., it was approximately 154 Hz. With increasing fuel flowrate a similar transition occurred around C where the frequency jumped to 193 Hz for D_I = 13 and 16 mm. and to 240 Hz for D_I = 19 mm. At D, the frequency jumped again for D_I = 16 mm. to 280 Hz. For clarity, the transition frequencies are shown in Table 4.A.

Table 4.A. Transition frequencies

D_I	13,16 mm.	19 mm.
Transition frequency, f	59	80
	117	154.
	193	240
	280 (16 mm. only)	
	Hz	Hz

Figure 4.8. also shows that, for a given mode of operation, the frequency increases with fuel flowrate. The slope of the lines is approximately 100 Hz per kg/h fuel flowrate. The only exception is for D_I = 19 mm. at 154 Hz where the slope is approximately 2 Hz per kg/h. The explanation for the rise in frequency lies in the increasing mean temperature of the gases within the resonating section.

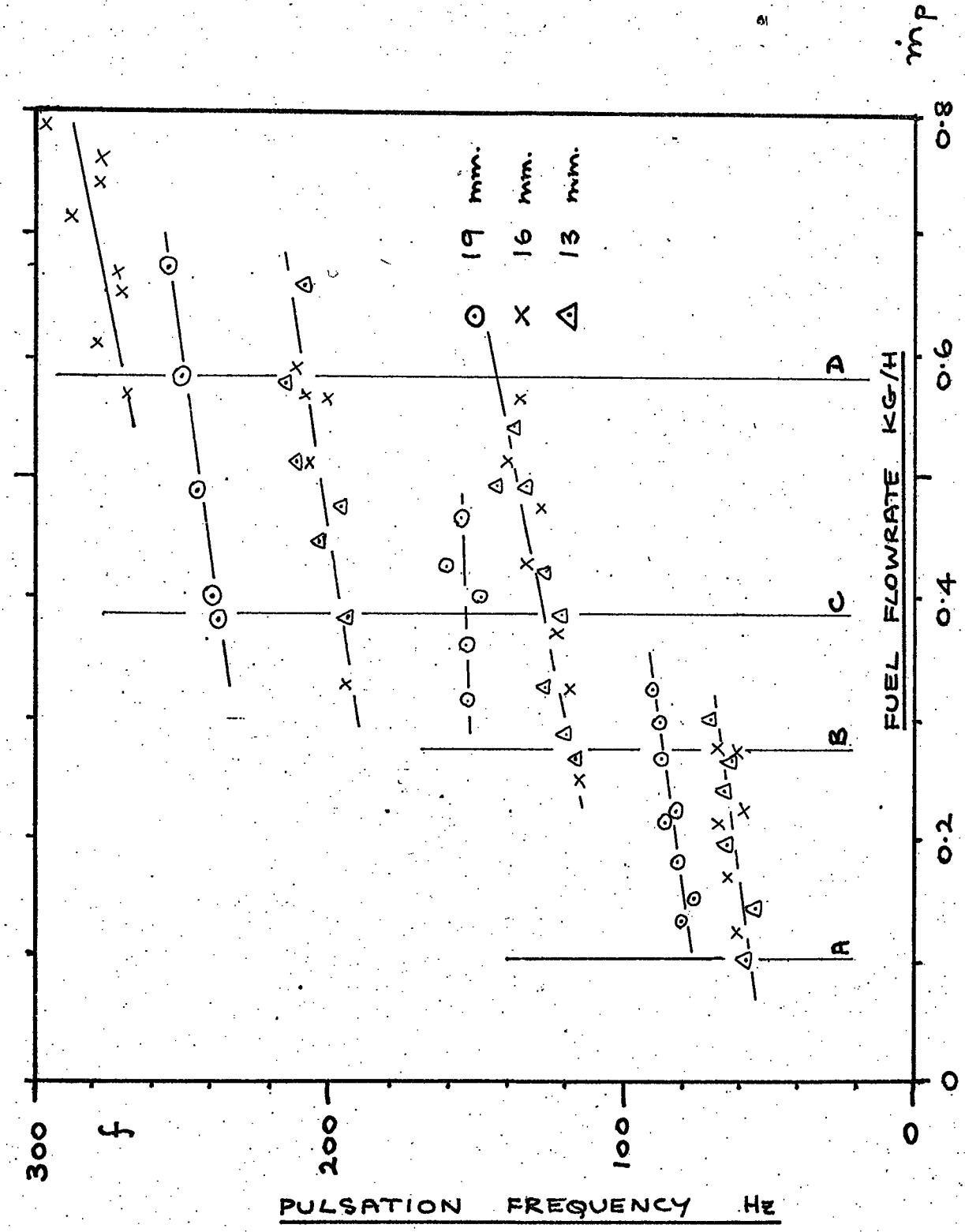

FIGURE 4.8 : VARIATION OF COMBUSTOR PULSATION FREQUENCY WITH FUEL FLOWRATE

4.3.1. Waveform

Due to the assumption of a sinusoidal pressure variation in Section 2, it was necessary to investigate the nature of the waveform. It was found that, at low fuel flowrates, the oscillations were irregular. This is demonstrated by Figures 4.9. and 4.10 which show the pressure variation in the combustion chamber for D_I = 19 mm. and for two low fuel flowrates. From Figure 4.8. it will be seen that, for $\dot{m}_p \simeq$ 0.27 kg/h, the frequency is in an unstable region and can jump to approximately 154 Hz, whereas, for $\dot{m}_p \simeq$ 0.18 kg/h the frequency is stable at approximately 80 Hz. Figure 4.10. shows that the fundamental frequency of 80 Hz is extremely irregular. In Figure 4.9. the waveform is more regular and its amplitude has increased from 2.5 to 5 divisions.

Figure 4.11. shows the pressure variation for the same aerodynamic values and for $\dot{m}_p$ = 0.42 kg/h. The smoother nature of the oscillations is evident, and the amplitude has increased to 14 divisions. Figure 4.12. shows the pressure variation at 160 Hz which is fundamentally sinusoidal. It was found that the smoothness and stability of the oscillations at a particular fuel flowrate always improved when the combustor attained thermal equilibrium.

4.3.2. Pressure Amplitude Variation

The readings for the axial distribution of pressure amplitude in the resonating section were obtained by screwing the pressure transducer into each of the measuring sites in turn. During the experiments, the combustor was maintained in operation in order not to disturb its thermal equilibrium. The results of three such tests for $\dot{m}_p$ = 0.45 kg/h are shown in Figures 4.16., 4.17. and 4.18. The distributions each show slight irregularities in the region of the combustion chamber. This was felt to be acceptable due to the combustion process and the flux of the inlet and exhaust gases. At the cold end of the resonating section in Figures 4.16. and 4.18, the reading has not fallen to zero as expected. This was felt to be due to the 'end effect' found in organ pipes.

The originals of these photographs are held in the Science Library in the top copy.

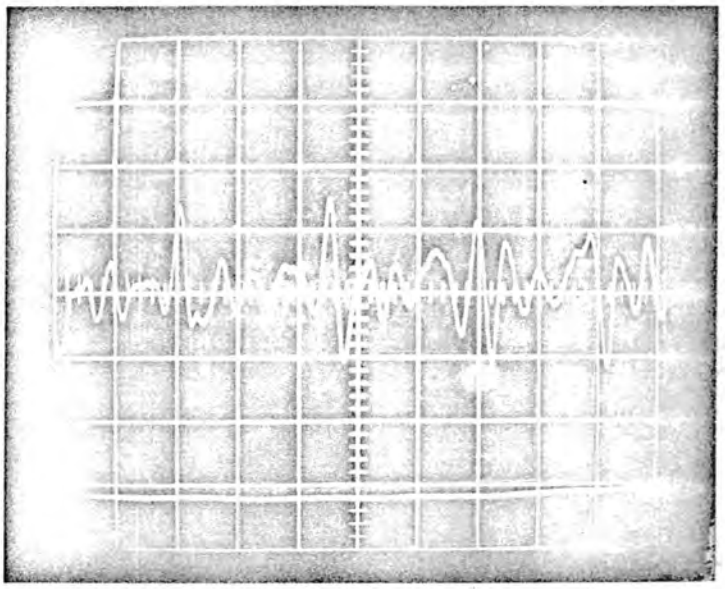

91 Hz

FIGURE 4.9 : PRESSURE VARIATION FOR D_I = 19 mm AND $\dot{m}_p$ = 0·27 KG/H

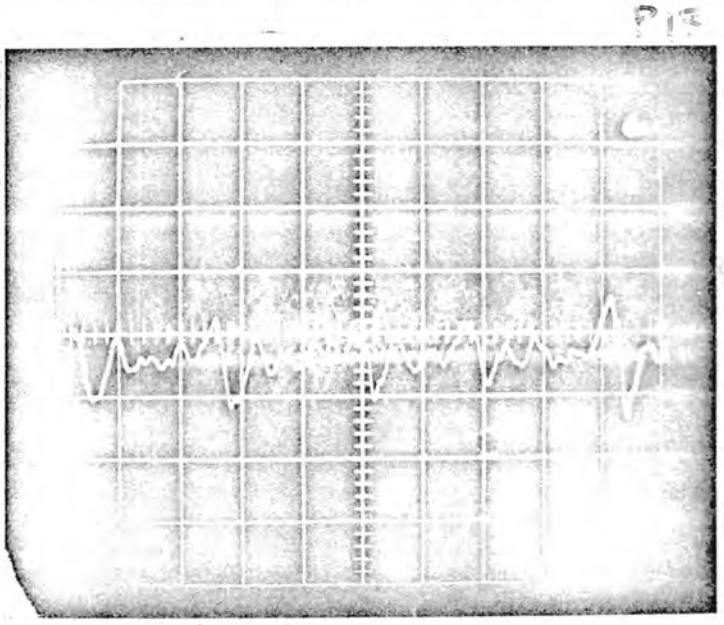

80Hz

FIGURE 4.10 : PRESSURE VARIATION FOR D_I = 19 mm. AND $\dot{m}_p$ = 0·18 KG/H

The originals of these photographs are held in the Science Library in the top copy.

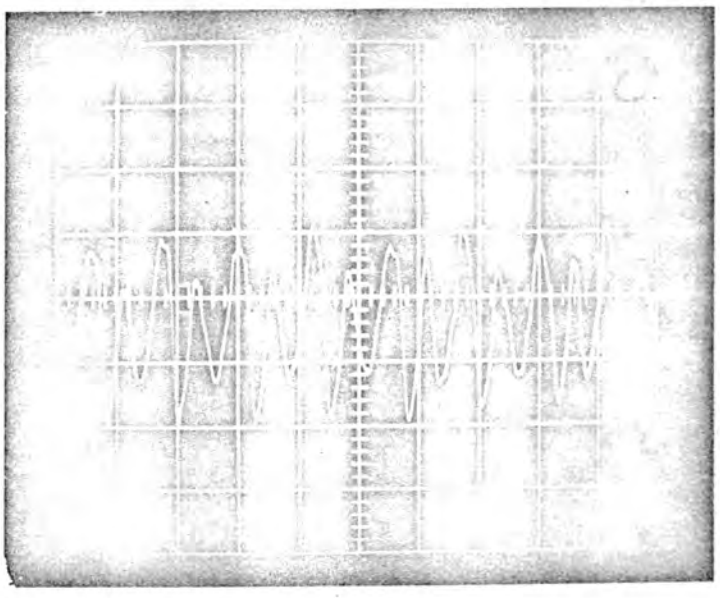

160 Hz

FIGURE 4.11 : PRESSURE VARIATION FOR D_I = 19 mm. AND $\dot{m}_p$ = 0·42 KG/H

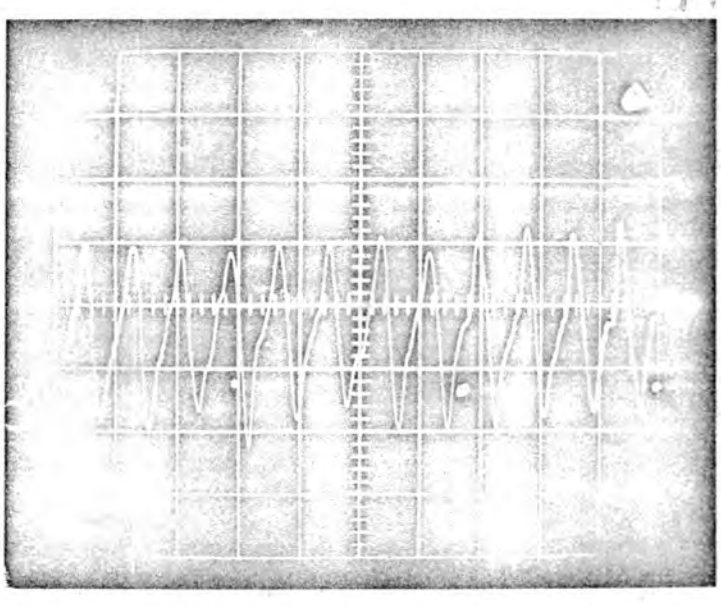

240 Hz

FIGURE 4.12: PRESSURE VARIATION FOR D_I = 19 mm. AND $\dot{m}_p$ = 0·47 KG/H

The distributions are generally smoother than those of Reay (20), as shown in Figure 4.13. Reay reported in the work that the pressure measurements were complicated by the presence of harmonics.

The phase of the readings was found by comparing on the oscilloscope two traces; one from the combustion chamber as a reference, and the one being measured. The nodes of the distribution are at x = 1.53 m, x = 1.0 and 2.21 m., and x = 1.68 m. for D_I = 13, 16 and 19 mm. respectively. An attempt was made to measure the exact position of these nodes by passing a long, tubular probe into the combustor from the cold end. The tube was connected to the pressure transducer. Although the method was found to work in principle, the probe interfered with the combustor operation and thus altered the frequency.

It may be concluded from the magnitude of the distributions at x = 0 and x = 3.05 m. that the resonating section behaved as an 'open-closed' organ pipe for D_I = 13 and 16 mm. and as an 'open-open' organ pipe for D_I = 19 mm. Table 4.A. may now be written;

4.B. Transition frequencies showing wavenumber, n

D_I = 13, 16 mm.	D_I = 19 mm.
59 n = 1 (40)	80 n = 1 (80)
117 n = 2 (120)	154 n = 2 (160)
193 n = 3 (200)	240 n = 3 (240)
280 n = 4 (280)	
Hz Hz	Hz Hz

In Table 4.E. the transition frequencies are shown together with wavenumber, n. For D_I = 13 and 16 mm., the behaviour of the combustor during warm-up follows the sequence given by the simple acoustic relation;

$$f = \frac{(2n-1)c}{4L} \quad \text{Hz} \qquad 4.3.1.$$

and for D_I = 19 mm.

$$f = \frac{nc}{2L} \quad \text{Hz} \qquad 4.3.2.$$

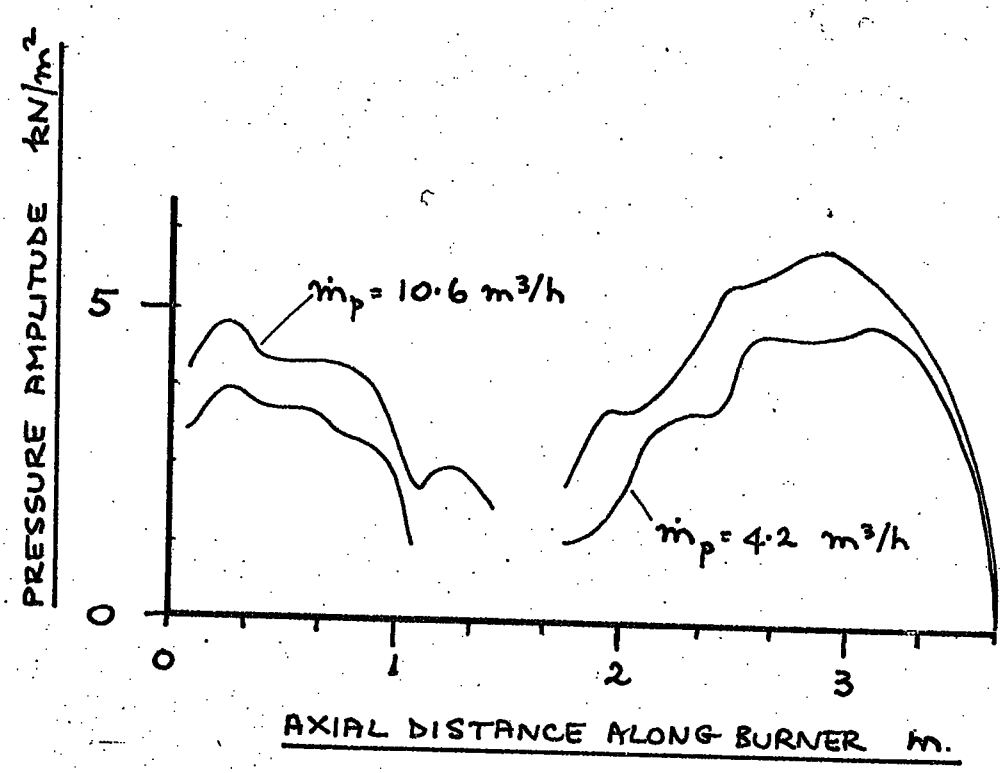

FIGURE 4.13: PRESSURE AMPLITUDE DISTRIBUTION IN A COMBUSTOR BY REAY (20) FOR TWO FUEL FLOWRATES

The exception occurs for D_T = 13 and 16 mm. with the initial frequency of 60 Hz. It is felt that, in this particular case, the resonating section behaves as an 'open-open' organ pipe. The objection to this is that the initial frequency is 21 Hz below that for D_T = 19 mm. It is possible that the mean temperature pf the gases was lower for D_T = 13 and 16 mm. but no measurements are available to support this view.

A Dawe Wave Analyser was used to examine the warm-up waveforms, illustrated by Figures 4.9. and 4.10. It was found that the waveform contained a frequency double that of the main one, but of lesser magnitude, in all cases. This observation could explain the first jumps of frequency at line B in Figure 4.8. With increasing fuel flowrate, the magnitude of the 80 Hz frequency, for example, decreased while that of the 160 Hz frequency increased. At a critical fuel flowrate, approximately 0.27 kg/h, both frequencies became unstable. With a further increase in fuel flowrate, the oscillations settled at 160 Hz.

4.3.3. Axial temperature distribution

Figure 4.14. shows the axial gas temperature distribution in Heat Exchanger A for D_T = 16 mm. and for four fuel flowrates. The temperature falls between 950 and 1450 K over the length of the heat exchanger. It was found that the exit temperature of the gases was generally below the condensing temperature, 100 °C.

Figure 4.15. shows the fitting of curves to the experimental gas temperature distributions. The isothermal line, T = 715 K, is clearly very poor. The exponential curves were fitted to the temperatures T_{A1} and T_{A8} It was found that the resultant curve was very flat and tended to a straight line. In Figure 4.15 , the exponential curve fits the experimental points to within 26%. For the case of the general solution, Equation 2.3.24., it was decided that a sinusoidal curve was the best fit, as shown in Figure 4.15. The sine curve fits the points to within 8%, and it was found to fit all the temperature distributions to within 12%. As for the exponential curve, the

FIGURE 4.14: AXIAL GAS TEMPERATURE DISTRIBUTION IN HEAT EXCHANGER A FOR D_t = 16 mm. AND FOUR FUEL FLOWRATES

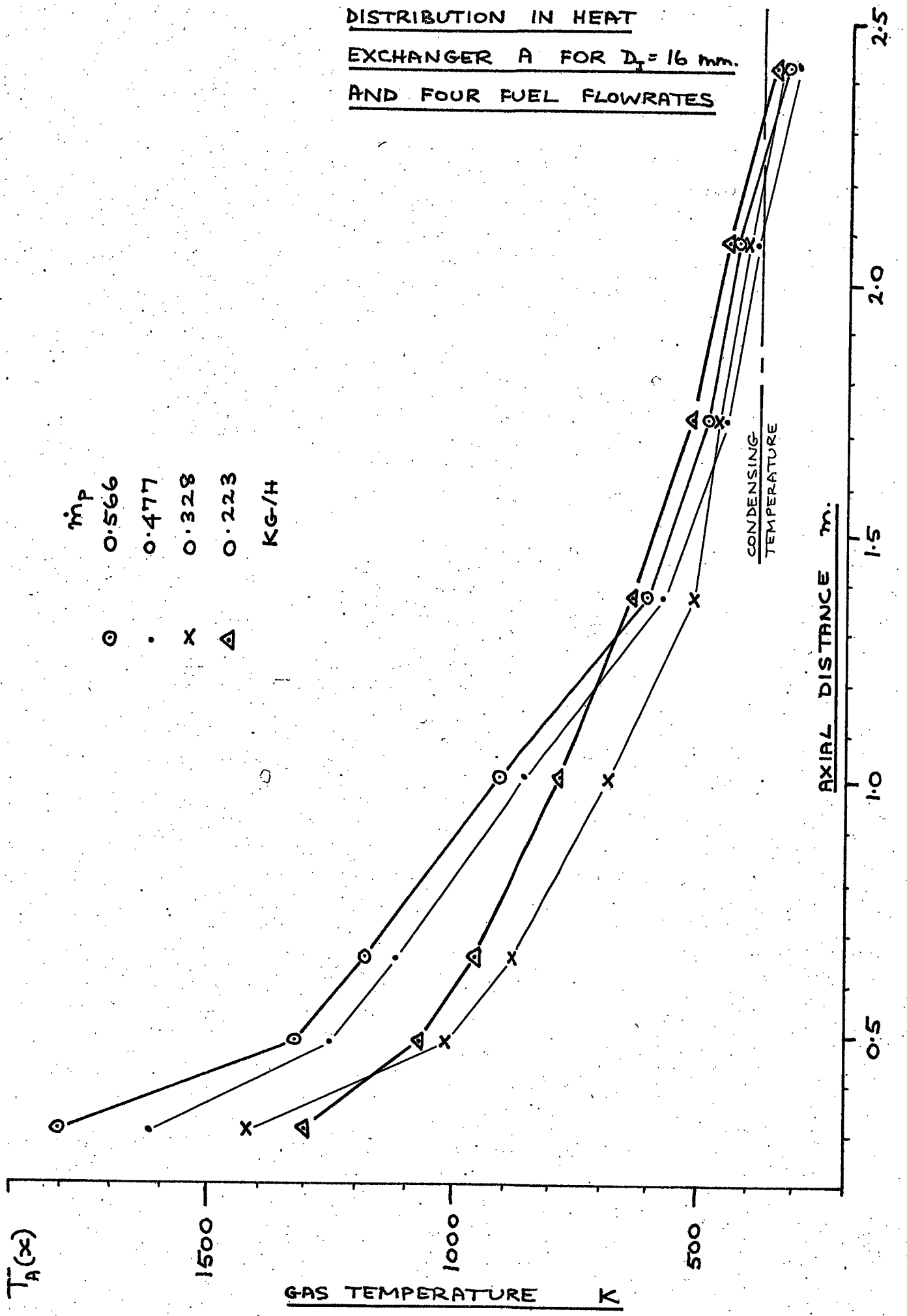

FIGURE 4.15: FITTING OF CURVES TO AXIAL GAS TEMPERATURE DISTRIBUTION IN RESONATING SECTION FOR $D_I = 16$ mm. AND $\dot{m}_p = 0.24$ KG/H

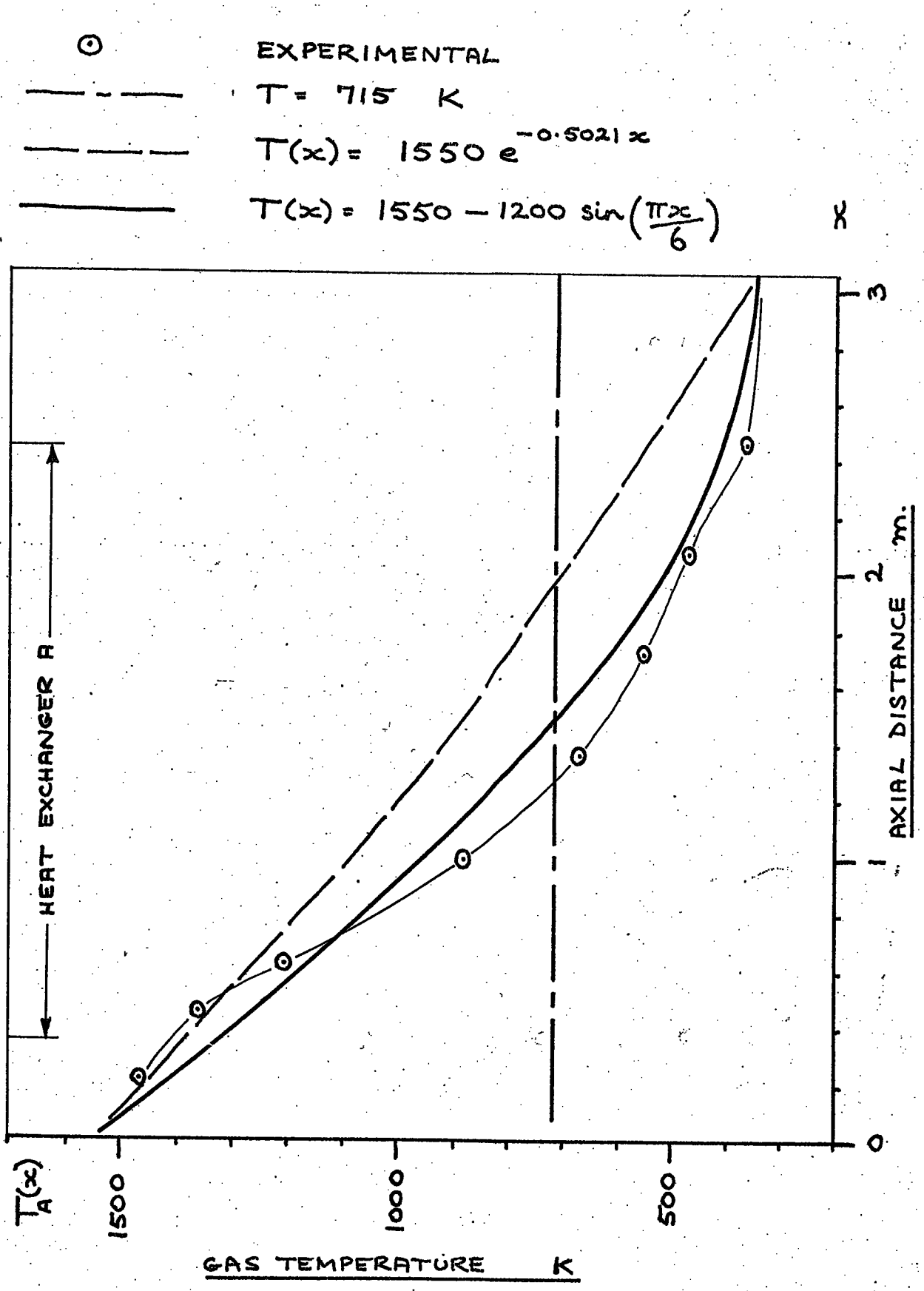

fitted points were T_{A1} and T_{A8}.

4.3.4. Frequency & Pressure Amplitude Predictions

Table 4.C. shows the comparison between the experimental values and the analytical predictions, based on the temperature measurements.

TABLE 4.C.

Frequencies

Experimental	Isothermal	Exponential	General
116	126 (+ 8%)	111 (- 4.5%)	115 (- 0.8%)
195	223 (+ 12.6%)	188 (- 3.8%)	193 (- 1.0%)
132.5	121 (- 9.5%)	111 (- 19.5%)	132 (- 0.5%)
201	217 (+ 7.2%)	188 (- 7.0%)	198 (- 1.9%)
75.5	87 (+ 13.2%)	-	77 (+ 2.0%)
145	178 (- 19.5%)	-	146 (+ 0.7%)
Hz			

The agreement between the isothermal frequency and the experimental ones is not better than 7.2%, and is on average 11%. The agreement between the exponential frequencies and the experimental ones lies in the range 3.8 to 8.5%. The prediction by the general solution, using the sinusoidal fit, is clearly the best, being on average 1.1%.

The predictions of the general solution for the axial distributions of pressure amplitude have been plotted in Figures 4.16., 4.17 and 4.18. For D_I = 13 mm. and 116 Hz, the general solution fits the experimental points to within 8%. For D_I = 16 and 19 mm., the fit improved to within 6%. The curves demonstrate the increase in pressure amplitude at the cobler end of the resonating section, predicted in Section 2.3. In Figure 4.16., this is 15%, in Figure 4.17., 8%, and in Figure 4.18., 17%. The results also demonstrate the nodal shift towards the cold end. These are 0.51, 0.19 and 0.15 m. respectively for the three figures.

FIGURE 4.16 : AXIAL DISTRIBUTION OF PRESSURE AMPLITUDE IN THE RESONATING SECTION

D_I = 13 mm.

f = 111 Hz

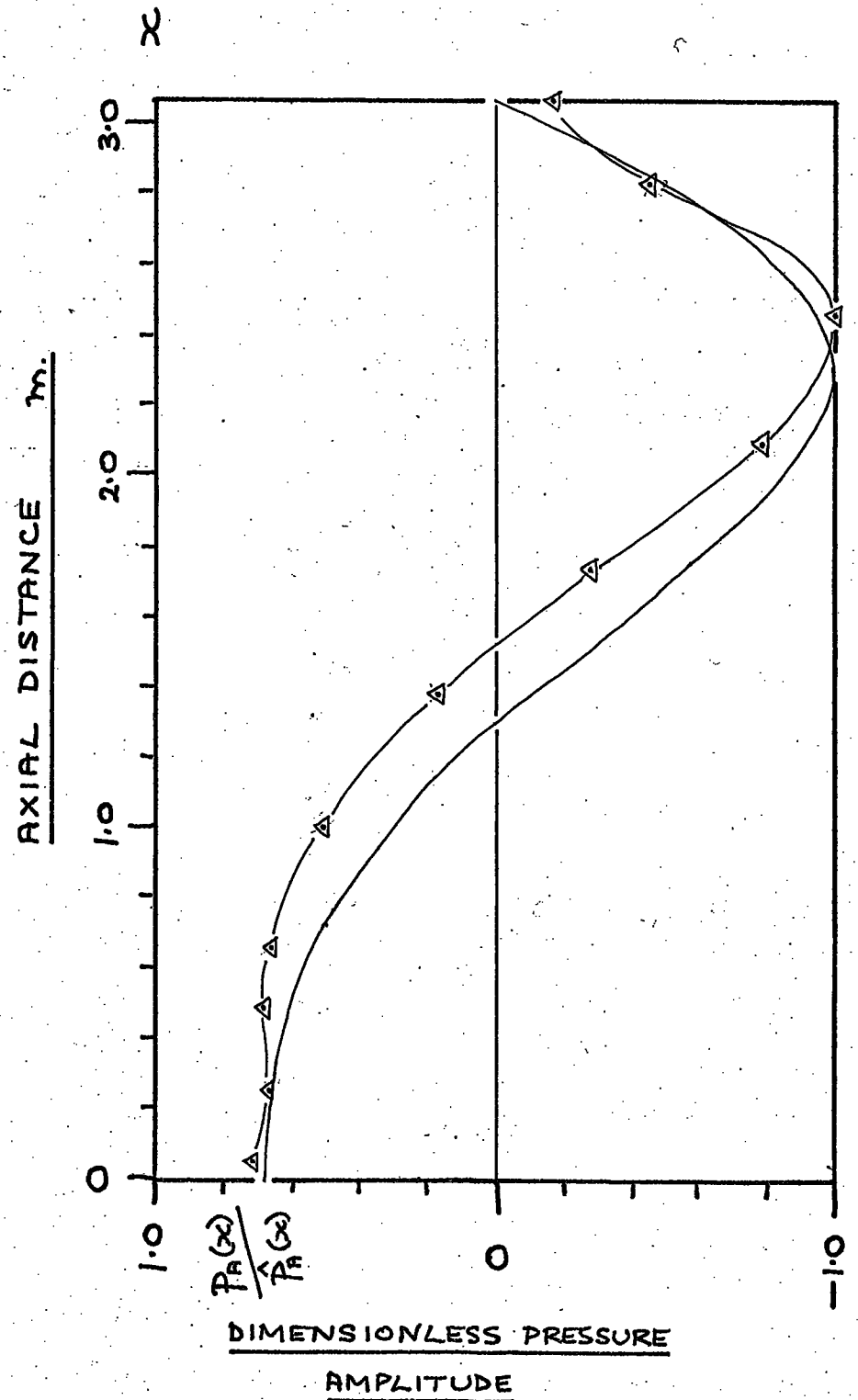

FIGURE 4.17 : AXIAL DISTRIBUTION OF PRESSURE AMPLITUDE IN THE RESONATING SECTION

$D_T = 16$ mm.

$f = 202$ Hz

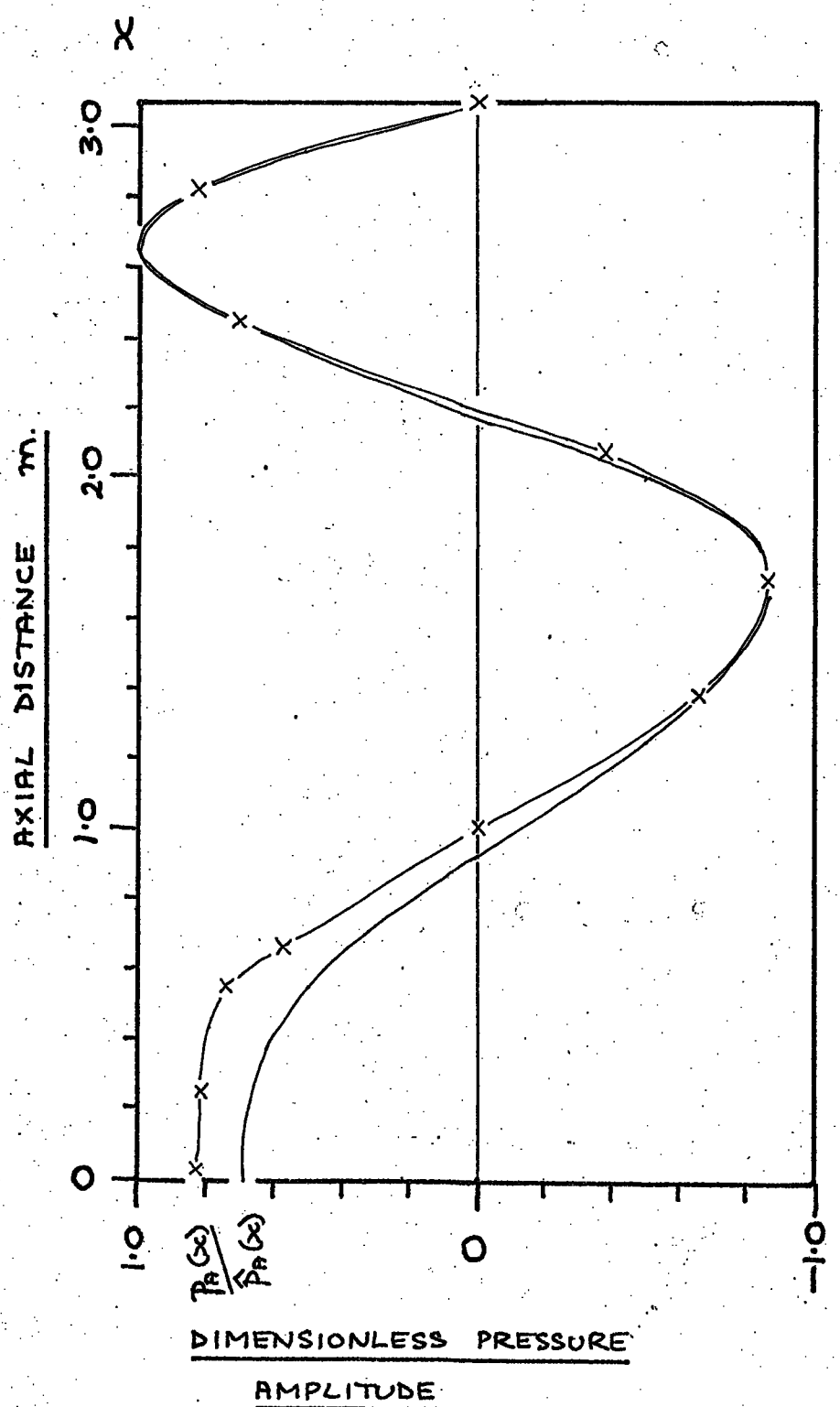

FIGURE 4.18 : AXIAL DISTRIBUTION OF PRESSURE AMPLITUDE IN THE RESONATING SECTION

D_t = 19 mm.

f = 145 Hz

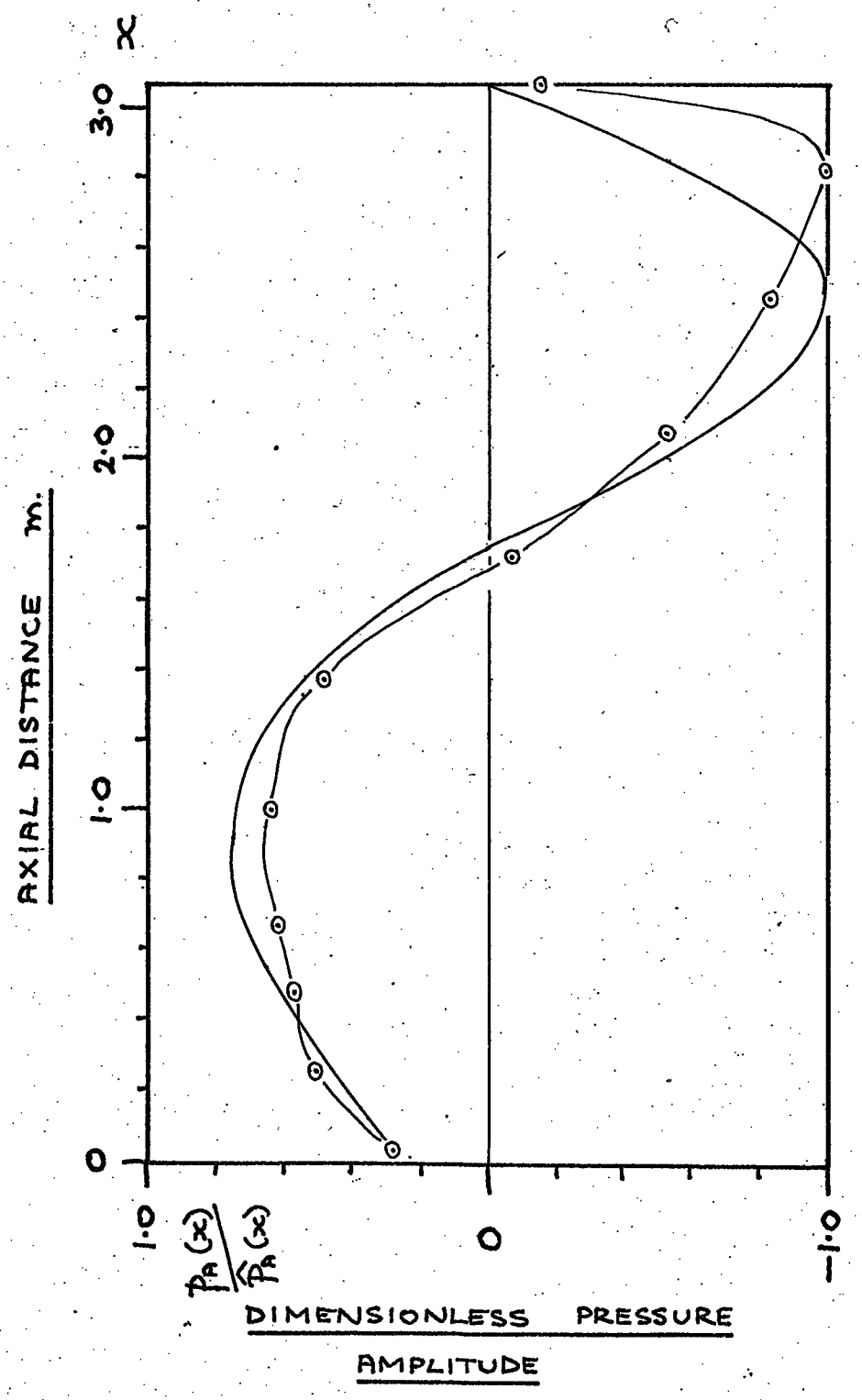

4.4. Heat Transfer

The results of Experiment 3 are tabulated in Appendix E. Both the readings, from which the heat transfer coefficients were calculated, and the derived parameters, are presented in Table E.4. et. seq. The overall heat transfer coefficient, U_A, lay in the range 32.8 to 61.0 W/m^2 K. The value of Reynolds Number, Re_w, for the water flow in Heat Exchanger A lay in the range 655 to 1256. The flow was therefore predominantly laminar. The value of Reynolds Number, $\overline{Re}_A$, for the gas flow through the Heat Exchanger was based on the mean gas velocity, $\bar{u}_A$. Thus;

$$\overline{Re}_A = \frac{\bar{u}_A D_o \rho_A}{\mu_A} \qquad 4.4.1.$$

$\overline{Re}_A$ lay in the range 1846 to 6689, and the gas flow was therefore predominantly turbulent. For a tube of 26 mm. diameter, a length of 0.5 m. would normally be required to allow a steady flow to become hydrodynamically developed. Thus it was assumed that the pulsating gas flow became fully developed in the lagged settling length of 0.22 m.

4.4.1. Experimental heat transfer coefficients

The experimental heat transfer coefficients were calculated by dividing the heat exchanger into the seven sections, lying between the gas temperature thermocouples. A typical section is shown in Figure 4.19. Application of the First Law to the control volume leads to the heat transfer coefficients:

$$h_{AS} = \frac{\Delta H_A}{S_S(\overline{T}_A - \overline{T}_S)} \qquad 4.4.2.$$

where S_S is the surface area based on the outside diameter of the inner tube,

$\overline{T}_A$ is the mean gas temperature,

$\overline{T}_S$ is the mean surface temperature,

ΔH_A is the change of enthalpy of the gas (equal to that of the water, assuming negligible losses through the lagging).

The water and surface temperatures corresponding to the points were found by linearly interpolating between the nearest adjacent readings. These calc-

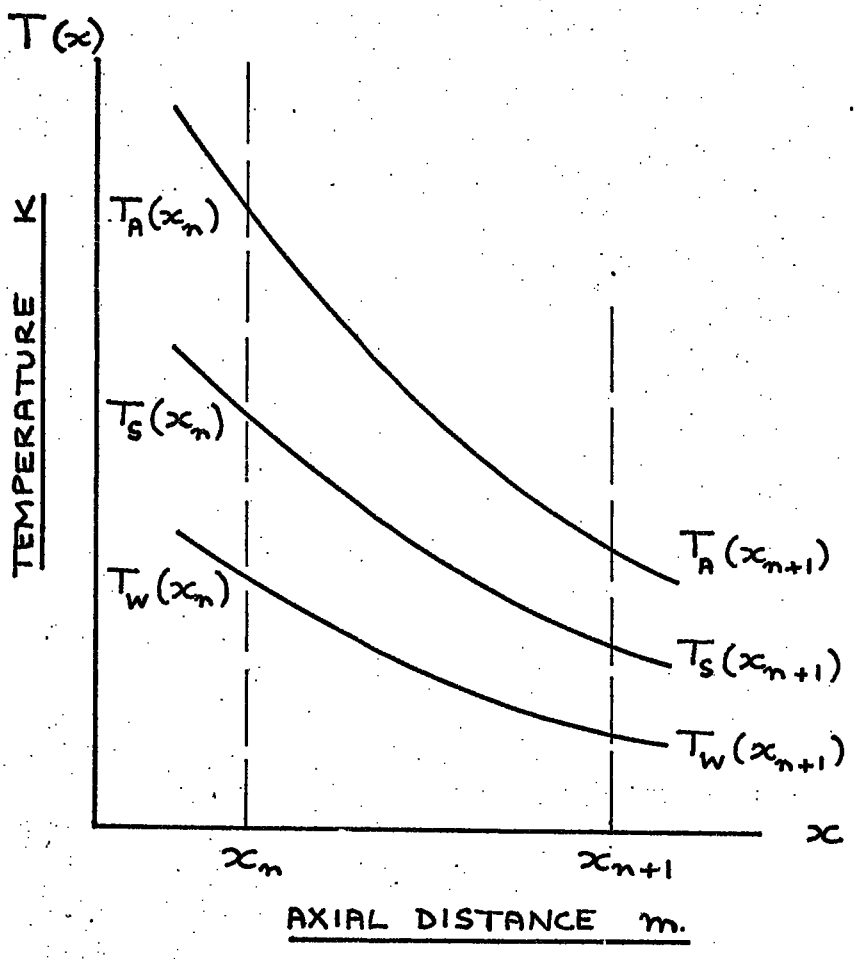

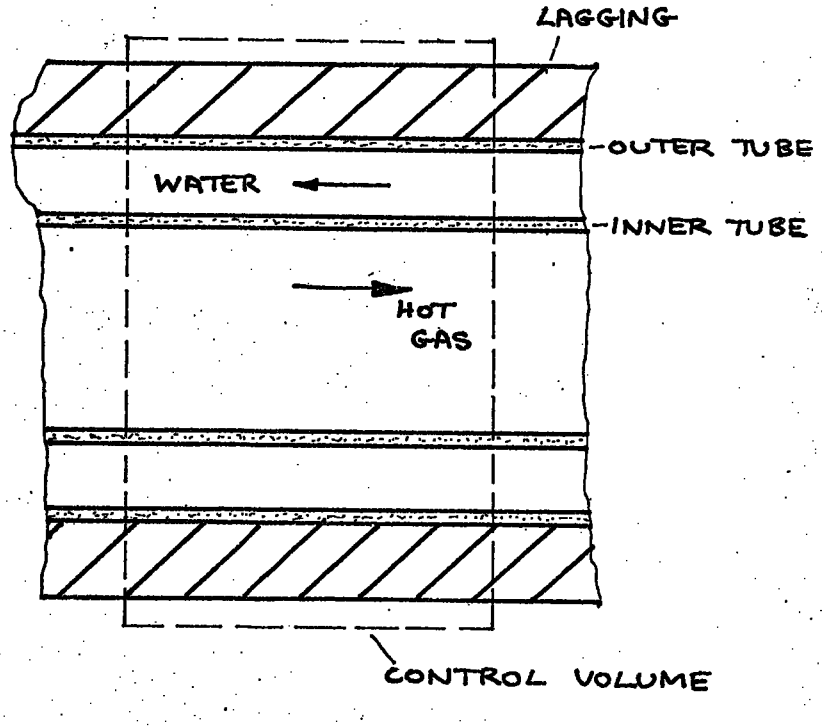

FIGURE 4.19 : TYPICAL SECTION OF HEAT EXCHANGER A

ulations were performed with the computer programme shown in Appendix F. The properties of the gas and water were evaluated at the corresponding mean temperatures. The Nusselt numbers were also calculated, using:

$$\overline{Nu}_p = \frac{h_{AS} D_o}{k_A} \qquad 4.4.3.$$

$$Nu_w = \frac{h_{gw} D_{eq}}{k_w} \qquad 4.4.4.$$

It will be seen from Table 4.F. that the heat transfer coefficients between the water and the tube surface, h_{gw}, lie in the range 1391 $< h_{gw} <$ 2327 $W/m^2 K$.

4.4.2. Steady state heat transfer

In order to be able to correlate the experimental results, an estimate of the equivalent steady flow heat transfer was required. It was not possible to run the apparatus under identical conditions without oscillations. Therefore the empirical equation of Seider and Tate was used (see equation 2.4.5.). The procedure was to calculate the heat transfer in fully developed steady turbulent flow, using the same values of $\dot{m}_w$, $\dot{m}_{AA}$, T_{AI}, and T_{WQ} as in the experiments. The calculations were performed by the programme CKBA in Appendix F. This had to be started with an estimate of the outlet water temperature, T_{WI}. It was found that a step length of $\frac{4K}{50}$ converged satisfactorily, and by successively changing the original estimate, the inlet water temperature was obtained. The water side heat transfer coefficients lay within an average of 14% of the experimental ones, and the Reynolds numbers corresponded to within 5%. With this agreement established, the steady state gas to surface Nusselt numbers could be used as a basis of comparison for the experimentally measured ones.

4.4.3. Heat Transfer Correlations

The local heat transfer coefficients, h_{AS}, in the heat exchanger were correlated with local velocity amplitude, $\hat{u}$ by plotting $\frac{\overline{Nu}_p}{Nu}$, the ratio

of pulsating to steady state Nusselt number, against $\frac{\hat{u}}{\bar{u}_A}$, the ratio of the velocity amplitude to the mean flow velocity. The latter was deduced from the continuity equation, thus;

$$\bar{u}_A = \frac{\dot{m}_{AA}}{\bar{\rho}_{Ax} S_o} \qquad 4.4.5.$$

where $\bar{\rho}_{Ax}$ is the density of the gases at point x. The velocity amplitude at any point were derived from equation 2.4.13;

$$\hat{u} = \frac{1}{\omega \bar{\rho}_{Ax}} \frac{\partial p_x}{\partial x}$$

The correlations for D_I = 13, 16 and 19 mm. are shown in Figures 4.20, 4.21. and 4.22 respectively. Also shown on each graph is the quasi-steady-state relation, equation 2.4.8. In Figure 4.20., the experimental points follow equation 2.4.8. to within 21% up to $\frac{\hat{u}}{\bar{u}_A} \simeq 1.5$, and then diverge along a steeper slope. For D_I = 16 mm. the agreement is approximately 16%, and again, a steeper slope is suggested after $\frac{\hat{u}}{\bar{u}_A} \simeq 1.0$. For D_I = 19 mm. the agreement is approximately 13%, and the same trend is apparent. These results substantially agree with those of Hanby (39) and do not exhibit as much scatter. They tend to conflict with those of Hirst (57) in that his results follow a slope below equation 2.4.8. as shown in Figure 4.23. Hirst examined the heat transfer from a heated tube to a flow of air passing through it while excited by a siren. The axial temperature gradient in the tube was less than 15% of that in this study, and there was no combustion process.

In Figure 4.24., the Nusselt Number ratio, $\frac{\overline{Nu}_p}{Nu}$, has been plotted against distance in Heat Exchanger A, x, for D_I = 13, 16 and 19 mm. On these graphs, the position of the velocity antinodes has been marked V.A. In Figure 4.24 (a) the variation of $\frac{\overline{Nu}_p}{Nu}$ with x is approximately sinusoidal and reaches a local maximum of 2.23 at x = 1.18 m. The nearest velocity antinode is at 0.92 m. The next velocity antinode is at x = 2.16 m. but here the value of $\frac{\overline{Nu}_p}{Nu}$ is large due to the end effect. In Figure 4.24 (b), the velocity antinodes do not coincide with local maxima. In

FIGURE 4.20: GRAPH OF NUSSELT NUMBER RATIO AGAINST DIMENSIONLESS VELOCITY AMPLITUDE FOR D_T = 13 mm.

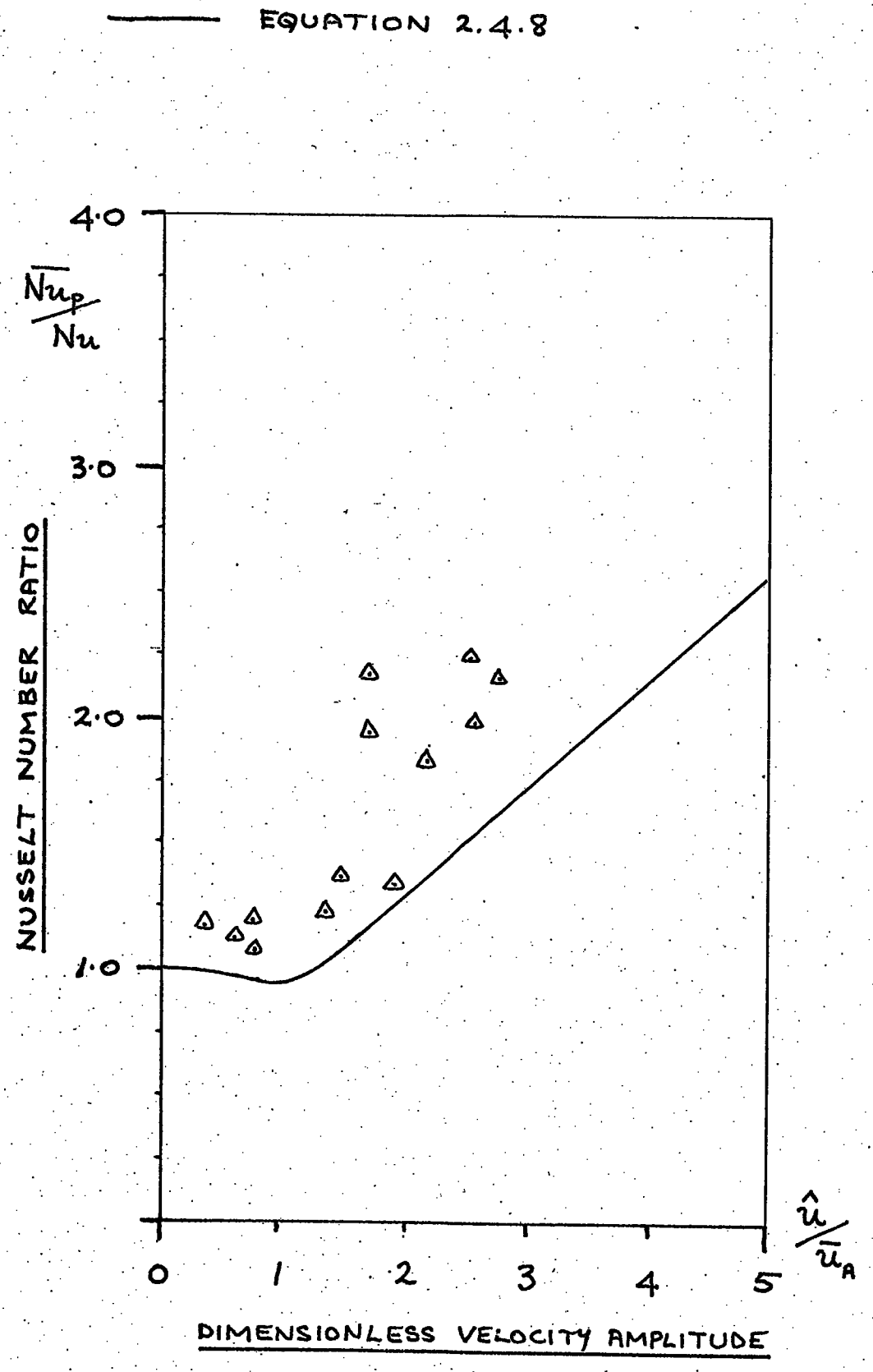

FIGURE 4.21: GRAPH OF NUSSELT NUMBER RATIO AGAINST DIMENSIONLESS VELOCITY AMPLITUDE FOR D_L = 16 mm.

——— EQUATION 2.4.8

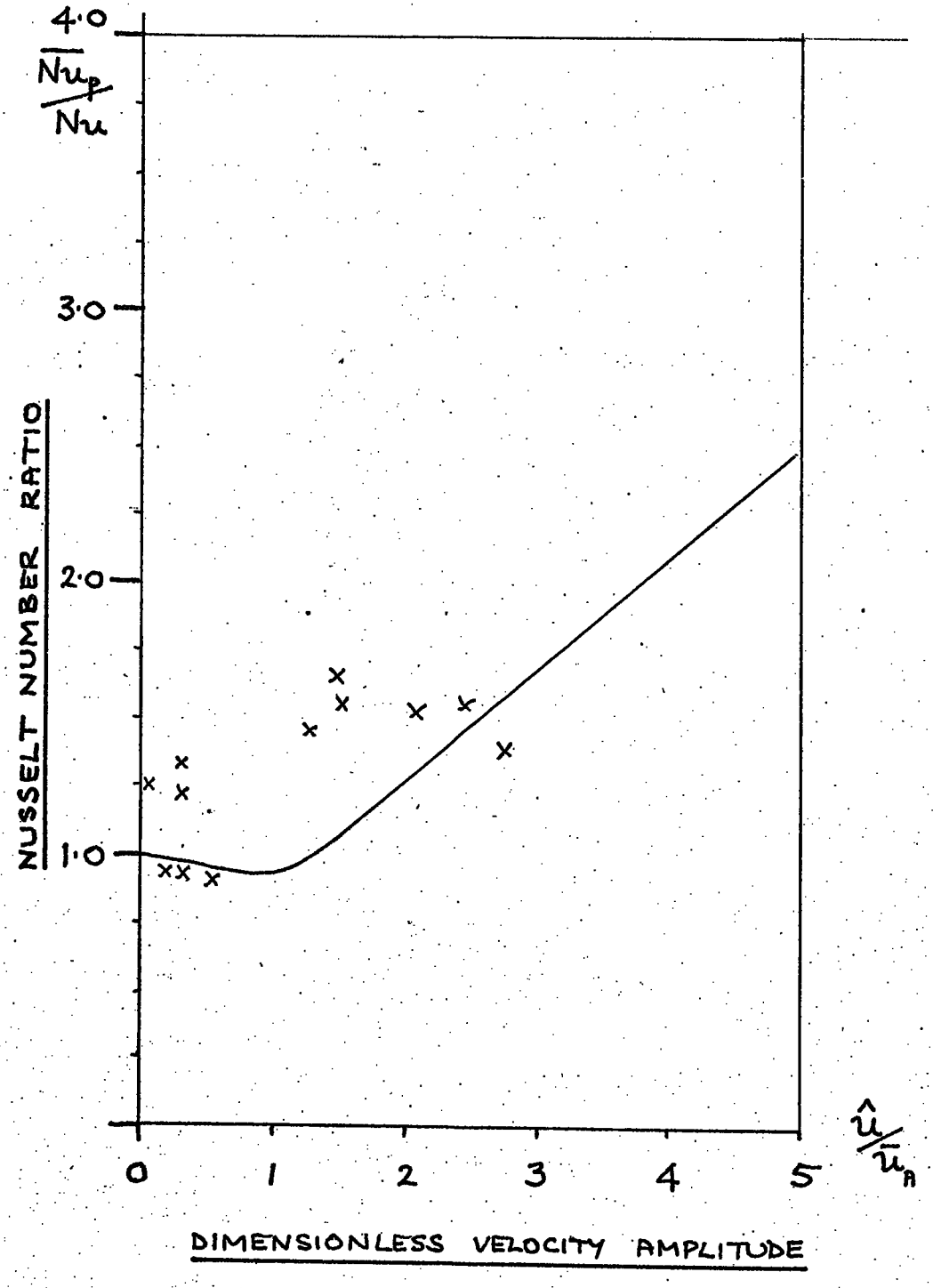

FIGURE 4.22: GRAPH OF NUSSELT NUMBER RATIO AGAINST DIMENSIONLESS VELOCITY AMPLITUDE FOR D_I = 19 mm.

——— EQUATION 2.4.8

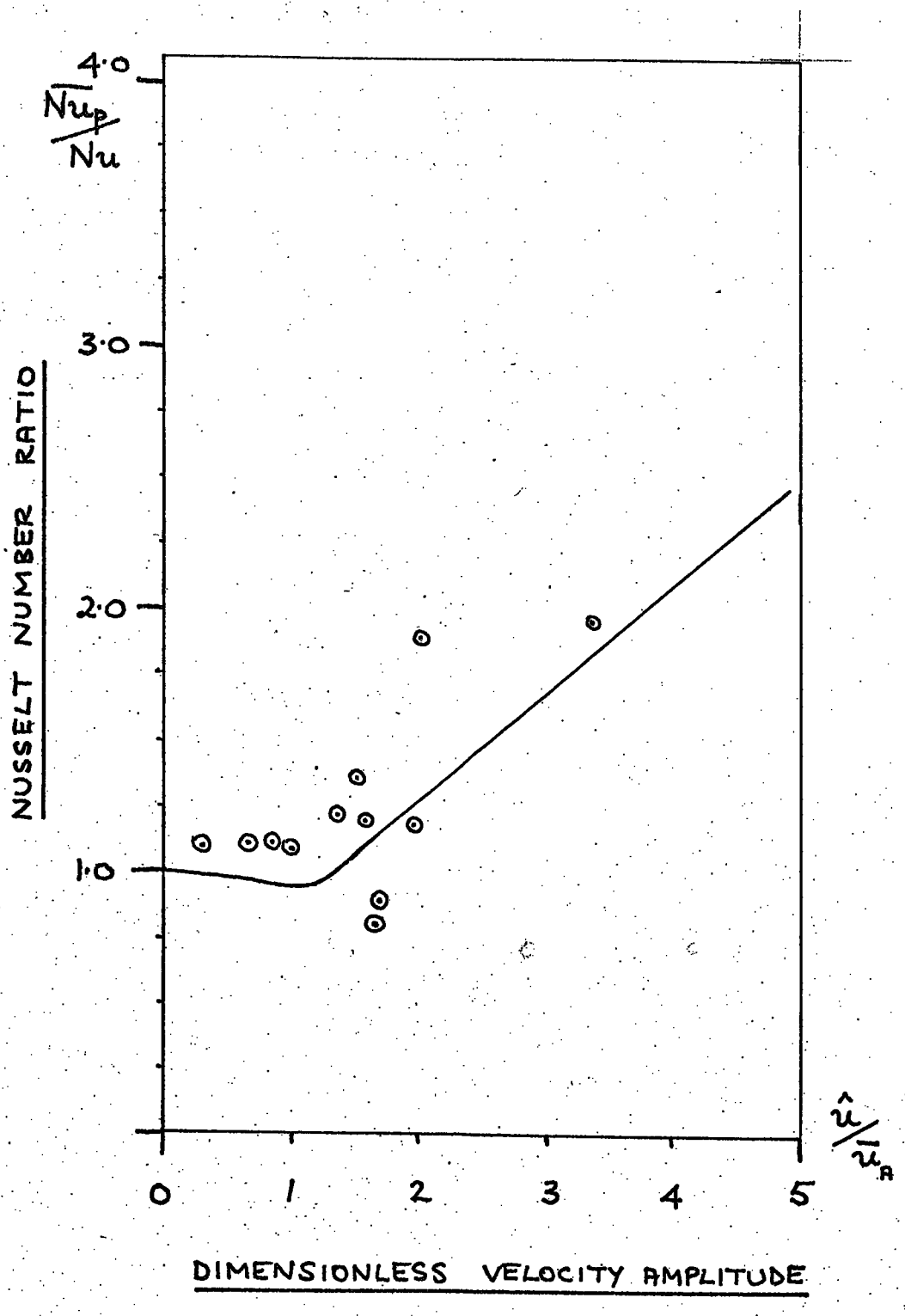

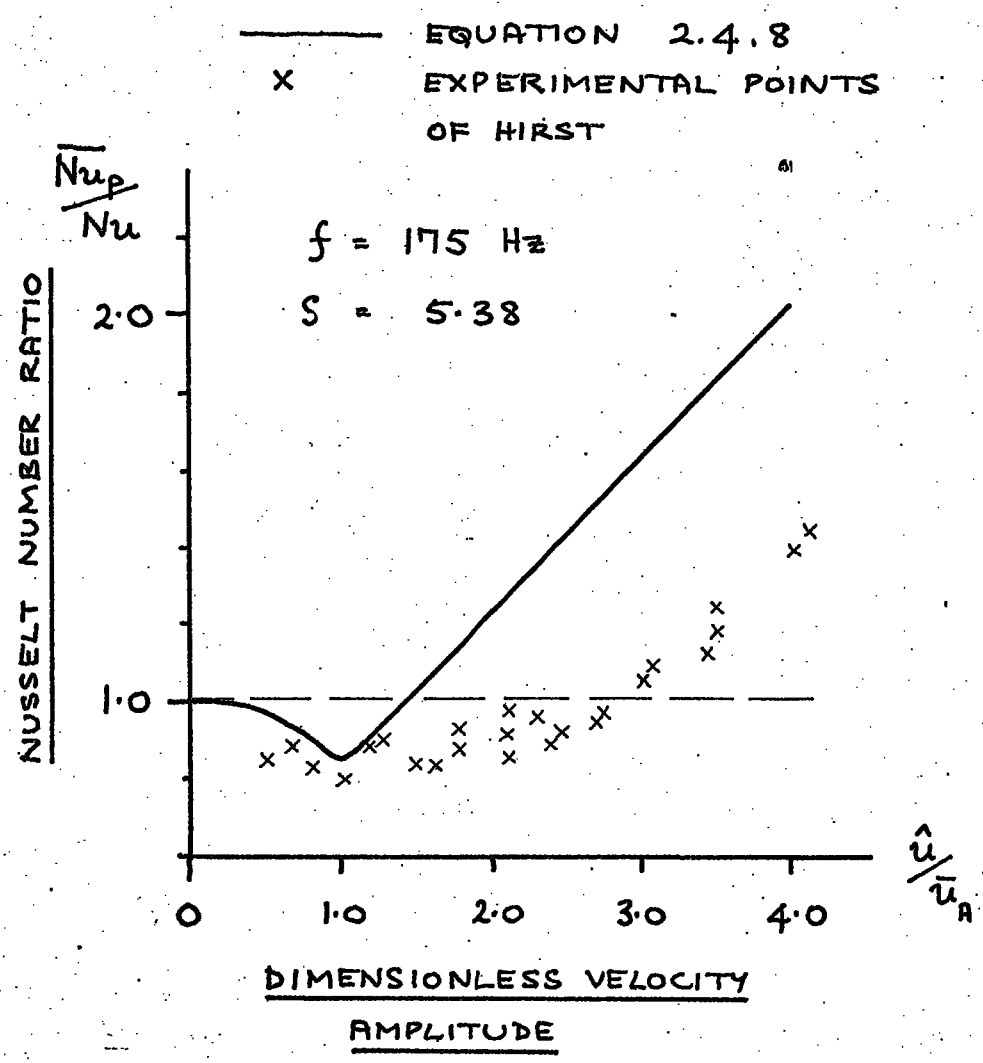

FIGURE 4.23 : GRAPH OF NUSSELT NUMBER RATIO AGAINST DIMENSIONLESS VELOCITY AMPLITUDE FROM HIRST (57)

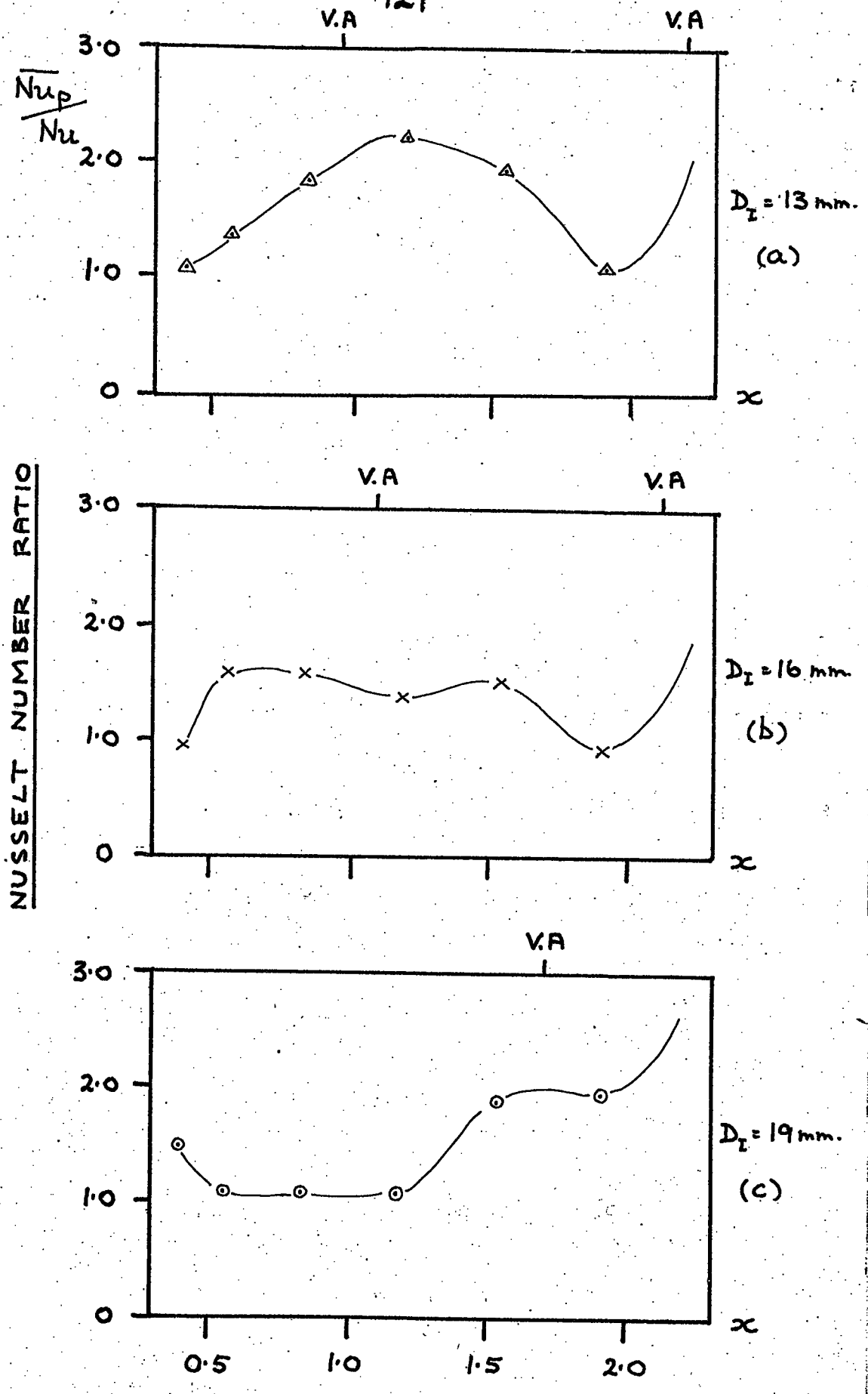

FIGURE 4.24: GRAPHS OF NUSSELT NUMBER RATIO AGAINST DISTANCE IN HEAT EXCHANGER A FOR D_I = 13, 16 & 19 mm.

$$\overline{Nu_p}/Nu = 1.0 + 0.20\,S$$

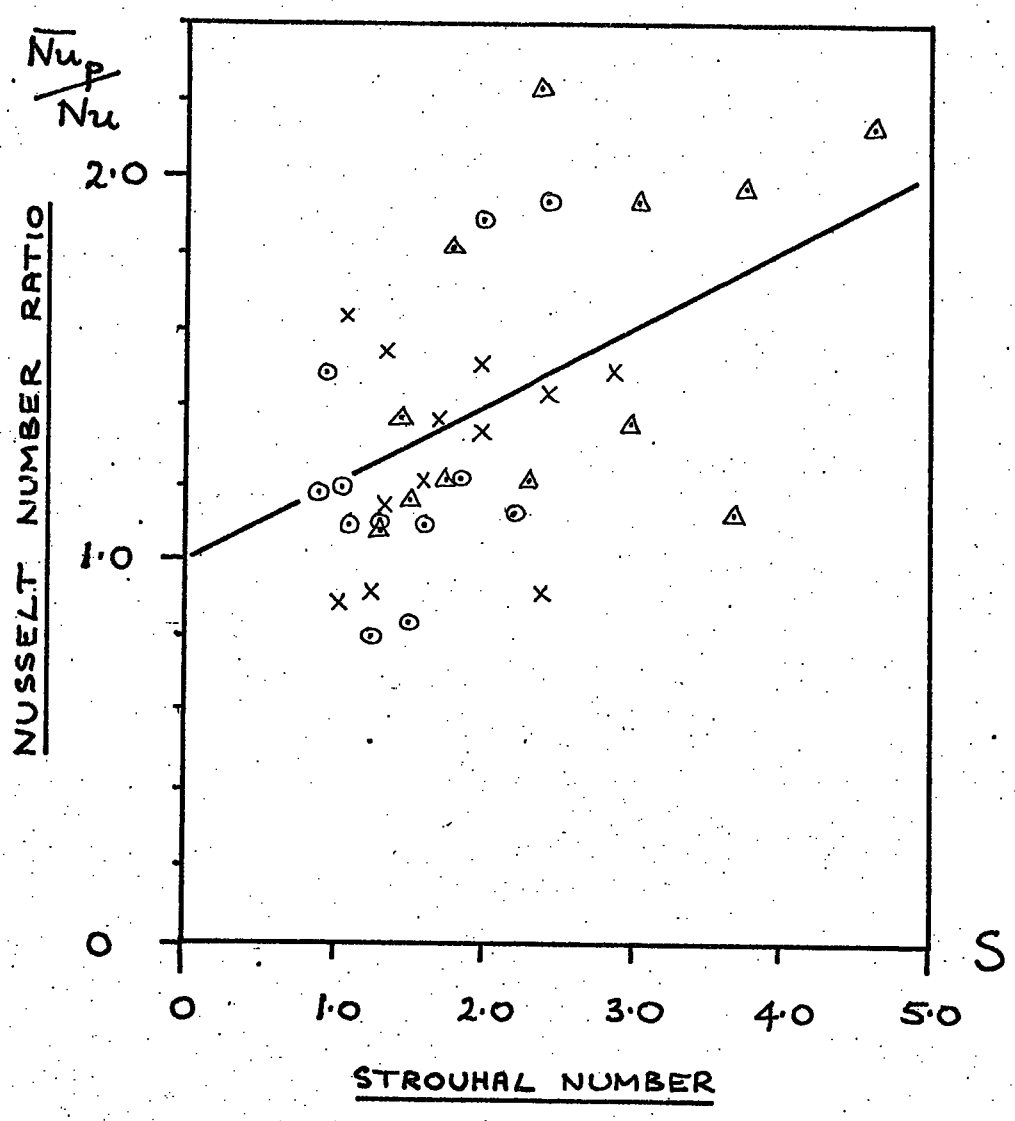

FIGURE 4.25: GRAPH OF NUSSELT NUMBER RATIO AGAINST STROUHAL NUMBER

Figure 4.24 (c), the velocity antinode occurs at x = 1.70 m. and coincides with a local plateau in the curve where $\frac{\overline{Nu}_p}{Nu} \simeq 1.91$. These results are not as clear as those of Jackson and Purdy (34), discussed in Section 1.3.

In Section 2.4.1., dimensional analysis pointed to a relationship between $\overline{Nu}_p$, $\frac{\hat{u}}{\bar{u}_A}$, $\overline{Re}_A$ and S. In order to be able to derive an empirical relationship it is necessary to keep two factors constant while examining the other two. This was not possible with this apparatus due to its feature of pumping its own combustion air, which meant that $\overline{Re}_A$ could not be fixed while altering $\hat{u}$, for example. In Figure 4.25., $\frac{\overline{Nu}_p}{Nu}$ has been plotted against Strouhal number, S. The points are scattered, and the straight line shown is a least squares fit. The line is;

$$\frac{\overline{Nu}_p}{Nu} = 1.0 + 0.20\,S \qquad 4.4.6.$$

Hirst (57) produced a similar empirical relationship which related his experimental results to the quasi-steady state predictions.

5. Conclusions

A naturally-aspirating propane-fired pulsating combustor was constructed with aerodynamic valves of diameters 13, 16 and 19 mm. Provision was made to measure the fluid flowrates, and fluid temperatures and pressure amplitude of the oscillations at regular intervals along the resonating section. A linearised wave equation, governing the propagation of sound waves through a gas exhibiting an axial temperature gradient, was obtained, together with exact solutions of an exponential temperature gradient.

The results of an energy balance of the apparatus lay within - 5.7% to + 10.0%. It was found that the overall thermal efficiency of the combustor decreased with increasing fuel flowrate. It was found that the airflow through the resonating section lay in the range 6 to 17 kg/h. A quasi-steady-state analysis of the aerodynamic valve overestimated this airflow by two to three magnitudes. This was felt to be caused by the assumptions of isentropic, frictionless flow in the analysis.

It was found that, at low fuel flowrates and low mean temperatures, the combustor ran at a fundamental frequency of approximately 60 Hz for D_I = 13 and 16 mm. and approximately 80 Hz for D_I = 19 mm. With increasing fuel flowrates, the combustor 'jumped' to harmonics based on the mode of operation. This were 'closed-open' organ pipe and 'open-open' organ pipe for D_I = 13, 16 mm. and D_I = 19 mm. respectively. The waveform of the oscillations was found to be sinusoidal only at high fuel flowrates and high frequencies.

The prediction of the operating frequency by the exponential analysis lay within 3.8 to 19.5%, of the experimental readings, and that by the general wave equation lay within 0.5 to 2.0%. The predictions by the general wave equation for the axial distributions of pressure amplitude lay within 6 to 8%.

The heat transfer results sought relationships between a) $\frac{\overline{Nu}_p}{Nu}$ and $\frac{\hat{u}}{\bar{u}_A}$, and b) $\frac{\overline{Nu}_p}{Nu}$ and S. The results of a) suggested a steeper relationship than predicted by the quasi-steady-state theory (based on an empirical steady state heat transfer equation). The results of b) produced

a scatter of points which were correlated by a least-squares line;

$$\frac{\overline{Nu}_p}{Nu} = 1.0 + 0.20\,S$$

The range of the major parameters was;

$\overline{Re}_A$	1800	-	6690
$\hat{u}/\bar{u}_A$	0.04	-	3.54
S	0.8	-	4.7

REFERENCES

1. Higgins, B. On the sound produced by a current of hydrogen gas passing through a tube. By editor, Mr. Nicholson, with a letter from Dr. Higgins respecting the time of its discovery. J. Nat. Philos. Chem. and the Arts v1 p. 129 1802.

2. Rijke, Pl L. Nature of a new method of causing a vibration of the air contained in a tube open at both ends. Phil. Mag. v17 p.419 1859.

3. Mallard, E. and Le Chatelier, H. Recherches experimentelles et theoriques sur la combustion des melanges gazeux explosifs. Annales des Mines, Partie Scientifique et Technique Series 8 n4 p.274 1883.

4. Reynst, F.H. Pulsating Combustion (collected works of F.H. Reynst. M.W. Thring, ed.) Pergamon Press, London, 1961.

5. Reynst, F.H. Pulsating Combustion (collected works of F.H. Reynst. M.W. Thring, ed.) Pergamon Press, London, 1961.

6. French Patent No. 373141.

7. French Patent No. 374124.

8. French Patent No. 376176.

9. French Patent No. 412478.

10. Dutch Patent No. 768 part 18 folio 38.

11. Reynst, F.H. Pulsating Combustion (collected works of F.H. Reynst. M.W. Thring ed.) Pergamon Press, London, 1961.

12. Swiss Patent No. 196312, Cl. 13b.

13. Reynst, F.H. Pulsating Combustion (see 11)

14. Huber, L. Central Heating, Air and Water-Heating with Pulsating Combustors. Paper presented at First Int. Symp. Pulsating Combustion, Univ. of Sheffield, 1971.

15. Alebon, J., Lee, G.K. & Geller, L.B. A Pulsating Combustion system for space heating. Proc. Boyar Conference pp. 61-89 May 1963 Univ. of Montreal.

16. Bottoms, C.H. Discussion of Paper.

17. Francis, W.E., Hoggarth, M.L. and Reay, D. A Study of gas-fired pulsating combustors for industrial applications. J. Inst. Gas Engrs. v3 p.301 1963.

18. Lord Rayleigh, Theory of Sound Vol. I & II.

19. Muller, J.L. The development of a resonant combustion heater for frying applications. The S.A. Mech. Engineer v137 February 1967 pp.137-146.

20. Reay, D. The thermal efficiency, silencing and practicability of gas-fired industrial pulsating combustors. J. Inst. Fuel v42 n339 p.135 1969.

21. Biffra, F.E.J., Staddon, P.W., Phillips, R.N. et Romaine, D.R. A study of unvalved pulse combustors. Inst. Gas Engineers Communication 860 37th Autumn Research Meeting, London 1971.

22. Reynst F.H. Pulsating Combustion (see 11)

23. Reynst, F.H. Pulsating Combustion (see 11).

24. Babkin, Yu. L. Pulsating Combustion Chambers as furnaces for steam boilers. Teploenergetika v12 n9 p.23 1959.

25. Hanby, V.I. and Brown, D.J. A 50 lb/h pulsating combustor for pulverised coal. J. Inst. Fuel v41 p.423 1968.

26. Martinelli, R.C. & Boelter, L.M.K. The Effect of Vibration on Heat Transfer by Free Convection from a Horizontal Cylinder. Proc. 5th Int. Congress Applied Mechanics 1938.

27. Martinelli, R.C., Boelter, L.M.K. Weinberg, E.B. and Yakati, S. Heat Transfer to a fluid flowing periodically at low frequencies in a vertical tube. A.S.M.E. v65 p.789 1943.

28. Schultz-Grunow, F. Pulsierender Durchfluss durch Rohre. Forschung auf dem Gebiere des Ingenieurewesens v11 pp.170-187 1940.

29. Estel see Bibliography No. 16.

30. Jackson, T.W., Harrison, W.B. & Boteler, W.C. Free convection, Forced convection and Acoustic Vibrations in a Constant Temperature Vertical Tube. J. Heat Transfer pp.68-74 February 1959 A.S.M.E. Paper No. 58-HT-6.

31. Zartmann, W.N. & Churchill, S.W. Heat transfer from acoustically resonating gas flames in a cylindrical burner A.I.Che.E. v7 n4 p.589 1961.

32. Sundstrom, D.W. & Churchill, S.W. Heat transfer from Premixed Gas Flames in a Cooled Tube. Che E Progress Symp. Series v56 n30 pp.65-73 1960.

33. Harrje, D.T. & Crocco, L. Heat Transfer in Oscillating Flow. Aeronautical Engineering Reports No. 483 - a,b,c 1959,60,61 Princeton University, New Jersy Contract USN-NONR 1858(29)

34. Jackson, T.W. & Purdy, K.R. Resonant Pulsating Flow and Convective Heat Transfer. J. Heat Transfer pp.507-512 Nov. 1965 A.S.M.E. Paper No. 65-HT-30

35. Miller, J. & Fejer, A. Transition phenomena in oscillating boundary layer flows. Jnl. Fluid Mech. v18 p.438 1974.

36. Purdy, K.R., Jackson, T.W. & Gorton, C.W. Viscous Fluid Flow under the Influence of a Resonant Acoustic Field. J. Heat Transfer pp.97-106 February 1964 A.S.M.E. Paper No. 62-WA-116.

37. Koshkin, V.K., Danilov, Y.I., Kalinin, E.K. Dreitser, D.A., Galitseysky, B.M. & Izosimov, V.G. Unsteady Heat Transfer in Tubes resulting from changes in Heat Flow, Gas Mass Flow Rate and Acoustic Resonance. 3rd Int. Heat Transfer Conf., Chicago 7-12 August 1966.

38. Galitseyskiy, B.M., Danilov, Yu. I., Dreytser, G.A., Kalinin, E.K. & Koshkin, V.N. Convective Heat Transfer for a flow in a pipe fluctuating about the first resonant harmonic. Heat Transfer - Soviet Research v1 n2 pp.164-176 1969.

39. Hanby, V.I. Convective Heat Transfer in a Gas-Fired Pulsating Combustor. Trans. A.S.M.E. v91 series a n1 p.48 1969.

40. Bogdanoff, D.W. A study of the mechanisms of heat transfer in oscillating flow. Technical Report No. 483-f Dep. Aerospace and Mech. Sci. Princeton, Oct. 1967.

41. Kapur, A., Cummings, A. et Mungur, P. Sound propagation in a combustion car with axial temperature and density gradients. J. Sound and Vibration v25 n1 pp.129-138 1972.

42. Morrell, G. An empirical method for calculating heat transfer rates in resonating gaseous pipe flow. Jet propulsion pp.829-831 Dec. 1958.

43. Holland, F. et al. Heat Transfer. Heinemann 1970.

44. Lewitt. Handbook of Mathematics.

45. Shapiro, A.H. Dynamics and Thermodynamics of compressible fluid flow. Vols I & II, Ronald Press Co. 1954.

46. Brudenberg Gauge Co. Handbook.

47. Thermal Syndicate Ltd. Handbook on use of Thermocoax

48. Holman, J.P. Experimental Methods for Engineers. McGraw-Hill, 1971.

49. Poole, K. Private Communication. Univ. of Durham 1973.

50. Numac Handbook - IBM Systems Reference Library 1972.

51. B.S. 726.

52. Beale, C.K., Clarke, P.H. & Everson, G. A Comparison of the dependence of the Pulsations in a single-orifice and a double-orifice Combustor on heat transfer or acoustic processes.

53. Simonson, J.R. An Introduction to Engineering Heat Transfer. McGraw Hill 1967

54. Holman, J.P. Experimental methods for Engineers. McGraw-Hill 1966.

55. Chapman, A.J. Heat Transfer. Macmillan 1967.

56. Bayley, F et al, Heat Transfer. Nelson 1972.

57. Hirst, S.L. Heat Transfer to a Resonant Pulsating Air Stream in a Pipe. Ph.D Thesis. Univ. of Durham 1974.

BIBLIOGRAPHY

1. A.A. Putnam — General survey of pulse combustion. 1st Int. Symposium on Pulsating Combustion, University of Sheffield. Sept. 1971.

2. G.H. Markstein ed. — Non-steady flame propatation Pergamon Press 1964.

3. A.A. Putnam — Combustion-driven oscillations in industry American Elsevier 1971.

4. D.D. McCracken — A guide to Fortran IV Programming Wiley 1966.

5. F. West, A. Taylor — Effect of pulsations on heat transfer. Chemical Engineering Progress. Vol. 48, No. 1, 1952 Pg. 39-43.

6. P.G. Morgan — The effect of vibration and pulsation on heat transfer. Engineering and Boiler House Review. April 1963, Pg. 128-129.

7. H. Havemann — Heat transfer in pulsating flow. Nature No. 4418, July 3, 1954, Pg. 41.

8. F. Romie — Heat transfer to fluids flowing with velocity pulsations in pipes. Thesis, University of California, 1956.

9. D.T. Harrje — Heat transfer in oscillating flow. Aero. Eng. Rep. No. 483c, Princeton University, Sept. 1961.

10. D. Bogdanoff, D.T. Harrje — A study of the mechanisms of heat transfer in oscillating flow. Aero. Eng. Rep. No. 483f, Princeton University, Sept.1967.

11. C. Feiler, E. Yeager — Effect of large amplitude oscillations on heat transfer. N.A.S.A. Tech. Report R-142, 1962.

12. A.H. Shapiro — Dynamics and thermodynamics of compressible fluid flow. Vol. I and II, Ronald Press Co. 1954.

13. R. Beyer — Physical Acoustics Vol. II, Part B. Academic Press 1965.

14. A.B. Wood — Textbook of Sound G. Bell and Sons Ltd., 1932.

15. C.E. Froberg — Introduction to numerical analysis. Addson-Wesley Pub. Co. Ltd., 1964.

16. W.M. Kays — Convective heat and mass transfer. McGraw-Hill Co. Ltd. 1966.

17. H. Schlichting — Boundary layer theory. Pergamon 1955.

18. J.K. Kilham et al — Oscillatory combustion in tunnel burners. 10th International Symp. on Combustion, 1965.

19. Arranged by T.R. Mayhew, G.F.C. Rogers — Thermodynamic and transport properties of fluids. Oxford 1967.

20. P.J. Westervelt — Effect of sound waves on heat transfer. Journal of Acoustical Society of America, Vol. 32, No. 3 March 1960, Pg. 337-338.

21. M.H.I. Baird — Vibrations and Pulsations British Chemical Engineering, Vol. 11, No. 1, Jan. 1966 Pg. 20-25.

22. R. Wick — Unsteady boundary layer and heat transfer phenomena - a literature survey. California Institute Technology, Technical Report 20-279, 1955.

23. G. Morell — An Empirical method for calculating heat transfer rates in resonating gaseous pipe flow. Jet Propulsion, Dec. 1958, Pg. 829-831.

24. R. Lemlich — A musical heat exchanger. Trans. A.S.M.E. - Journal of Heat Transfer, Aug. 1961 Pg. 385-386.

25. J. Dent — Effect of vibration on condensation heat transfer to a horizontal tube. Institute of Mechanical Eng. Proc. 1969/70, Vol 184, Part 1, No. 5.

26. M.J. Lighthill — The response of laminar skin friction and heat transfer to fluctuations of the stream velocity. Proceedings of Royal Soeiety, Series A, Vol. 224, No. 1156 June 1954.

27. T. Sarpkaya — Experimental determination of critical Reynolds number for pulsating flow. Journal of Basic Engineering, Vol. 88, No. 3, Sept. 1966, Pg. 5-9.

28. P.M. Morse — Vibration and Sound McGraw-Hill 1948.

29. P.M. Morse, K.U. Ingard — Theoretical Acoustics. McGraw Hill 1968.

30. A. Cambel, B.H. Jennings — Gas Dynamics. McGraw Hill 1958.

31. F. Cheers — Elements of Compressible Flow Wiley 1963.

32. A.J. Ede — An Introduction to Heat Transfer Pergamon Press 1967.

33. F. Holland et al — Heat Transfer
Heinemann 1970.

34. R.P. Benedict — Fundamentals of Temperature, Pressure and Flow Measurements.
Wiley 1969.

35. E. Owen, R.C. Pankhurst — Measurement of Air Flow.
Pergamon 1966.

36. C. Rektorys — Survey of Applicable Mathematics.
Iliffe 1969.

37. Owen, E, Pankhurst, R.C. — The Measurement of Airflow.
Pergamon 1966.

38. Lewis, B, von Elbe, G. — Combustion Flames and Explosions of Gases.
Academic Press 1961.

39. D.D. McCracken, W.S. Dorn — Numerical Methods and Fortran Programming.
Wiley 1964.

40. J.M. Beer, N.A. Chigier — Combustion Aerodynamics.
Applied Science Publ. 1972.

41. F. Cheers — Elements of Compressible flow.
Wiley 1963.

42. NPL — Noise Measurement Techniques - Notes of Applied Sci. No. 10.
HMSO 1958.

43. A. Schack — Industrial Heat Transfer.
Chapman and Hall 1965.

44. W.M. Kays — Convective Heat & Mass Trans.
McGraw Hill 1966.

45. C.C. Lin, ed. — Vol. 5 high speed Aero & Jet Propulsion
Turbulent flows and heat transfer.
Oxford 1959.

46. R.P. Benedict — Fundamentals of T, P and flow measurements.
Wiley 1969.

47. J. Heading — Mathematical Methods.
Univ. Press Belfast 1963.

48. D.C. Baird — Exptn. - An Introduction to Measurement Theory and Expt. design.
Prentice-Hall 1962.

49. Bruel & Kjoer — Instructions, Applications & Calibration.

50. B.V. Ranshenbakh — Vibrational Combustion.
FTD-TT-62-942/1 & 2
AD 402909 1963.

51. The Rayleigh Criterion — Stability of Systems Containing a Heat Source - Boa-Teh Chn
NACA RM 56D27 1956.

6.A Solution of the general wave equation

Equation 2.3.24 is:

$$\frac{d^2p}{dx^2} - \frac{1}{\bar{\rho}} \frac{d\bar{\rho}}{dx} \frac{dp}{dx} + \frac{\omega^2}{c^2} p = 0$$

where $\bar{\rho} = \bar{\rho}(x)$

$\bar{c} = \bar{c}(x)$

It may be written in the form:

$$p'' + f(x)\, p' + g(x)\, p = 0$$

where $f(x) = -\frac{1}{\bar{\rho}} \frac{d\bar{\rho}}{dx}$

$g(x) = \frac{\omega^2}{c^2}$

This may be split up into two simultaneous first order differential equations by writing:

$$y = p'$$
$$y' = p''$$

thus giving:

$$y' = -f(x)\, y - g(x)\, p$$

The boundary conditions for the tube are:

$$p(0) = P_0$$
$$p(L) = 0$$

This is an initial value problem and was solved using the subroutine DRKGS in the Numac Library (50). This uses a fourth-order Runga-Kutta method, and requires only the values of $p(0)$ and $p'(0)$ to start it. In order to meet the boundary condition $p(L) = 0$, a Newton-Raphson iteration loop was written into the procedure. The output of the programme was the pressure amplitude at any required point in the tube.

```
C  CKBGPX -- GENERAL SOLN.
      IMPLICIT REAL*8(A-Z)
      DIMENSION Y(2),DERY(2),AUX(16,2),PRMT(5)
      INTEGER NDIM,J,N,NUM,JM
      COMMON OMEGA
      EXTERNAL FCT,OUTP
      N=0
      READ(5,1000)OMEGA,PAC,GRAD
 1000 FORMAT(4(F10.3))
C  COMPUTE STARTING VALUE OF P(L)
      Y(1)=PAC
      Y(2)=GRAD
      DERY(1)=0.5
      DERY(2)=0.5
      PRMT(1)=0.0
      PRMT(2)=3.3
      PRMT(3)=0.3
      PRMT(4)=0.0001
      NDIM=2
      CALL DRKGS(PRMT,Y,DERY,NDIM,IHLF,FCT,OUTP,AUX)
      FA=Y(1)
      WA=OMEGA
C  START ZERO SEEKING LOOP
      OMEGA=OMEGA+25.0
   10 CONTINUE
C  RESET INPUT PARAMETERS FOR DRKGS
      Y(1)=PAC
      Y(2)=GRAD
      DERY(1)=0.5
      DERY(2)=0.5
      PRMT(1)=0.0
      PRMT(2)=3.3
      PRMT(3)=0.3
      PRMT(4)=0.0001
      NDIM=2
      CALL DRKGS(PRMT,Y,DERY,NDIM,IHLF,FCT,OUTP,AUX)
      FB=Y(1)
      WB=OMEGA
      K=(FB-FA)/(WB-WA)
      OMEGA=WB-(FB/K)
      IF(DABS(OMEGA-WB).LE.0.01.OR.N.GE.20)GO TO 9
      N=N+1
      WRITE(6,3311)N,OMEGA
 3311 FORMAT(4X,I2,3(F15.2))
      FA=FB
      WA=WB
      GO TO 10
    9 CONTINUE
C
      X=0.0
      DO 12 J=1,12
      Y(1)=PAC
      Y(2)=GRAD
      DERY(1)=0.5
      DERY(2)=0.5
      PRMT(1)=0.0
      PRMT(2)=X
      PRMT(3)=X/10
```

```
      PRMT(4)=0.0001
      NDIM=2
      CALL DRKGS(PRMT,Y,DERY,NDIM,IHLF,FCT,OUTP,AUX)
      WRITE(6,9091)J,X,Y(1),DERY(1)
 9091 FORMAT(6X,I2,3(4X,F10.3))
      X=X+0.3
   12 CONTINUE
      WRITE(6,9092)OMEGA
 9092 FORMAT(4X,'OMEGA =   ',F10.2)
      STOP
      END
      SUBROUTINE FCT(X,Y,DERY)
      IMPLICIT REAL*8(A-Z)
      DIMENSION Y(2),DERY(2)
      COMMON OMEGA
C
      DATA A,B,RR,GAMMA/-373.4,1400.0,287.1,1.4/
      TX=1500.0-1200.0*DSIN((X-0.3)*3.14159/6)
      DTX=-200.0*3.14159*DCOS((X-0.3)*3.14159/6)
      FX=DTX/TX
      GX=(OMEGA**2)/(GAMMA*RR*TX)
      DERY(1)=Y(2)
      DERY(2)=-FX*Y(2)-GX*Y(1)
      RETURN
      END
      SUBROUTINE OUTP(X,Y,DERY,IHLF,NDIM,PRMT)
      IMPLICIT REAL*8(A-Z)
     *DIMENSION Y(2),DERY(2),AUX(16,2),PRMT(5)
      INTEGER NDIM,IHLF
      RETURN
      END
```

6.B. The Preliminary Investigation

The first combustor to be constructed was based on a design of the Gas Council (17) and is shown in Figure B.1. It was found that stable combustion oscillations could be sustained only by directing a blast of air continuously towards the aerodynamic valve. The mean static pressure in the chamber was 0.3 kN/m^2g for an energy release of 18 kW on propane fuel, and the exhaust temperature was approximately 1350°C. It was observed that flames emerged from both ends of the chamber.

A number of modifications were made to the design in order to measure the overall rate of heat transfer, and the result of these is shown in Figure B.2. The fuel injection was changed to a radial configuration, a system used by Francis et al. (17) and Muller (19), and a heat exchanger was fitted to the exhaust end of the chamber. The combustion chamber was fitted with a cooling jacket. It was found that the maximum volumetric combustion rate was 78 MW/m^3, that the operating frequency was 175 Hz and that the overall rate of heat transfer was 64 kW/m^2. These figures were compared with those of Reynst (13), Muller (19) and Alebon et al. (15), which were 17.5 MW/m^3, 71 and 150 MW/m^3, and 44.5 MW/m^3 and 59 kW/m^2 respectively. A sample of exhaust gas from the centre of the heat exchanger was analysed with an Orsat apparatus, which yielded 6.5 per cent carbon dioxide, 3.6 per cent oxygen and 0.1 per cent carbon monoxide. It was concluded from this analysis that the combustor was inducting excess air and that, therefore, the dimensions of the aerodynamic valve could be reduced without detriment to the combustion process.

As the original combustion chamber had become distorted, a new one of 51 mm. internal diameter was constructed, and a tail-pipe added to the heat exchanger to prevent end-effects due to reverse flow. The revised apparatus is shown in Figure B.3. It was found that, over the range of fuel flowrate, 0.68 to 0.92 kg/h, the gas temperature at the exit of the heat exchanger fell from 260 to 175°C while that of a thermocouple placed just outside the aero-

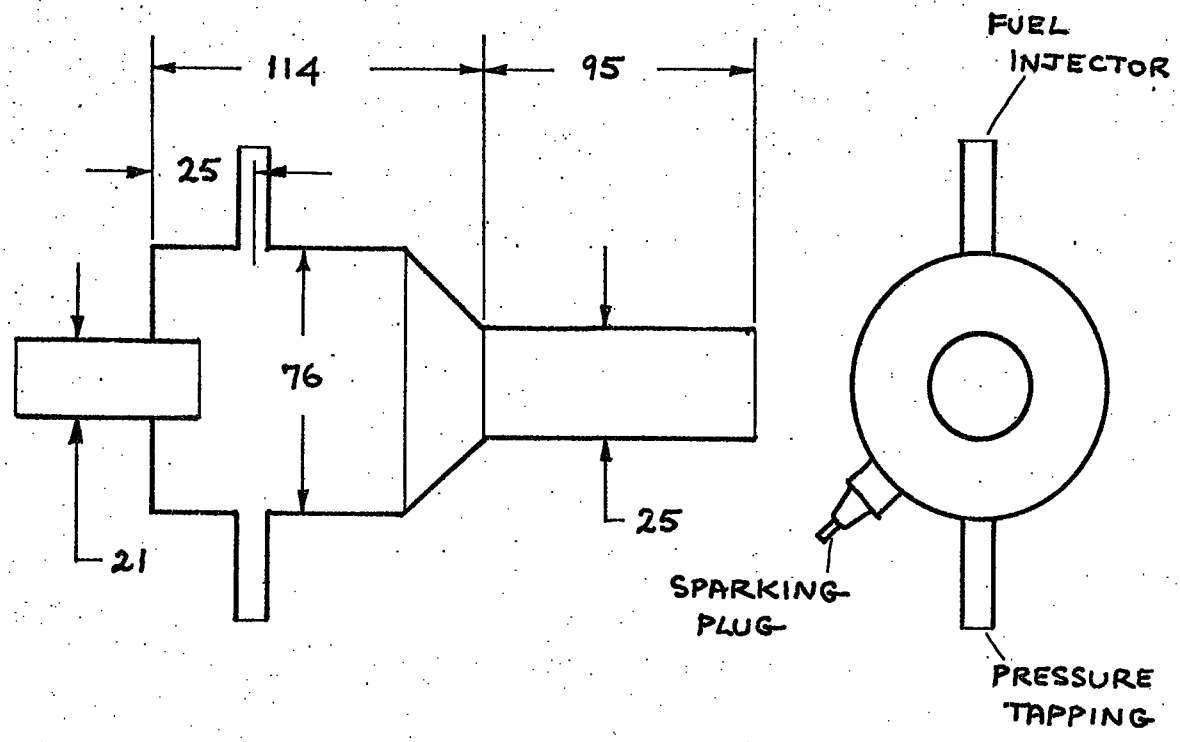

FIGURE B.1 : FIRST COMBUSTION CHAMBER
(DIMENSIONS IN MM)

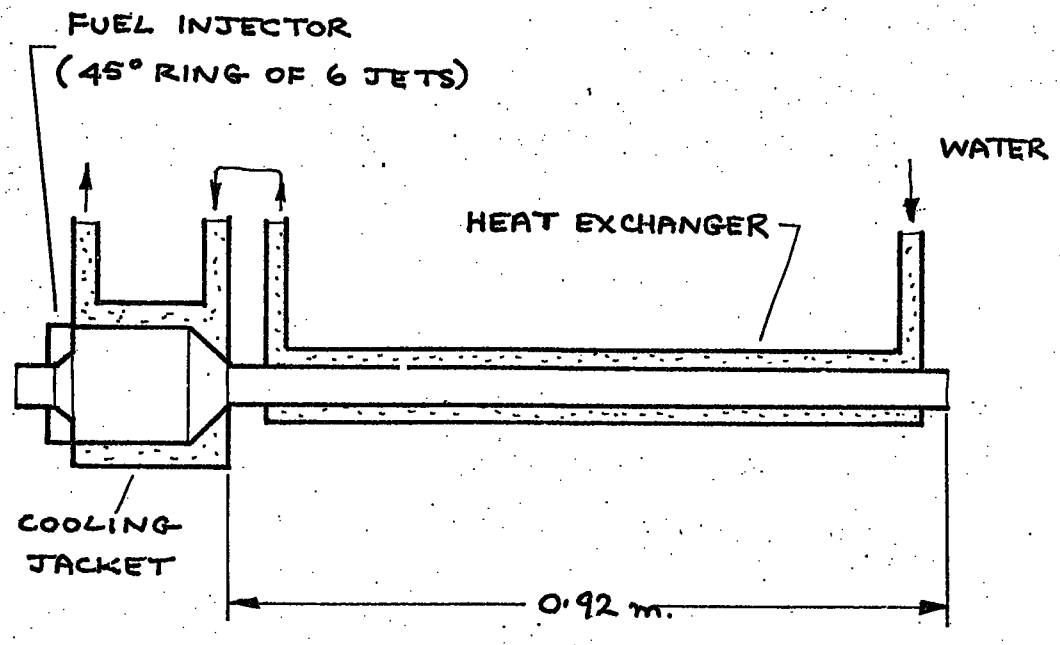

FIGURE B.2 : FIRST COMBUSTION CHAMBER WITH HEAT EXCHANGER, COOLING JACKET AND MODIFIED FUEL INJECTION

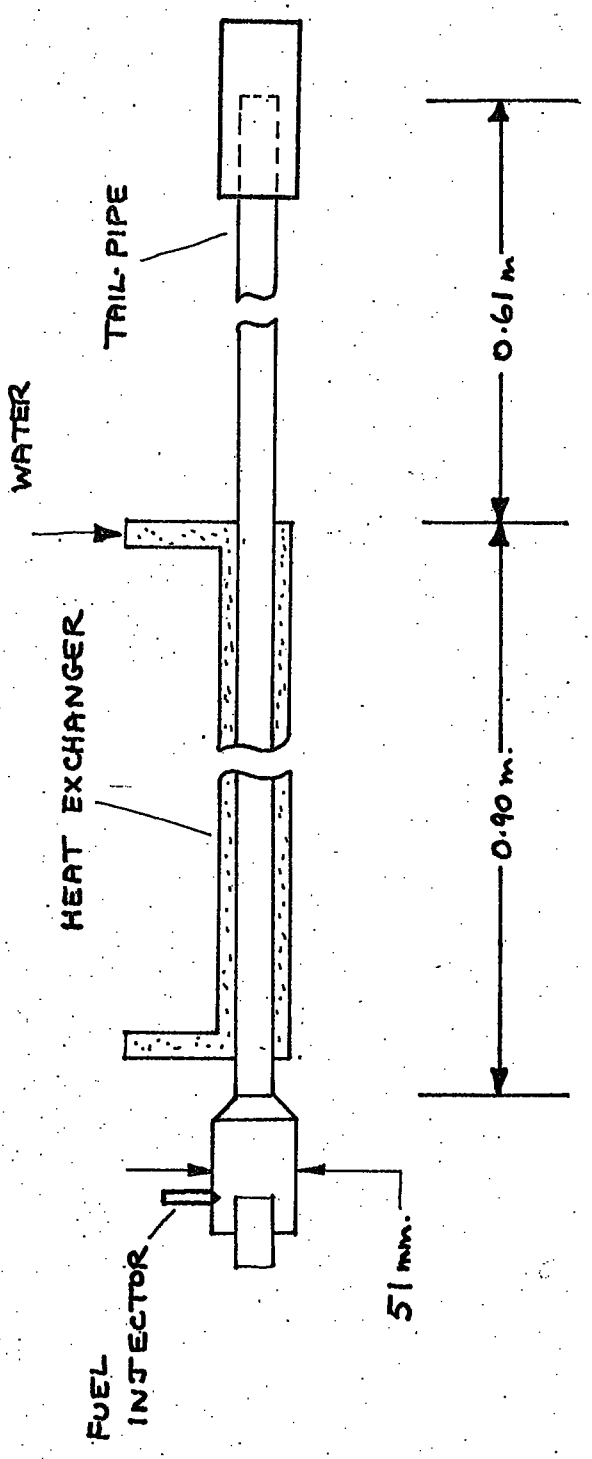

FIGURE B.3 : SECOND COMBUSTOR WITH HEAT EXCHANGER AND AUGMENTER

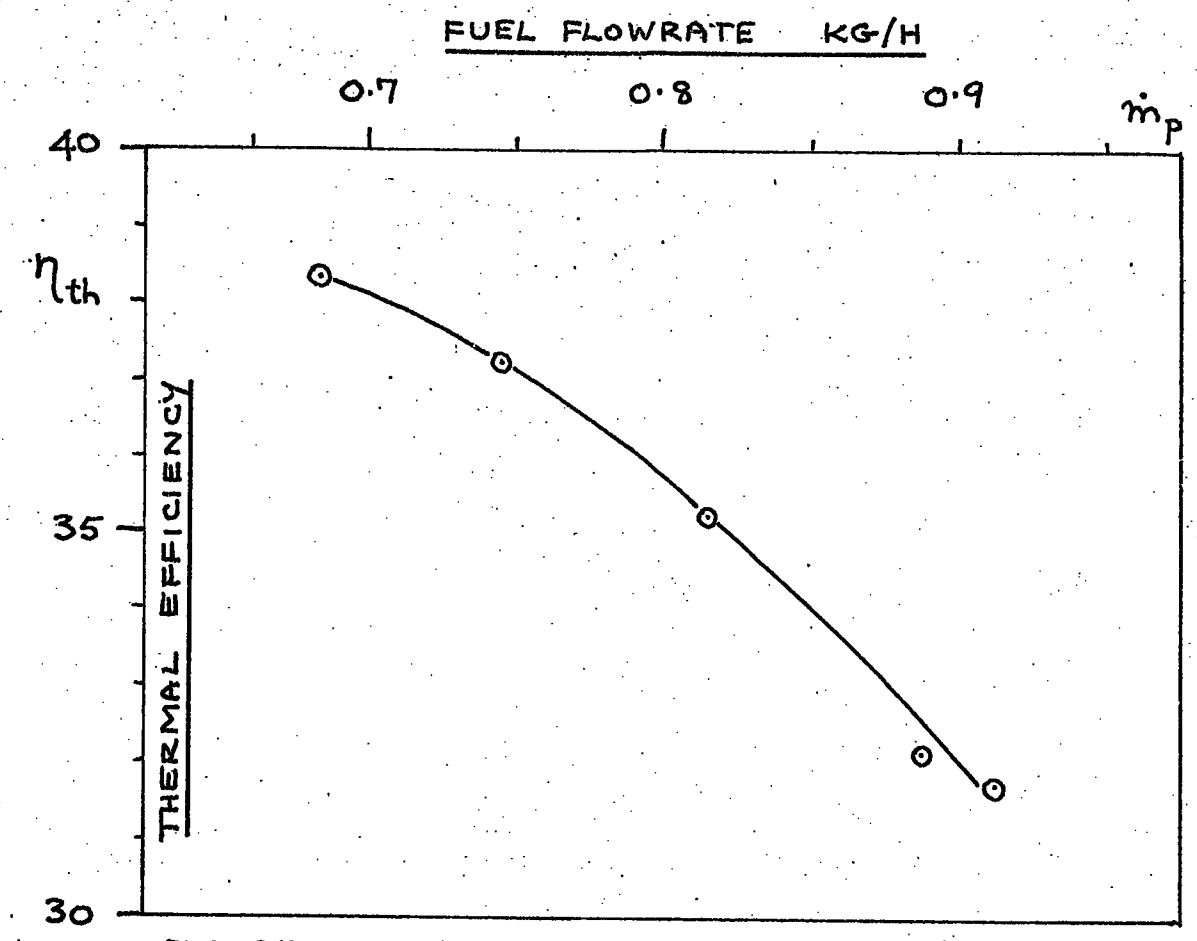

FIGURE B.5: VARIATION OF THERMAL EFFICIENCY WITH FUEL FLOWRATE

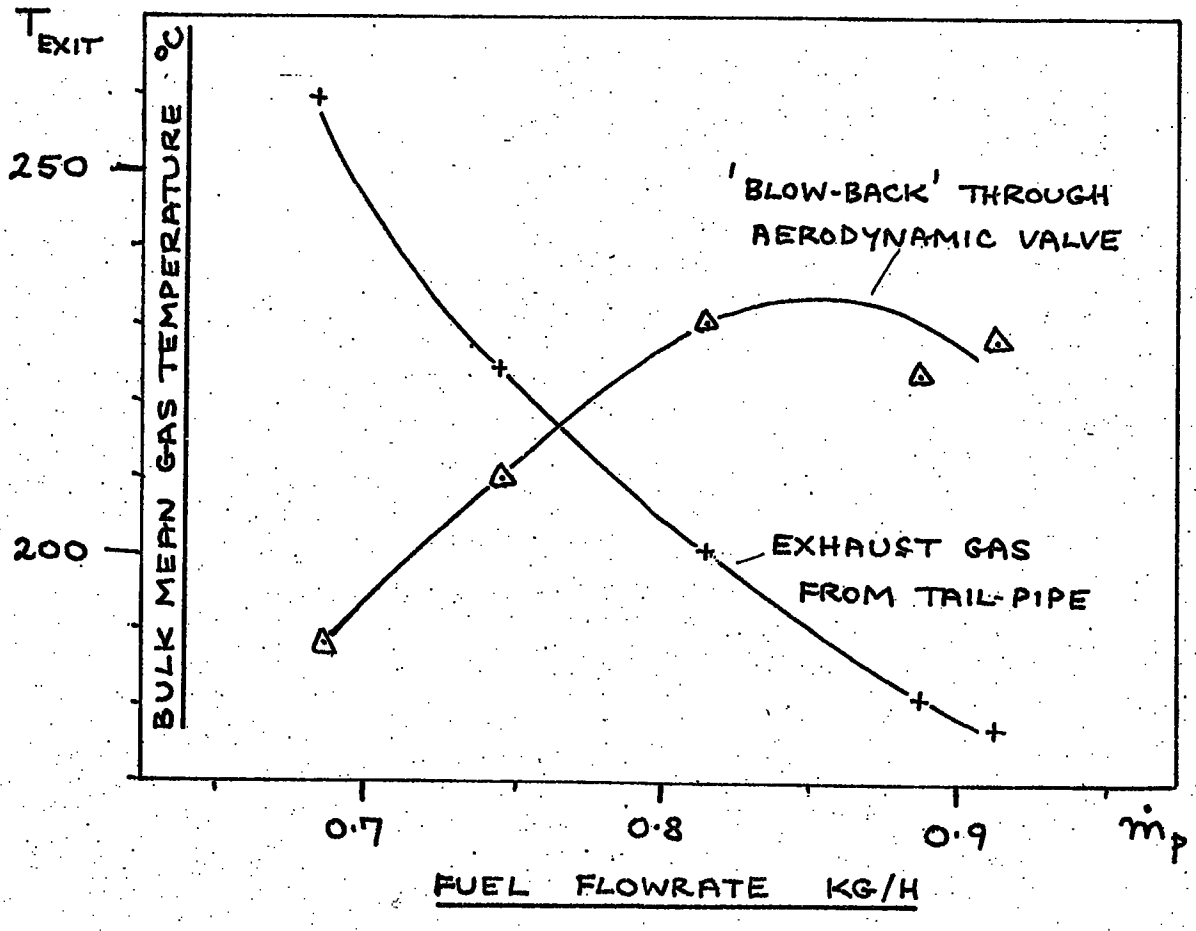

FIGURE B.4: VARIATION OF GAS OUTLET TEMPERATURES WITH FUEL FLOWRATE

dynamic valve rose from 185 to 225°C, as may be seen from Figure B.4. It was also found that, over the same range of fuel flowrate, the thermal efficiency (Figure B.5.) of the combustor fell from 38.5 to 32 per cent. It was concluded from these observations that the reverse flow of hot gases through the aerodynamic valve ('blowback') represented a significant energy loss which would be difficult to measure without placing heat exchangers suitably. It was realised that, if this was done, cool air would be entrained into such a heat exchanger, thus reducing the temperature difference between the hot gases and the cooled walls. A further experiment was made to determine the effect of aerodynamic valve length upon the volumetric combustion rate. The results are shown in Figure B.6. where maximum fuel flowrate is plotted against valve length for an internal diameter of 16 mm. It was concluded from this graph that, in order to obtain a wide turn-down ratio, a short valve was desirable.

It was decided then to construct an apparatus in which local heat transfer coefficients could be measured, (see Figure B.7.). Two identical combustors were aligned horizontally opposite each other. It was intended that, by operating the combustor under counterphase conditions, the blow-back from one valve would be inducted by the other, and thus virtually eliminate energy losses. The combustion chambers were mounted on a slide within a large wooden box so that the gap between the two valves could be varied from 5 to 260 mm. The box was lined with tin foil to reduce radiation losses from the unlagged chambers. Its purpose was to act as a smoothing reservoir so that a measurement of the airflow could be made. The volume of the box was 0.45 m^3, calculated from the formula in B.S.726 (51).

The design of the combustors is shown in more detail in Figures B.8. & 9. The aerodynamic valves were 50 mm. long and 16 mm. internal diameter. Each combustor had nine sampling sites; those of Combustor A were used to measure gas and water temperatures, while those of Combustor B were for pressure measurements and exhaust sampling. The gas temperatures were measured by

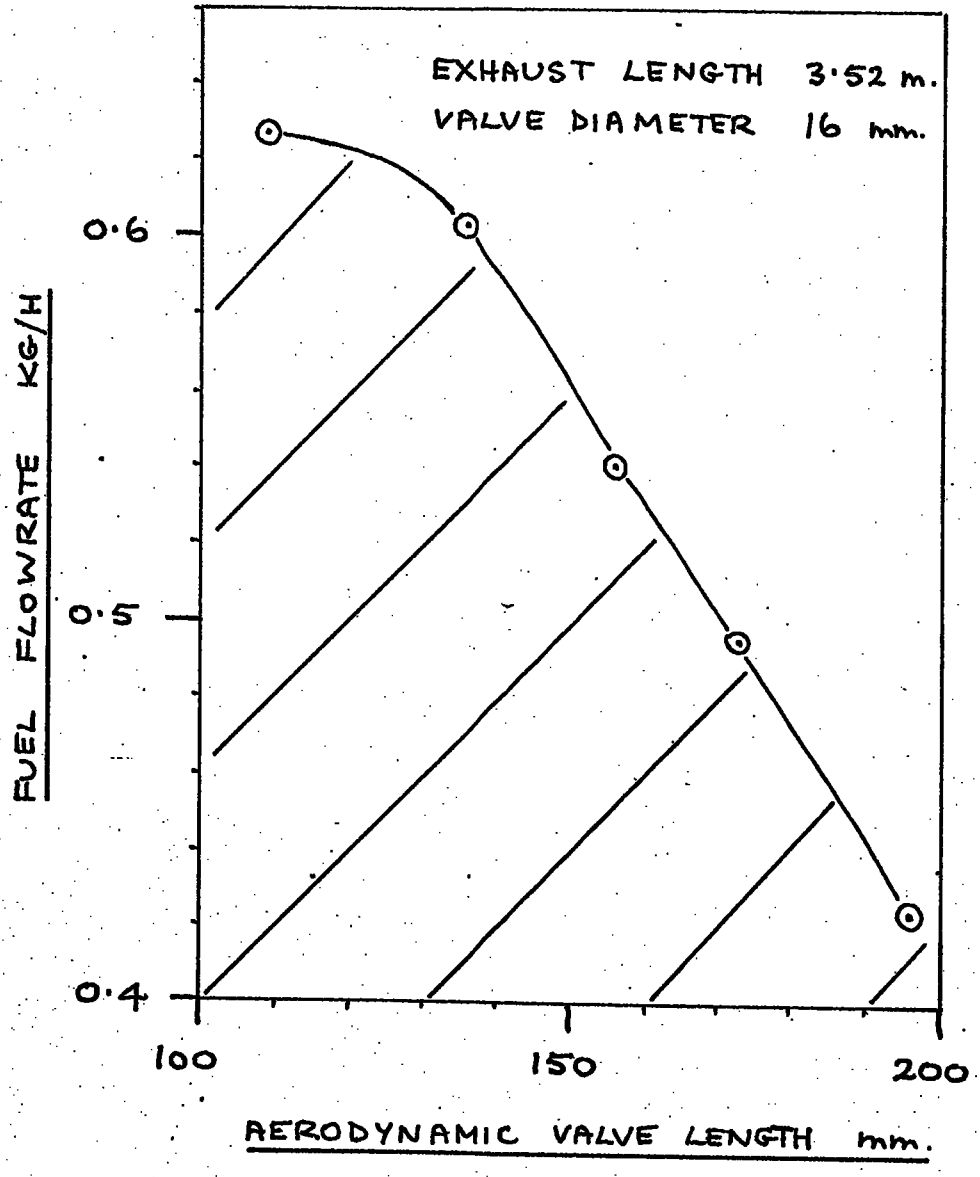

FIGURE B.6 : VARIATION OF 'BLOW-OFF' LIMIT WITH AERODYNAMIC VALVE LENGTH

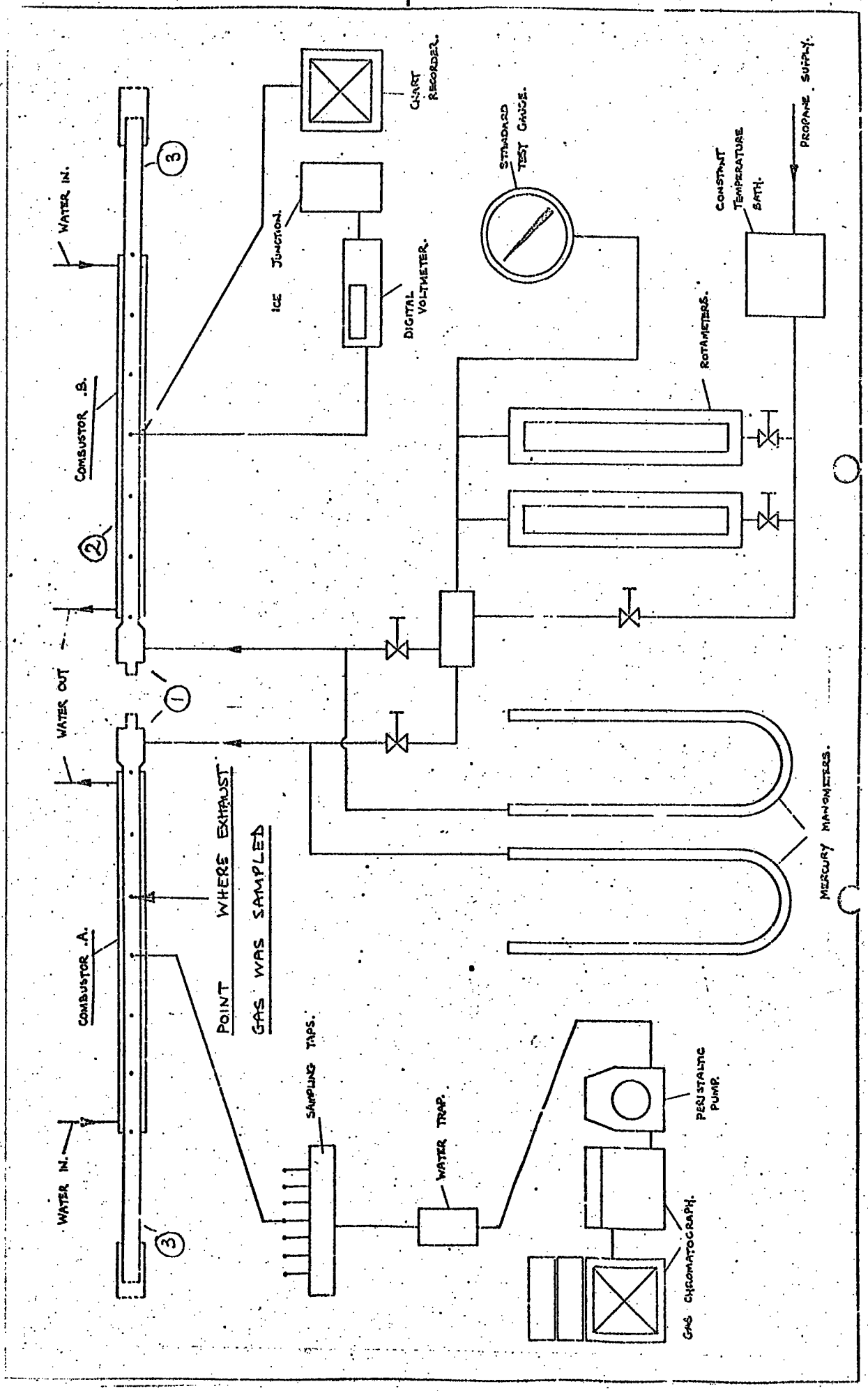

FIGURE B.7 : OPPOSED COMBUSTOR APPARATUS

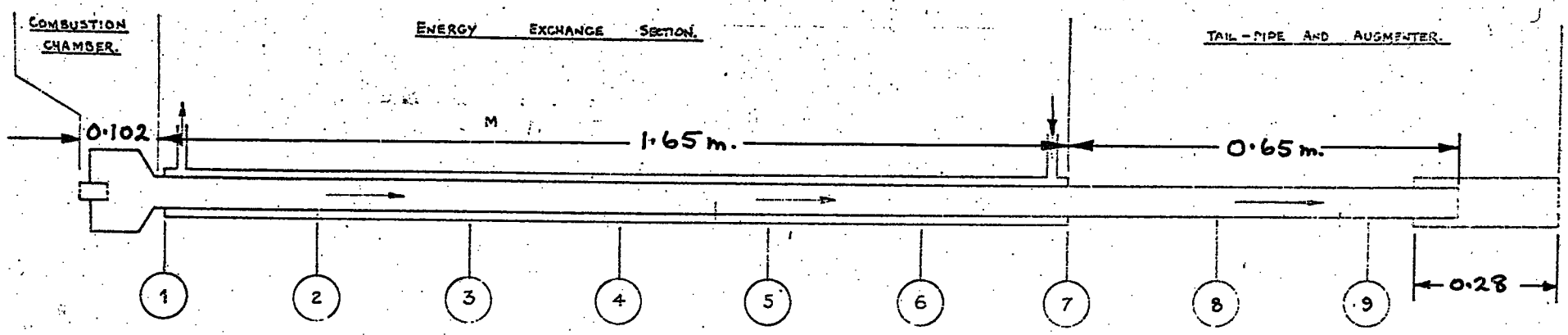

FIGURE B.8: LAY-OUT OF INSTRUMENTED COMBUSTOR

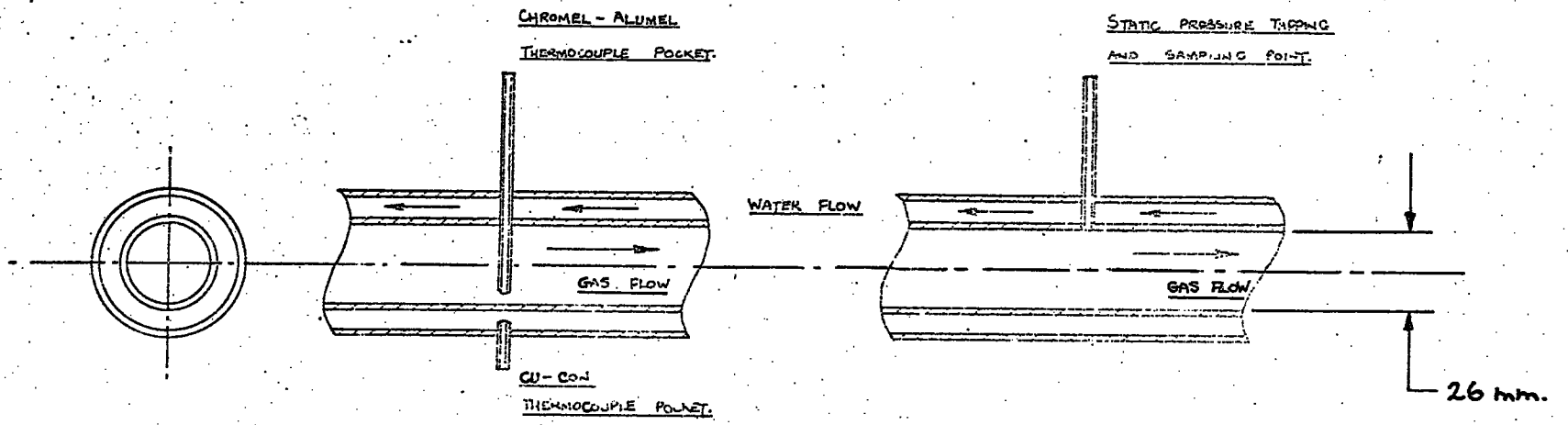

FIGURE B.9: SAMPLING SITES IN THE HEAT EXCHANGERS

inserting a chromel-alumel thermocouple into the chosen pocket, which was sealed when not in use. The water temperature sites were all provided with copper-constantan thermocouples which indicated directly on a chart recorder. The static pressure measurements were measured by an inclined water multi-manometer.

During early experiments on this apparatus it was observed that a short length of 37 mm. diameter tube, when held over the end of the tail-pipe, caused the combustion-driven oscillations to jump to a higher frequency. In addition the pressure variation became very regular, and the maximum volumetric combustion rate was increased. This tube is similar to the augmenters of Muller (19), and, although he intended them to perform as ejectors and used slightly divergent tubes, this term is used henceforward. The diameter of the augmenter was found not to be critical, but its length was important, and one of 0.45 m. gave the best results. The reason for the improving effect of the augmenter was not clear.

Results

The results of tests on Combustor 4 are presented here. Figure B.10. illustrates a typical sequence of frequency jumps during the warm-up period of the combustor. The frequency was measured by a piezo-electric transducer, and the chamber wall temperature by a chromel-alumel thermocouple. The frequency jumped from 93 to 160 to 245 Hz. If the mean gas temperature is taken to be 500°C, and the length of the resonator being 2.4 m., the natural frequencies are given by simple acoustic theory to be:

open-open tube; 104, 208, 312 Hz

closed-open tube; 52, 156, 260 Hz

The bands have been marked to show a region of instability in which the operating frequency of the combustor alternated randomly. From the comparison of the experimental and calculated operating frequencies shown, it was evident that simple acoustic theory was inadequate.

FIGURE B.10: VARIATION OF COMBUSTOR FREQUENCY WITH COMBUSTION CHAMBER WALL TEMPERATURE DURING WARM-UP

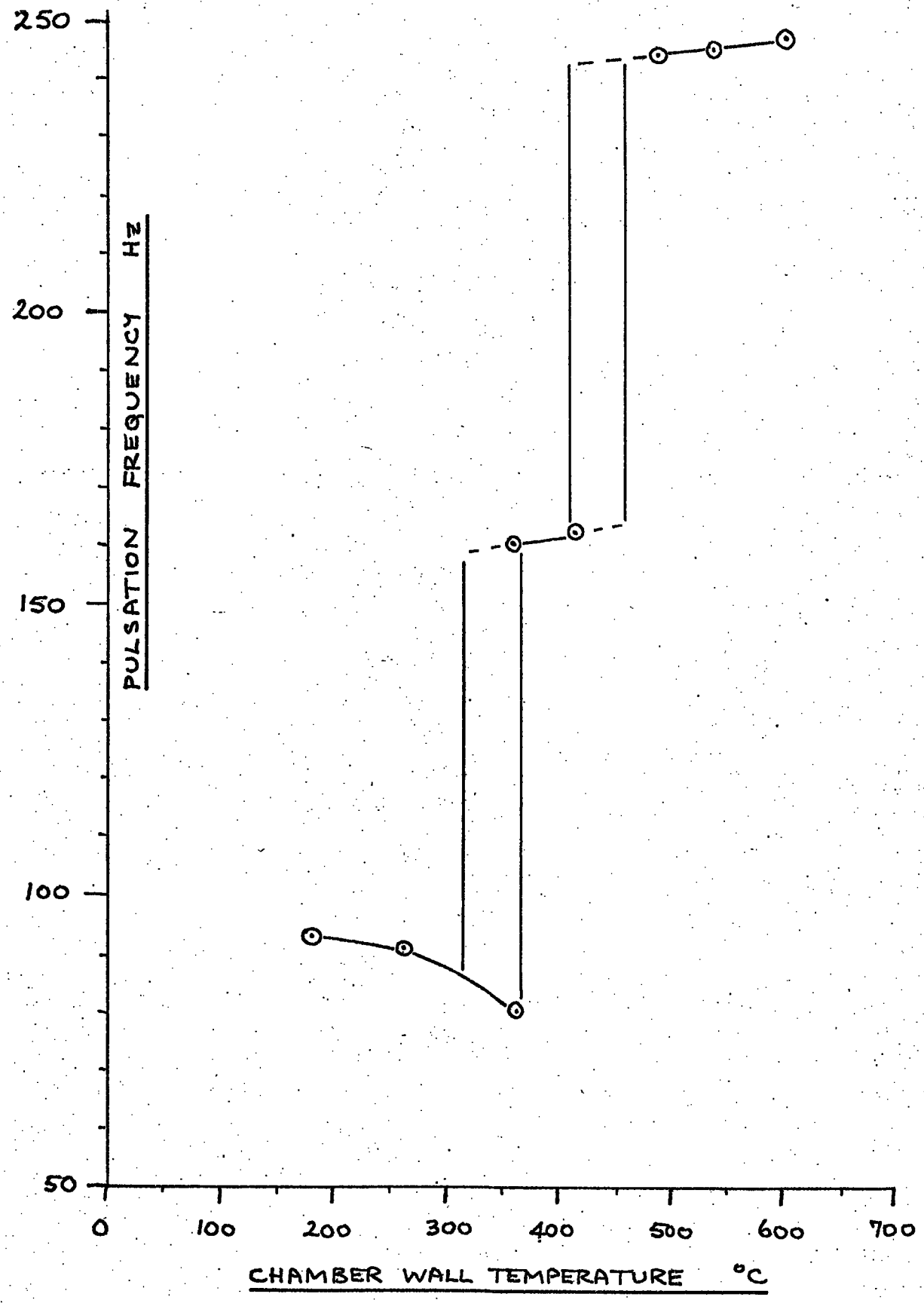

FIGURE B.11 : VARIATION OF COMBUSTOR FREQUENCY WITH COMBUSTION CHAMBER WALL TEMPERATURE

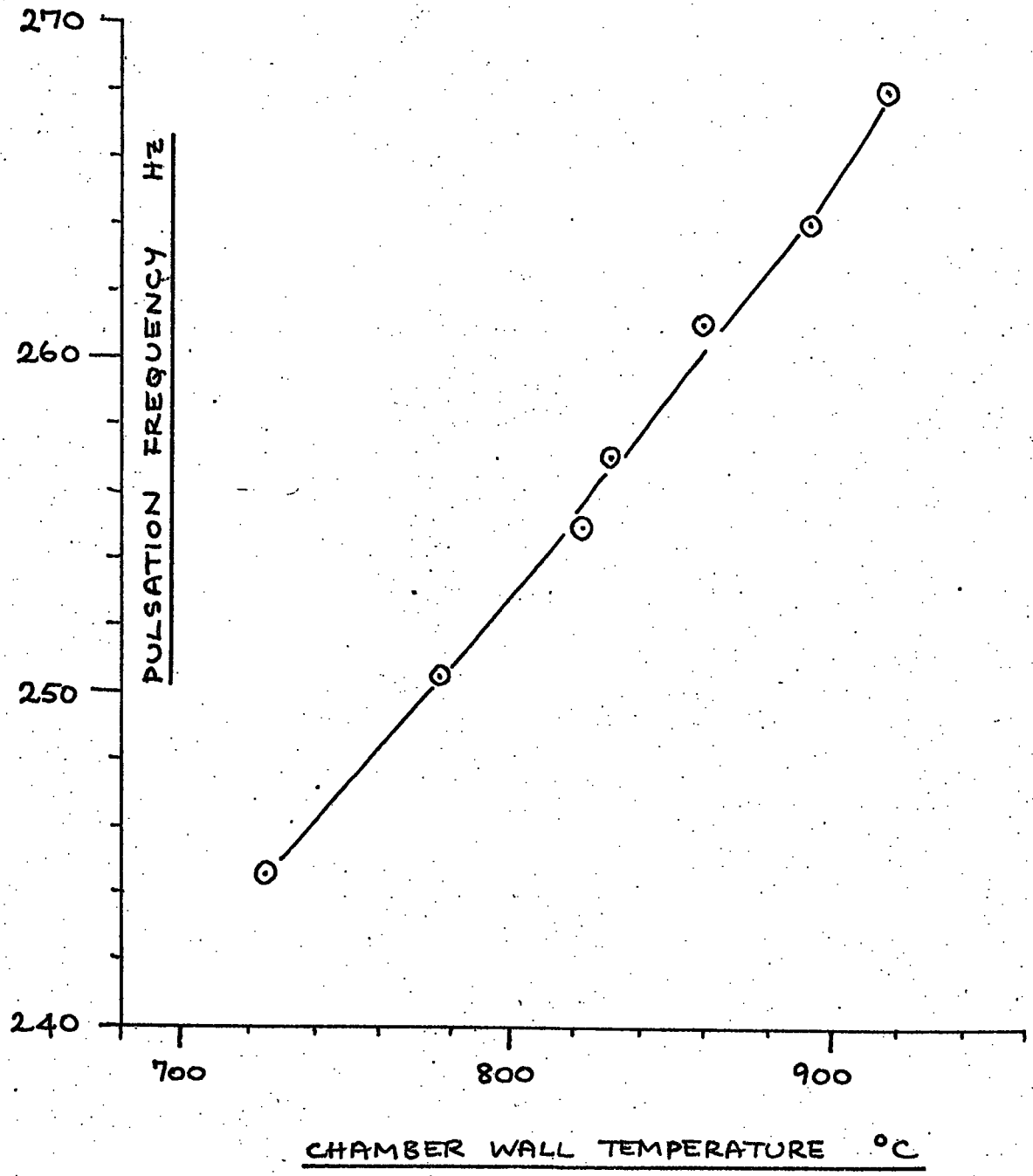

Figure B.11. shows that, having reached the 245 Hz mode, the combustor frequency rose at the rate of 0.25 Hz/°C but did not jump higher as the chamber reached its maximum temperature of approximately 920°C. The rise was attributed to the increasing velocity of sound in the gases.

Figures B.12. and B.13. illustrate the gas and water temperature distributions found within the heat exchanger of Combustor A. The gas temperature fell approximately 380°C in the final 1.375 m. of the heat exchanger. No measurement at the entrance was taken, but from Figure B.11, it was approximately 900°C. Thus the gas temperature fell 600°C in the first 0.275 m. of the heat exchanger. The water temperature showed the greatest rise, of 60°C, in the first 0.54 m. of the heat exchanger, the rise up to that point, of 18°C, being approximately linear. The greatest energy transfer therefore occurred at the entrance to the heat exchanger. This was expected because the difference in temperature between the gases and the water was greatest in this region. During the tests the Reynolds number of the water flow in the annulus was 650, and that of the gas flow ranged from 2700 at the hot end to 6750 at the cold end. It was concluded from this that the water flow was essentially laminar, and that the gas flow could be regarded as turbulent.

The data permitted heat transfer coefficients to be calculated. By drawing a control volume around each of the six sections of the heat exchanger and applying the First Law, the mean heat transfer coefficient, based on the area separating the two fluids, was:

$$h = \frac{\dot{m}_w c_{p_w} \Delta T_w}{\pi d_o \Delta x (T_{Bm} - T_{wm})} \qquad 6\text{-B.1}$$

The heat transfer coefficients thus calculated are plotted against distance along the combustor in Figure B.14. The coefficients fall steeply from a value of 240 W/m^2 °K at the hot end to a minimum of 22 W/m^2 °K and then rise again to 137 W/m^2 °K at the cold end. Shown on the same graph is the variation in the pressure amplitude along the combustor. This was assumed to be sinusoidal, and the combustor was assumed to be operating as a closed-

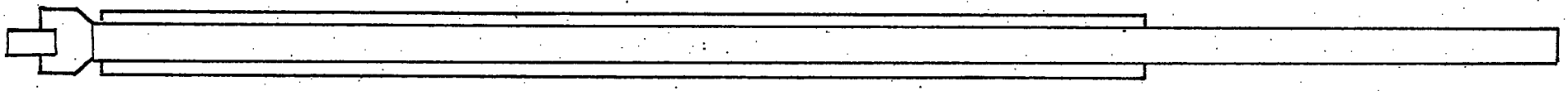

FIGURE B.14 : VARIATION OF HEAT TRANSFER COEFFICIENT AND PRESSURE AMPLITUDE ALONG COMBUSTOR

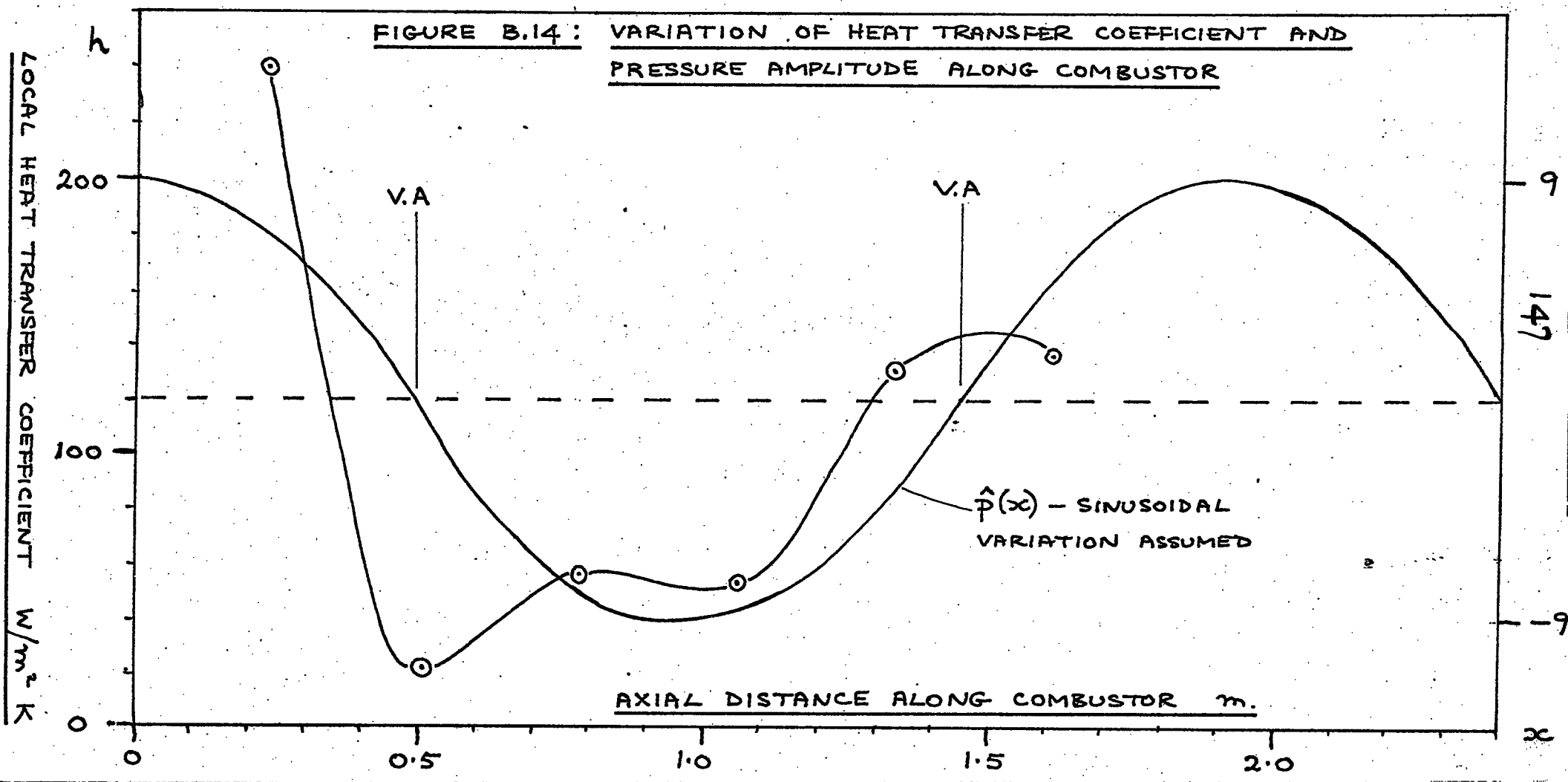

FIGURE B.15: CORRELATION BETWEEN OVERALL HEAT TRANSFER COEFFICIENT IN HEAT EXCHANGER A AND COMBUSTION CHAMBER PRESSURE AMPLITUDE

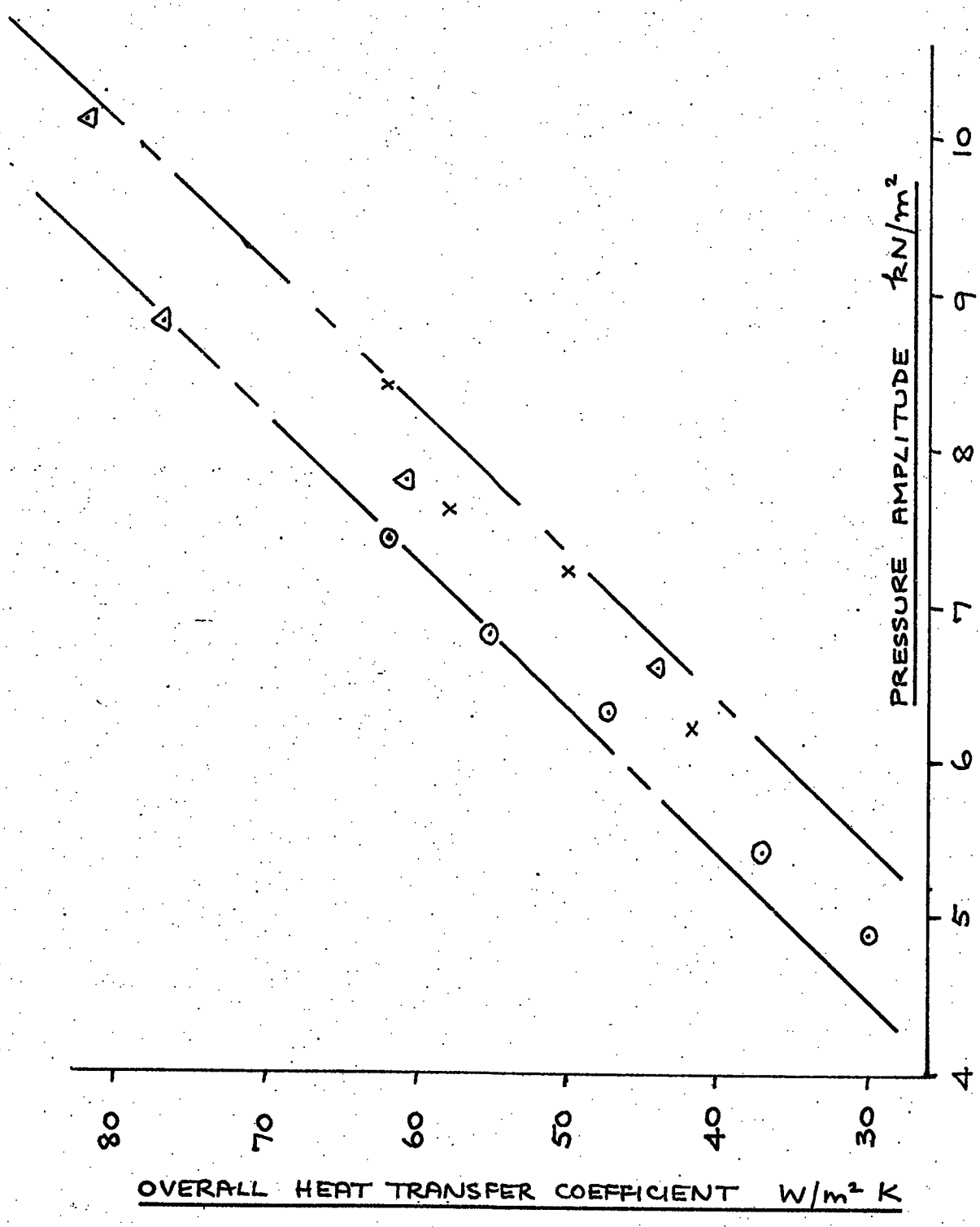

open tube. The only measurement of pressure amplitude was taken at the combustion chamber with a piezo-electric transducer. Assuming that oscillations in particle velocity within the tube were phased 90° ahead of the pressure oscillations, the velocity antinodes may be taken to lie on the graph at the pressure nodes. At the first velocity antinode at x = 0.48 m, the heat transfer coefficient reaches a minimum. At x = 0.96 m, a velocity node, the heat transfer coefficient is approximately constant. At x = 1.44 m, the heat transfer coefficient attains a local maximum. According to this evidence, therefore, it appears that the local velocity variations in the gas flow affect the heat transfer coefficient in opposite ways. This anomaly was caused by:

a) the pressure amplitude variation shown took no account of the severe axial temperature gradient existing in the gas flow;

b) the uncertainty in the deduction of the heat transfer coefficient.

The effect of a) is that, in reality, the waveform would be compressed towards the cold exhaust end because, for a given frequency, the decrease of the sound velocity in the cooling gases would be accompanied by a shorter wavelength. This means that the pressure nodes, as shown, are shifted towards the combustion chamber. Regarding b), an analysis of equation 6-B.1 showed that the temperature rise in the water, ΔT_w, was calculated by subtracting two values taken from the chart recorder. It was estimated that the maximum possible error arising from this source was 25%, with an expected highest error of 15%.

Figure B.15 shows a graph of overall heat transfer coefficient against combustion chamber pressure amplitude. The overall heat transfer coefficient was based on the logarithmic mean temperature difference. The linear character of the graph is evident.

As the apparatus had given a great deal of trouble in operation, it was decided to construct a single new combustor, incorporating a longer heat exchange section and improved measurement techniques.

Exhaust Gas Analysis

A Pye Series 104 Gas Chromatograph was used to analyse the products of combustion passing through the heat exchangers of the combustor. The carrier gas was argon, which was passed through a drying agent before entering the instrument. A coiled tube, 1 m. long and filled with Molecular sieve was used to elute hydrogen, oxygen, nitrogen and carbon monoxide from the sample, and a similar one filled with Silica Gel to elute carbon dioxide. A peristaltic pump drew samples from the combustor, in which the mean pressure was approximately atmospheric, through a water trap.

It was found by experiment that the best settings for the chromatograph were:

Detector oven temperature	50°C
Analyser oven temperature	50°C
Argon flowrate	22 ml/min
Sample flowrate	33 ml/min
Katherometer current	60 mA
Chart speed	12 in/h

A typical chromatogram is shown in Figure B.16 and Figure B.17 shows the result of the tests. It is evident that the combustor operated on the lean side of stoichiometric. With increasing fuel flowrate the air/fuel ration approached stoichiometric. The graph suggests a connection between the maximum volumetric combustion intensity and the attainment of stoichiometric conditions. If this were so, it could be concluded that pulsating combustors extinguish under fuel rich conditions. It was also observed that no carbon monoxide was present in measurable quantities, although up to 0.5 per cent hydrogen was found occasionally.

Summary

The preliminary work showed that the Helmholtz-type combustor would be satisfactory for the investigation. It was felt that it could be improved

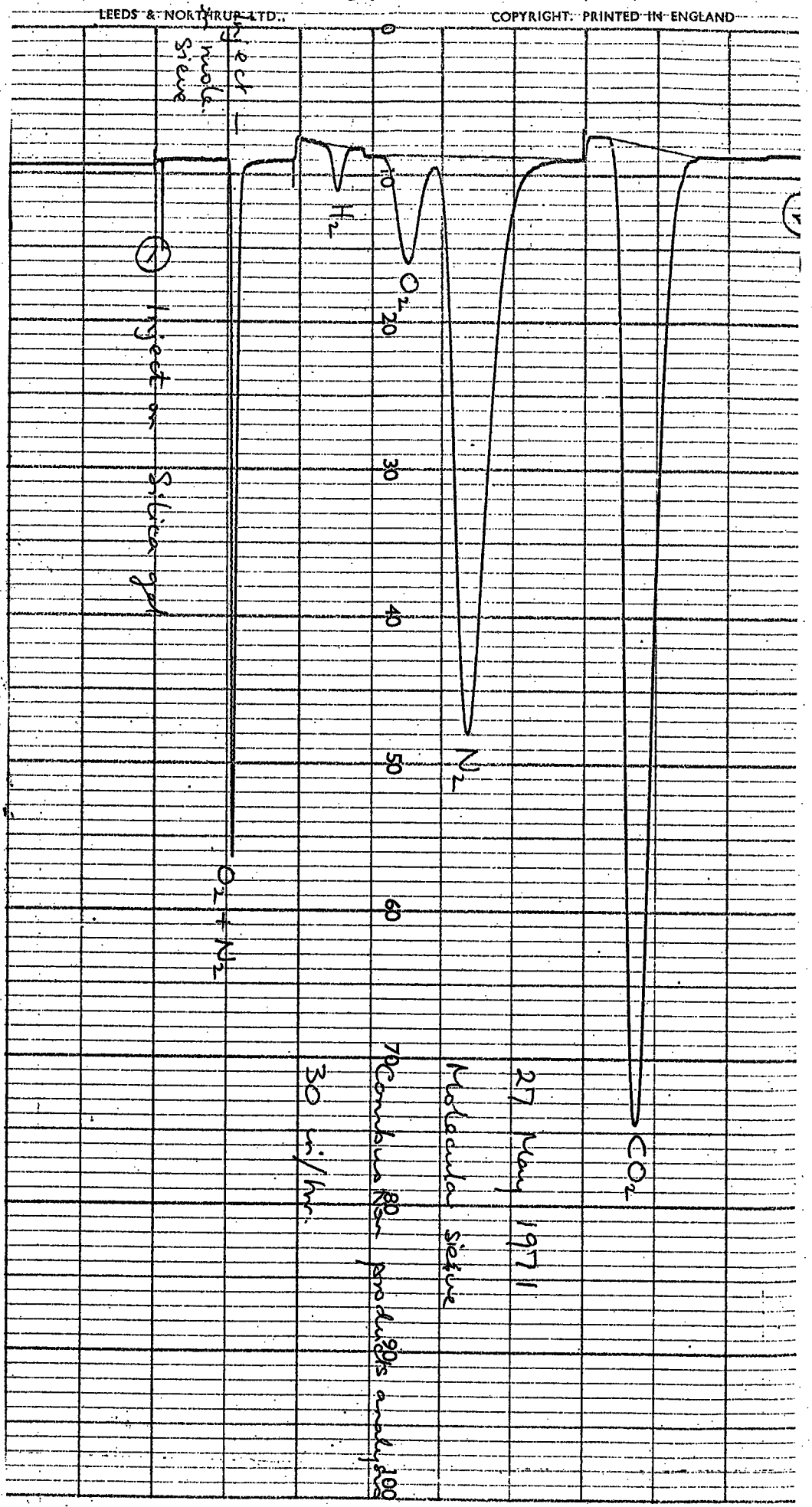

FIGURE B.16 : CHROMATOGRAM OF EXHAUST GASES

FIGURE B.17: RESULT OF DRY VOLUMETRIC ANALYSIS OF EXHAUST PRODUCTS

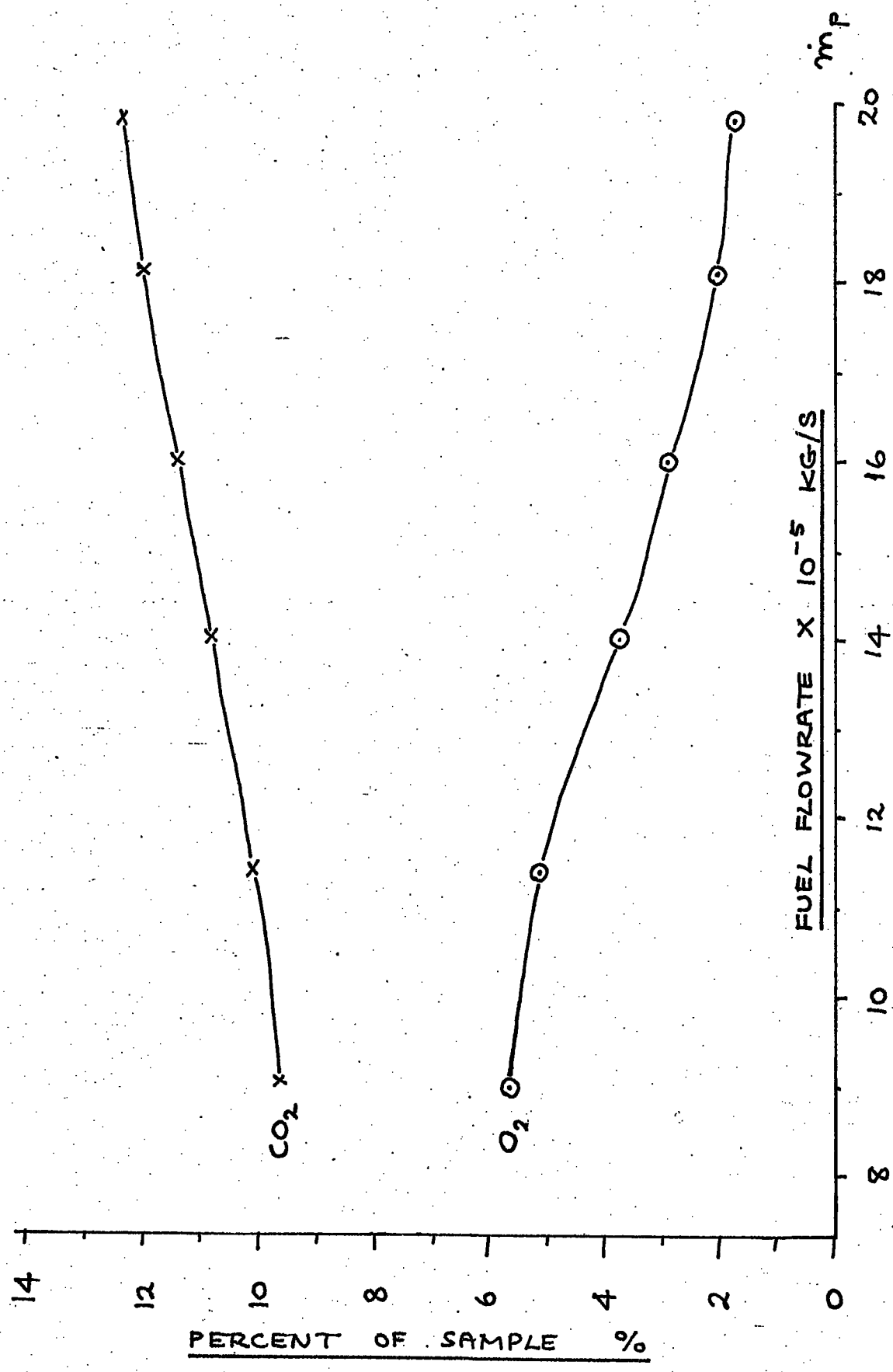

by lengthening the heat exchanger to spread out the effects under observation, and by adding heat exchangers to the inlet side to recover the energy loss caused by blowback through the valve. It was felt that the dimensions of the valve should lie in the range 12 - 26 mm. diameter and be 50 mm. long. It was found that the waveform of the pressure oscillation was approximately sinusoidal, and that, compared to it, the mean static pressure within the combustor was approximately atmospheric. It was decided that the accuracy of the fuel flowrate measurement should be improved.

6.C. Gas Temperature Corrections

As stated in Section 3.4.1., two types of thermocouple were used to measure the gas temperature. These were a bare Type S junction mounted on a silica rod and a Type K sheathed thermocouple. The temperature of the junction in both cases required corrections for three reasons:

a) convective and radiant heat exchange occurred between the gas, tube walls and the thermocouple, as well as conduction from the junction;

b) the thermocouple was heated due to stagnation of the gas velocity;

c) as the junctions were at fixed radii in the tube, the reading had to be corrected to the bulk fluid temperature.

a) Thermocouple A

This thermocouple junction, a bead of 0.8 mm. diameter, projected 9.0 mm. into the gas flow. It was supported by its two constituent wires, which were threaded through a silica rod of low thermal conductivity. It was decided that, even though the thermocouple wires did not run parallel to the flow for a few millimetres, the predominant influences on the bead were radiation and convection. To simplify calculation, it was assumed that the surroundings were large and that the effective radiation temperature of the surroundings was $T_{S\phi}$. The following energy balance may then be made, as in Figure C.1;

$$h_c S_B (T_{A1} - T_{A1}') = S_B \sigma \varepsilon_B (T_{A1}'^4 - T_{S\phi}^4) \qquad 6\text{-C.1}$$

where T_{A1}' is the temperature recorded by the thermocouple. The normal total emissivity of a platinum filament lies in the range 0.036 to 0.192 over the temperature range 27 to 1230°C, according to Simonson (53). Thus was taken to be 0.19. The correlation used for forced convection over spheres was taken from Holman (54):

$$Nu_d = 0.37 (Re_d)^{0.6} \qquad 6\text{-C.2}$$

Thus:

$$h_c = 462 k_A \left\{ \frac{0.8}{10^3} \frac{\bar{u}_A \rho_A}{\mu_A} \right\}^{0.6} \qquad 6\text{-C.3}$$

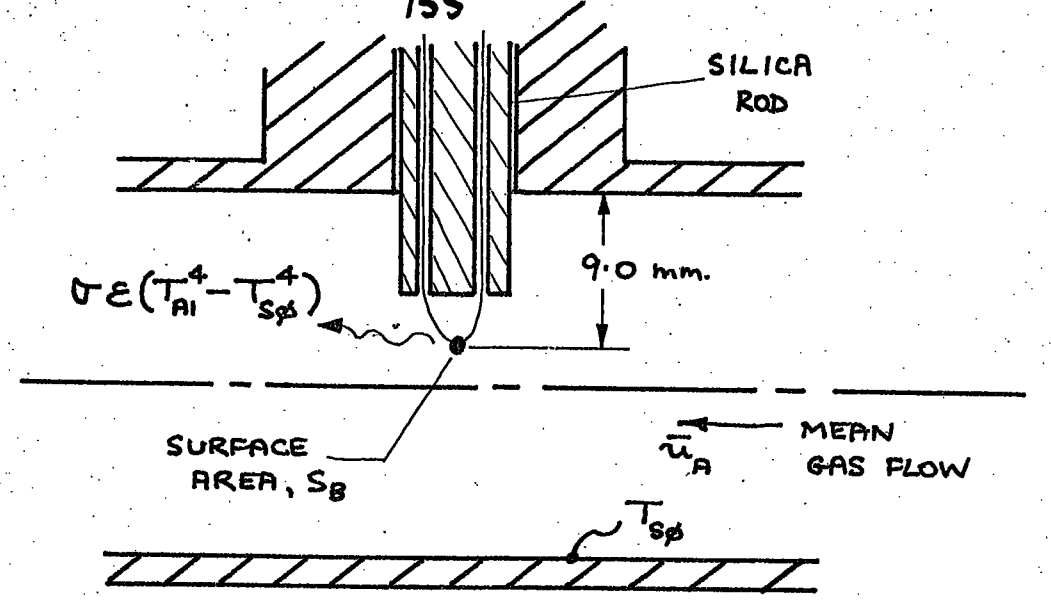

FIGURE C.1 : EXAGGERATED T_{AI} INSTALLATION

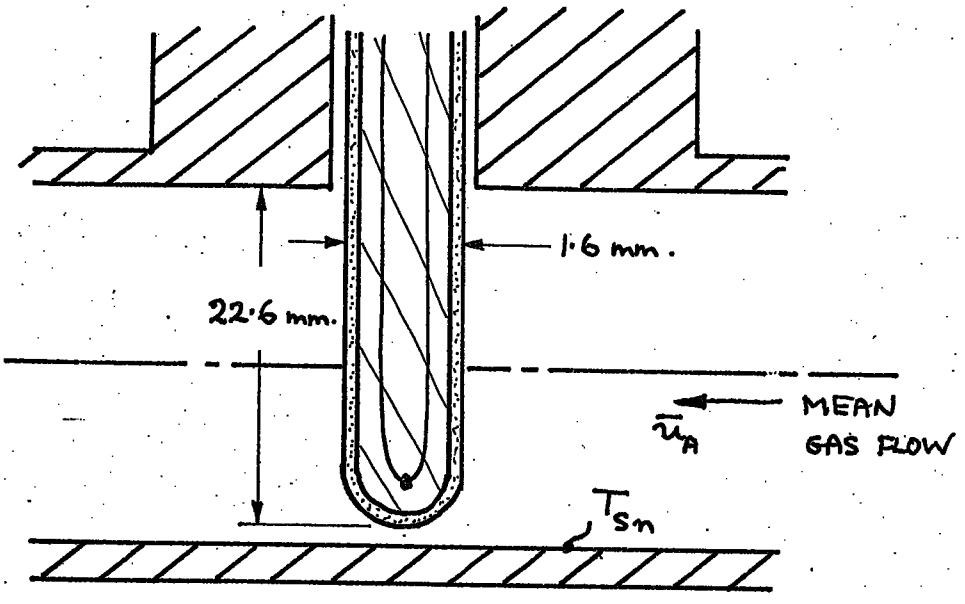

FIGURE C.2: EXAGGERATED T_{Am} INSTALLATION

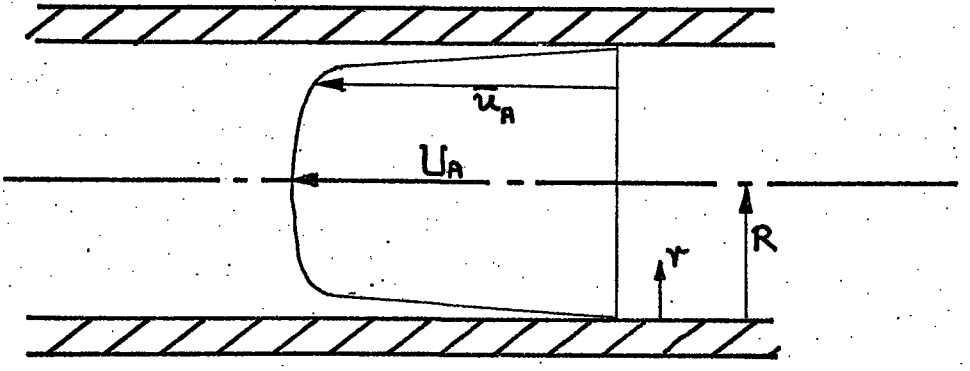

FIGURE C.3 : TIME-AVERAGED VELOCITY PROFILE

The properties of air in equation 6-C.3 were evaluated at T'_{A1}, and u_A was deduced from $\dot{m}_{AA}$ by the continuity equation:

$$\bar{u}_A = \frac{\dot{m}_{AA}}{3600\, \rho_A\, S_\phi} \qquad 6\text{-C.4}$$

The total correction is, from equations 6-C.1:

$$T_{A1} = T'_{A1} + \frac{1.08\,(T'^4_{A1} - T^4_{S\phi})}{10^8\, h_c} \qquad 6\text{-C.5}$$

where h_c is calculated from equations 6-C.3 and 6-C.4.

Thermocouple B

This thermocouple junction was embedded in magnesium silicate powder and sheathed in 25/20 Chromium/Nickel steel. It projected 22.6 mm. into the flow and was mounted in a brass collar so that it could be screwed into the measuring sites on the resonating section. (See Figure C.2). Due to this requirement, the thermocouple was straight, and again not bent along an isothermal to reduce conduction. It was decided that the temperature of the junction was affected by radiation, convection and conduction, and the analysis of Chapman (55) was used:

$$\frac{T'_{An} - T_{Sn}}{T_{An} - T_{Sn}} = \frac{h_c}{h_c + h_r} \cdot \frac{\cosh(m_1 L) - 1}{\cosh(m_1 L)} \qquad 6\text{-C.6}$$

where T'_{An} was the reading of the thermocouple at the Site number n, L was the immersion of the thermocouple and m_1 was given by:

$$m_1 = \left\{ \frac{h_c + h_r}{k_{sh}\, t_{sh}} \right\}^{1/2} \qquad 6\text{-C.7}$$

t_{sh}, the thickness of the sheath wall, was 0.15 mm. The radiation and convection coefficients were taken from Chapman and Holman respectively:

$$h_r = \sigma\, \varepsilon_{sh}\, \frac{(T'^4_{An} - T^4_{Sn})}{(T'_{An} - T_{Sn})} \qquad 6\text{-C.8}$$

$$h_c = 0.5\, \frac{k_{sh}}{d_{sh}}\, R_d^{0.5} \qquad 6\text{-C.9}$$

Again, the properties of air were evaluated at T'_{An} . The normal total emissivity of the sheath was taken from Simonson to be 0.82, as the surface became blackened with use. The thermal conductivity of 18/8 Chromium Nickel steel is 22.5 W/m°K at 600°C, and this value was used for k_{sh} .

b) Assuming that the two installations completely stagnate the moving gas adiabatically, the thermocouples recorded the total temperature of the gas. Therefore:

$$T'_{An} = T_{An} + \frac{u_A^2}{2 c_{p_A}} \qquad 6\text{-C.10}$$

Now, the velocity of the gas at any instant, u_A, is given by equation 2.3.6:

$$u_A = \bar{u}_A + u'_A \qquad 2.3.6.$$

The stagnation temperature of the gas at any instant thus depends on the velocity amplitude of the oscillations as well as the mean velocity, $\bar{u}_A$, of the gas.

c) The bulk fluid temperature at a cross-section may be defined, for an incompressible fluid of constant properties, as:

$$T_B = \frac{\int_0^R c_p T \rho u r \, dr}{c_p \int_0^R \rho u r \, dr} \qquad 6\text{-C.11}$$

T_B is dependent on the velocity distribution across the tube. In the absence of a direct measurement, which would have required a special hot-wire anemometer, it was assumed that the time-averaged velocity distribution in the tube was given by an equation of the type:

(see Figure C.3)

$$\frac{u}{U} = \left(\frac{r}{R}\right)^{1/n} \qquad 6\text{-C.12}$$

For Re = 4000, Bayley et al (56) give $n = 6$ and the ratio:

$$\frac{\bar{u}_A}{U_A} = 0.791 \qquad \text{6-C.13}$$

Now equation 6-C.11 may be written:

$$T_B = \frac{3600}{\dot{m}_{AA}} \rho_A \int_0^R T_A u_A r \, dr \qquad \text{6-C.14}$$

Substitution of 6-C.4, 6-C.12 and 6-C.13 into 6-C.14 yields:

$$T_B = \frac{1}{0.791 \, S_\phi} \int_0^R T_A(r) \left(\frac{r}{R}\right)^{1/6} r \, dr \qquad \text{6-C.15}$$

It was therefore necessary to measure the temperature profile, $T_A(r)$ at a cross-section. This was done at Site 7 for two fuel flowrates, and the results are shown in Figure C.4. A Type K thermocouple, of 0.5 mm. diameter, was mounted on a slide with a micrometer and traversed across the tube. Immediately after the traverse, the Pyrotenax Type K thermocouple was inserted, and a reading obtained under the same conditions. It was assumed that the corrections to the readings from these thermocouples were identical, although this is an approximation since the immersion of the traversing thermocouple necessarily changed.

The data from the traverses was used to integrate equation 6-C.15 by Simpson's Rule, and the results are shown in Table C.1.

Table C.1.

Comparison of experimental reading with corrected temperature

$\bar{Re}_A$	Experimental Reading	T_B
3840	152	141
4800	144	128
	°C	°C

FIGURE C.4 : GAS TEMPERATURE PROFILE AT SITE 7 FOR TWO FUEL FLOWRATES.

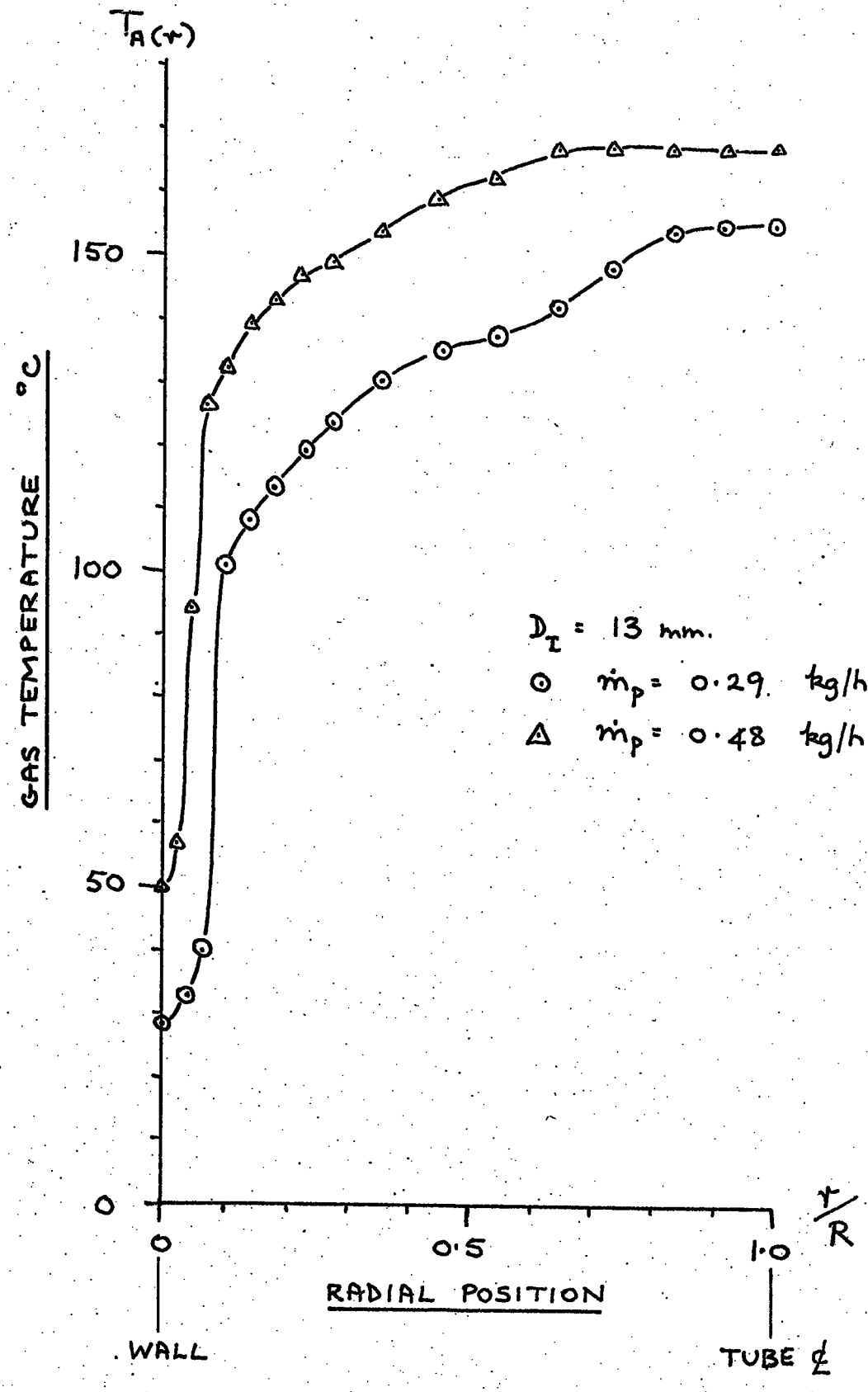

It transpired that the product $m_1 L$ always exceeded 5, and thus equation 6-C.6 became:

$$T_{An} = T_{Sn} + \left(\frac{h_c + h_r}{h_c} \right) \left(T'_{An} - T_{Sn} \right) \qquad 6\text{-C.17}$$

The correction to the Pyrotenax installation therefore depended only on the relative magnitudes of the convection and radiation coefficients. The ratio $(h_c + h_r / h_c)$ lay in the range 1.01 to 1.2, corresponding to corrections of approximately 0.5°C and 130°C at the cold and hot ends respectively.

The gas temperature corrections were applied using the programmes overleaf.

```
C  TA1 TEMP. CORRECTION PROG
      IMPLICIT REAL*8(A-Z)
    3 CONTINUE
      READ(5,1000)TA,TS,MAA
      IF(TA)6,6,4
    4 CONTINUE
      RED=MAA/(2497*MUA(TA))
      HC=462*KA(TA)*(RED**0.6)
      TA=TA+1.08*(TA**4-TS**4)/(100000000*HC)
      WRITE(6,1001)TA
 1001 FORMAT(6X,F10.2)
 1000 FORMAT(5(F10.3))
      GO TO 3
    6 CONTINUE
      STOP
      END
```

```
C  TAN TEMP. CORRECTION PROG
      IMPLICIT REAL*8(A-Z)
    3 CONTINUE
      READ(5,1000)TA,TS,MAA
 1000 FORMAT(5(F10.3))
      IF(TA)6,6,4
    4 CONTINUE
      RED=0.0016*MAA/MUA(TA)
      HC=384*KA(TA)*(RED**0.47)
      HR=(TA**4-TS**4)*4.69/((TA-TS)*100000000)
      R=(HC+HR)/HC
      TA=TS+(R*(TA-TS))
      WRITE(6,1001)TA
 1001 FORMAT(6X,F10.2)
      GO TO 3
    6 CONTINUE
      STOP
      END
```

Type T thermocouple Calibrations

This was achieved by lagging the resonating section thoroughly with Cosywrap and running a constant flow of water through the heat exchangers without firing up the combustor. The system was allowed to reach equilibrium and then readings of all the surface and water thermocouples were taken, together with the mercury-in-glass thermometer readings T_{W1} and T_{W9}. The mean of these last two was taken, and all other readings compared. In the case of the surface thermocouples, the corrections lay in the range -1.7 to +1.3 K, and in the case of the water thermocouples, the corrections lay in the range -0.3 to +1.3 K. These corrections were applied to the experimental readings by the programme CKBC.

6.D. Calibration of Pressure transducer mountings

The Kistler pressure transducer mountings were calibrated by comparing their response to a range of frequencies with that of a calibrated Bruel and Kjer microphone. The apparatus is shown in Figure D.1 and was set up in the middle of high, open laboratory to minimise reflections. The loud-speaker was excited by an audio wave generator at the highest level that could be sustained over the range 60 to 220 Hz without overloading the cone. The transducer mountings and calibrated microphone were held by a clamp so that the open end of the tubes and the diaphragm, respectively, were in the same position relative to the loudspeaker. The procedure followed was to set the sound level, run through the frequency range at 10 Hz intervals taking the transducer readings, and then, having exchanged the microphone for the transducer, repeat the experiment. The transducer signal was amplified using the same amplifier and oscilloscope as was used in the main experiments, and was transmitted by the same connecting cables. The results of the calibration are shown in Figure 3.19.

The charge sensitivity of the Bruel and Kjer Type 4117 Microphone was calculated as follows, from (57);

Charge sensitivity, $S_{charge} = S_v \times C_m$

and the voltage sensitivity was given as:

$$S_v = 0.37 \ mV/\mu Bar$$

The sensitivity correction was:

$$S_{v(c)} = \frac{S_v (C_m + 0.1)}{C_m + C_c + C_i}$$

where

$C_m = 4.2 \ nF$

$C_c = 3.04 \ m \times 90 \ pF/m$

$C_i = 0.0001 \ pF$

Thus $S_{v(c)} = 0.3556 \ mV/\mu Bar$

and $S_{charge} = 14.9 \ pC / \ N/m^2$

FIGURE D.1 : APPARATUS FOR CALIBRATION OF PRESSURE MEASURING SYSTEM

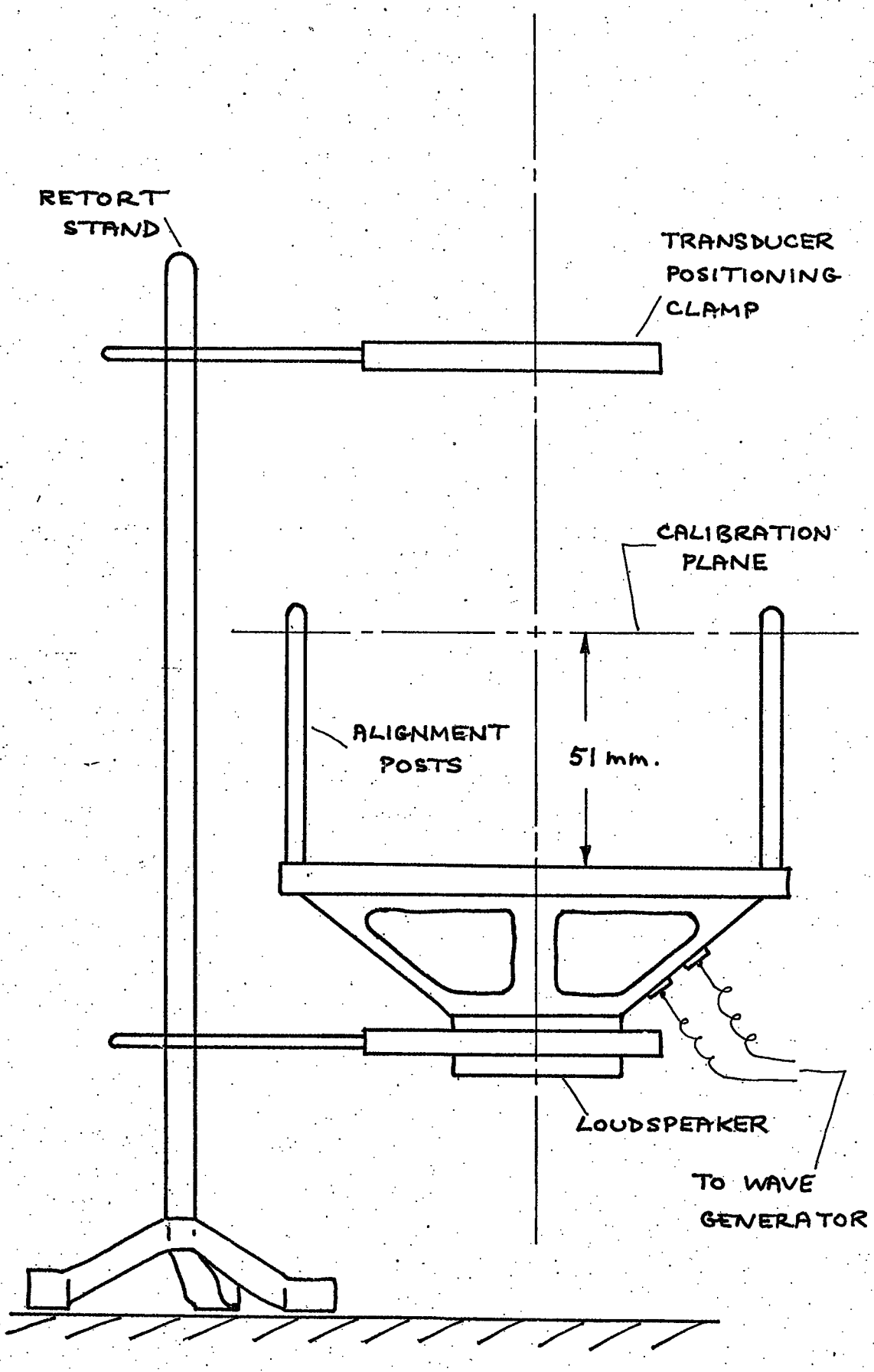

The amplifier was set to an amplification of 1.49 x 1000 and the time-constant to 0.1 m S . From the Vibro-Meter Ag Handbook (Bib/16.49), and the setting of the oscilloscope, the final amplification was, on the oscilloscope screen:

$$1\ V \equiv 10 \pm 0{\cdot}05\ N/m^2$$

X

6.E.1. The Energy Balance

The readings for Experiment 1 were converted to S.I. units and corrected to a standard temperature and pressure, 293.16 K and 101.325 kN/m^2 respectively. The following correction factors were used:

Temperature, T $\quad T \times T_o/T_{A_o}$ E.1.1

Pressure, p $\quad p \times P_o/P_{A_o}$ E.1.2

Mass flowrate, $\dot{m}$ $\quad \dot{m} \times \frac{P_o}{P_{A_o}} \times \left\{\frac{T_{A_o}}{T_A}\right\}^{1/2}$ E.1.3

where T_{A_o}, P_{A_o} were the ambient conditions. The mass flowrate, of fuel, water and coolant air were obtained with the following factors to give kg/h:

$\dot{m}_p$ 1.905 x reading E.1.4

$\dot{m}_w$ 105.64 + (37.512 x reading) E.1.5

$\dot{m}_{gc}$ 0.1168 x reading E.1.6

The thermocouple readings were converted by subroutines of the main computation which interpolated quadratically the reference tables. All these operations were performed by a computer programme, CKBC, listed in Appendix F.

E.1.1 Application of the First Law

The Steady Flow Energy Equation is;

$$\dot{Q} - \dot{W}_x = \Sigma_{OUT}\, \dot{m}\left(h + \frac{u^2}{2g_o} + \frac{a_g z}{g_o}\right) - \Sigma_{IN}\, \dot{m}\left(h + \frac{u^2}{2g_o} + \frac{a_g z}{g_o}\right) + \left[\Delta \dot{H}'\right]_{t_o} \qquad \text{E.1.7}$$

where the terms accounting for the effects of capillarity, electricity and magnetism have been ignored. The streams of material entering the control volume are cold water, cold air, propane and cold coolant water, and those leaving were hot water, two streams of combustion products, and hot coolant water. There are no work interactions at the control boundary, if the radiation of sound waves from the open ends of the combustor is regarded as negligible. There are heat interactions in the form of heat transfer through the lagging.

Assuming that the heat transfers through the heat exchanger lagging were negligible, and that the conduction through the combustion chamber lagging is given by;

$$\dot{Q}_{LCL} = - \frac{2\pi k_{LAG} (T_{LAG} - T_{gc}) L_{CL}}{\log_e (D_{L2} / D_{L1})} \qquad \text{E.1.8}$$

Ignoring changes in kinetic and potential energy, equation E.1.7 may be written:

$$\dot{Q}_{LCL} = \dot{m}_w \Delta h_w + \dot{m}_A \Delta h_A + \dot{m}_{WTR} \Delta h_{WTR} + \dot{m}_{WIN} \Delta h_{WIN} + \dot{m}_{gc} \Delta h_{gc} + \dot{m}_p [\Delta h']_{t_o} \qquad \text{E.1.9}$$

The connecting pipe carrying the water flow from Heat Exchangers B and C to A lies outside the control volume in Figure 4.1, so:

$$\Delta h_w = \Delta h_{WA} + \Delta h_{WBC} \qquad \text{E.1.10}$$

and by continuity:

$$\dot{m}_A = \dot{m}_{AA} + \dot{m}_{ABC} \qquad \text{E.1.11}$$

The assumption is now made that the combustion products flowing through the apparatus are predominantly air, and the properties used hereafter for the combustion products are those of pure air. Assuming that air and water behave as pure substance, the changes in enthalpy through the control volume are:

$$\Delta h_{AA_o} = \bar{c}_{p_{AA_o}} (T_{A8} - T_{A_o}) \qquad \text{E.1.12}$$

$$\Delta h_{AC_o} = \bar{c}_{p_{AC_o}} (T_{A23} - T_{A_o}) \qquad \text{E.1.13}$$

$$\Delta h_{WTR} = \bar{c}_{p_{WTR}} (T_{WTR} - T_{W23}) \qquad \text{E.1.14}$$

$$\Delta h_{WIN} = \bar{c}_{p_{WIN}} (T_{WIN} - T_{W23}) \qquad \text{E.1.15}$$

$$\Delta h_{gc} = \bar{c}_{p_{gc}} (T_{gc2} - T_{gc1}) \qquad \text{E.1.16}$$

where the specific heats of the substances are evaluated at the arithmetic mean of the inlet and outlet temperatures.

The mass flowrates of the two streams of air flowing through the apparatus

may be deduced by applying equation E.1.7 to control volumes around Heat Exchanger A and around Heat Exchangers B and C. Using the assumptions already made, the mass flowrates are given by:

$$\dot{m}_{AA} = - \frac{\dot{m}_W \bar{c}_{pWA} (T_{W1} - T_{W9})}{\bar{c}_{pAA} (T_{A8} - T_{A1})} \qquad \text{E.1.17}$$

and

$$\dot{m}_{ABC} = - \frac{\dot{m}_W \bar{c}_{pABC} (T_{W21} - T_{W23})}{\bar{c}_{pABC} (T_{A23} - T_{A21})} \qquad \text{E.1.18}$$

In equation E.1.17, and specific heat, $\bar{c}_{pAA}$, is evaluated at a mean temperature, $\bar{T}_A$, defined by:

$$\bar{T}_A = \frac{1}{(x_e - x_H)} \int_{x_H}^{x_e} T_A(x)\, dx \qquad \text{E.1.19}$$

which may conveniently be integrated by Simpson's Rule;

$$\bar{T}_A = \frac{\Delta L_A}{3} \left[T_{A1} + 4T_{A3} + 2T_{A4} + 4T_{A5} + 2T_{A6} + 4T_{A7} + T_{A8} \right] \qquad \text{E.1.20}$$

where $\Delta L_A = 0.345 \quad m.$

In equation E.1.18, the specific heats are evaluated as for equations E.1.12 to E.1.16.

These calculations were performed also by computer programme CKBC.

E.1.2 Results of the Energy Balance

The results of the energy balance are shown in Tables E.1, E.2 and E.3 where the discrepancy between the two sides of equation 4.1.9 is expressed as a percentage of the energy released, $[\Delta \dot{H}']_{t_o}$ The discrepancy lies within the limits -5.7 to +10.0%. This was regarded as satisfactory. In the next column, the overall thermal efficiency of the combustor has been calculated, using:

$$\eta_{th} = - \frac{(\Delta \dot{H}_{WA} + \Delta \dot{H}_{WBC} + \Delta \dot{H}_{WTR} + \Delta \dot{H}_{WIN} + \Delta \dot{H}_{gc})}{[\Delta \dot{H}']_{t_o}} \qquad 1.21$$

		TABLE E.1				
$\dot{m}_p$		0·479	0·391	0·292	0·223	kg/h
$\dot{Q}_{LCL}$		−319	−244	−197	−203	W
$\Delta\dot{H}_{WA}$		4186	3348	2511	2104	W
$\Delta\dot{H}_{WBC}$		886	635	577	518	W
$\Delta\dot{H}_{AA\phi}$		47	62	38	37	W
$\Delta\dot{H}_{AC\phi}$		250	250	199	134	W
$\Delta\dot{H}_{WTR}$		54	56	30	37	W
$\Delta\dot{H}_{WIN}$		220	222	216	149	W
$\Delta\dot{H}_{QC}$		200	102	58	0	W
$[\Delta\dot{H}']_{t\phi}$		−6662	−5432	−4061	−3098	W
ENERGY BALANCE		+8·2	+10·0	+6·0	−2,7	%
η_{th}		0·886	0·85	0·882	0·906	–
		TABLE E.2				
$\dot{m}_p$	0·562	0·477	0·383	0·328	0·223	kg/h
$\dot{Q}_{LCL}$	−294	−237	−217	−204	−182	W
$\Delta\dot{H}_{WA}$	4278	3660	3266	2848	2307	W
$\Delta\dot{H}_{WBC}$	1827	1432	1104	723	381	W
$\Delta\dot{H}_{AA\phi}$	68	62	48	95	111	W
$\Delta\dot{H}_{AC\phi}$	422	372	298	164	92	W
$\Delta\dot{H}_{WTR}$	52	66	67	52	53	W
$\Delta\dot{H}_{WIN}$	230	225	226	198	168	W
$\Delta\dot{H}_{QC}$	–	–	–	–	–	W
$[\Delta\dot{H}']_{t\phi}$	−7818	−6627	−5332	−4558	−3107	W
ENERGY BALANCE	+8·2	+8·8	+2·0	+6·0	−5·7	%
η_{th}	0·853	0·849	0·874	0·838	0·936	–

D_I = 13 mm.

D_I = 16 mm.

D_H = 19 mm.

TABLE E.3

$\dot{m}_p$	0·563	0·477	0·381	0·330	0·224	kg/h
$\dot{Q}_{LCL}$	− 331	− 245	− 227	− 211	− 190	W
$\Delta\dot{H}_{WA}$	4185	3784	3107	2828	2185	W
$\Delta\dot{H}_{WBC}$	1765	1491	1132	780	297	W
$\Delta\dot{H}_{AA\phi}$	112	100	89	79	86	W
$\Delta\dot{H}_{AC\phi}$	362	298	157	126	110	W
$\Delta\dot{H}_{WTR}$	64	65	51	42	31	W
$\Delta\dot{H}_{WIN}$	250	219	217	204	173	W
$\Delta\dot{H}_{QC}$	-	-	-	-	-	W
$[\Delta\dot{H}']_{t\phi}$	-7820	-6627	-5352	-4564	-3112	W
ENERGY BALANCE	+9·5	+6·5	+7·1	+6·2	+4·5	%
η_{th}	0·842	0·879	0·882	0·872	0·893	-

TABLE E.4

D_I	13	13	16	16	19	19
$\dot{m}_p$	0·292	0·572	0·291	0·569	0·293	0·573
$\dot{m}_w$	145	141	151	144	149	159
$\dot{m}_{AA}$	7·16	11·8	9·57	14·2	7·30	11·7
T_{S1}	311·7	320·2	314·6	327·2	312·9	321·2
T_{S2}	310·8	325·7	318·4	333·1	309·3	322·8
T_{S3}	300·7	308·8	306·9	317·1	303·4	309·0
T_{S4}	293·9	297·7	301·0	305·7	295·7	300·3
T_{S5}	293·9	299·4	300·0	306·9	298·1	300·5
T_{W1}	301·4	310·0	307·1	319·2	302·4	310·1
T_{W2}	297·8	301·3	303·0	307·2	297·9	303·8
T_{W3}	294·9	298·9	300·0	304·0	295·0	299·8
T_{W4}	292·9	294·1	297·3	299·7	293·3	295·7
T_{W5}	292·4	292·9	296·8	297·5	292·8	294·5
T_{W6}	291·4	290·7	295·4	295·5	291·5	292·9
T_{W7}	290·2	288·0	293·1	291·1	289·6	289·2
T_{W8}	290·0	287·5	292·6	290·4	289·3	288·5
T_{W9}	289·3	287·1	291·7	289·9	289·4	288·6
$\Delta\dot{H}_{WA}$	2028	3770	2705	4907	2246	3966
U_A	37·5	53·3	41·2	61·0	32·8	49·8
$\bar{c}_{PAA}$	1061	1087	1081	1110	1082	1096
f	115	193	132	198	77	146

TABLE E.5

D_I	13	13	16	16	19	19
GAS TEMPERATURE						
T_{A1}	1289	1420	1308	1509	1385	1497
T_{A2}	997	1176	1091	1298	1088	1195
T_{A3}	891	1076	989	1177	973	1090
T_{A4}	705	837	817	968	824	911
T_{A5}	573	650	681	823	701	764
T_{A6}	454	544	574	697	582	621
T_{A7}	385	464	495	598	498	522
T_{A8}	328	362	367	388	361	384
CORRECTED GAS TEMPERATURE						
T_{A1}	1336	1479	1351	1580	1454	1573
T_{A2}	1131	1368	1252	1549	1270	1399
T_{A3}	980	1215	1102	1353	1094	1236
T_{A4}	743	893	874	1055	891	988
T_{A5}	590	672	710	871	738	804
T_{A6}	461	555	589	723	600	640
T_{A7}	388	470	503	612	508	531
T_{A8}	329	363	368	390	363	386

TABLE E.6

D_I	13	13	16	16	19	19
$\overline{Re}_A$ (1)	1846	2771	2382	3136	1764	2671
(2)	2046	2953	2545	3293	1936	2890
(3)	2339	3375	2856	3720	2172	3230
(4)	2775	4109	3306	4310	2475	3724
(5)	3262	4836	3774	4885	2822	4298
(6)	3800	5471	4246	5498	3207	4950
(7)	4321	6352	4984	6689	3802	5870
Re_W (1)	903	1041	1057	1256	947	1177
(2)	885	1004	1031	1205	927	1138
(3)	855	944	987	1123	894	1074
(4)	814	870	935	1018	849	995
(5)	774	796	882	916	804	916
(6)	792	724	828	820	835	836
(7)	698	655	875	784	720	766
$\bar{u}_A$ (1)	12·5	23·8	17·6	31·5	14·1	24·6
(2)	10·7	21·6	16·0	29·2	12·2	21·8
(3)	8·75	17·6	13·4	24·2	10·3	18·4
(4)	6·78	13·1	10·7	19·4	8·43	14·9
(5)	5·34	10·3	8·83	16·0	6·93	12·0
(6)	4·32	8·58	7·43	13·5	5·75	9·73
(7)	3·70	6·98	5·94	10·1	4·53	7·65

TABLE E.7

D_I	13	13	16	16	19	19
$\hat{u}$ (1)	4·2	17·8	5·14	8·7	41·4	33·8
(2)	7·95	31·7	0·59	21·2	37·8	21·4
(3)	11·8	37·7	4·12	29·2	34·1	5·4
(4)	13·0	33·0	8·0	26·8	26·9	9·7
(5)	13·5	17·3	11·0	16·5	19·8	24·0
(6)	11·9	5·1	11·5	1·2	10·6	32·4
(7)	8·45	24·6	10·0	18·6	0·8	32·8
Nu (1)	9·1	9·4	9·3	9·9	9·5	9·8
(2)	9·9	10·1	9·6	10·7	10·3	10·1
(3)	11·5	11·7	11·4	11·9	11·4	10·6
(4)	12·0	12·3	11·9	12·9	12·4	11·7
(5)	13·2	13·4	13·0	14·1	13·5	12·8
(6)	14·4	14·5	14·1	15·3	14·5	13·9
(7)	15·3	15·5	15·1	16·2	15·3	15·1
$\overline{Nu}_p$ (1)	10·7	10·2	8·7	8·9	11·2	14·7
(2)	12·1	14·0	12·1	17·6	11·6	11·2
(3)	14·2	21·4	13·9	18·6	9·3	11·7
(4)	16·5	27·6	16·0	17·9	10·6	12·9
(5)	26·2	26·2	18·8	21·4	15·0	24·1
(6)	30·8	16·4	21·2	14·3	16·4	27·1
(7)	62·3	91·3	77·5	119	62·5	84·1

TABLE E.8

D_I	13	13	16	16	19	19
h_{gw} (1)	1275	1391	1394	2021	1246	1810
(2)	1328	1415	1424	1987	1262	1820
(3)	1426	1456	1476	1932	1292	1834
(4)	1580	1516	1552	1865	1333	1855
(5)	1773	1581	1636	1801	1377	1876
(6)	1638	1326	1730	1743	1146	1898
(7)	2327	1727	1456	1374	1472	1920
h_{AS} (1)	42.6	32.8	26.1	10.0	35.0	48.6
(2)	31.4	41.9	36.8	57.0	32.6	43.1
(3)	31.7	55.5	34.4	53.0	23.0	39.6
(4)	30.2	57.2	33.5	43.3	22.7	38.8
(5)	39.7	44.8	33.6	45.0	27.5	47.0
(6)	39.4	46.9	33.2	44.5	25.9	44.8
(7)	69.5	115	101.1	174	81.5	114
S (1)	1.5	1.32	1.23	1.03	0.89	0.97
(2)	1.75	1.46	1.35	1.11	1.03	1.09
(3)	2.3	1.79	1.61	1.34	1.22	1.29
(4)	2.97	2.4	2.02	1.67	1.49	1.6
(5)	3.78	3.06	2.44	2.02	1.81	1.98
(6)	4.67	3.67	2.9	2.4	2.19	2.45
(7)	5.45	4.52	3.64	3.2	2.77	3.11

6.F. Computer Programmes

The following programmes are listed in this Appendix:

CKBA - This programme calculated the steady state heat transfer coefficients and flow parameters according to Section 4.4.2 for given air and water mass flow-rates and inlet and outlet temperatures.

CKBB - This programme calculated the experimental heat transfer coefficients according to Section 4.4.1. from data provided by CKBC.

CKBC - This programme read in the experimental data, corrected it according to Section 4.1 and calculated the energy balance. All water and air properties were obtained by quadratic interpolation.

PCVPP01 - This programme solved the Bessel boundary conditions for an exponential gas temperature gradient according to Section 2.2 for given T_{A1} and T_{A8}.

VALVE - This programme calculated the air mass flow through the aerodynamic valve according to Section 2.5 for a given pressure amplitude and valve diameter.

The programmes are written in Fortran IV and were run on N.U.M.A.C.

```
C  CKBA  --  THEORETICAL STEADY STATE HEAT TRANSFER IN HEAT EXCHANGER
      REAL*8 XH,XC,DO,SO,SANN,DEQ,DEP,SS,DL,TA1,TW1,TA2,TW2,TAX1,TWX1,
     >X,DH,DHA,TWL,REA,REW,NUA,NUW,MUA,MUW,PRA,PRW,CPA,CPW,KA,KW,TA,TW
     >MUAS,MUWS,U,H1,H2,TAXM,TSXM,TWXM,XX
     >,MAA,MW,DHR
      DATA XH,XC,DO,SO,SANN,DEQ,DEP
     >/0.33,2.40,0.026594,0.00055546,0.00061322,0.027616,0.011478/
      J=50
    3 CONTINUE
      READ(5,1070)MAA,MW,TAX1,TWX1,TWL
 1070 FORMAT(5(F10.5))
      IF(MAA.LE.0.0)GO TO 33
      WRITE(6,2073)
 2073 FORMAT(6X,'XX',5X,'TAXM',6X,'TSXM',6X,'TWXM',6X,'NUA',7X,'NUW',
     >7X,'REA',7X,'REW',7X,'H1',8X,'H2'//)
C
      DL=(XC-XH)/J
      SS=3.14159265358*DO*DL
      MAA=MAA/3600.0
      MW=MW/3600.0
      TW1=TWX1
  200 CONTINUE
      DH=0.0
      TA1=TAX1
      DHA=0.0
      X=XH
      DO 80 IJ=1,J
      X=X+DL
      TA=TA1
      TW=TW1-273.16
      PRA=CPA(TA)*MUA(TA)/KA(TA)
      PRW=CPW(TW)*MUW(TW)/KW(TW)
      REA=4.0*MAA/(3.14159265358*DO*MUA(TA))
C  EQU, 8.15 P.336 CHAPMAN
      NUA=0.023*(REA**0.8)*(PRA**0.3)
      H1=(NUA*KA(TA))/DO
      REW=MW*DEP/(SANN*MUW(TW))
C  EQU, 8.11 P.333 CHAPMAN    (LESS VISCOSITY TERM)
      NUW=0.023*(REW**0.8)*(PRW**0.4)
      H2=(NUW*KW(TW))/DEQ
      U=H1*H2/(H1+H2)
C  ENTHALPY CHANGES
      DH=U*SS*(TA1-TW1)
C  CALC. FIRST ESTIMATE OF OUTLET TEMPS. FROM SECTION
      TA2=TA1-(DH/(MAA*CPA(TA)))
      TW2=TW1-(DH/(MW*CPW(TW)))
      TAXM=0.5*(TA1+TA2)
      TWXM=0.5*(TW1+TW2)
      TSXM=((H1*TAXM)+(H2*TWXM))/(H1+H2)
C  CALC. AGAIN USING DYNAMIC VISCOSITY RATIO & MEAN TEMPS.
      TA=TSXM
      TW=TSXM-273.16
      MUAS=MUA(TA)
      MUWS=0.0001798
```

```
      TA=TAXM
      TW=TWXM-273.16
      PRA=CPA(TA)*MUA(TA)/KA(TA)
      PRW=CPW(TW)*MUW(TW)/KW(TW)
      REA=4.0*MAA/(3.14159265358*DO*MUA(TA))
C   EQU, 8.16 P.336 CHAPMAN
C
      IF(TAXM.LE.373.16)GO TO 73
      NUA=0.023*(REA**0.8)*(PRA**0.3)
      GO TO 76
   73 CONTINUE
      NUA=5.03*(REA**0.33333333)*(PRA**0.33333333)
      GO TO 76
   76 CONTINUE
C
      H1=(NUA*KA(TA))/DO
      REW=MW*DEP/(SANN*MUW(TW))
C   EQU, 8.11 P.333 CHAPMAN
      NUW=0.023*(REW**0.8)*(PRW**0.4)
C
      H2=(NUW*KW(TW))/DEQ
      U=H1*H2/(H1+H2)
C   ENTHALPY CHANGES
      DH=U*SS*(TAXM-TWXM)
C   CALC. FIRST ESTIMATE OF OUTLET TEMPS. FROM SECTION
      TA2=TA1-(DH/(MAA*CPA(TA)))
      TW2=TW1-(DH/(MW*CPW(TW)))
      TAXM=0.5*(TA1+TA2)
      TWXM=0.5*(TW1+TW2)
      TSXM=((H1*TAXM)+(H2*TWXM))/(H1+H2)
      DH=U*SS*(TAXM-TWXM)
      DHR=0.17*SS*(((TAXM/100)**4)-((TSXM/100)**4))
      DH=DH+DHR
      DHA=DHA+DH
      XX=X-DL/2
      WRITE(6,2010)IJ,XX,TAXM,TSXM,TWXM,NUA,NUW,REA,REW,H1,H2
 2010 FORMAT(1H ,I3,F7.3,10(1PD10.3))
      TA1=TA2
      TW1=TW2
   80 CONTINUE
C   TEST FOR TW2 = TWL
      IF(DABS(TW2-TWL).LE.0.8)GO TO 100
      TW1=TWX1-(TW1-TWL)
      GO TO 200
  100 CONTINUE
      WRITE(6,2020)MAA,MW,TAX1,TWX1,TWL,J
 2020 FORMAT(7X,'MA =',1PD12.5/7X,'MW =',1PD12.5/5X,'TAX1 =',
     +1PD12.5/5X,'TWX1 =',1PD12.5/6X,'TWL =',1PD12.5/8X,'J =',I3)
      WRITE(6,2017)DHA
 2017 FORMAT(10X,'DHA =',5X,1PD10.3)
      GO TO 3
   33 CONTINUE
      STOP
      END
```

```
C  EXPERIMENTAL RESULTS PROG
      IMPLICIT REAL*8(A-Z)
      DIMENSION XA(20),XS(20),XW(20),TG(20),TS(20),TF(20),
     >UA(20),CVEL(20),HAS(20),HSW(20),NUA(20),NUW(20),REA(20),REW(20)
      INTEGER I,J,K
      DATA XA/0.33,0.477,0.654,1.011,1.366,1.722,2.077,2.4/
      DATA XS/0.33,0.84,1.375,1.93,2.4/
      DATA XW/0.33;0.450,0.628,0.805,1.162,1.518,1.874,2.23,2.4/
      DATA DO,SO,SAN,CEQ,DEP
     >/0.026594,0.00055546,0.00061322,0.027616,0.011478/
      READ(5,1000)(TG(I),I=1,8)
      READ(5,1000)(TS(I),I=1,5)
      READ(5,1000)(TF(I),I=1,9)
      READ(5,1000)MAA,MW
1000  FORMAT(10(F10.4))
      GRADS=(TS(1)-TS(5))/(XS(1)-XS(5))
      GRADW=(TF(1)-TF(9))/(XW(1)-XW(9))
      CONSTS=(XS(1)*TS(5)-XS(5)*TS(1))/(XS(1)-XS(5))
      CONSTW=(XW(1)*TF(9)-XW(9)*TF(1))/(XW(1)-XW(9))
      DA=0.0
      DW=0.0
      X1=0.33
      TS1=CONSTS+GRADS*X1
      TW1=CONSTW+GRADW*X1
      DO 10 I=1,7
      X2=XA(I+1)
      TS2=CONSTS+GRADS*X2
      TW2=CONSTW+GRADW*X2
      SS=3.14159265358*DO*(X2-X1)
      TAXM=0.5*(TG(I)+TG(I+1))
      TSXM=0.5*(TS1+TS2)
      TWXM=0.5*(TW1+TW2)
      TA=TAXM
      TW=TWXM-273.16
      UA(I)=MAA/(SO*3600*RHOA(TA))
      CVEL(I)=CA(TA)
      DHA=MAA*CPA(TA)*(TG(I)-TG(I+1))/3600
      DHW=MW*CPW(TW)*(TW1-TW2)/3600
      HAS(I)=DHA/(SS*(TAXM-TSXM))
      HSW(I)=DHW/(SS*(TSXM-TWXM))
      NUA(I)=HAS(I)*DO/KA(TA)
      NUW(I)=HSW(I)*DEQ/KW(TW)
      REA(I)=4*MAA/(3.14159265358*DO*3600*MUA(TA))
      REW(I)=MW*DEP/(SAN*3600*MUW(TW))
      DW=DW+DHW
      DA=DA+DHA
      TS1=TS2
      TW1=TW2
      X1=X2
   10 CONTINUE
      DO 20 I=1,7
      WRITE(6,3030)I,REA(I),REW(I),NUA(I),NUW(I),HAS(I),
     >HSW(I),UA(I),CVEL(I)
3030  FORMAT(I10,10(F10.2))
   20 CONTINUE
      WRITE(6,3040)DA,DW




3040  FORMAT(F10.2/F10.2)
      STOP
      END
```

```
C  @KBC  A PROGRAM TO PROCESS EXPERIMENTAL READINGS FROM THE DOUBLE
C  ORIFICE COMBUSTOR .
      REAL*8 PAO,TAO,PO,TO,TFAC,PFAC,MFAC,MP,MW,MWTR,MWIN,CM,ROTAMW,
     >PAMP,F,PSCALE,TSO,TS1,TS2,TS3,TS4,TS5,TYPEK,TYPES,TYPET,E,
     >TW1,TW2,TW3,TW4,TW5,TW6,TW7,TW8,TW9,TW21,TW22,TW23,TWTR,TWIN,
     >TA1,TA2,TA3,TA4,TA5,TA6,TA7,TA8,TA21,TA22,TA23,LAUG,XAUG,DI,
     >TGC1,TGC2,MGC,TREF,TLAG,ROTAMA,HCVP,KLAG,AA,AB,AC,TW,CPWC,CPWB,
     >CPWA,CPWTR,CPWIN,CPWBC,TA,CPAC,CPAB,CPABC,CPAA,CPAAO,CPACO,
     >CPGC,CPA,CPW,MAC,MAB,MABC,MAA,QLCL,DHW,DHA,DHWTR,DHWIN,DHGC,
     >DHTO,EQ1,TAM,TBM,TCM,UA,UB,UC,NUTH,NUVOL,TYPEK,TYPES,TYPET,
     >TREFK,TREFS,TREFT,TAMB,VOLC,DHWA,PERC,
     >XA1,XA2,XA3,XA4,XA5,XA6,XA7,XA8,XS1,XS2,XS3,XS4,XS5,
     >XW1,XW2,XW3,XW4,XW5,XW6,XW7,XW8,XW9
     >,DX,VAL(10),TEMP1(10)
C  PART 1 - READ IN DATA AND CORRECT TO S.I. UNITS & TO CHOSEN DATUM .
      READ(5,1000)PAO,TAO
 1000 FORMAT(2(F10.4))
      READ(5,1001)MP,MW,MWTR,MWIN
 1001 FORMAT(4(F10.4))
      READ(5,1002)PAMP,F
 1002 FORMAT(2(F10.4))
      READ(5,1003)TSO,TS1,TS2,TS3,TS4,TS5
 1003 FORMAT(6(F10.4))
      READ(5,1004)TW1,TW2,TW3,TW4,TW5,TW6,TW7,TW8,TW9,TW21,TW22,TW23,
     >TWTR,TWIN
 1004 FORMAT(8(F10.4)/6(F10.4))
      READ(5,1005)TA1,TA2,TA3,TA4,TA5,TA6,TA7,TA8,TA21,TA22,TA23
 1005 FORMAT(8(F10.4)/3(F10.4))
      READ(5,1006)LAUG,XAUG,DI,NJET
 1006 FORMAT(3(F10.4),I3)
      READ(5,1007)TGC1,TGC2,MGC,TREF,TLAG
 1007 FORMAT(5(F10.4))
      PAO=PAO*133.333333
      TAO=TAO+273.16
C  CALCULATE CORRECTION FACTORS
      PO=101325.0
      TO=293.16
      TFAC=TO/TAO
      PFAC=PO/PAO
      MFAC=PFAC/(DSQRT(TFAC))
      MP=MP*1.905*MFAC
      MWTR=MWTR*3.6*MFAC
      MWIN=MWIN*3.6*MFAC
      CM=MW
      MW=ROTAMW(CM)*MFAC
      PAMP=PAMP*1723.69*PFAC
      TAMB=0.5*(TREF+TAO-273.16)
      E=TSO
      E=E+TREFK(TAMB)
      TSO=TYPEK(E)*TFAC
      E=TS1
      E=E+TREFT(TAMB)
      TS1=TYPET(E)*TFAC
      E=TS2
      E=E+TREFT(TAMB)
      TS2=TYPET(E)*TFAC
      E=TS3
      E=E+TREFT(TAMB)
```

```
      TS3=TYPET(E)*TFAC
      E=TS4
      E=E+TREFT(TAMB)
      TS4=TYPET(E)*TFAC
      E=TS5
      E=E+TREFT(TAMB)
      TS5=TYPET(E)*TFAC
      E=TW2
      E=E+TREFT(TAMB)
      TW2=TYPET(E)*TFAC
      E=TW3
      E=E+TREFT(TAMB)
      TW3=TYPET(E)*TFAC
      E=TW4
      E=E+TREFT(TAMB)
      TW4=TYPET(E)*TFAC
      E=TW5
      E=E+TREFT(TAMB)
      TW5=TYPET(E)*TFAC
      E=TW6
      E=E+TREFT(TAMB)
      TW6=TYPET(E)*TFAC
      E=TW7
      E=E+TREFT(TAMB)
      TW7=TYPET(E)*TFAC
      E=TW8
      E=E+TREFT(TAMB)
      TW8=TYPET(E)*TFAC
      TW1=(TW1+273.16)*TFAC
      TW9=(TW9+273.16)*TFAC
      TW21=(TW21+273.16)*TFAC
      TW22=(TW22+273.16)*TFAC
      TW23=(TW23+273.16)*TFAC
      TWTR=(TWTR+273.16)*TFAC
      TWIN=(TWIN+273.16)*TFAC
      E=TA1
      E=E+TREFS(TAMB)
      TA1=TYPES(E)*TFAC
      E=TA2
      E=E+TREFK(TAMB)
      TA2=TYPEK(E)*TFAC
      E=TA3
      E=E+TREFK(TAMB)
      TA3=TYPEK(E)*TFAC
      E=TA4
      E=E+TREFK(TAMB)
      TA4=TYPEK(E)*TFAC
      E=TA5
      E=E+TREFK(TAMB)
      TA5=TYPEK(E)*TFAC
      E=TA6
      E=E+TREFK(TAMB)
      TA6=TYPEK(E)*TFAC
      E=TA7
      E=E+TREFK(TAMB)
      TA7=TYPEK(E)*TFAC
      E=TA8
      E=E+TREFK(TAMB)
      TA8=TYPEK(E)*TFAC
      E=TA21
      E=E+TREFK(TAMB)
      TA21=TYPEK(E)*TFAC
      E=TA22
      E=E+TREFK(TAMB)
      TA22=TYPEK(E)*TFAC
      E=TA23
      E=E+TREFK(TAMB)
      TA23=TYPEK(E)*TFAC
      E=TGC1
      E=E+TREFK(TAMB)
      TGC1=TYPEK(E)*TFAC
      E=TGC2
      E=E+TREFK(TAMB)
      TGC2=TYPEK(E)*TFAC
      TREF=(TREF+273.16)*TFAC
      TLAG=(TLAG+273.16)*TFAC
      CM=MGC
      MGC=ROTAMA(CM)*TFAC
C     SET CONSTANTS
      HCVP=50060000.0
      KLAG=0.0845
      AA=0.183862
      AB=0.108856
      AC=0.072759
C     CALCULATE MEAN SPECIFIC HEATS FOR
      TW=0.5*(TW23+TW22)-273.16
      CPWC =CPW(TW)
      TW=0.5*(TW22+TW21)-273.16
      CPWB =CPW(TW)
      TW=0.5*(TW9 +TW1 )-273.16
      CPWA =CPW(TW)
      TW=0.5*(TW23+TWTR)-273.16
      CPWTR=CPW(TW)
      TW=0.5*(TW23+TWIN)-273.16
      CPWIN=CPW(TW)
      TW=0.5*(TW23+TW21)-273.16
      CPWBC=CPW(TW)
      TA=0.5*(TA23+TA22)
      CPAC =CPA(TA)
      TA=0.5*(TA22+TA21)
      CPAB =CPA(TA)
      TA=0.5*(TA23+TA21)
      CPABC=CPA(TA)
      TA=TA1
      VAL(1)=CPA(TA)
      TA=TA3
      VAL(2)=CPA(TA)
      TA=TA4
      VAL(3)=CPA(TA)
      TA=TA5
      VAL(4)=CPA(TA)
      TA=TA6
      VAL(5)=CPA(TA)
      TA=TA7
      VAL(6)=CPA(TA)
      TA=TA8
      VAL(7)=CPA(TA)
      DX=2.132/6.0
      NORD=7
      CALL DQSF(DX,VAL,TEMP1,NORD)
```

```
      CPAA=TEMP1(NORD)/2.132
      TA=0.5*(TA0 +TA8 )
      CPAA0=CPA(TA)
      TA=0.5*(TA0 +TA23)
      CPAC0=CPA(TA)
      TA=0.5*(TGC2+TGC1)
      CPGC =CPA(TA)
C  PART 2(A) - APPLY S.F.E.E. TO CONTROL VOLUME AROUND HEAT EXCHANGER
      MAC=-MW*(CPWC/CPAC)*(TW22-TW23)/(TA23-TA22)
C  PART 2(B) - APPLY S.F.E.E. TO CONTROL VOLUME AROUND HEAT EXCHANGER
      MAB=-MW*(CPWB/CPAB)*(TW21-TW22)/(TA22-TA21)
C  PART 2(C) - APPLY S.F.E.E. TO CONTROL VOLUME AROUND HEAT EXCHANGERS
      MABC=-MW*(CPWBC/CPABC)*(TW21-TW23)/(TA23-TA21)
C  PART 2(D) - APPLY S.F.E.E. TO CONTROL VOLUME AROUND HEAT EXCHANGER
      MAA=-MW*(CPWA/CPAA)*(TW1-TW9)/(TA8-TA1)
C  PART 2(E) - APPLY S.F.E.E. TO CONTROL VOLUME AROUND WHOLE DOUBLE OR
C  COMBUSTOR
C  CALCULATE QLCL & SEPARATE ENTHALPY CHANGES FIRST .
      QLCL=-2.0*3.14159265358*0.43*KLAG*(TSO-TLAG)*0.99969873436
      DHW=MW*(CPWA*(TW1-TW9)+CPWBC*(TW21-TW23))
      DHW=DHW/3600.0
      DHA=MAA*CPAA0*(TA8-TA0)+MABC*CPAC0*(TA23-TA0)
      DHA=DHA/3600.0
      DHWTR=MWTR*CPWTR*(TWTR-TW23)
      DHWTR=DHWTR/3600.0
      DHWIN=MWIN*CPWIN*(TWIN-TW23)
      DHWIN=DHWIN/3600.0
      DHGC=MGC*CPGC*(TGC2-TGC1)
      DHGC=DHGC/3600.0
      DHTO=MP*HCVP
      DHTO=DHTO/3600.0
      EQ1=DHW+DHA+DHWTR+DHWIN+DHGC+(-DHTO)-QLCL
C  PART 3     - OVERALL HEAT TRANSFER COEFFICIENTS .
C  CALCULATE LOG. MEAN TEMPERATURES DIFFERENCES FIRST .
      TAM=(TA1-TW1-TA8+TW9)/DLOG((TA1-TW1)/(TA8-TW9))
      TBM=(TA21-TW21-TA22+TW22)/DLOG((TA21-TW21)/(TA22-TW22))
      TCM=(TA22-TW22-TA23+TW23)/DLOG((TA22-TW22)/(TA23-TW23))
      UA=MW*CPWA*(TW1-TW9)/(AA*TAM)
      UA=UA/3600.0
      UB=MW*CPWB*(TW21-TW22)/(AB*TBM)
      UB=UB/3600.0
      UC=MW*CPWC*(TW22-TW23)/(AC*TCM)
      UC=UC/3600.0
C  PART 4     - THERMAL EFFICIENCY OF DOUBLE ORIFICE COMBUSTOR .
      NUTH=(DHW+DHWTR+DHWIN)/DHTO
C  PART 5     - VOLUMETRIC COMBUSTION EFFICIENCY .
      VOLC=0.00018
      NUVOL=DHTO/VOLC
      DHWA=MW*CPWA*(TW1-TW9)/3600.0
      PERC=100.0*EQ1/DHTO
C  PRINT OUT CORRECTED EXPERIMENTAL DATA & CALCULATED PARAMETERS .
      WRITE(6,8000)MP,MW,MWTR,MWIN,MAC,MAB,MABC,MAA,MGC,PAMP,F
 8000 FORMAT(
     >11H  MP       =,1PD16.5,8H    KG/H/
     >11H  MW       =,1PD16.5,8H    KG/H/
     >11H  MWTR     =,1PD16.5,8H    KG/H/
     >11H  MWIN     =,1PD16.5,8H    KG/H/
     >11H  MAC      =,1PD16.5,8H    KG/H/
     >11H  MAB      =,1PD16.5,8H    KG/H/
     >11H  MABC     =,1PD16.5,8H    KG/H/
```

```
     >11H  MAA      =,1PD16.5,8H     KG/H/
     >11H  MGC      =,1PD16.5,8H     KG/H/
     >11H  PAMP     =,1PD16.5,8H   N/M**2/
     >11H  F        =,1PD16.5,8H       HZ/
     >//)
      WRITE(6,8001)
     >TS0,TS1,TS2,TS3,TS4,TS5,TW1,TW2,TW3,TW4,TW5,TW6,TW7,TW8,TW9
8001 FORMAT(
     >11H  TS0      =,1PD16.5,8H        K/
     >11H  TS1      =,1PD16.5,8H        K/
     >11H  TS2      =,1PD16.5,8H        K/
     >11H  TS3      =,1PD16.5,8H        K/
     >11H  TS4      =,1PD16.5,8H        K/
     >11H  TS5      =,1PD16.5,8H        K/
     >11H  TW1      =,1PD16.5,8H        K/
     >11H  TW2      =,1PD16.5,8H        K/
     >11H  TW3      =,1PD16.5,8H        K/
     >11H  TW4      =,1PD16.5,8H        K/
     >11H  TW5      =,1PD16.5,8H        K/
     >11H  TW6      =,1PD16.5,8H        K/
     >11H  TW7      =,1PD16.5,8H        K/
     >11H  TW8      =,1PD16.5,8H        K/
     >11H  TW9      =,1PD16.5,8H        K/
     >//)
      WRITE(6,8002)
     >TW21,TW22,TW23,TWTR,TWIN,TA1,TA2,TA3,TA4,TA5,TA6,TA7,TA8
8002 FORMAT(
     >11H  TW21     =,1PD16.5,8H        K/
     >11H  TW22     =,1PD16.5,8H        K/
     >11H  TW23     =,1PD16.5,8H        K/
     >11H  TWTR     =,1PD16.5,8H        K/
     >11H  TWIN     =,1PD16.5,8H        K/
     >11H  TA1      =,1PD16.5,8H        K/
     >11H  TA2      =,1PD16.5,8H        K/
     >11H  TA3      =,1PD16.5,8H        K/
     >11H  TA4      =,1PD16.5,8H        K/
     >11H  TA5      =,1PD16.5,8H        K/
     >11H  TA6      =,1PD16.5,8H        K/
     >11H  TA7      =,1PD16.5,8H        K/
     >11H  TA8      =,1PD16.5,8H        K/
     >//)
      WRITE(6,8003)
     >TA21,TA22,TA23,LAUG,XAUG,TGC1,TGC2,TREF,TLAG,DHW,DHA,DHWTR
8003 FORMAT(
     >11H  TA21     =,1PD16.5,8H        K/
     >11H  TA22     =,1PD16.5,8H        K/
     >11H  TA23     =,1PD16.5,8H        K/
     >11H  LAUG     =,1PD16.5,8H        M/
     >11H  XAUG     =,1PD16.5,8H        M/
     >11H  TGC1     =,1PD16.5,8H        K/
     >11H  TGC2     =,1PD16.5,8H        K/
     >11H  TREF     =,1PD16.5,8H        K/
     >11H  TLAG     =,1PD16.5,8H        K/
     >11H  DHW      =,1PD16.5,8H        W/
     >11H  DHA      =,1PD16.5,8H        W/
     >11H  DHWTR    =,1PD16.5,8H        W/
     >//)
      WRITE(6,8004)
     >DHWIN,DHGC,DHTO,QLCL,EQ1,PERC,DHWA,UA,UB,UC,NUTH,NUVOL,DI
8004 FORMAT(
```

```
     >11H  DHWIN    =,1PD16.5,8H        W/
     >11H  DHGC     =,1PD16.5,8H        W/
     >11H  DHTO     =,1PD16.5,8H        W/
     >11H  QLCL     =,1PD16.5,8H        W/
     >11H  EQ1      =,1PD16.5,8H        W/
     >11H  PERC     =,1PD16.5,8H        %/
     >11H  DHWA     =,1PD16.5,8H        W/
     >11H  UA       =,1PD16.5,10H  W/M**2 K/
     >11H  UB       =,1PD16.5,10H  W/M**2 K/
     >11H  UC       =,1PD16.5,10H  W/M**2 K/
     >11H  NUTH     =,1PD16.5,8H        %/
     >11H  NUVOL    =,1PD16.5,8H  W/M**3/
     >11H  DI       =,1PD16.5,8H        M/
     >//)
      WRITE(6,8010)NJET
8010 FORMAT(19H  AMAL JET NUMBER =,I6/)
      DATA XA1,XA2,XA3,XA4,XA5,XA6,XA7,XA8/
     >0.33,0.477,0.654,1.011,1.366,1.722,2.077,2.4/
      DATA XS1,XS2,XS3,XS4,XS5/0.33,0.84,1.375,1.93,2.4/
      DATA XW1,XW2,XW3,XW4,XW5,XW6,XW7,XW8,XW9/
     >0.33,0.45,0.628,0.805,1.162,1.518,1.874,2.23,2.4/
      DATA M1,XA9/8,3.05/
      WRITE(2,5050)M1
      WRITE(2,5000)XA1,XA3,XA4,XA5,XA6,XA7,XA8,XA9
      WRITE(2,5000)TA1,TA3,TA4,TA5,TA6,TA7,TA8,TA8
      WRITE(2,5000)XS1,XS5
      WRITE(2,5000)TS1,TS5
      WRITE(2,5000)XW1,XW9
      WRITE(2,5000)TW1,TW9
5000  FORMAT(9(1PD10.3))
5050  FORMAT(I1)
      WRITE(2,9898)MP,MW,MAA,PAMP,F,LAUG,XAUG,DHWA,UA
9898  FORMAT(5(1PD16.5)/4(1PD16.5))
      STOP
      END
      FUNCTION TYPEK(E)
C  SUBROUTINE TO PERFORM QUADRATIC INTERPOLATION ON THERMOCOUPLE REFER
C  TABLES .  E - E.M.F. IN MILLIVOLTS TO DEGREES CELSIUS .
C      TYPEK - NICKEL-CHROMIUM / NICKEL-ALUMINIUM
C  REFERENCE :  B.S.4937:PART 4:1973
      REAL A
      REAL*8 TEMP(60),EMF(60),E,H01,H02,H03,D1,D2,D3,D12,D23,D123
     >,TYPEK,TYPES,TYPET,TREFK,TREFS,TREFT
      DATA EMF/
     >   0.0,      1.0,      2.0,      3.0,      4.0,      5.0,
     >   6.0,      7.0,      8.0,      9.0,     10.0,     11.0,
     >  12.0,     13.0,     14.0,     15.0,     16.0,     17.0,
     >  18.0,     19.0,     20.0,     21.0,     22.0,     23.0,
     >  24.0,     25.0,     26.0,     27.0,     28.0,     29.0,
     >  30.0,     31.0,     32.0,     33.0,     34.0,     35.0,
     >  36.0,     37.0,     38.0,     39.0,     40.0,     41.0,
     >  42.0,     43.0,     44.0,     45.0,     46.0,     47.0,
     >  48.0,     49.0,     50.0,     51.0,     52.0,     53.0,
     >  54.0/
      DATA TEMP/
     >     0.0,    25.0,    49.5,    73.6,    97.7,   122.0,   146.6,
     >   171.5,   196.6,   221.5,   246.3,   270.7,   295.0,   319.1,
     >   343.0,   366.9,   390.6,   414.3,   437.9,   461.5,   485.0,
     >   508.4,   531.9,   555.3,   578.8,   602.3,   625.9,   649.5,
     >   673.2,   696.9,   720.8,   744.8,   769.0,   793.3,   817.7,
```

```
     >   842.3,   867.0,   891.9,   916.9,   942.2,   967.5,   993.1,
     >  1018.8,  1044.7,  1070.8,  1097.1,  1123.7,  1150.4,  1177.4,
     >  1204.7,  1232.3,  1260.3,  1288.6,  1317.3,  1346.3/
      DATA H01,H02,H03/1.0,1.0,0.5/
      IF(E.LE.0.9)GO TO 21
      IF(E.LT.53.2)GO TO 22
      IF(E.GT.54.0)GO TO 23
      N=53
      GO TO 24
   21 CONTINUE
      IF(E.LT.0.0)GO TO 23
      N=1
      GO TO 24
   22 CONTINUE
      A=SNGL(E/H01)
      N=IFIX(A)
   24 CONTINUE
      D1=E-EMF(N)
      D2=E-EMF(N+1)
      D3=E-EMF(N+2)
      D12=(D1*TEMP(N+1)-D2*TEMP(N))*H02
      D23=(D2*TEMP(N+2)-D3*TEMP(N+1))*H02
      D123=((D1*D23)-(D3*D12))*H03
      TYPEK=D123+273.16
      GO TO 25
   23 CONTINUE
      TYPEK=0.0
   25 CONTINUE
      RETURN
      END
      FUNCTION TYPES(E)
C  SUBROUTINE TO PERFORM QUADRATIC INTERPOLATION ON THERMOCOUPLE REFER
C  TABLES .  E - E.M.F. IN MILLIVOLTS TO DEGREES CELSIUS .
C     TYPES - PLATINUM-10%RHODIUM/PLATINUM
C  REFERENCE :  B.S.4937:PART 1:1973
      REAL A
      REAL*8 TEMP(60),EMF(60),E,H01,H02,H03,D1,D2,D3,D12,D23,D123
     >,TYPEK,TYPES,TYPET,TREFK,TREFS,TREFT
      DATA EMF/
     >  0.0,    0.5,    1.0,    1.5,    2.0,    2.5,    3.0,    3.5,
     >  4.0,    4.5,    5.0,    5.5,    6.0,    6.5,    7.0,    7.5,
     >  8.0,    8.5,    9.0,    9.5,   10.0,   10.5,   11.0,   11.5,
     >12.0,   12.5,   13.0,   13.5,   14.0,   14.5,   15.0,   15.5,
     > 16.0,   16.5,   17.0,   17.5,   18.0,   18.5/
      DATA TEMP/
     >     0.0,    79.8,   146.4,   207.1,   264.3,   319.3,   372.7,
     >   425.0,   476.3,   526.8,   576.6,   625.7,   673.9,   721.3,
     >   768.1,   814.2,   859.7,   904.6,   948.9,   992.6,  1035.8,
     >  1078.5,  1120.8,  1162.7,  1204.4,  1245.9,  1287.2,  1328.5,
     >  1369.7,  1410.9,  1452.2,  1493.6,  1535.3,  1577.2,  1619.4,
     >  1661.9,  1705.1,  1749.7/
      DATA H01,H02,H03/0.5,2.0,1.0/
      IF(E.LE.0.4)GO TO 21
      IF(E.LT.18.1)GO TO 22
      IF(E.GT.18.5)GO TO 23
      N=36
      GO TO 24
   21 CONTINUE
      IF(E.LT.0.0)GO TO 23
      N=1
```

```
      GO TO 24
   22 CONTINUE
      A=SNGL(E/H01)
      N=IFIX(A)
   24 CONTINUE
      D1=E-EMF(N)
      D2=E-EMF(N+1)
      D3=E-EMF(N+2)
      D12=(D1*TEMP(N+1)-D2*TEMP(N))*H02
      D23=(D2*TEMP(N+2)-D3*TEMP(N+1))*H02
      D123=((D1*D23)-(D3*D12))*H03
      TYPES=D123+273.16
      GO TO 25
   23 CONTINUE
      TYPES=0.0
   25 CONTINUE
      RETURN
      END
      FUNCTION TYPET(E)
C  SUBROUTINE TO PERFORM QUADRATIC INTERPOLATION ON THERMOCOUPLE REFER
C  TABLES .  E - E.M.F. IN MILLIVOLTS TO DEGREES CELSIUS .
C     TYPET - COPPER-CONSTANTAN .
C  REFERENCE :  B.S.1828:1961
      REAL A
      REAL*8 TEMP(60),EMF(60),E,H01,H02,H03,D1,D2,D3,D12,D23,D123
     >,TYPEK,TYPES,TYPET,TREFK,TREFS,TREFT
      DATA EMF/
     >  0.0,    0.5,    1.0,    1.5,    2.0,    2.5,    3.0,    3.5,
     >  4.0,    4.5,    5.0,    5.5,    6.0,    6.5,    7.0,    7.5,
     >  8.0,    8.5,    9.0,    9.5,   10.0,   10.5,   11.0,   11.5,
     >12.0,   12.5,   13.0,   13.5,   14.0,   14.5,   15.0,   15.5,
     > 16.0,   16.5,   17.0,   17.5,   18.0,   18.5,   19.0,   19.5,
     > 20.0,   20.50/
      DATA TEMP/
     >    0.0,   12.9,   25.4,   37.6,   49.5,   61.2,   72.6,   83.8,
     >   94.8,  105.6,  116.3,  126.8,  137.1,  147.3,  157.4,  167.4,
     >  177.2,  187.0,  196.6,  206.1,  215.6,  224.9,  234.2,  243.4,
     >  252.5,  261.6,  270.5,  279.5,  288.3,  297.1,  305.8,  314.5,
     >  323.1,  331.7,  340.2,  348.6,  357.1,  365.4,  373.8,  382.0,
     >  390.3,  398.5/
      DATA H01,H02,H03/0.5,2.0,1.0/
      IF(E.LE.0.49)GO TO 21
      IF(E.LT.20.1)GO TO 22
      IF(E.GT.20.5)GO TO 23
      N=40
      GO TO 24
   21 CONTINUE
      IF(E.LT.0.0)GO TO 23
      N=1
      GO TO 24
   22 CONTINUE
      A=SNGL(E/H01)
      N=IFIX(A)
   24 CONTINUE
      D1=E-EMF(N)
      D2=E-EMF(N+1)
      D3=E-EMF(N+2)
      D12=(D1*TEMP(N+1)-D2*TEMP(N))*H02
      D23=(D2*TEMP(N+2)-D3*TEMP(N+1))*H02
      D123=((D1*D23)-(D3*D12))*H03
```

```
      TYPET=D123+273.16
      GO TO 25
   23 CONTINUE
      TYPET=0.0
   25 CONTINUE
      RETURN
      END
      FUNCTION TREFK(TAMB)
C  SUBROUTINE TO PERFORM QUADRATIC INTERPOLATION ON THERMOCOUPLE TABLE
C  FOR A GIVEN RANGE OF ATMOSPHERIC TEMPERATURE          0 < TAMB < 30.0
C     TYPEK - NICKEL-CHROMIUM / NICKEL-ALUMINIUM
C  DEGREES CELSIUS TO MILLIVOLTS .
C  REFERENCE :  B.S.4937:PART 4:1973
      REAL A
      REAL*8 TEMP(60),EMF(60),E,H01,H02,H03,D1,D2,D3,D12,D23,D123
     >,TYPEK,TYPES,TYPET,TREFK,TREFS,TREFT,TAMB
      DATA TEMP/ 0.0,   2.0,   4.0,   6.0,   8.0,  10.0,  12.0,  14.0,
     >    16.0,  18.0,  20.0,  22.0,  24.0,  26.0,  28.0,  30.0/
      DATA EMF/  0.000,  0.079,  0.158,  0.238,  0.317,  0.397,  0.477
     >   0.557,  0.637,  0.718,  0.798,  0.879,  0.960,  1.041,  1.122
     >   1.203/
      DATA H01,H02,H03/2.0,0.5,0.25/
      IF(TAMB.LE.1.8)GO TO 21
      IF(TAMB.LT.28.4)GO TO 22
      IF(TAMB.GT.30.0)GO TO 23
      N=14
      GO TO 24
   21 CONTINUE
      IF(TAMB.LT.0.0)GO TO 23
      N=1
      GO TO 24
   22 CONTINUE
      A=SNGL(TAMB/H01)
      N=IFIX(A)
   24 CONTINUE
      D1=TAMB-TEMP(N)
      D2=TAMB-TEMP(N+1)
      D3=TAMB-TEMP(N+2)
      D12=(D1*EMF(N+1)-D2*EMF(N))*H02
      D23=(D2*EMF(N+2)-D3*EMF(N+1))*H02
      D123=((D1*D23)-(D3*D12))*H03
      TREFK=D123
      GO TO 25
   23 CONTINUE
      TREFK=0.0
   25 CONTINUE
      RETURN
      END
      FUNCTION TREFS(TAMB)
C  SUBROUTINE TO PERFORM QUADRATIC INTERPOLATION ON THERMOCOUPLE TABLE
C  FOR A GIVEN RANGE OF ATMOSPHERIC TEMPERATURE          0 < TAMB < 30.0
C     TYPES - PLATINUM-10%RHODIUM/PLATINUM
C  DEGREES CELSIUS TO MILLIVOLTS .
C  REFERENCE :  B.S.4937:PART 1:1973
      REAL A
      REAL*8 TEMP(60),EMF(60),E,H01,H02,H03,D1,D2,D3,D12,D23,D123
     >,TYPEK,TYPES,TYPET,TREFK,TREFS,TREFT,TAMB
      DATA TEMP/ 0.0,   2.0,   4.0,   6.0,   8.0,  10.0,  12.0,  14.0,
     >    16.0,  18.0,  20.0,  22.0,  24.0,  26.0,  28.0,  30.0/
      DATA EMF/  0.000,  0.011,  0.022,  0.033,  0.044,  0.055,  0.067
```

```
     >   0.078,  0.090,  0.101,  0.113,  0.125,  0.137,  0.148,  0.161
     >   0.173/
      DATA H01,H02,H03/2.0,0.5,0.25/
      IF(TAMB.LE.1.8)GO TO 21
      IF(TAMB.LT.28.4)GO TO 22
      IF(TAMB.GT.30.0)GO TO 23
      N=14
      GO TO 24
   21 CONTINUE
      IF(TAMB.LT.0.0)GO TO 23
      N=1
      GO TO 24
   22 CONTINUE
      A=SNGL(TAMB/H01)
      N=IFIX(A)
   24 CONTINUE
      D1=TAMB-TEMP(N)
      D2=TAMB-TEMP(N+1)
      D3=TAMB-TEMP(N+2)
      D12=(D1*EMF(N+1)-D2*EMF(N))*H02
      D23=(D2*EMF(N+2)-D3*EMF(N+1))*H02
      D123=((D1*D23)-(D3*D12))*H03
      TREFS=D123
      GO TO 25
   23 CONTINUE
      TREFS=0.0
   25 CONTINUE
      RETURN
      END
      FUNCTION TREFT(TAMB)
C  SUBROUTINE TO PERFORM QUADRATIC INTERPOLATION ON THERMOCOUPLE TABLE
C  FOR A GIVEN RANGE OF ATMOSPHERIC TEMPERATURE          0 < TAMB < 30.0
C     TYPET - COPPER-CONSTANTAN .
C  DEGREES CELSIUS TO MILLIVOLTS .
C  REFERENCE :  B.S.1828:1961
      REAL A
      REAL*8 TEMP(60),EMF(60),E,H01,H02,H03,D1,D2,D3,D12,D23,D123
     >,TYPEK,TYPES,TYPET,TREFK,TREFS,TREFT,TAMB
      DATA TEMP/ 0.0,   2.0,   4.0,   6.0,   8.0,  10.0,  12.0,  14.0,
     >    16.0,  18.0,  20.0,  22.0,  24.0,  26.0,  28.0,  30.0/
      DATA EMF/  0.000,  0.077,  0.154,  0.232,  0.309,  0.388,  0.466
     >   0.545,  0.624,  0.703,  0.783,  0.863,  0.944,  1.025,  1.106
     >   1.188/
      DATA H01,H02,H03/2.0,0.5,0.25/
      IF(TAMB.LE.1.8)GO TO 21
      IF(TAMB.LT.28.4)GO TO 22
      IF(TAMB.GT.30.0)GO TO 23
      N=14
      GO TO 24
   21 CONTINUE
      IF(TAMB.LT.0.0)GO TO 23
      N=1
      GO TO 24
   22 CONTINUE
      A=SNGL(TAMB/H01)
      N=IFIX(A)
   24 CONTINUE
      D1=TAMB-TEMP(N)
      D2=TAMB-TEMP(N+1)
      D3=TAMB-TEMP(N+2)
```

```
      D12=(D1*EMF(N+1)-D2*EMF(N))*H02
      D23=(D2*EMF(N+2)-D3*EMF(N+1))*H02
      D123=((D1*D23)-(D3*D12))*H03
      TREFT=D123
      GO TO 25
   23 CONTINUE
      TREFT=0.0
   25 CONTINUE
      RETURN
      END
      FUNCTION ROTAMW(CM)
C  REFERENCE ; CALIBRATION OF METRIC 24E ROTAMETER FOR WATER . 21 SEPT
      REAL*8 ROTAMW,CM
      ROTAMW=105.64+(37.512*CM)
C  UNITS  ---    KG/H
      RETURN
      END
      FUNCTION ROTAMA(CM)
      REAL*8 ROTAMA,CM
      ROTAMA=CM*0.1168
      RETURN
      END
      FUNCTION CPA(TA)
C     SUBROUTINE TO PERFORM QUADRATIC INTERPOLATION ON DATA FOR
C  SPECIFIC HEAT AT CONSTANT PRESSURE OF
C  DRY AIR AT ONE ATMOSPHERE
C  REFERENCE :   TABLES OF THERMODYNAMIC & TRANSPORT PROPERTIES OF
C  AIR,AR,CO2,CO,H2,N2,O2 & H2O .
C  HILSENRATH,J. ET AL .     PERGAMON  1960
      REAL A
      REAL*8 TAB(30),TT(30),TA,H01,H02,H03,D1,D2,D3,D12,D23,D123,
     +CPA
      DATA TT/200.0,300.0,400.0,500.0,600.0,700.0,800.0,900.0,1000.0,
     +1100.0,1200.0,1300.0,1400.0,1500.0,1600.0,1700.0,1800.0,1900.0,
     +2000.0,2100.0,2200.0,2300.0,2400.0,2500.0,2600.0,
     +2700.0,2800.0,2900.0,3000.0/
      DATA TAB/
     +     3.5062,    3.5059,    3.5333,    3.5882,    3.6626,    3.7455,
     +     3.828,     3.906,     3.979,     4.046,     4.109,     4.171,
     +     4.230,     4.289,     4.352,     4.418,     4.487,     4.566,
     +     4.662,     4.781,     4.947,     5.179,     5.484,     5.882,
     +     6.40,      7.06,      7.87,      8.86,      9.96
     +/
      DATA H01,H02,H03/100.0,0.01,0.005/
      IF(TA.LE.299.0)GO TO 21
      IF(TA.LT.2940.0)GO TO 22
      IF(TA.GT.3000.0)GO TO 23
      N=16
      GO TO 24
   21 CONTINUE
      IF(TA.LT.200.0)GO TO 23
      N=1
      GO TO 24
   22 CONTINUE
      A=SNGL(TA/H01)
      N=IFIX(A)-2
   24 CONTINUE
      D1=TA-TT(N)
      D2=TA-TT(N+1)
      D3=TA-TT(N+2)
```

```
      D12=(D1*TAB(N+1)-D2*TAB(N))*H02
      D23=(D2*TAB(N+2)-D3*TAB(N+1))*H02
      D123=((D1*D23)-(D3*D12))*H03
      CPA=D123*287.041
C  UNITS OF CPA :  J/KG  K
      GO TO 25
   23 CONTINUE
      WRITE(6,700)TA
  700 FORMAT('CPA   ARGUMENT OF ',F12.5,' IS OUTSIDE TEMPERATURE RANGE
     +OF 200.0 --  3000.0  DEG. K')
   25 RETURN
      END
      FUNCTION CPW(TW)
C     SUBROUTINE TO PERFORM QUADRATIC INTERPOLATION ON DATAFOR
C     SPECIFIC HEAT AT CONSTANT PRESSURE FOR WATER
C     FROM TABLE 5 ,PAGE 119 ,UK STEAM TABLES IN SI UNITS 1970 .
      REAL A
      REAL*8 TAB(11),TT(11),TW,H01,H02,H03,D1,D2,D3,D12,D23,D123,
     +CPW
      DATA TT/10.0,20.0,30.0,40.0,50.0,60.0,70.0,80.0,90.0,100.0,
     +110.0/
      DATA TAB/4.194,4.182,4.179,4.179,4.181,4.185,4.191,4.198,
     +4.207,4.218,4.230/
      DATA H01,H02,H03/10.0,0.1,0.05/
      IF(TW.LE.19.0)GO TO 21
      IF(TW.LT.104.0)GO TO 22
      IF(TW.GT.110.0)GO TO 23
      N=9
      GO TO 24
   21 CONTINUE
      IF(TW.LT.10.0)GO TO 23
      N=1
      GO TO 24
   22 CONTINUE
      A=SNGL(TW/H01)
      N=IFIX(A)-1
   24 CONTINUE
      D1=TW-TT(N)
      D2=TW-TT(N+1)
      D3=TW-TT(N+2)
      D12=(D1*TAB(N+1)-D2*TAB(N))*H02
      D23=(D2*TAB(N+2)-D3*TAB(N+1))*H02
      D123=((D1*D23)-(D3*D12))*H03
      CPW=D123*1000.0
      GO TO 25
   23 CONTINUE
      WRITE(6,700)TW
  700 FORMAT(' CPW  ARGUMENT OF ',F12.5,' IS OUTSIDE TEMP RANGE OF
     + 10.0 ---  110.0  DEG. C')
   25 RETURN
      END
```

```
C      PCFPP01
C PULSATING COMBUSTOR FREQUENCY PREDICTION PROGRAM  --  CNE
C THE PURPOSE OF THIS PROGRAM IS TO SOLVE THE BESSEL BOUNDARY
C CONDITIONS FOR AN EXPONENTIAL GAS TEMPERATURE GRADIENT IN THE
C HEAT EXCHANGER SECTIONS OF THE MARK 5 COMBUSTOR .
C            6 JUNE 1972
C  NUMBER CODE : M = 1      OPEN-OPEN       MODEL
C                M = 2      OPEN-CLOSED     MODEL
       IMPLICIT REAL*8(A-H,O-Z)
       DIMENSION BJ(6),BY(6),IER(12)
       REAL*8 LANDA
   18 CONTINUE
       READ(5,7799)T1,T2
 7799 FORMAT(2(F10.3))
       IF(T1)53,53,12
   12 CONTINUE
       DATA X1,X2/0.33,2.4/
       ALPHA=(-DLOG(T1/T2))/(2*(X1-X2))
       TO=T1/(DEXP(-2*ALPHA*X1))
       CO=DSQRT(401.94*TO)
       EL=3.3
       M=2
C
       WRITE(6,2000)M,ALPHA,CO,EL
 2000 FORMAT(3X,'M =',I3,4X,'OPEN-CLOSED MODEL'//8X,'ALPHA = ',1PE12.6
     1//11X,'CO = ',1PE12.6,3X,'METRE/SECOND'//11X,'EL = ',1PE12.6,
     23X,'METRE'/)
C234567
C CALCULATE A & B
       A=(DEXP(ALPHA*EL))/ALPHA
       B=1.0/ALPHA
C
       WRITE(6,9111)T1,T2
 9111 FORMAT(11X,'T1 = ',1PD12.6,7X,'K'/11X,'T2 = ',1PD12.6,7X,'K'/)
C
       D=0.001
C READ STARTING VALUE OF LANDA
   11 READ(5,1001)LANDA
 1001 FORMAT(F10.5)
C
C
       IF(LANDA)18,18,10
   10 CONTINUE
C SET N EQUAL TO ZERO
       N=0
C
C
C
    4 CONTINUE
       ALANDA=A*LANDA
       BLANDA=B*LANDA
C CALCULATE BESSEL ARRAYS FOR GIVEN ORDER AND ARGUEMENT
       CALL DBESJ(ALANDA,0,BJ(1),D,IER(1))
       CALL DBESJ(BLANDA,0,BJ(2),D,IER(2))
       CALL DBESJ(ALANDA,1,BJ(3),D,IER(3))
       CALL DBESJ(BLANDA,1,BJ(4),D,IER(4))
       CALL DBESJ(ALANDA,2,BJ(5),D,IER(5))
       CALL DBESJ(BLANDA,2,BJ(6),D,IER(6))
```

```
C234567
      CALL DBESY(ALANCA,0,BY(1),IER(7))
      CALL DBESY(BLANDA,0,BY(2),IER(8))
      CALL DBESY(ALANDA,1,BY(3),IER(9))
      CALL DBESY(BLANCA,1,BY(4),IER(10))
      CALL DBESY(ALANCA,2,BY(5),IER(11))
      CALL DBESY(BLANCA,2,BY(6),IER(12))
      FLANDA=BJ(2)*BY(3)-BJ(3)*BY(2)
      GLANDA=B*BJ(3)*BY(4)-B*BY(3)*BJ(4)+0.5*A*BJ(2)*(BY(1)-BY(5))
     >-0.5*A*BY(2)*(BJ(1)-BJ(5))
      IF(DABS(GLANDA) .LT. 1.0D-06)GO TO 90
      Y=LANDA-(FLANDA/GLANDA)
      IF(DABS(LANDA-Y) .LT. 1.0D-06 .OR. N .GT. 50)GO TO 9
      N=N+1
      LANDA=Y
C
C
      GO TO 4
    9 WRITE(6,2004)Y,N
 2004 FORMAT(4X,'FINAL VALUE OF LANDA =',2X,1PE12.6,4X,'AT N =',I3//)
      FREQ=CO*Y/6.2831853072
      WRITE(6,2005)FREQ
 2005 FORMAT(10X,'COMPUTED FREQUENCY =',2X,1PE12.6,6X,' HERTZ'/)
      GO TO 11
   90 WRITE(6,2150)
 2150 FORMAT(3X,' GLANCA DEFAULT '//)
      GO TO 11
   53 STOP
      END
C     PCFPP01
C PULSATING COMBUSTOR FREQUENCY PREDICTION PROGRAM -- ONE
C THE PURPOSE OF THIS PROGRAM IS TO SOLVE THE BESSEL BOUNDARY
C CONDITIONS FOR AN EXPONENTIAL GAS TEMPERATURE GRADIENT IN THE
C HEAT EXCHANGER SECTIONS OF THE MARK 5 COMBUSTOR .
C           6 JUNE 1972
C  NUMBER CODE : M = 1     OPEN-OPEN     MODEL
C                M = 2     OPEN-CLOSED   MODEL
      IMPLICIT REAL*8(A-H,O-Z)
      DIMENSION BJ(6),BY(6),IER(12)
      REAL*8 LANDA
   18 CONTINUE
      READ(5,7799)T1,T2
 7799 FORMAT(2(F10.3))
      IF(T1)53,53,12
   12 CONTINUE
      DATA X1,X2/0.33,2.4/
      ALPHA=(-DLOG(T1/T2))/(2*(X1-X2))
      TO=T1/(DEXP(-2*ALPHA*X1))
      CO=DSQRT(401.94*TO)
      EL=3.3
      M=1
      WRITE(6,2000)M,ALPHA,CO,EL
 2000 FORMAT(3X,'M = ',I2,4X,'OPEN-OPEN MODEL'//8X,'ALPHA = ',1PE12.6
     1//11X,'CO = ',1PE12.6,3X,'METRE/SECOND'//11X,'EL = ',1PE12.6,
     23X,'METRE'/)
C234567
C CALCULATE A & B
      A=(DEXP(ALPHA*EL))/ALPHA
      B=1.0/ALPHA
      WRITE(6,9111)T1,T2
```

```
 9111 FORMAT(11X,'T1 = ',1PD12.6,7X,'K'/11X,'T2 = ',1PD12.6,7X,'K'/)
      WRITE(6,2001)A,B
 2001 FORMAT(7X,'A = ',1PE12.6/7X,'B = ',1PE12.6/)
      D=0.001
C READ STARTING VALUE OF LANDA
   11 READ(5,1001)LANCA
 1001 FORMAT(F10.5)
      WRITE(6,2002)LANDA
 2002 FORMAT(3X,'LANDA STARTING VALUE = ',1PE12.6/)
      IF(LANDA)18,18,10
   10 CONTINUE
C SET N EQUAL TO ZERO
      N=0
      WRITE(6,6000)
 6000 FORMAT(3X,'N',6X,'ALANDA',6X,'BLANDA',6X,'FLANCA',6X,'GLANCA',
     46X,'LANDA'//)
    4 CONTINUE
      ALANDA=A*LANDA
      BLANCA=B*LANDA
C CALCULATE BESSEL ARRAYS FOR GIVEN ORDER AND ARGUEMENT
      CALL DBESJ(ALANDA,0,BJ(1),D,IER(1))
      CALL DBESJ(BLANCA,0,BJ(2),D,IER(2))
      CALL DBESJ(ALANCA,1,BJ(3),D,IER(3))
      CALL DBESJ(BLANDA,1,BJ(4),D,IER(4))
      CALL DBESJ(ALANCA,2,BJ(5),D,IER(5))
      CALL DBESJ(BLANDA,2,BJ(6),D,IER(6))
C234567
      CALL DBESY(ALANCA,0,BY(1),IER(7))
      CALL DBESY(BLANDA,0,BY(2),IER(8))
      CALL DBESY(ALANCA,1,BY(3),IER(9))
      CALL DBESY(BLANCA,1,BY(4),IER(10))
      CALL DBESY(ALANDA,2,BY(5),IER(11))
      CALL DBESY(BLANDA,2,BY(6),IER(12))
      FLANDA=BJ(4)*BY(3)-BJ(3)*BY(4)
      GLANDA=0.5*B*BY(3)*(BJ(2)-BJ(6))+0.5*A*BJ(4)*(BY(1)-BY(5))
     >-0.5*A*BY(4)*(BJ(1)-BJ(5))-0.5*B*BJ(3)*(BY(2)-BY(6))
      IF(DABS(GLANCA) .LT. 1.0D-06)GO TO 90
      Y=LANDA-(FLANDA/GLANDA)
      IF(DABS(LANDA-Y) .LT. 1.0D-06 .OR. N .GT. 50)GO TO 9
      N=N+1
      LANCA=Y
      WRITE(6,7000)N,ALANDA,BLANDA,FLANDA,GLANDA,LANDA
 7000 FORMAT(2X,I2,4X,5(1PE12.5))
      GO TO 4
    9 WRITE(6,2004)Y,N
 2004 FORMAT(4X,'FINAL VALUE OF LANDA =',2X,1PE12.6,4X,'AT N =',I3//)
      FREQ=C0*Y/6.2831853072
      WRITE(6,2005)FREQ
 2005 FORMAT(10X,'COMPUTED FREQUENCY =',2X,1PE12.6,6X,' HERTZ'/)
      GO TO 11
   90 WRITE(6,2150)
 2150 FORMAT(3X,' GLANDA DEFAULT '//)
      GO TO 11
   53 STOP
      END
C     TEST PROGRAM                10 SEPT 1972
C     EVALUATION OF P(X,T) FOR C(X) = C0*EXP(ALPHA*X)
      IMPLICIT REAL*8(A-H,O-Z)
      REAL*8 LANDA
      DIMENSION BJ(9),BY(9),IER(9)
```

```
      DATA BA,EL,D/135000.0,3.3,0.00001/
    4 READ(5,1050)ALPHA,CO,PMAX
      IF(ALPHA)24,24,73
   73 CONTINUE
1050 FORMAT(5(F10.7))
      WRITE(6,5000)CO,ALPHA,EL,PMAX,BA
5000 FORMAT(2X,'   CO = ',1PD12.5,' METRES/SEC'/2X,'ALPHA = '
     1,1PD12.5/2X,'   EL = ',1PD12.5,' METRES'/2X,' PMAX = '
     2,1PD12.5,' N/M**2'/2X,'   BA = ',1PD12.5,' N/M**2'//)
      READ(5,1000)LANDA
1000 FORMAT(F15.6)
      WRITE(6,4000)LANDA
4000 FORMAT(2X,'LANDA = ',1PD12.5/)
      IF(LANDA)24,24,25
   25 CONTINUE
      ZL=(DEXP(ALPHA*EL))*LANDA/ALPHA
      Z0=LANDA/ALPHA
      CALL DBESJ(Z0,0,BJ(1),D,IER(1))
      CALL DBESY(Z0,0,BY(1),IER(2))
      RMN=-BY(1)/BJ(1)
      CALL DBESJ(Z0,1,BJ(2),D,IER(3))
      CALL DBESY(Z0,1,BY(2),IER(4))
      CONST=(RMN*BJ(2))+BY(2)
      WRITE(6,2001)
2001 FORMAT(4X,'J',9X,'X',15X,'P',13X,'V'//)
      X=0.0
      DO 90 J=1,12
      Z=(DEXP(ALPHA*X))*LANDA/ALPHA
      CALL DBESJ(Z,1,BJ(3),D,IER(5))
      CALL DBESY(Z,1,BY(3),IER(6))
      P=PMAX*DEXP(ALPHA*X)*((RMN*BJ(3))+BY(3))/CONST
      CALL DBESJ(Z,0,BJ(4),D,IER(7))
      CALL DBESY(Z,0,BY(4),IER(8))
      V=PMAX*CO*((RMN*BJ(4))+BY(4))/(BA*CONST)
      WRITE(6,2000)J,X,P,V
2000 FORMAT(I5,3(5X,1PD10.3))
      X=X+0.3
   90 CONTINUE
      WRITE(6,2002)
2002 FORMAT(//4X,'-',7X,'METRES',10X,'N/M**2',9X,'M/SEC'//)
      GO TO 4
   24 STOP
      END
```

```
C  PROGRAMME TO CALCULATE AIR MASS FLOW THROUGH AERODYNAMIC VALVE ;
C  CALCULATION BASED ON QUASI-STEADY-STATE THEORY . THUS MASS FLOW
C  IS INDEPENDENT OF FREQUENCY .      5  MARCH  1973
      REAL*8 MAIN(200),MAEX(200),RHO1,RHO2,P1,P2,GAM1,GAM2,GAMMA,TA,
     +M1,M2,A,AE,CD,C1,C2,PXO,PAT,D,KG,KP,T,DT,RR,U1(200),U2(200)
C  READ  D        INTERNAL DIAMETER OF VALVE
C        PXO      PRESSURE AMPLITUDE IN COMBUSTION CHAMBER
C        TA       MEAN TEMPERATURE IN COMBUSTION CHAMBER
   98 CONTINUE
      READ(5,1000)D,PXO,TA
      IF(D)94,94,95
   95 CONTINUE
 1000 FORMAT(3(F10.0))
C  SET CONSTANTS FOR INDUCTION PART OF CYCLE ;  2PI >  T  >  PI
      PAT=101350.0
      RHO1=1.177
      NORD=20
      T=3.14159265358
      DT=3.14159265358/NORD
      P1=PAT
      NORD=NORD+1
      GAM1=1.4
      KG=(GAM1-1.0)/GAM1
      RR=287.1
      C1=DSQRT(GAM1*RR*300.0)
      WRITE(6,3003)
 3003 FORMAT(10X,'T',13X,'U1(I)'//)
      DO 10 I=1,NORD
      P2=PAT+PXO*DSIN(T)
      KP=P2/P1
      RHO2=RHO1*(KP**(1.0/GAM1))
C  CALCULATE INSTANTANEOUS VELOCITY & MACH NO.
      U1(I)=DABS((2.0*P1/(KG*RHO1))*(1.0-KP**KG))
      U1(I)=DSQRT(U1(I))
      M1=U1(I)/C1
C  CALCULATE COEFFICIENT OF DISCHARGE & EFFECTIVE AREA
      CD=0.5+(M1**2)*0.125+(M1**4)*0.04166666667
      AE=3.14159265358*(D**2)*CD*0.25
C  CALCULATE INSTANTANEOUS AIR MASS FLOWRATE
      MAIN(I)=RHO2*AE*U1(I)
C  WRITE ANGLE & VELOCITY
      WRITE(6,3000)T,U1(I)
 3000 FORMAT(2(4X,1PD13.5))
      T=T+DT
   10 CONTINUE
C  INTEGRATE BY SIMPSONS RULE
      CALL DQSF(DT,MAIN,MAIN,NORD)
      WRITE(6,3010)MAIN(NORD)
 3010 FORMAT(4X,'INDUCTION AIR MASS =',1PD13.5//)
C  RESET CONSTANTS FOR EXHAUST PART OF CYCLE ;  0  <  T  <  PI
      NORD=20
      T=0.0
      DT=3.14159265358/NORD
      GAM2=1.3
      KG=(GAM2-1.0)/GAM2
      C2=DSQRT(GAM2*RR*TA)
      NORD=NORD+1
      RHO2=P1/(RR*TA)
```

```
      WRITE(6,3004)
 3004 FORMAT(10X,'T',13X,'U2(J)'//)
      DO 11 J=1,NORD
      P2=PAT+PX0*DSIN(T)
      KP=P1/P2
      RHO1=RHO2*(KP**(1.0/GAM2))
C  CALCULATE INSTANTANEOUS VELOCITY & MACH NO.
      U2(J)=CQ
      U2(J)=DSQRT((2.0*P2/(KG*RHO2))*(1.0-KP**KG))
      M2=U2(J)/C2
C  CALCULATE COEFFICIENT OF DISCHARGE & EFFECTIVE AREA
      CD=0.5+(M2**2)*0.125+(M2**4)*0.04166666667
      AE=3.14159265358*(D**2)*CD*0.25
C  CALCULATE INSTANTANEOUS AIR MASS FLOWRATE
      MAEX(J)=RHO1*AE*U2(J)
C  WRITE ANGLE & VELOCITY
      WRITE(6,3006)T,U2(J)
 3006 FORMAT(2(4X,1PD13.5))
      T=T+DT
   11 CONTINUE
C  INTEGRATE BY SIMPSONS RULE
      CALL DQSF(DT,MAEX,MAEX,NORD)
      WRITE(6,3007)MAEX(NORD)
 3007 FORMAT(4X,'EXHAUST AIR MASS =',1PD13.5//)
      MAIN(NORD)=MAIN(NORD)-MAEX(NORD)
      WRITE(2,1235)MAIN(NORD)
 1235 FORMAT(4X,' MAA = ',1PD13.5)
      WRITE(2,2222)D,PX0,TA
 2222 FORMAT(4X,'D =',F10.5/4X,'PX0 =',F10.2/4X,'TA =',F10.2//)
      GO TO 98
   94 CONTINUE
      STOP
      END
```